Modelling, Simulation & Performance Analysis of Permanent Magnet Brushless DC Motor

A THESIS SUBMITTED IN PARTIAL FULFILLMENT OF THE REQUIREMENTS FOR THE DEGREE OF DOCTOR OF PHILOSOPHY

By

ARVIND KUMAR SINGH

Registration No. 011/2003

SCHOOL OF ENERGY, ENVIRONMENT AND NATURAL RESOURCES

Department of Energy
Tezpur University
Tezpur, Assam
INDIA

August, 2005

Certificate of the supervisor(s)

This is to certify that the matter embodied in the thesis titled "**Modelling, Simulation & Performance Analysis of Permanent Magnet Brushless DC Motor**" by Sri Arvind Kumar Singh for the award of Degree of Doctor of Philosophy of Tezpur University is a record of bonafide research work carried out by him under our joint supervision and guidance. The results embodied in this thesis have not been submitted to any other University or Institute for the award of any degree or diploma.

P.K. Bordoloi

Prof. P. K. Bordoloi

Dated: 22/8/2005

K. Kumar

Prof. Kalyan Kumar

Dated: 22/8/2005

SIN

ACKNOWLEDGEMENT

The author wishes to express his deep gratitude to the guides Prof. P. K. Bordoloi, Professor& Head, Department of Energy, Tezpur University, Tezpur, Assam, and Prof. Kalyan Kumar, (Professor in Electrical Engineering, Ex-Dean (P&D) & Ex-HoD (EE), North Eastern Regional Institute of Science and Technology (NERIST), Nirjuli, Arunachal Pradesh for their valuable guidance received throughout the research work. Their fruitful suggestions and guidance have always been a source of inspiration to the author.

The author remains ever grateful to His Excellency Hon'ble Governor of Arunachal Pradesh and the chairman, NERIST Society, Sri S. K. Singh for his constant encouragement during the course of investigation.

The author remains grateful to Prof. D. Konwar, Dean, School of Energy, Environment and Natural Resources and Prof. B.D. Phukan, H.o.D, Department of Electronics, Tezpur University, Tezpur.

The author appreciates the co-operation, help and encouragement received from his friends and colleagues Dr. O.P. Roy, Dr. T. Thakur, Mr. S. K. Bhagat, Mr. Radak Blage, Mr. P.D. Kashayap, Mr. S. Gao, Mr. Ratan Singh and Mr. M.D. Singh of the Department of Electrical Engineering, NERIST; Dr. R.P. Singh and Mr. H.P. Singh of the Department of Civil Engineering, NERIST; and Dr. B.K. Singh of the Department of Mathematics, NERIST; Mr. Ashok Singh, Dy Registrar, Tezpur University, Ramesh Chand, Scientist, in Electronics Niketan, New Delhi, Dr. Narendra Kumar, Department of Electrical Engineering, D.C.E, Delhi, Dr. Arvind Pandey and Mr. S.K. Tripathi, in the Department of Physics, NERIST.

The author acknowledges the support received from the faculty and staff of the Department of Energy, Tezpur University, Tezpur and the faculty and staff of NERIST, Nirjuli, Arunachal Pradesh during the course of research work.

The author is also thankful to the authorities of North Eastern Regional Institute of Science and Technology (NERIST), Nirjuli, Arunachal Pradesh for providing the research facilities.

The author would like to express his heartfelt gratitude to his beloved mother, father, uncles, brothers, sister and brother in law.

The author wishes to record his appreciation for his wife Shikha Singh for her constant inspiration, patience and co-operation throughout the period of research and affection for son (Harsh) and daughter (Anshika).

Date: 22/8/2005

aksingl

(ARVIND KUMAR SINGH)

Modelling, Simulation & Performance Analysis of Permanent Magnet Brushless DC Motor

Abstract

The rapid development in power electronics and microelectronics has made it possible to apply modern control techniques particularly in the area of motion control. Numerous References were collected to study the efforts of researchers in bringing about considerable improvements in design of motors, sources of excitation and control techniques used with a view to meeting the ever increasing requirements of different kinds of industrial applications in handling of loads. Traditionally, induction motors were preferred for constant speed operation while DC motors, due to their inherent flexibility, were exclusively used for variable-speed loads. Advances in solid-state devices have paved the way for the development of controllers which made it possible to provide the induction motor with some of the desirable features of DC motors. However, these machines though equipped with controllers, were not able to cope with more stringent requirements of handling loads used in high performance applications. Increase in the power-to-weight ratio and reduction in machine size became essential for aerospace applications as well as for servo drives used in robotics and material handling. Similarly, for applications requiring high power rating such as line-start pumps, fans and compressors, improving the operational features became very important from the point of view of energy conversion, while requirements of precise control of speed and position became critical for machine tool applications. Improvement in solid state devices and the availability of improved magnetic materials have generally contributed to the development of Permanent Magnet Brushless DC (PMBLDC) motor which will go a long way in squarely meeting these requirements. A number of research papers are available which claims the superiority of PMBLDC motors over DC, induction and synchronous motors in terms of efficiency, size and other performance indices. The design engineers are now selecting PMBLDC motor over conventional dc, induction or synchronous motor drives.

The major effort of the research reported in the thesis is centered around dynamic performance evaluation of PMBLDC motor. The investigation reported in this thesis seeks to develop a suitable model for the PMBLDC motor with the help of which the dynamic performances of the drive system can be studied and analyzed. This model is used with the various controllers and/or excitation schemes apart from making attempt to improve upon its overall performance.

The results of the investigation have confirmed the viability of the simplified model used in the simulation of PMBLDC motor drive. The different types of control structures proposed in the work are capable of taking care of transients in speed, current and torque during starting, speed reversal and load perturbations. Since the transient currents drawn by the motor never exceeded the maximum permissible, the motor control structure was able to take care of the over current protection. The proposed models examine the suitability of the various controllers and/or excitation schemes with a view to improve upon the drive's overall performance besides exploring the possibility of cost reduction in terms of sensorless operation and/or design optimization.

The modern drive incorporates an impressive range of technology: new materials, motors, sensors, powerful processors and control electronics, and software. Traditionally interfacing the control circuit with the power circuit has been achieved by using large number of discrete components. However, higher level of system integration is now possible using compact products and IC's. Very-Large-Scale-Integrated circuits (VLSI) and Application-Specific-Integrated-Circuits (ASIC) are becoming more and more popular in PM brushless motor drive applications. Now-a-days, manufacturers of industrial control systems are looking for higher levels of system integration, coupled with increasing sophistication in control techniques at comparatively lower costs. Depending on the application, driver and control products for PM brushless motor, drives are available with voltages upto 600V and varying degrees of control and logic complexity.

The performance of close-loop control drive system depends upon the choice of controllers. Several papers are published dealing with speed and current controllers for different drives and it is found that each of these controllers has its own advantages and disadvantages. Many control strategies have been proposed on classical linear control theory. It is well known that PI and PID controllers are mostly used in industry due to their simple structure and ease of implementation. The PI

controllers have failed to perform upto mark under parametric variation, non-linearity and load disturbances. This has resulted in excessive use of modern non-linear control schemes such as state feedback controllers, self-tuning controllers, model reference adaptive systems, and variable structure control. These controllers also need mathematical models and are quite sensitive to parameteric variations. Several adaptive control algorithms have been theoretically developed and proposed in recent years. An attempt was made to study the simulation results of controllers designed with the fuzzy logic. Also, the thesis illustrates the manner in which the switching options of the motor are decided by employing a current controller, namely Pulse Width Modulation (PWM). In a PWM controller, PWM bandwidth gives a near rectangular phase current with small current ripple but requires high frequency inverter. PWM controller gives faster response and it is easy to implement. MOSFET based inverter is used and higher switching frequencies are applied. The use of fast processors like micro-controllers, digital signal processing (DSP) and the new switching devices made it possible to implement intelligent controllers for the efficient operation of the drive system.

Another type of controller based on Fuzzy logic is being increasingly applied to systems with non-linearity and uncertainty. In the light of these observations, a range of speed controllers starting from conventional controllers to the modern controllers has been used for the simulation of the PMBLDC motor drive. Among different current controllers the PWM current controller has been used in the investigations. A 'C' language program is developed for the simulation in real time operating conditions. Two PMBLDC drives are used for simulation with machines of ratings: (1) 2.0 HP, 4A, 4pole, 3phase, star-connected, 1500rpm; and (2) 0.5 HP, 4 pole, 3 phase, star-connected, 1A, and 1500rpm.

The work carried out during the course of research and the observations made can be summarized as follows:

1. Models for the purpose of simulating the dynamic performance of both the PMBLDC motor and PMSM have been developed. The model for PMBLDC motor has been developed using a-b-c reference frame and the performance of the system has been analyzed using different types of speed controllers. The simulated results are obtained for different operating conditions of the drive such as starting, speed reversal and load perturbations.

2. Five different types of speed controllers for the PMBLDC motor have been considered, namely, PI (Proportional plus Integral), PID (Proportional plus Integral plus Derivative), SM (Sliding Mode), FPID (Fuzzy Proportional plus Integral plus Derivative) and FSM (Fuzzy Sliding Mode) controllers.
3. For the PMSM drive, the model has been developed using d-q reference frame. In this case, vector control method has been used for the purpose of predicting the motor's dynamic performance. The simulated results have been obtained for PI and PID speed controller with the understanding that what can be done with two speed controllers could easily be extended to others.
4. The current research focuses on modelling and simulation of PMBLDC motor drive system for predicting its dynamic performances.
5. The mathematical models of both the PMBLDC motor (in a-b-c reference frame) and the PMSM drive (in d-q reference frame) are expressed in the form of differential equations from which state-space equations for motor winding currents, rotor speed and rotor position are derived. For this purpose, all the subsystems of the drive are modelled separately and then they are integrated to provide the model for the complete system with the help of which the closed loop performance of the drive has been studied. The models so developed are quite useful to design and application engineers not only for analyzing the performance of the drive but also for selecting a drive for a specific application.
6. As the model equations are nonlinear in nature, a numerical technique called the Runge-Kutta method is being used to get the solutions.
7. The electromagnetic torque, stator winding currents, rotor speed and winding voltage are stored for studying the dynamic responses of the drive. PWM current controllers are used for maintaining the winding currents in the vicinity of their reference values.
8. Based on the simulated results of both the PMBLDC motor and the PMSM drive, it is observed that these motors, along with speed controllers exhibit good dynamic performances. The reference speed of the motor was set at 157 rad/sec (1500 rpm). The starting responses of the drive were studied with PI, PID, SM, FPI, FPID, FSM, Self-Organizing Fuzzy Logic, Gain Scheduling PI and Hybrid (FP+ID) Controllers, respectively.

9. The motor takes nearly (125 – 170) msec, depending upon the type of speed controller used, to reach the set reference speed. One can find the difference in time between the fastest (125 msec by FSM) and the slowest (170 msec by PID) controllers.

10. It may also be observed that in all the cases (with different controllers), as soon as the rotor speed reaches the set reference value, the controller becomes effective in maintaining the rotor speed at the set reference value without oscillations in speed. Only during the starting, the speed shows marginal oscillations.

11. With PI and PID controllers, more oscillations are observed in speed, current and torque during the settling period. These oscillations get improved with SM controller in which case the change over is relatively smooth during the time of transition from starting to the running condition. Moreover, the starting performance is significantly improved with Fuzzy based controllers (all types). The winding voltage is the same in all types of controllers.

12. On changing the reference speed from +157 rad/sec to -157.0 rad/sec, the control structure activated the regenerative braking at controlled frequencies and followed by the reverse motoring upto the set reference speed.

13. It is observed that right at the moment when the reference speed is changed from positive value to the negative value there is an instantaneous change in reference currents. The motor current follows the change in reference currents. This is possible due to the fast and accurate close-loop control structure used in the present investigation. In the case of reverse speed operation, the spikes are observed in PI and PID controllers during the settling period. While this problem is minimized to a great extent in the case of SM controller, the results get further improved in FL controller, namely FPI, FPID, FSM, Gain Scheduling PI and hybrid (FP+ID) controllers.

14. The responses of the drive system were studied under load perturbations with PI, PID, SM, FPI, FPID, FSM, Self-Organizing Fuzzy Logic, Gain Scheduling PI and Hybrid (FP+ID) controllers.

15. It is observed that the motor takes time to recover from load perturbations (nearly 5–100 msec) depending upon the type of speed controller used in order to reach the set reference speed. The sudden application of the load on the

motor causes a small dip in the motor speed, which should recover due to the fast controller action.

16. It can be observed that, almost immediately after the change of load the speed recovers and comes back to its normal value.
17. Under the SM control scheme, using PI and PID controllers, some small oscillations are observed during the load perturbations in speed, torque and current but winding voltages of all phases remain same in all the three phases. The performance of the drive system is more improved in the case of all types of FL controllers in terms of speed, torque and current responses.
18. The developed models are, therefore, effective in improving the dynamic responses of the drive, and further to this, these provide the basis on which the effectiveness of different speed controllers can be compared.
19. It is also observed that PMBLDC motor drive system shows a dynamic performance of the same level with speed controllers (PI, PID, SM, FPI, FPID, FSM, Gain scheduling PI, Self-Organizing fuzzy logic and hybrid (FP+ID) types). In SM controller, the dip in speed caused by load application is relatively lower as compared to PI and PID controllers and this dip remains intact till the withdrawal of the load. Unlike the PID controller there is no overshoot in this case, however, it suffers from the problem of chattering.
20 Use of Fuzzy based controllers such as FPI, FPID, FSM, Gain scheduling PI, Self-Organizing fuzzy logic, and hybrid (FP+ID) controllers, in general, lead to faster responses and they bring intelligence into the system. Among these Fuzzy based controllers, the FSM controller is the most robust while the FPID is easiest to implement.

It can be concluded that the motor control structure takes care of the over-current protection requirement of devices used in the inverter circuit. It has also been shown from this study that there is a quick and instantaneous corrective change in the motor current in response to any disturbances in the set operating conditions of the drive system. The oscillations present in the current and torque in the PI and PID speed controllers during change over from starting to steady state condition have been found to be curbed considerably when the SM and FL controllers are used in the closed loop operation of the drive. It has been observed that the PI and PID controllers are simpler and easier to implement in comparison to Fuzzy PI and Fuzzy PID speed

controllers. But they exhibit a slower response and cause some steady-state errors with a settling period. The SM, on the other hand, is found to be robust but slower. Apart from being relatively difficult to realize FSM controller, the latter is found to be superior to SM controller in terms of intelligence robustness. FPID and hybrid (FP+ID) controllers are more intelligent than FSM controller and exhibits the fastest response. Gain Scheduling PI controller is also superior to the PI controller.

***

CONTENTS

		Page Nos.
CERTIFICATE OF THE SUPERVISOR		ii
ACKNOWLEDGMENT		iii
ABSTRACT		iv
CONTENTS		xi
LIST OF TABLES		xx
LIST OF FIGURES		xxi
LIST OF SYMBOLS AND ABBREVIATIONS		xxix
CHAPTER 1: INTRODUCTION		1
1.1	General	1
1.2	Scope of the Problem Identified for the Research	2
1.3	State-of–the-Art	4
1.4	About the Proposed Research	6
	1.4.1 Analysis of PMBLDC Drive	6
	1.4.2 Real Time Simulation	7
	1.4.3 Different Speed Controllers	7
	1.4.4 Sensorless Speed Control of PMBLDC Motor	8
1.5	Proposed Research Methodology	8
	1.5.1 Development of System Model	8
	1.5.2 Cost Reduction	9
	1.5.3 Improved Performance	9
	1.5.4 Specifications of the PMBLDC motor and PMSM Drive System	9
	1.5.5 Modelling of PMBLDC Motor Drive System	9
	1.5.6 Main Features of the model of the PMBLDC Motor	12
1.6	Organization of the Thesis	13
CHAPTER 2:	A CRITICAL REVIEW OF THE AVAILABLE LITERATURE	15
2.1	General	15
2.2	Literature Review on PMBL Motor and PMSM Drive	15

2.3 Permanent Magnet Motor Drives 17
2.4 Trends in Permanent Magnet Motors and Drive Industry 19
2.5 Classifications of Permanent Magnet Brushless DC Motor 19
2.6 Permanent Magnets 20
2.6.1 Permanent Magnets and characteristics 21
2.6.2 Properties of Permanent Magnets 23
2.6.3 Permanent Magnet versus Electromagnetic Excitation 23
2.6.4 Electric Motor Design with NdFeB: Problems and Advantages 24
2.6.5 Applications of Permanent Magnet Brushless DC Motor 24
2.7 Source of Excitation 26
2.8 Rotor Position Sensing of DC Brushless Motors 26
2.8.1 Encoders 26
2.8.2 Resolvers 28
2.9 Different Types of Speed Controllers 30
2.10 Sensorless Control of PMBL Motors 31
2.11 Design Optimization of PM Brushless Motor 32
2.11.1 Formulation of PM Motor Design Optimization Problem 34
2.11.2 Design variables 34
2.11.3 Design constraint 35
2.11.4 Design objectives 35
2.11.5 Optimization Technique 36
2.11.6 Sequential Unconstrained Minimization Technique 36
2.11.7 Algorithm 37
2.11.8 Rosen Brock's method 38
2.12 Conclusion 42

CHAPTER 3: MATHEMATICAL MODELLING OF PMBLDC MOTOR 43
3.1 General 43
3.2 Description of the PMBLDC Motor Drive System 43
3.3 Types of Speed Controllers 44
3.3.1 PI speed controller 45
3.3.2 PID speed controller 45
3.3.3 Sliding mode controller (SMC) 45

3.3.4 Fuzzy Logic controller 46
3.3.4.1 Fuzzy Precompensated PI Controller 47
3.3.4.2 Fuzzy PID Controller 47
3.3.4.3 Fuzzy Sliding Mode Controller 48
3.3.4.4 Self Organizing Fuzzy Logic Controller 48
3.3.4.5 Gain Scheduled PI controller 49
3.3.4.6 Hybrid Fuzzy Controller 49
3.4 Modelling of the PMBLDC Motor Drive System 49
3.4.1 Modelling of speed controller 49
3.4.2 PI Speed Controller Modelling 50
3.4.3 PID Speed Controller Modelling 50
3.4.4 Modelling of Sliding Mode Controller 51
3.4.5 Modelling of Fuzzy Logic Controller 52
3.4.5.1 Modelling of Fuzzy Precompensated PI Controller 54
3.4.5.2 Modelling of Self-Organizing Fuzzy Logic Controller 57
3.4.5.3 Modelling of Gain Scheduled PI Speed Controller 59
3.4.5.4 Modelling of Hybrid FP+ID controller structure 61
3.4.6 Modelling of Reference Current Generator 63
3.4.7 Modelling of PWM Current Controller 63
3.4.8 Modelling of back EMF using rotor position 63
3.4.9 Modelling of PMBLDC Motor and Inverter 64
3.5 Sensorless Control of PMBLDCM Drive System 67
3.5.1 General 67
3.5.2 Different Sensorless Schemes of PMBLDC motor 67
3.5.2.1 Terminal voltage sensing 67
3.5.2.2 Third Harmonic voltage Integration 68
3.5.2.3 Method based on monitoring switching states in the inverter 68
3.5.2.4 Position detection using phase current sensing 69
3.5.2.5 Observer methods 69
3.5.2.6 By using a special windings 69
3.5.3 Different Starting Strategies of PMBL Motor 69
3.6 Mathematical Modelling of Sensorless speed controller 71
3.6.1 Modelling of Speed Controller 71

3.6.2 Modelling of position detection using Back EMF 72
3.7 Conclusion 73

CHAPTER 4: MATHEMATICAL MODELLING OF PMSM MOTOR DRIVE 74
4.1 General 74
4.2 Principle of PMSM Motor Drive 75
4.3 Description of the PMSM Motor Drive System 76
4.4 Types of Speed Controllers 78
4.4.1 Proportional Type of Controller 79
4.4.2 Proportional and Derivative Controller 79
4.4.3 Proportional and Integral Controller 80
4.4.4 Proportional Plus Derivative Plus Integral (PID) controller 81
4.5 Modelling of a Drive System 81
4.5.1 Modelling of speed controller 82
4.5.2 Modelling of Vector Control 82
4.5.3 Modelling of reference current generator 83
4.5.4 Modelling of PWM current controller 83
4.5.5 Modelling of Inverter and motor 84
4.5.6 Phase Voltage Reconstruction from DC Link Voltage 85
4.5.7 PI Speed Controller Modelling 85
4.6.8 PID Speed Controller 85
4.6 Conclusion 86

CHAPTER 5: SIMULATION RESULTS OF PMBLDC MOTOR 87
5.1 General 87
5.2 Simulation Results of PMBLDC Motor with PI controller 88
5.2.1 Responses of Current during starting 88
5.2.1.1 Response of Speed during starting 89
5.2.1.2 Response of Torque during starting 89
5.2.1.3 Response of Voltage during starting 90
5.2.2 Responses of Current during Reversal 90
5.2.2.1 Response of Speed during Reversal 92
5.2.2.2 Response of Torque during Reversal 92

5.2.2.3 Response of Voltage during Reversal 93
5.2.3 Responses of Current during Load Perturbations 93
5.2.3.1 Response of Speed during Load Perturbations 94
5.2.3.2 Response of Torque during Load Perturbations 95
5.2.3.3 Response of Voltage during Load Perturbations 95
5.3 PID Speed Controller 95
5.3.1 Responses of Current during starting 96
5.3.1.1 Response of Speed during starting 97
5.3.1.2 Response of Torque during starting 97
5.3.1.3 Response of Voltage during starting 98
5.3.2 Responses of Current during Reversal 98
5.3.2.1 Response of Speed during Reversal 99
5.3.2.2 Response of Torque during Reversal 100
5.3.2.3 Response of Voltage during Reversal 100
5.3.3 Responses of Current during Load Perturbations 101
5.3.3.1 Response of Speed during Load Perturbations 102
5.3.3.2 Response of Torque during Load Perturbations 102
5.3.3.3 Response of Voltage during Load Perturbations 103
5.4 SMC Speed Controller 103
5.4.1 Responses of Current during Starting 103
5.4.1.1 Response of Speed during Starting 104
5.4.1.2 Response of Torque during Starting 105
5.4.1.3 Response of Voltage during Starting 105
5.4.2 Response of Current during Reversal 106
5.4.2.1 Response of Speed during Reversal 107
5.4.2.2 Response of Torque during Reversal 107
5.4.2.3 Response of Voltage during Reversal 108
5.4.3 Responses of Current during Load Perturbations 108
5.4.3.1 Response of Speed during Load Perturbations 110
5.4.3.2 Response of Torque during Load Perturbations 110
5.4.3.3 Response of Voltage during Load Perturbations 111
5.5 Fuzzy Precompensated PI Speed Controller 111
5.5.1 Responses of Current during Starting 111
5.5.1.1 Response of Speed during Starting 112

5.5.1.2 Response of Torque during Starting 113
5.5.1.3 Response of Voltage during Starting 114
5.5.2 Responses of Current during Reversal 114
5.5.2.1 Response of Speed during Reversal 115
5.5.2.2 Response of Torque during Reversal 116
5.5.2.3 Response of Voltage during Reversal 117
5.5.3 Responses of Current during Load Perturbations 117
5.5.3.1 Responses of Speed during Load Perturbations 118
5.5.3.2 Responses of Torque during Load Perturbations 119
5.5.3.3 Responses of Voltage during Load Perturbations 119
5.6 Fuzzy PID Speed Controller 120
5.6.1 Responses of Current during Starting 120
5.6.1.1 Response of Speed during Starting 121
5.6.1.2 Response of Torque during Starting 122
5.6.1.3 Response of Voltage during Starting 122
5.6.2 Responses of Current during Reversal 123
5.6.2.1 Response of Speed during Reversal 124
5.6.2.2 Response of Torque during Reversal 125
5.6.2.3 Response of Voltage during Reversal 126
5.6.3 Responses of Current during Load Perturbations 126
5.6.3.1 Responses of Speed during Load Perturbations 127
5.6.3.2 Responses of Torque during Load Perturbations 128
5.6.3.3 Responses of Voltage during Load Perturbations 128
5.7 Fuzzy SMC Speed Controller 129
5.7.1 Responses of Current during Starting 129
5.7.1.1 Response of Speed during Starting 130
5.7.1.2 Response of Torque during Starting 131
5.7.1.3 Response of Voltage during starting 132
5.7.2 Responses of Current during Reversal 132
5.7.2.1 Response of Speed during Reversal 133
5.7.2.2 Response of Torque during Reversal 134
5.7.2.3 Response of Voltage during Reversal 134
5.7.3 Responses of Current during Load Perturbations 135
5.7.3.1 Responses of Speed during Load Perturbations 136

5.7.3.2 Responses of Torque during Load Perturbations 137
5.7.3.3 Responses of Voltage during Load Perturbations 137
5.8 Self-Organizing Fuzzy Logic Speed Controller 137
5.8.1 Responses of Current during Starting 138
5.8.1.1 Response of Speed during Starting 139
5.8.1.2 Response of Torque during Starting 139
5.8.1.3 Response of Voltage during starting 140
5.8.2 Responses of Current during Reversal 140
5.8.2.1 Response of Speed during Reversal 141
5.8.2.2 Response of Torque during Reversal 142
5.8.2.3 Response of Voltage during Reversal 143
5.8.3 Responses of Current during Load Perturbations 143
5.8.3.1 Responses of Speed during Load Perturbations 144
5.8.3.2 Responses of Torque during Load Perturbations 145
5.8.3.3 Responses of Voltage during Load Perturbations 145
5.9 Gain-scheduling PI Speed Controller 146
5.9.1 Responses of Current during Starting 146
5.9.1.1 Response of Speed during Starting 148
5.9.1.2 Response of Torque during Starting 148
5.9.1.3 Response of Voltage during Starting 149
5.9.2 Responses of Current during Reversal 149
5.9.2.1 Response of Speed during Reversal 150
5.9.2.2 Response of Torque during Reversal 151
5.9.2.3 Response of Voltage during Reversal 152
5.9.3 Responses of Current during Load Perturbations 152
5.9.3.1 Responses of Speed during Load Perturbations 153
5.9.3.2 Responses of Torque during Load Perturbations 154
5.9.3.3 Responses of Voltage during Load Perturbations 154
5.10 Hybrid FP+ID Speed Controller 155
5.10.1 Responses of Currents during Starting 155
5.10.1.1 Response of Speed during Starting 157
5.10.1.2 Response of Torque during Starting 157
5.10.1.3 Response of Voltage during Starting 158
5.10.2 Responses of Current during Reversal 158

5.10.2.1 Response of Speed during Reversal 159
5.10.2.2 Response of Torque during Reversal 160
5.10.2.3 Response of Voltage during Reversal 161
5.10.3 Responses of Current during Load Perturbations 161
5.10.3.1 Response of Speed during Load Perturbations 162
5.10.3.2 Response of Torque during Load Perturbations 163
5.10.3.3 Response of Voltage during Load Perturbations 163
5.11 Performance Comparison of Controllers 164
5.12 Simulation Results of Sensorless Control of PMBLDC Motor Drive 169
5.12.1 Starting Algorithm 169
5.12.2 Results and Discussions 169
5.12.3 Responses of Sensorless Control of Current during Starting 169
5.12.4 Responses of Sensorless Control of Speed during Starting 171
5.12.5 Responses of Sensorless Control of Torque during Starting 171
5.12.6 Response of the back emf and its corresponding Position Signal of Sensorless Control of PMBLDC Motor 172
5.12.7 Responses of three back emf and its corresponding three Positions Signal of Sensorless Control of PMBLDC Motor 172
5.13 Conclusion 173

CHAPTER 6: SIMULATION RESULTS OF PMSM DRIVE 174
6.1 General 174
6.2 Simulation Results of PMSM drive with PI controller 175
6.2.1 Responses of Currents during starting 175
6.2.2 Responses of Speed during starting 176
6.2.3 Responses of Torque during starting 177
6.2.4 Responses of Voltage during starting 177
6.3 Responses of Current during Reversal 177
6.3.1 Response of Speed during Reversal 179
6.3.2 Response of Torque during Reversal 179
6.3.3 Response of Voltage during Reversal 180
6.4 Responses of Current during Load Perturbations 180
6.4.1 Response of Speed during Load Perturbations 182

6.4.2 Response of Torque during Load Perturbations 182
6.4.3 Response of Voltage during Load Perturbations 183
6.5 6.5 Response of PMSM with PID Controller 183
6.5.1 Responses of Current during starting 183
6.5.2 Response of Speed during starting 185
6.5.3 Response of Torque during starting 185
6.5.4 Response of Voltage during starting 186
6.6 Responses of Current during Reversal 186
6.6.1 Response of Speed during Reversal 188
6.6.2 Response of Torque during Reversal 188
6.6.3 Response of Voltage during Reversal 189
6.7 Responses of Current during Load Perturbations 189
6.7.1 Response of Speed Controller during Load Perturbations 191
6.7.2 Response of Torque during Load Perturbations 191
6.7.3 Response of Voltage during Load Perturbations 192
6.8 Comparison of PMSM with PMBLDC Motor Drive System 192
6.9 Conclusion 195

CHAPTER 7: SUMMARY AND CONCLUSIONS 196
7.1 General 196
7.2 Major Contributions and Summary of the Main Conclusions Drawn 196
7.3 Limitations 199
7.4 Scope for Future Work 199

REFERENCES 201
APPENDIX [A] Parameters of PMBLDC Motors 213
APPENDIX [B] - Parameters of PMSM Motor 214
APPENDIX [C] - Controller Parameters for PMBLDC Motor 215
APPENDIX [D] - Electrical & Electronics Circuit Parameters 217

LIST OF TABLES

Table 2.1	Choronical Development of Permanent Magnet	21
Table 2.2	Properties of PM Materials	23
Table 3.1	Rule base Table for the Fuzzy Logic based speed Controller	54
Table 3.2	Rule base Table for Fuzzy Precompensated PI controller	57
Table 3.3	Rule base table for the Self-organizing fuzzy logic controller	58
Table 3.4	Fuzzy members	62
Table 3.5	Fuzzy Logic Rules for hybrid (FP+ID) controller	62
Table 3.6	Reference currents corresponding to the Position Signals	63
Table 3.7	Summary of indirect position sensing methods in brushless PM motors	70
Table 3.8	Conduction period	73
Table 5.1	Performance comparison of the drive with different Speed Controllers	168
Table 5.2	Performance summary	168
Table A.1	PMBLDC motor (1) Specifications	213
Table A.2	PMBLDC Motor (2) Specifications	213
Table B.1	PMSM Motor Specifications	214
Table C.1	Controller gains for PI Speed Controller	215
Table C.2	Controller gains for PID Speed Controller	215
Table C.3	Controller gains for SMC Speed Controller	215
Table C.4	Controller gains for FP-PI Speed Controller	215
Table C.5	Controller gains for Fuzzy PID Speed Controller	215
Table C.6	Controller gains for Fuzzy SMC Speed Controller Simulation	215
Table C.7	Controller gains for Self-Organizing Fuzzy Speed Controller Simulation	216
Table C.8	Controller gains for Gain-scheduling PI Speed Controller Simulation	216
Table C.9	Controller gains for Hybrid (FP+ID) Speed Controller Simulation	216
Table C.10	Controller gains for PI Speed Controller for PMSM Drive	216
Table C.11	Controller gains for PID Speed Controller	216
Table D.1	Electrical and Electronic Circuit Parameters	217
Table D.2	Power Supply	217

LIST OF FIGURES

Figure 1.1	Schematic Block Diagram of PMBLDC Motor	11
Figure 1.2	Schematic Block Diagram of PMSM Drive	11
Figure 2.1	Armature waveforms for sinusoidally excited and square wave	18
Figure 2.2	Second Quadrant B-H characteristics of Permanent Magnets	21
Figure 2.3	Incremental and absolute encoders (a) disk of an incremental encoder, (b) Quadrature output signals, (c) disk of an absolute encoder, (d) Absolute encoder output signals	28
Figure 2.4	Brushless resolver.1-stator, 2-rotor, 3-rotary transformer	29
Figure 2.5	Principle of operation of a rotary resolver: (a) winding Configuration,(b) resolver output waves and 4-pole voltages. The interval $0 \leq p\theta \leq 720^0$ corresponds to one revolution	29
Figure 2.6	Flow Chart of 'SUMT' For PM Motor Design Optimization	38
Figure 2.7	Flow Chart of 'Rosen Brock's method' For PM Motor Design Optimization	41
Figure 3.1	Schematic Block Diagram of PMBLDC Motor	44
Figure 3.2	Block Diagram representation of PI Speed controller	50
Figure 3.3	Block Diagram representation of PID Speed Controller	51
Figure 3.4	Block Diagram representation of Sliding Mode Controller	52
Figure 3.5	Basic diagram of Fuzzy Logic Controller	52
Figure 3.6	Membership functions used in fuzzy logic controller	53
Figure 3.7(a)	Basic control structure of the fuzzy Precompensated PI controller	55
Figure 3.7(b)	Basic control structure of the fuzzy Precompensated PI controller	55
Figure 3.8	Membership function for speed error	56
Figure 3.9	Block diagram representation of Self-Organizing Fuzzy Logic Controller	58
Figure 3.10	Basic Diagram of Gain Scheduling Speed Controller for PMBLDC Motor	60
Figure 3.11	Block diagram hybrid FP+ID of PMBLDC motor	61
Figure 3.12	Back EMF of PMBLDC Motor drive	64
Figure 3.13	Inverter Circuit of PMBLDC Motor drive	65
Figure 3.14	Zero crossing instants of the back emf and the Corresponding Position Signals	72
Figure 4.1	Schematic Diagram of PMSM motor Drive	76

Figure 4.2	Schematic Block Diagram of PMSM Drive	77
Figure 4.3	Proportional type of controller	79
Figure 4.4	Proportional and Derivative controller	80
Figure 4.5	Proportional and Integral controller	80
Figure 4.6	Proportional plus Derivative plus Integral (PID) controller	81
Figure 5.1	Motor Current 'i_a'	88
Figure 5.2	Motor Current 'i_b'	88
Figure 5.3	Motor Current 'i_c'	89
Figure 5.4	Rotor speed Vs time plot during starting	89
Figure 5.5	Electromagnetic Torque Vs time plot during starting	90
Figure 5.6	Motor winding Voltage Vs time plot during starting	90
Figure 5.7	Motor Current 'i_a'	91
Figure 5.8	Motor Current 'i_b'	91
Figure 5.9	Motor Current 'i_c'	91
Figure 5.10	Rotor speed Vs time plot during Reversal	92
Figure 5.11	Electromagnetic Torque Vs time plot during Reversal	92
Figure 5.12	Motor winding Voltage Vs time plot during Reversal	93
Figure 5.13	Motor Current 'i_a'	93
Figure 5.14	Motor Current 'i_b'	94
Figure 5.15	Motor Current 'i_c'	94
Figure 5.16	Rotor speed Vs time plot during Load Perturbations	94
Figure 5.17	Electromagnetic Torque Vs time plot during Load Perturbations	95
Figure 5.18	Motor winding Voltage Vs time plot during Load Perturbations	95
Figure 5.19	Motor Current 'i_a'	96
Figure 5.20	Motor Current 'i_b'	96
Figure 5.21	Motor Current 'i_c'	96
Figure 5.22	Rotor speed Vs time plot during Starting	97
Figure 5.23	Electromagnetic Torque Vs time plot during Starting	97
Figure 5.24	Motor winding Voltage Vs time plot during Starting	98
Figure 5.25	Motor Current 'i_a'	98
Figure 5.26	Motor Current 'i_b'	99
Figure 5.27	Motor Current 'i_c'	99

Figure 5.28	Rotor speed Vs time plot during Reversal	99
Figure 5.29	Electromagnetic Torque Vs time plot during Reversal	100
Figure 5.30	Motor winding Voltage Vs time plot during Reversal	100
Figure 5.31	Motor Current 'i_a'	101
Figure 5.32	Motor Current 'i_b'	101
Figure 5.33	Motor Current 'i_c'	101
Figure 5.34	Rotor speed Vs time plot during Load Perturbations	102
Figure 5.35	Electromagnetic Torque Vs time plot during Load Perturbations	102
Figure 5.36	Motor winding Voltage Vs time plot during Load Perturbations	103
Figure 5.37	Motor Current 'i_a'	103
Figure 5.38	Motor Current 'i_b'	104
Figure 5.39	Motor Current 'i_c'	104
Figure 5.40	Rotor speed Vs time plot during Starting	104
Figure 5.41	Electromagnetic Torque Vs time plot during Starting	105
Figure 5.42	Motor winding Voltage Vs time plot during Starting	105
Figure 5.43	Motor Current 'i_a'	106
Figure 5.44	Motor Current 'i_b'	106
Figure 5.45	Motor Current 'i_c'	106
Figure 5.46	Rotor speed Vs time plot during Reversal	107
Figure 5.47	Electromagnetic Torque Vs time plot during Reversal	108
Figure 5.48	Motor winding Voltage Vs time plot during Reversal	108
Figure 5.49	Motor Current 'i_a'	109
Figure 5.50	Motor Current 'i_b'	109
Figure 5.51	Motor Current 'i_c'	109
Figure 5.52	Rotor speed Vs time plot during Load Perturbations	110
Figure 5.53	Electromagnetic Torque Vs time plot during Load Perturbations	110
Figure 5.54	Motor winding Voltage Vs time plot during Load Perturbations	111
Figure 5.55	Motor Current 'i_a'	112
Figure 5.56	Motor Current 'i_b'	112
Figure 5.57	Motor Current 'i_c'	112
Figure 5.58	Rotor speed Vs time plot during Starting	113

Figure 5.59	Electromagnetic Torque Vs time plot during Starting	113
Figure 5.60	Motor winding Voltage Vs time plot during Starting	114
Figure 5.61	Motor Current 'i_a'	114
Figure 5.62	Motor Current 'i_b'	115
Figure 5.63	Motor Current 'i_c'	115
Figure 5.64	Rotor speed Vs time plot during Reversal	116
Figure 5.65	Electromagnetic Torque Vs time plot during Reversal	116
Figure 5.66	Motor winding Voltage Vs time plot during Reversal	117
Figure 5.67	Motor Current 'i_a'	117
Figure 5.68	Motor Current 'i_b'	118
Figure 5.69	Motor Current 'i_c'	118
Figure 5.70	Rotor speed Vs time plot during Load Perturbations	119
Figure 5.71	Electromagnetic Torque Vs time plot during Load Perturbations	119
Figure 5.72	Motor winding Voltage Vs time plot during Load Perturbations	120
Figure 5.73	Motor Current 'i_a'	120
Figure 5.74	Motor Current 'i_b'	121
Figure 5.75	Motor Current 'i_c'	121
Figure 5.76	Rotor speed Vs time plot during Starting	122
Figure 5.77	Electromagnetic Torque Vs time plot during Starting	122
Figure 5.78	Motor winding Voltage Vs time plot during Starting	123
Figure 5.79	Motor Current 'i_a'	123
Figure 5.80	Motor Current 'i_b'	124
Figure 5.81	Motor Current 'i_c'	124
Figure 5.82	Rotor speed Vs time plot during Reversal	125
Figure 5.83	Electromagnetic Torque Vs time plot during Reversal	125
Figure 5.84	Motor winding Voltage Vs time plot during Reversal	126
Figure 5.85	Motor Current 'i_a'	126
Figure 5.86	Motor Current 'i_b'	127
Figure 5.87	Motor Current 'i_c'	127
Figure 5.88	Rotor speed Vs time plot during Load Perturbations	128
Figure 5.89	Electromagnetic Torque Vs time plot during Load Perturbations	128
Figure 5.90	Motor winding voltage Vs time plot during load perturbations	129

Figure 5.91	Motor Current 'i_a'	130
Figure 5.92	Motor Current 'i_b'	130
Figure 5.93	Motor Current 'i_c'	130
Figure 5.94	Rotor speed Vs time plot during Starting	131
Figure 5.95	Electromagnetic Torque Vs time plot during Starting	131
Figure 5.96	Motor winding Voltage Vs time plot during Starting	132
Figure 5.97	Motor Current 'i_a'	132
Figure 5.98	Motor Current 'i_b'	133
Figure 5.99	Motor Current 'i_c'	133
Figure 5.100	Rotor speed Vs time plot during Reversal	133
Figure 5.101	Electromagnetic Torque Vs time plot during Reversal	134
Figure 5.102	Motor winding Voltage Vs time plot during Reversal	134
Figure 5.103	Motor Current 'i_a'	135
Figure 5.104	Motor Current 'i_b'	135
Figure 5.105	Motor Current 'i_c'	136
Figure 5.106	Rotor speed Vs time plot during Load Perturbations	136
Figure 5.107	Electromagnetic Torque Vs time plot during Load Perturbations	137
Figure 5.108	Motor winding Voltage Vs time plot during Load Perturbations	137
Figure 5.109	Motor Current 'i_a'	138
Figure 5.110	Motor Current 'i_b'	138
Figure 5.111	Motor Current 'i_c'	139
Figure 5.112	Rotor speed Vs time plot during Starting	139
Figure 5.113	Electromagnetic Torque Vs time plot during Starting	140
Figure 5.114	Motor winding Voltage Vs time plot during Starting	140
Figure 5.115	Motor Current 'i_a'	141
Figure 5.116	Motor Current 'i_b'	141
Figure 5.117	Motor Current 'i_c'	141
Figure 5.118	Rotor speed Vs time plot during Reversal	142
Figure 5.119	Electromagnetic Torque Vs time plot during Reversal	142
Figure 5.120	Motor winding Voltage Vs time plot during Reversal	143
Figure 5.121	Motor Current 'i_a'	143
Figure 5.122	Motor Current 'i_b'	144

Figure 5.123 Motor Current 'i_c' 144

Figure 5.124 Rotor speed Vs time plot during Load Perturbations 145

Figure 5.125 Electromagnetic Torque Vs time plot during Load Perturbations 145

Figure 5.126 Motor winding Voltage Vs time plot during Load Perturbations 146

Figure 5.127 Motor Current 'i_a' 147

Figure 5.128 Motor Current 'i_b' 147

Figure 5.129 Motor Current 'i_c' 147

Figure 5.130 Rotor speed Vs time plot during Starting 148

Figure 5.131 Electromagnetic Torque Vs time plot during Starting *148*

Figure 5.132 Motor winding Voltage Vs time plot during Starting 149

Figure 5.133 Motor Current 'i_a' 149

Figure 5.134 Motor Current 'i_b' 150

Figure 5.135 Motor Current 'i_c' 150

Figure 5.136 Rotor speed Vs time plot during Reversal 151

Figure 5.137 Electromagnetic Torque Vs time plot during Reversal 151

Figure 5.138 Motor winding Voltage Vs time plot during Reversal 152

Figure 5.139 Motor Current 'i_a' 152

Figure 5.140 Motor Current 'i_b' 153

Figure 5.141 Motor Current 'i_c' 153

Figure 5.142 Rotor speed Vs time plot during Load Perturbations 154

Figure 5.143 Electromagnetic Torque Vs time plot during Load Perturbations 154

Figure 5.144 Motor winding Voltage Vs time plot during Load Perturbations 155

Figure 5.145 Motor Current 'i_a' 156

Figure 5.146 Motor Current 'i_b' 156

Figure 5.147 Motor Current 'i_c' 156

Figure 5.148 Rotor speed Vs time plot during Starting 157

Figure 5.149 Electromagnetic Torque Vs time plot during Starting 158

Figure 5.150 Motor winding Voltage Vs time plot during Starting 158

Figure 5.151 Motor Current 'i_a' 159

Figure 5.152 Motor Current 'i_b' 159

Figure 5.153 Motor Current 'i_c' 159

Figure 5.154	Rotor speed Vs time plot during Reversal	160
Figure 5.155	Electromagnetic Torque Vs time plot during Reversal	160
Figure 5.156	Motor winding Voltage Vs time plot during Reversal	161
Figure 5.157	Motor Current 'i_a'	161
Figure 5.158	Motor Current 'i_b'	162
Figure 5.159	Motor Current 'i_c'	162
Figure 5.160	Rotor speed Vs time plot during Load Perturbations	163
Figure 5.161	Electromagnetic Torque Vs time plot during Load Perturbations	163
Figure 5.162	Motor winding Voltage Vs time plot during Load Perturbations	164
Figure 5.163	Response of Sensorless Control of PMBLDC Motor Current 'i_a' during starting	170
Figure 5.164	Response of Sensorless Control of PMBLDC Motor Current 'i_b' during starting	170
Figure 5.165	Response of Sensorless Control of PMBLDC Motor Current 'i_c' during starting	170
Figure 5.166	Rotor Speed Vs time plot during Starting	171
Figure 5.167	Electromagnetic Torque Vs time plot during Starting	171
Figure 5.168	Motor back emf and its corresponding position signal	172
Figure 5.169	Motor back emf and its corresponding three Position Signal	172
Figure 6.1	Response of Motor Current (i_a) with PI Controller	175
Figure 6.2	Response of Motor Current (i_b) with PI Controller	175
Figure 6.3	Response of Motor Current (i_c) with PI Controller	176
Figure 6.4:	Response of Motor Currents (i_a, i_b and i_c) with PI Controller	176
Figure 6.5	Rotor speed Vs time plot during starting	176
Figure 6.6	Electromagnetic Torque Vs time plot during starting	177
Figure 6.7	Motor winding Voltage Vs time plot during starting	177
Figure 6.8	Response of Motor Current (i_a) during Reversal	178
Figure 6.9	Response of Motor Current (i_b) during Reversal	178
Figure 6.10	Response Motor Current (i_c) during Reversal	178
Figure 6.11	Response of Motor Currents (i_a, i_b and i_c) during Reversal	179
Figure 6.12	Rotor speed Vs time plot during Reversal	179
Figure 6.13	Electromagnetic Torque Vs time plot during Reversal	180
Figure 6.14	Motor winding Voltage Vs time plot during Reversal	180

Figure 6.15	Response of Motor Current (i_a) during load Perturbations	181
Figure 6.16	Response of Motor Current (i_b) during load Perturbations	181
Figure 6.17	Response of Motor Current (i_c) during load Perturbations	181
Figure 6.18	Response of Motor Currents (i_a, i_b and i_c) during load Perturbations	182
Figure 6.19	Rotor speed Vs time plot during load Perturbations	182
Figure 6.20	Electromagnetic Torque Vs time plot during load Perturbations	183
Figure 6.21	Motor winding Voltage Vs time plot during load Perturbations	183
Figure 6.22	Response of Motor Current (i_a) with PI Controller	184
Figure 6.23	Response of Motor Current (i_b) with PI Controller	184
Figure 6.24	Response of Motor Current (i_c) with PI Controller	184
Figure 6.25	Response of Motor Currents (i_a, i_b and i_c) with PI Controller	185
Figure 6.26	Rotor speed Vs time plot during starting	185
Figure 6.27	Electromagnetic Torque Vs time plot during starting	186
Figure 6.28	Motor winding Voltage Vs time plot during starting	186
Figure 6.29	Response of Motor Current (i_a) during Reversal	187
Figure 6.30	Response of Motor Current (i_b) during Reversal	187
Figure 6.31	Response Motor Current (i_c) during Reversal	187
Figure 6.32	Response of Motor Currents (i_a, i_b and i_c) during Reversal	188
Figure 6.33	Rotor speed Vs time plot during Reversal	188
Figure 6.34	Electromagnetic Torque Vs time plot during Reversal	189
Figure 6.35	Motor winding Voltage Vs time plot during Reversal	189
Figure 6.36	Response of Motor Current (i_a) during load Perturbations	190
Figure 6.37	Response of Motor Current (i_b) during load Perturbations	190
Figure 6.38	Response of Motor Current (i_c) during load Perturbations	190
Figure 6.39	Response of Motor Currents (i_a, i_b and i_c) during Load Perturbations	191
Figure 6.40	Rotor speed Vs time plot during load Perturbations	191
Figure 6.41	Electromagnetic Torque Vs time plot during load Perturbations	192
Figure 6.42	Motor winding Voltage Vs time plot during load Perturbations	192

LIST OF SYMBOLS AND ABBREVIATIONS

K_p	=	Proportional gain
K_d	=	Derivative gain
K_i	=	Integral gain
T^*	=	Reference torque
θ_r	=	Position signal
i_a^*	=	Reference current at phase a
i_b^*	=	Reference current at phase b
i_c^*	=	Reference current at phase c
i_a, i_b , i_c	=	Winding current of phase 'a','b' and 'c'
S_1 and S_2	=	Values of Switching functions
X_1	=	Speed error
X_2	=	Derivative of the speed error
σ	=	Switching hyper plane of SMC controller
K_1 and K_2	=	Controller gain on speed locus
V	=	Output of SMC controller
K	=	Adjustable parameters
E_1	=	Error between reference speed and speed of the motor
E_2	=	Change in speed error
e(k), Δe(k)	=	Input error
$\hat{u}$ (k)	=	Output fuzzy control
NB	=	Negative big
NM	=	Negative medium
NS	=	Negative small
Z0	=	Zero
PS	=	Positive small
PM	=	Positive Medium
PB	=	Positive big
C_1 and C_2	=	Adjustable parameters of SMC controller Gains
E_1, E_2, E_3	=	Inputs of fuzzy controller
$K_p(t)$	=	Proprtional speed error

$K_I(t)$	=	Integral gain
$e(t)$	=	Speed error
$p\theta_r$	=	Derivative of the rotor position
PI	=	Proportional Plus Integral
PID	=	Proportional Plus Integral Plus Derivative
SMC	=	Sliding mode controller
FLC	=	Fuzzy Logic controller
h_b	=	Hysteresis band
PWM	=	Pulse Width Modulation
PMBLDCM	=	Permanent Magnet Brushless DC Motor
Hybrid(FP+ID)	=	Hybrid Fuzzy Proportional Plus Integral Plus Derivative
FP-PI	=	Fuzzy Precompensated Proportional Plus Integral
DSPs	=	Digital Signal processors
PMBLM	=	Permanent Magnet Brushless Motor
PM	=	Permanent Magnet
CC-VSI	=	Current controlled- Voltage source Inverter
VC-VSI	=	Voltage controlled- Voltage source Inverter
SUMT	=	Sequential Unconstrained Minimization Technique
e_{an}	=	Back emf of phase a
e_{bn}	=	Back emf of phase b
e_{cn}	=	Back emf of phase c
V_{an}	=	Phase voltage of phase a
V_{bn}	=	Phase voltage of phase b
V_{cn}	=	Phase voltage of phase c
λ_a	=	Flux linkage of phase winding 'a'
λ_b	=	Flux linkage of phase winding 'b'
λ_c	=	Flux linkage of phase winding 'c'
L_s	=	Self Inductance
M	=	Mutual inductance
K_b	=	Back emf constant
$f_a(\theta_r), f_b(\theta_r), f_c(\theta_r)$	=	Function of rotor position of phase a, b and c
p	=	Derivative of d/dt
T_e	=	Electromagnetic Torque

V_{ao}, V_{bo}, V_{co}	=	Phase to neutral voltage referred to 'o' Potential at mid point of d.c link
V_{no}	=	The potential of neutral point with respect to the zero potential (V_{no})
R	=	*Stator resistance*
Lw	=	Stator winding inductance
ω_r	=	Rotor speed
ω_r^*	=	Reference speed of the motor
B	=	Frictional coefficient
J	=	Moment of inertia
P	=	No. of poles
T_l	=	Load Torque
T(n)	=	Output Torque at nth sampling instant
T^*	=	Reference value of the torque produced by the PMBLDC motor drive or output of the limiter
$T_{(n-1)}$	=	Output Torque at (n-1)th sampling instant
$w_r(n)$	=	*Rotor Speed*
$\omega_r^*(n)$	=	Reference Speed of the motor
$\omega_{e\,(n)}$	=	Speed error at n th sampling instant
$\omega_{e\,(n-1)}$	=	Speed error at (n -1)th sampling instant
V_{dc}	=	D.C. link voltage
i_s	=	Stator current
i_d	=	Direct axis current
i_q	=	Quadrature axis current
V_d	=	Direct axis voltage
V_q	=	Quadrature axis voltage
L_d	=	Direct axis inductance
L_q	=	Quadrature axis inductance
λ_d	=	Direct axis stator flux
λ_q	=	Quadrature axis stator flux
λ_{af}	=	Rotor flux linkage (Excitation Flux)
δ	=	Torque angle
θ_r	=	Rotor position signal
K_t	=	Torque constant
SF	=	switching function

CHAPTER 1

INTRODUCTION

1.1 General

The Permanent Magnet Brushless PMBLDC motor is identified as the combination of AC machine, rotor position sensor and inverter to represent a system producing linear speed-torque characteristics at par with the conventional DC motor. The output torque is dependent upon the stator current, and the electrical and mechanical equations of motion are simple linear differential equations easing evaluation and implementation. The use of rare earth magnet material has resulted in reduced motor weight, increased efficiency, high torque and low rotor inertia imparting fast response. There have been rapid developments in the solid state components and power conditioner technology to accompany the advancement in motors and in rotor position sensors.

The availability of high-energy permanent magnets, high-power solid-state switching components like MOSFET, IGBT, MCTs and digitally compatible sensing devices have resulted in great application possibilities for brushless DC motors utilizing PM rotors. Electric vehicles, flight control actuators, submersibles, medical systems, machine tools and robotics are noted to illustrate the broad range of applications of brushless DC motors (Irdand, 1968; Howlett, 1982; Kenjo and Nagamori, 1985; Miller, 1989; Dote and Kinoshita, 1990; Kumar, 1993; Hanselman,, 1994; Gieras and Wing, 1996; Gieras, and Wing, 2000; Gieras and Marler, 2002).

The permanent-magnet brushless motors are of two types. They are the permanent -magnet synchronous (PMSM) and the brushless DC motor (PMBLDCM). PMSM and the PMBLDCM have sinusoidal and trapezoidal back emfs respectively, exhibiting different operating characteristics and requirements. Comparing these two motors (Kim and Cho, 1994; Friedrich and Kant, 1998), the PMBLDCM has the distinct advantages over PMSM in terms of (i) higher power density provided the core losses are equal and ii) higher torque at same rated speed.

In this chapter, the state-of-art of the PMBL motor is discussed to illustrate all the recent developments of the drive for achieving improved performance. A brief

presentation of the proposed work is also given. Finally, the outline of different chapters is explained briefly.

1.2 Scope of the Problem Identified for the Research

Permanent magnet (PM) machines have received considerable attention in recent years for variable speed drives. Permanent-magnet brushless motor enhances the dynamic responses of a drive due to its lower rotor inertia and commutatorless operation. PM brushless motor is also a good competitor to the induction motor drive due to its high efficiency and power factor and ease of control. Recent developments in permanent- magnet materials, micro and power electronics, fast digital signal processors and modern control technologies have significantly influenced the widespread use of permanent- magnet motor drives in order to meet the competitive world market demands of manufactured goods, devices, products and processors. Large, medium, small as well as micro permanent-magnet motors are extensively sought for applications in all sorts of motion control apparatus and systems. The stupendous increase in the popularity of the permanent-magnet motor drives among engineers bears testimony to its industrial usefulness in terms of superior performance, better efficiency, compact size and low cost. Numerous references are available on the efforts of researchers in improving the design of motors, sources of excitation and/or control techniques in meeting the varied requirements of loads (Gieras and Wing, 1996; Gieras and Marler, 2002; Miller, Popescu, Cossar, McGilp and Walker, 2003)

In order to fulfill the stringent requirements of modern drive systems, researchers are developing drives with high efficiency, high power-density and fast dynamic performance. Permanent-magnet motors are considered favourably to meet these needs. In recent years the advances in high-energy permanent-magnet materials, semi-conductor power devices and control theories have made PMBLDC drives play an important role in motion-control applications in the low-to-medium power range. The desirable features of a PM servomotor are its compact structure, high torque-to-inertia ratio, and high torque capability. Moreover, compared to an induction servomotor, a PM brushless motor has the advantages of higher efficiency; lower no-load current below the rated speed and its control performance is much less sensitive to the parametric variation of the motor. These factors make the PMBLDC

motor an attractive alternative to the induction motor in which overall efficiency is critical, mainly in pump, compressor and fan drives.

The brushless dc motors are generally controlled using a three-phase power semiconductor inverter bridge. The motors are equipped with encoder for providing proper commutation to turn on the power devices in the inverter bridge. The dynamic performance of PMBLDC motor with different speed controllers is evaluated in this investigation. The main thrust is to develop the model of a PMBLDC motor drive to optimize the dynamic performance of the system and to identify a drive to suit a particular application. The model of the drive consists of a speed controller, reference current generator, PWM current controller, inverter and the PMBLDC motor. All these components are modelled and integrated for simulation. In the investigation, dynamic performance of the system is analyzed using different types of speed controllers and the simulated results are obtained for different operating conditions such as starting, speed reversal and load perturbation. In this work different types of speed controllers have been considered namely PI (Proportional plus Integral), PID (Proportional plus Integral plus Derivative), SMC (Sliding Mode Control), different types of Fuzzy Logic based controllers. Out of the various current controllers, the PWM current controller has been chosen in this investigation.

Commercial developments in both metallic and bonded PM materials (Sawyer, and Edge, 1977; Ritchter, Eike, Miller and Neumann and Hudson, 1985; Rahman and Slemon, 1985) have taken place in quantum steps with the introduction of Alnicos, Ferrites, Samarium Cobalts and Neodymium Boron Iron (NdBFe) families of magnets during last four decades. The critical parameters required for successful application in PM motors are high residual flux density (B_r), large coercive force (H_c), maximum energy product $(B_rH_c)_{max}$, good temperature tolerance and the lowest per unit cost. The upsurge in PM materials technology has placed PM motor drives on the top in the field of electronics.

The availability of smart power-electronics devices and their optimal topologies have accelerated unprecedented growth of cost effective and reliable inverter and converter systems. Software controlled on-line implementation of sophisticated and a robust controller has advanced the art of computer control of permanent motor drives. Motor drives are traditionally designed with relatively inexpensive analog components.

Conventional controllers such as PI need accurate mathematical models describing the dynamics of the system under control. This can be a major limiting factor for systems with unknown varying dynamics. Even if a model can be obtained for the system under control, unknown conditions such as saturation, disturbances, parameter drifts and noise may limit the level of accuracy. For most of the basic electric drive applications, these unknown conditions and system nonlinearities may be ignored. In the present work, besides PI controller, emphasis has also been directed towards SMC (Sliding Mode Controller) and fuzzy logic-based controllers.

The high performance of Digital Signal Processors (DSPs) allows them to perform with high-resolution control and minimum control loop delays. These efficient controllers make it possible to reduce torque ripples and harmonics and improve dynamic behavior in all speed ranges. The motor design is optimized due to lower vibrations and lower power losses such as harmonic losses in the rotor. Smooth waveforms allow optimization of power elements and input filters. Besides, these improvements result in a reduction of system cost and enhancement of reliability allowing efficient energy management and conservation.

The conventional PI speed controller is simulated and the dynamic performance of the PMBLDC drive system is examined. A sliding mode controller is also simulated for the speed control of PMBLDC drive. Intelligent, knowledge-based controllers like fuzzy logic and self-organizing fuzzy logic have been recently recognized as important tools for enhancing the performance of electric drives. The motor generally requires a rotor-position sensor for starting and for providing proper commutation sequence to turn- on the power devices in the inverter bridge. In many applications, however, the use of direct position sensors is not desired due to its reliability, cost, mechanical and environmental constraints. The work reported in the thesis also explores the sensorless operation based on back-emf sensing of the PMBLDC motor drive. The position detection scheme based on terminal-voltage sensing is found to be simple and cost effective for steady-state operation.

1.3 State-of-the-Art

The modern drive incorporates an impressive range of technology: new materials, motors, sensors, powerful processors and control electronics and software. Traditionally interfacing the control circuit with the power circuit has been achieved by using large number of discrete components. However, higher levels of system

integration are now possible using compact products and ICs. Very-Large-Scale-Integrated (VLSI) circuits and Application-Specific-Integrated-Circuits (ASICs) are becoming popular in PM brushless motor drive applications (Kappas, Kinniment and Acarhley, 1990; Patterson and Morley, 1992; Galvan, Torralba and Franquelo, 1996; Tzou and Kuo, 1997). Now-a-days, manufacturers of industrial control systems are looking for higher levels of systems integration, coupled with increasing sophistication in control techniques at lower costs. Depending on the particular type of application, driver and control products for PM brushless motor drives are available for voltages upto 600V and varying degrees of control and logic complexity.

The performance of closed-loop-controlled drive system depends upon the choice of controllers. Several papers refer to dealing with speed and current controllers for different drives (Cerrupto, Consoli and Raciti, 1995; Gieras and Wing, 2002; Singh and Kumar, 2002), and it is found that each of these controllers has its own advantages and disadvantages. Many control strategies have been proposed on classical linear control theory. It is well known that PI, PID controllers are mostly used in industry due to its simple structure and ease of implementation. The PI controllers have failed to perform satisfactorily under parametric variation, non-linearity and load disturbances (Panda, Lim and Dash, 1997; Kumar, Singh and Bordoloi, 2005). This has boosted the use of modern non-linear control schemes such as state feedback controllers, self-tuning controllers, model reference adaptive systems, and variable structure control (Chern and Chang, 1991; Souza and Bose, 1994; Hu, Dawson and Anderson, 1995; Cerrupto, Consoli and Raciti, 1995; Singh, Murthy, Singh, Reddy and Singh, 1999; Singh. and Kumar, 2005). These controllers also need mathematical models, and are sensitive to parametric variations. Several adaptive control algorithms have been theoretically developed and proposed in recent years (Ertugal, 1992; Ertugrul and Acarnley, 1994; Ceruto, Cosoli, Raciti and Testa, 1995; Silva, Neto and Huy, 1997; Ehasani and Rahman, 1997; Chung and Gweon, 2002; Lee and Ehsani, 2003; Singh and Kumar, 2005). Since in electrical drives all the control loop actions must be performed in small time, practical implementation of adaptive algorithms is possible with the aid of DSPs. Another type of controller based on fuzzy logic is being increasingly used in many systems with non-linearity and uncertainty, and many papers are available on the application of fuzzy logic to different drive systems (Matsunga and Kawaji, 1991; Souza and Bose, 1994; Kim and Chong, 1994; Kung and Liaw, 1994; Puttaswamy, 1995; Silva, Neto and Huy, 1997;

Cerrupto, Consoli and Raciti, 1997; Li, 1998; Kumar, Singh, and Bordoloi, 2005).

Various schemes which can be employed in a current controller, namely, hysteresis and PWM current controllers (Verster and Enslin, 1990; Yoshitsugu and Inove, 1997). In a hysteresis current controller hysteresis bandwidth gives a near-rectangular phase current with small current ripple but requires high frequency of inversion. Hysteresis controller (Krishnan and Rim, 1990; Chern and Chang, 1991; Jainhua and Rahman, 1993) gives faster response and it is easy to implement. In PWM current controller, the frequency is preset to ensure that the inverter can operate safely. MOSFET-based inverter is used and higher switching frequencies can be applied (Tripathi and Sen, 1992). The use of fast processors like micro-controllers, DSP and the new switching devices make it possible to implement intelligent controllers for the drive system (Chern and Chang, 1991; Matsui, and Ohashi, 1992; Dote and Kano, 1992; Zhang, Li, and Zuo, 2000).

The current interest is directed towards development of techniques for eliminating the rotor position-sensing device and sensing position by analyzing the motor voltages and current waveforms (Nobuyuki and Shigyo, 1992; Cassat and Jufer, Consoli, Alfo, Musumeci, Raciti and Tesla, 1994; Ertugrul and Acarnley, 1994; Hu, Dawson and Anderson, 1995; Cardoletti, 1995; Rajasekhara, Kawamura and Matsuse, 1996; Kumar and Singh, 2002; Zhu, Zhu, Ede and Howe, 2002). In the near future, the high performance control of any type of PM brushless motors may be achieved by monitoring the motor's power terminals only.

1.4 About the Current Research

1.4.1 Analysis of PMBLDC Drive

The model of the drive consists of a speed controller, reference-current generator, PWM current controller, inverter and the PMBLDC motor. All these components are modelled and integrated for simulation and implementation (Luk and Lee, 1994; Lee and Ehsani, 2003; Miller, Popescu, Cossar, McGilp and Walker, 2003). In this investigation, dynamic performance of the system is analyzed using different types of speed controllers and the simulated results are obtained for different operating conditions such as starting, load perturbation and speed reversal.

1.4.2 Real Time Simulation

The performance of the closed-loop controlled drive system depends on the choice of the controllers. As the model of the PMBLDC motor is non-linear, Runge-Kutta method is used to get the solution of system equations for the variables such as motor currents (i_a, i_b, i_c), motor speed (ω_r) and position (θ_r). The motor torque, winding currents, rotor speed and winding voltages are stored for studying the behaviour of dynamic responses of the drive. There has been tremendous research on different speed controllers to improve upon the dynamic responses of the drive. It is well known that up till now a conventional PI controller is mostly used in industry due to its simple control structure and design and low cost. However, the control performance of PM drives is still influenced by uncertainties of the plant which features parameter variations, external load disturbances, and non-linear dynamics. This has boosted the use of non-linear control schemes such as model reference adaptive control and variable structure control. Another type of controller based on fuzzy logic is being increasingly used in systems with non-linearity and uncertainty. Based on above observations, a range of speed controllers starting from conventional controllers to the modern ones has been used for the simulation of the PMBLDC drive. Among different current controllers the PWM current controller has been used in this investigation. A C-language program is developed for the simulation in real-time operating conditions. Two PMBLDC drives are used for simulation with ratings: 1) 0.5 HP, 4-pole, 3-phase, star-connected, 1A, 1500rpm and 2) 2.0 HP, 4A, 4-pole, 3-phase, star-connected, 1500rpm.

1.4.3 Different Speed Controllers

In this investigation an attempt has been made to develop and simulate the speed controller for PMBLDC motor drive system. The conventional PI speed controller is simulated and the dynamic performance of the PMBLDC drive system is evaluated and examined. The response of the drive has an overshoot and an undershoot. An attempt has been made to implement Gain-Scheduling PI controller. In this, the PI gains are allowed to vary over a predetermined range for varying operating conditions. An advantage of this approach is that the existing PI control system can be easily modified for Gain-Scheduling control simply by adding auto-tuning techniques.

Intelligent and knowledge-based controllers (based on fuzzy logic) have also been studied as important tools to enhance the performance of the electric drives. The simulation of the fuzzy logic controller is also undertaken in this investigation. The fuzzy system has been simulated as a pre-calculated lookup table. The performance of the drive and the effectiveness of the proposed controllers are demonstrated by a wide range of simulation results.

1.4.4 Sensorless Speed control of PMBLDC Motor

The motor requires a rotor-position sensor for starting and for providing the proper commutation sequence to turn on the power devices in the inverter bridge. Encoders or resolvers have been used to sense the position. However, these position sensors are expensive and they need wiring and extra space. These sensors (particularly Hall sensors) are temperature sensitive, limiting the operation of the motor below 75°C. Absolute position sensors are generally used for speeds limited to about 6000 rpm. In many applications, however, the use of direct-position sensors is not desired due to reliability, cost, mechanical and environmental constraints. Due to the above limitations, sensorless operation of PM brushless motors is receiving wide attention. Several schemes for the position sensorless operation of PMBL motors have been reported, (Hzuka, Uzuhashi, Rano, Endo and Mohri, 1985; Ogasawara and Akagi, 1991; Rajeshekara and Kawannura, 1994; Hu, Dawson and Anderson, 1995; Rajasekhara, Kawamura and Matsuse, 1996; Kumar and Singh, 2002; Consoli and Musumeci, 2004).

In the present work, an attempt has been made to control the speed of the PMBLDC motor without using speed and position sensors. The back emf in the unexcited phase is measured to establish a switching sequence for commutation of the power devices in the three-phase inverter. This method is simple and cost effective for steady state operation.

1. 5 Proposed Research Methodology

1.5.1 Development of System Model

A simple model for the purpose of simulating the dynamic performance of the PMBLDC motor is proposed. The model for the PMBLDC motor is developed by using a-b-c reference frame and the performance of the system analyzed using

different types of speed controllers. The simulated results are obtained for different operating conditions of the drive such as starting, load perturbation and speed reversal. In this work, different types of speed controllers studied are PI (Proportional plus Integral), PID (Proportional plus Integral plus Derivative), SMC (Sliding Mode Control), FP-PI (Fuzzy Precompensated Proportional plus Integral), FPID (Fuzzy Proportional plus Integral plus Derivative), FSMC (Fuzzy Sliding Mode Controller), Self Organizing Fuzzy Logic controller and Gain scheduling PI controller, Hybrid (FP+ID) controllers.

1.5.2 Cost Reduction

Cost reduction is one of the most important objectives of any system design. This can be achieved in two ways, one by reducing the cost of the motor at the design stage itself; and another, by reducing or eliminating some of the costly components of the system.

1.5.3 Improved Performance

The model is extended to the case when PMBLDC motor is fed from an integrated current-controlled converter-inverter link. In this case the current-controlled converter can operate at unity power factor with negligible harmonic in AC mains and it facilitates regeneration of power.

1.5.4 Specifications of the PMBLDC motor and PMSM Drive System

The specifications of the system are chosen after some necessary tests on a smaller 2 hp, 4-pole, 1500 rpm (157 rad/sec) PMBLDC motor; and 0.5 hp, 6-pole and 1000 rpm (100 rad/sec). The power circuit of the inverter consists of a diode bridge rectifier; MOSFET or IGBT based current-controlled inverter and associated control circuit.

1.5.5 Modelling of PMBLDC Motor Drive System

Permanent magnet (PM) motors are broadly divided into two categories: one is trapezoidal motor called permanent-magnet brushless (PMBL) dc motor with trapezoidal flux-density waveforms and the other one is sinusoidal motor called PMSM with sinusoidal flux distribution. The excitation for PMBLDC motor is given in the form of pulses. As the rotor carries permanent magnets, it is necessary to excite

the phases which are under the influence of the magnets. The complete revolution is divided into six sectors. The reference current generation depends on these six sectors each of 60° intervals. The drive consists of speed controller, reference-current generator, hystresis current controller, brushless motor and current-controlled voltage-source inverter. The rotor speed is compared with the reference speed and an error in speed is fed to speed controller for generation of a reference torque to limit the speed error. The generation of reference currents depends on the position of the rotor. The hysteresis current controller compares the actual and reference values, limits the winding currents and generates switching signals for power devices depending on the current error. Figure1 shows the general block diagram of the PMBLDC drive system. The drive system consists of PMBLDC motor, controlled excitation source, current and speed controllers, position sensor and reference current generator. As shown in Figure 1.1, the feedback speed is compared with the set reference speed and the speed error is fed to the speed controller. A limiter is incorporated along the speed controller that limits the maximum value of the output signal. The output of the limiter is considered as the reference torque (T*) which decides the magnitude of the stator current I*. The limiter not only limits the stator winding currents within a prescribed value but also provides protection to inverter switches. The reference current generator block provides three- phase controlled-frequency reference currents (i_a^*, i_b^*, i_c^*). For this purpose, it uses the stator-current vector I* and the rotor position (θ_r). The three-phase reference currents have the shape of the quasi-square-wave in phase with respective back emfs to develop a constant unidirectional torque. The PWM current controller regulates the winding currents (i_a, i_b, i_c), which are compared with the reference currents and the switching commands are generated to drive the inverter devices. In response to three-phase quasi-square wave currents (i_a, i_b, i_c), the PMBLDC motor runs at the desired speed.

The winding currents (i_a, i_b, and i_c), are compared with the reference currents and the switching commands are generated to drive the inverter devices. In response to three- phase quasi-square-wave currents (i_a, i_b, and i_c), the PMBLDC motor runs at the synchronous speed.

Figure 1.2 shows the corresponding diagram for the PMSM drive. The drive functions in the manner similar to that of PMBLDC motor. The only difference is the decoupling of flux component (i_d) from the torque component (i_q) of the stator current

vector. These currents (i_d, i_q) are fed to the reference current generator block which is being used in control structure of the PMSM motor while in the earlier case (PMBLDCM), the magnitude of stator current 'I' was given as an input. This difference could be revealed from the fact that in the case of PMBLDC motor; the control is taken care of by torque component of the stator current alone since in this case the flux component is absent.

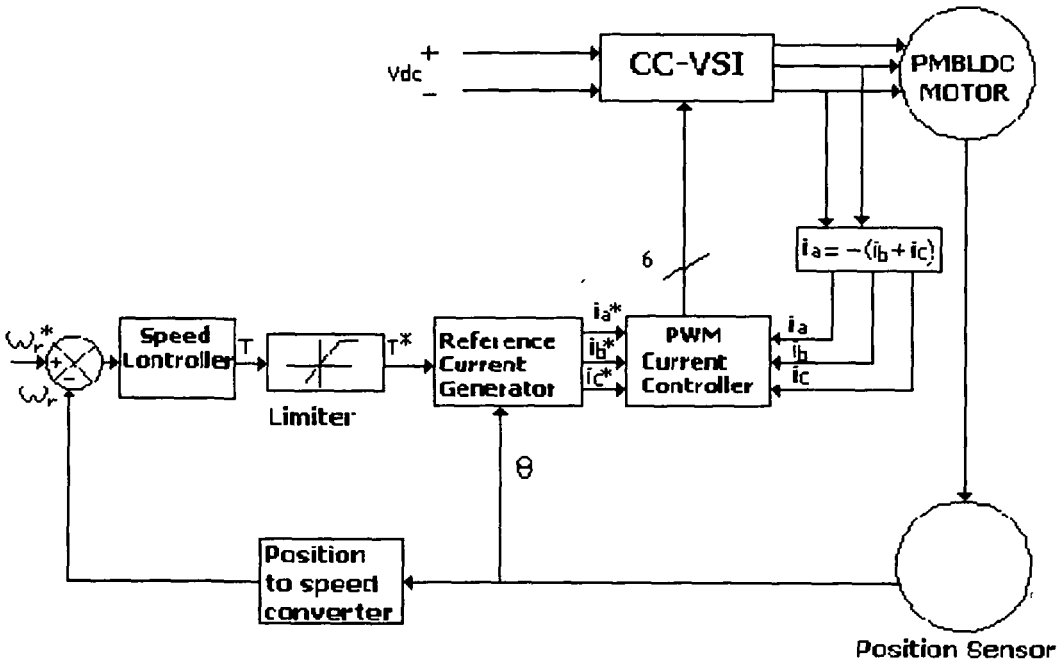

Figure1.1: Schematic Block Diagram of PMBLDC Motor

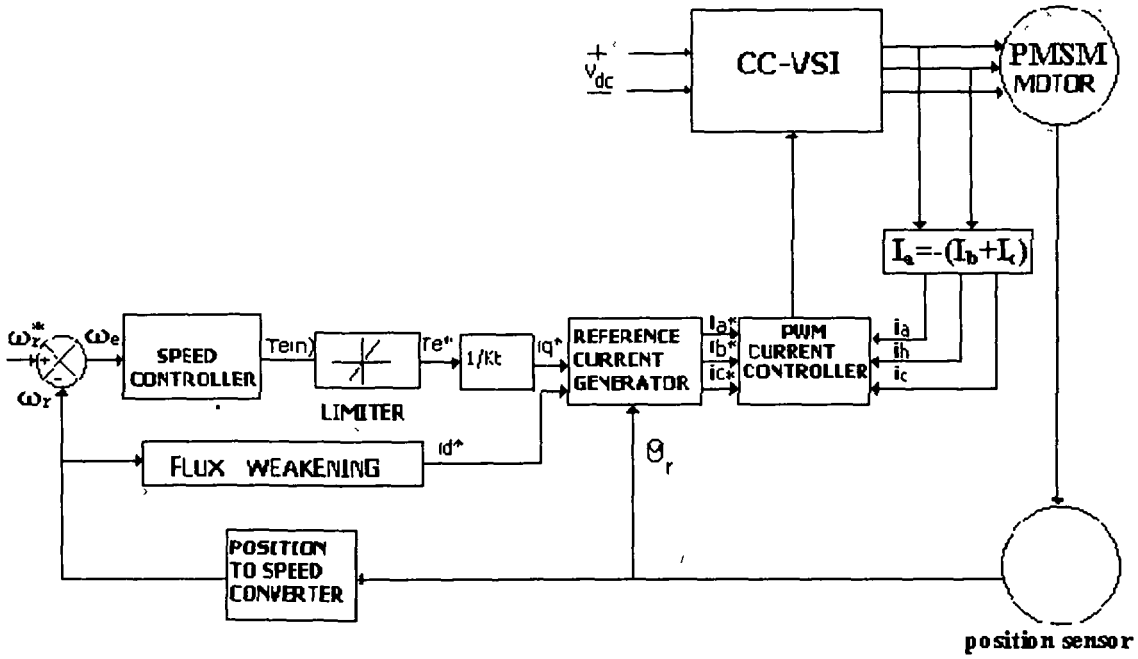

Figure 1.2: Schematic Block Diagram of PMSM Drive

1.5.6 Main Features of the model of the PMBLDC Motor

The PMBLDC motors have received considerable attention in recent years. Application engineers are more likely to select PM motors as against the brushed DC or Induction motor for the following reasons. (1) The presence of the brushes and commutator leads to increased maintaince and poor commutation, (2) The low inertia of rotor improves the mechanical response of the motor by reducing the acceleration and deceleration times, (3) Use of PM materials with higher coercive force results in higher power-to-weight ratio, (4) The absence of the commutator makes the motor construction simpler, (5) Losses are reduced and the motor proves to be energy efficient. These motors offer higher power density, improved efficiency, high torque-to-inertia ratio and faster dynamic response, (6) The efficiency of PMBLDC motors is 90-95% against 70-80% efficiency achieved by induction motors. Using PMBLDC motor in place of induction motor, one can save the energy significantly.

The high performance of Digital Signal Processors allows the motor perform with high-resolution, control and minimize control loop delays. These efficient controls make it possible to reduce torque ripples and harmonics and improve dynamic behavior in all speed ranges. The motor design is optimized due to lower vibrations and lower power losses such as harmonic losses in the rotor.

The preceding paragraphs have highlighted both the current state of knowledge and existing gap in knowledge on the PM brushless motor drive. The investigation reported in the thesis has the basic objective of the bridging the reported gap through:

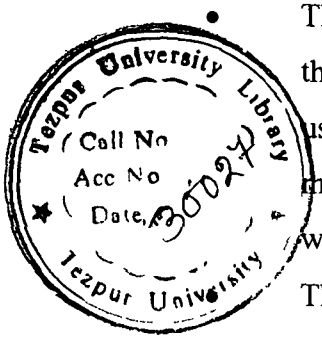

- The development of comprehensive mathematical model for carrying out the performance analysis of the PMBLDC motor and PMSM drives. The use of improved excitation enhances the performance levels of PMBLDC motor drive system so that it is capable of reactive power management without causing harmonic injection into the AC mains.
- The examination of the effectiveness of different types of speed controllers used in the PMBLDC motor drive system with a view to identifying an appropriate speed controller for a given application.
- The development and use of suitable algorithm for the elimination of Speed controller for a given application.
- The use of a suitable design optimization technique for facilitating comparison of cost with different objective functions with a view to reducing the cost of the overall drive system.

1.6 Organization of the Thesis

In Chapter 1, an overview of the PM brushless motor drives is given. The state-of -art of the PMBL motor is discussed to deal with the recent developments of the drive for achieving improved performance. A brief outline of the scope of work is presented.

In Chapter 2, an exhaustive literature survey and historical background of PM machines are presented along with their controls and developments till date. This is followed by a general review of the available literature on various aspects like selection of motors, controllers, sensorless control optimization etc.

Chapter 3 describes the development of a model of the PMBLDC motor drive system with different types of speed controllers. The basic mathematical equations for speed controllers, current controller, motor and inverter which are useful in simulation of PMBLDC motor drive system are derived. The chapter also describes sensorless operation of the drive system. Included are different schemes of sensorless operation used till today by different researchers. Since the motor in sensorless operation is not

self-starting, different starting schemes are explained. Sensorless simulation based on the back-emf sensing is discussed in detail. The simulated results are discussed.

Chapter 4 presents the modelling of control structure of the PMSM drive system to investigate its dynamic behavior. The basic mathematical model which is useful for simulation of the PMSM drive is considered for different operating conditions such as starting, speed reversal and load perturbation.

Chapter 5 describes the results of the simulation runs for the model developed for PMBLDC motor. Performance evaluation of the drive using different controllers such as PI, PID, SMC, Fuzzy Logic based controllers like Fuzzy precompensated PI, Fuzzy PID, Fuzzy SMC, Gain scheduling, Self organizing and hybrid (FP+ID) controllers are discussed in detail. All these controllers are compared for optimum performance of the drive. Real-time simulation aspects are also discussed in this chapter.

Chapter 6 illustrates the results of the simulation runs for the mathematical model developed for PMSM motor. Performance evaluation of the drive using different controllers such as PI and PID is presented and discussed in detail.

Chapter 7 presents the summary of the research along with the conclusions drawn on different aspects of PMBLDC motor drive. It also incorporates the relative difference in operation of PMBLDC motor drive with PMSM drive.

CHAPTER 2

A CRITICAL REVIEW OF THE AVAILABLE LITERATURE

2.1 General

This chapter deals with the brief description of the developments of PMBL motor drive system. It contains information which paved the way to the research reported in the Thesis. Advances in high-energy permanent-magnet materials and power electronics have widely enhanced the applications of brushless dc machines in variable speed drives. Early references also appear in space applications but only with the introduction of the silicon controlled rectifier interest has grown manifold in brushless DC motors. Throughout the sixties and up to 1972 a substantial amount of work has been done for NASA. Since that time the literature on brushless dc motors has grown rapidly with the publication of many papers on motor systems. A highly significant work has appeared in the paper of Sawyer and Edge, 1977 wherein the design of samarium cobalt brushless dc motor for electromechanical actuator applications has been presented. The use of rare-earth magnetic material has resulted in reduced weight, increased efficiency, high torque, low rotor inertia with associated fast response. There have been rapid developments in the solid-state components and power conditioner technology to accompany the advances in motors and in rotor-position sensors (Howlett, 1982). Switching devices of the inverter connected to PMBL motor in the drive system have passed stages from thyristor, transistor, MOSFET to fast IGBT devices. With the use of faster processors like microcontroller and DSP, complicated algorithms can be easily implemented and the drive system becomes more reliable with reduced hardware. The advantages such as light weight, precise speed control, faster response have increased the demand for these motors in medical and other applications.

2.2 Literature Review on PMBL motor drive

Low, Jabbar, and Rahman, 1980; Kenjo and Nagamori, 1985; Dote and Kinoshita, 1990; Chung and Gweon, 2002 have described the basic principle of operation of PMBL motor and its control features. Miller, 1989 has described the properties of magnetic materials and explained the need of high-density magnetic

material for PM motor. Some control aspects are also covered. Howlett, 1982 has reviewed terminology, history, motor design and has given examples of brushless DC motors in actuators, electric vehicles, heart pumps, submarines and robotics. Pillay and Krishnan, 1989 and Luk and Lee, 1994; Miller, Popescu, Cossar, McGilp and Walker, 2003 deal with modelling, simulation and analysis of PMBLDC motor drive. PuttaSwamy, Singh and Singh, 1995; Singh and Kumar, 2002; Lee and Ehsani, 2003 have dealt with PMBLDC and PMSM motor drive systems in considerable detail. Erdman and Harms, 1984 and Kumar, 1993 have outlined a transient performance model for a three-phase, full-bridge, surface-mounted-magnet brushless DC motor to give reliable estimates of the motor's speed-torque profile. The work reported by Jack and Acarnley, 1988, Hanselman, 1994; Gieras and Wing, 2002 is concerned with the design of small brushless DC drives such as laser scanners in which the requirement of stability is important. Several important features of brushless DC drives have been identified in this work. Luneau, 1984 explores the requirements of feedback devices for brushless DC and sine-wave PM servo motors. Important problems are identified in ensuring the reliability and also in minimizing the cost of the feedback devices. Luk and Lee, 1994 and Lee and Ehsani, 2003 have discussed an efficient model for brushless DC drive which allows engineers to investigate the performance of the system when a variation such as load or sampling rate of digital controller occurs. There has been considerable research towards reducing torque ripples in PMBLDC drives (Huy, Houng, Perret and Feuillet, 1986; Kim, Cho and Yoko, 1994; Sebastian and Gangla, 1996; Zhu and Howe, 2000; Qu and Lipo, 2002). With the growing potential for widespread use of PMBLDC motor drives in many low-cost applications such as HVAC, refrigerators and freezers in houses and low-velocity sensors in process industries, it has become important to minimize the cost. One obvious option for cost reduction is through the cost regulation of inverter and its associated controller. Krishnan and Lee, 1997 and Krishnan, 1997 have proposed "C dump" converter.

A common component which is used in adjustable speed drives is an incremental shaft encoder and an electronic circuit for velocity estimation. The usual method of counting pulses from the encoder in a fixed period of time produces high precision velocity estimation in high speed-range. High precision in the lower speed-range can be achieved by measuring the elapsed time between two successive pulses coming from the encoder. Galvan, Torralba and Franquelo, 1996 and Uddin, Radwan

and Rahman, 2002 have proposed a mixed method for speed measurement. Merits and demerits of the two methods are discussed in their paper.

Considerable research has been done in digital control of PM machines. Kappas, Kinniment and Acarhley, 1990; Patterson and Morley, 1992; Tzou and Kuo, 1997 have designed PMAC IC that can be incorporated with a general purpose microcontroller to provide a simple, compact, low-cost and effective solution for high performance AC drives. All the control functions including the PWM waveform generation, current control, vector control and position control have been realized using FPGA based programmable logic gates (Kappas, Kinniment and Acarhley, 1990; Patterson and Morley, 1992; Tzou and Kuo, 1997; Zhu, Zhu, Ede and Howe, 2002).

2.3 Permanent Magnet Motor Drives

In general, all electromechanical drives can be divided into constant-speed drives, servo-drives and variable-speed drives. A constant-speed drive usually employs a synchronous motor alone which can keep the speed constant without an electronic converter and feedback or any other motor when there is less restriction on the speed variation tolerance. A servo-system is a system consisting of several devices which continuously monitor the actual information (speed, position), compare these values to the desired outcome and make necessary corrections to minimize the difference. A servo- motor drive is a drive with a speed or position feedback for precise control where the response time and the accuracy with which the motor follows the speed and position commands are extremely important.

In variable-speed drive, the accuracy and the response time with which the motor follows the speed command are not important, but the main requirement is to change the speed over a wide range.

In all electromechanical drives where the speed and position are controlled, a power-electronic converter interfaces the power supply and the motor. There are three types of permanent magnet motor electromechanical drives:

- DC commutator motor drives,
- Brushless motor drives (DC and AC synchronous),
- Stepping motor drives.

Brushless motor drives fall into the two principal classes of sinusoidally-excited and square-wave (trapezoidal excited) motors. Sinusoidally-excited motors are fed with three-phase sinusoidal waveforms as shown in the Figure 2.1 and they operate on the principle of a rotating magnetic field. They are simply called sine-wave motors or permanent-magnet synchronous motors. All phase windings conduct current at a time. Square-wave motors are also fed with three-phase waveforms shifted by 120° one from another, but these wave shapes are rectangular or trapezoidal in the same figure. Such a shape is produced when the armature current (MMF) is precisely synchronized with the rotor instantaneous position and frequency (speed). The most direct and popular method of providing the required rotor position information is to use an absolute angular position sensor mounted on the rotor shaft. Only two phase windings (out of three) conduct current simultaneously and this is functionally equivalent to the mechanical commutation in d.c motors. This explains why motors with square wave excitation are called d.c brushless motors. An alternative term used in power electronics and motion control is self-controlled synchronization (Johns, 1994; Rahman, Vilathgamuwa, Uddin and Tseng, 2003). Although stepping motor electromechanical drives are a kind of synchronous motor drives, they are separately discussed due their different power electronic circuits and control strategies.

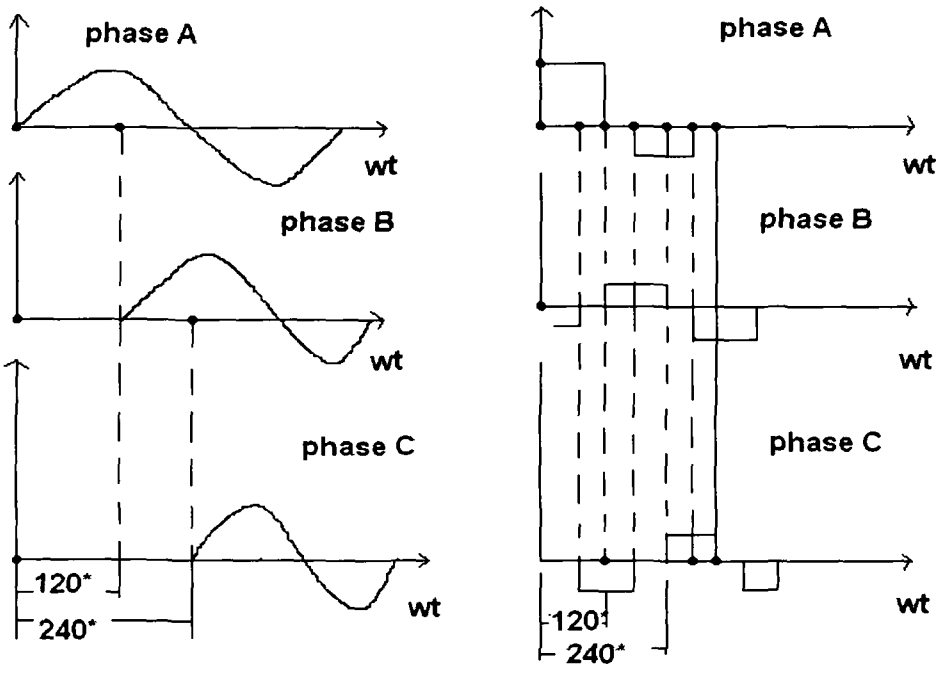

Figure 2.1: Armature waveforms: for sinusoidally excited and square wave

2.4 Trends in Permanent Magnet Motors and Drive Industry

The electromechanical drive has the biggest share in the electric and electronic market. The market analysis of electromechanical drive shows that the D.C. Commutator motor drive sales increase only slightly each year whilst the demand for a.c. motor drives increases substantially. The same trend is seen in the brushless PM motor drives vis-à-vis the PM DC Commutator motor drives.

Small PM motors are especially demanded by manufacturers of computer peripheral equipment, office equipment, medical instruments, measurement technology, automobiles, robots, and handling systems. From today's perspective, the Far East (principally Japan, China and South Korea), America and Europe will remain or become largest market areas.

Advances in electronics and PM quality have outpaced improvements in associated mechanical transmission system, making ball lead screws and gearing the limiting factors in motion control. For the small motor business, a substantially higher integration of motor components will increasingly help in bridging this gap in the future (Mayer, 1995). However, there is always the question of cost analysis, which ultimately is the key factor for specific customer needs.

2.5 Classifications of Permanent Magnet Brushless DC Motor

In general, permanent magnet motors are classified into:

- d.c commutator motors,
- d.c brushless dc motors,
- a.c synchronous motors.

The construction of a PMDC commutator motor is similar to a DC motor with the electromagnetic excitation system replaced by permanent magnets. PMBLDC and AC synchronous motor designs are practically the same with a polyphase stator and PMs located on the rotor. The only one difference is in the control and shape of the excitation voltage. AC synchronous motor is fed with more or less sinusoidal waveforms which in turn produce a rotating magnetic field. In PMBLDC motors the armature current has a shape of square (trapezoidal) waveform, only two phase windings (for Y connection) conduct the current at the same time and switching pattern is synchronized with the rotor angular position (electronic communication).

The armature current of synchronous and D.C. brushless motors is not transmitted through brushes, which are subject to wear and require maintenance. Another advantage of the brushesless motor is the fact that the power loss occurs in the stator, where heat transfer conditions are good. Consequently the power-density can be increased as compared with a D.C. Commutator motor. In addition, considerable improvements in dynamics can be achieved because the air-gap magnetic flux-density is high, the rotor has a lower inertia and there are no speed dependent current limitations. Thus, the volume of a brushless PM motor can be reduced by more than 40% for the same rating of a PM commutator motor.

The following constructions of PMDC commutator motor have been developed:

- Motors with conventional slotted rotors,
- Motors with slotless (surface wound) rotors,
- Motors with moving coil rotors.

2.6 Permanent Magnets

Materials to retain magnetism were introduced in electrical-machine research in 1950s. There has been a rapid progress in materials in the interim period. Materials that retain magnetism are known as hard magnetic materials. Various materials, such as Alnico-5, ferrites, samarium-cobalt, and neodymium-boron-iron are available as permanent magnets for use in machines (Irdand, 1968; Sawyer and Edge, 1977; Ritchter, Eike, Miller, Neumann and Hudson, 1985; Rahman and Slemon, 1985; Ramsden and Nguyen, 1987). The B-H demagnetization characteristics of these materials are shown in Figure 2.2 for second quadrant only, because the magnets do not have an external excitation once they are magnetized and therefore have to operate with a negative magnetic field strength. That includes the second and third quadrants of the B-H characteristics. It is not usual to encounter the third quadrant in operation; hence, only the second quadrant is considered here. The last three listed materials have straight-line B vs. H characteristics, whereas Alnico-5 has the highest remnant flux density but has nonlinear B vs H. Table 2.1 shows the history of permanent magnet.

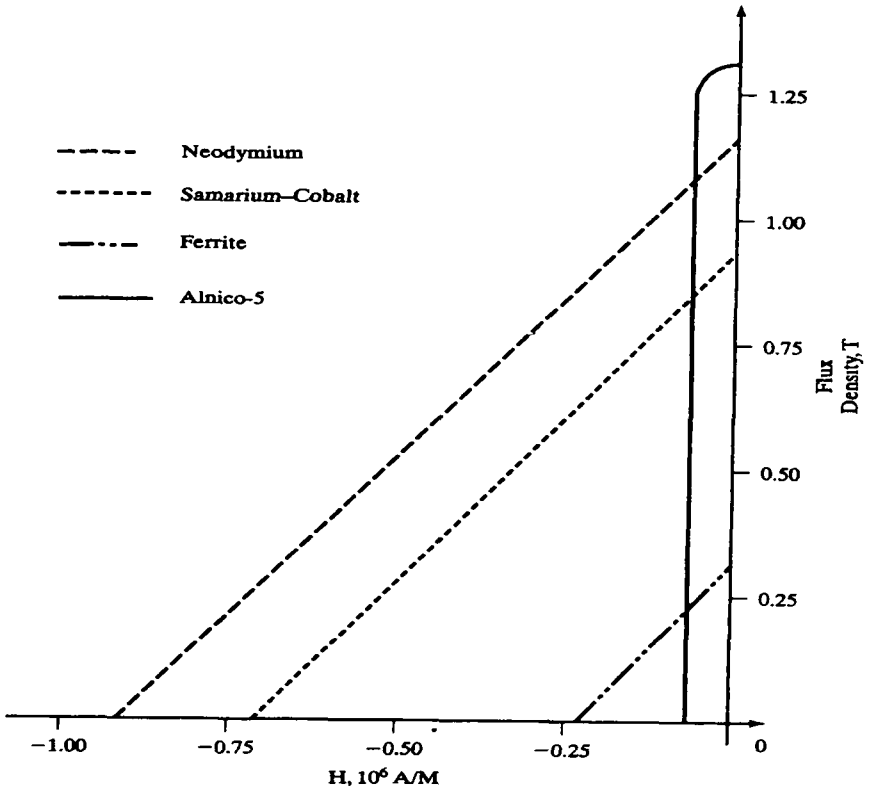

Figure 2.2: Second Quadrant B-H characteristics of Permanent Magnets

Table 2.1: Chronological Development of Permanent Magnet Materials

600 B.C.	Discovery of Natural lodestone
500 A.D.	Good Magnet Traced in China
1600	Gilbert invented the application of lodestone
1825	Invention of Electromagnets by Sturgeon
1917	Cobalt Steel
1931	Alnico discovered in Japan
1938	Powdered Oxide Magnet Invented in Japan
1940	Development of Ferrite Magnet
1950	Ceramic Magnet commercially used
1960	Samarium Cobalt
1989	Neodymium Iron Boron (Nd-Fe-B)

2.6.1 Permanent Magnets and characteristics

Permanent-magnet characteristics and their operation within a magnetic circuit are described in the available literature. The air-gap or load-line to determine the

operating point of the magnet is derived. The energy-density definition and magnet-volume calculation are given to clarify the rudiments of application considerations for the magnet in machine design.

The sustained success of the permanent-magnet industry in developing improved magnet characteristics is evident from Figure 2.2. The latest addition being neodymium-iron-boron which has been pioneered by Sumitomo as 'Neomax', by General motors as 'Magnequennch', Crucible ('Crumax') and IG Technologies. At the room temperature NdFeB has the highest energy product among all commercially available magnets. The high remanence and coericivity permit marked reductions in motor frame size for the same output compared with motors using ferrite (ceramic) magnets. However, ceramic magnets are considerably cheaper.

Both ceramic and NdFeB magnets are sensitive to temperature and special care must be taken in design for working temperatures above 100^0. For very high temperature applications Alnico or rare-earth cobalt magnets must be used.
The characteristics of NdFeB are compared with other materials such as:

1. Ferrite (Ceramic 8) 60^0 C
2. Bonded NdFeB (MQI) 80^0C
3. SmCo5 (Crucore 20)
4. Sintered NdFeB (Crumax 30) 80^0C
5. Alnico

There are two main manufacturing methods: (1) melt-spin process pioneered by general Motors (Delco Remy Div.) producing isotropic plastic bonded magnets ("Magnequench"), and (2) classical powder/ sinter process pioneered by Sumitomo Special Metal Co. producing higher quality, less easily machined anisotropic magnets. (Mitchell, 1985; Bleeke, 1986; Furukawa, 1985; Carlilse, 1986).

The theoretical limit to energy product for the material is 500 kJ/m^3, and its price should fall close to the cost of materials of about \$60/kg as the cost of manufacturing is low. These developments will bring the cost/Joule close to that of ferrite. As the cost of materials in Sm-Co is about \$290 /kg, it is not expected that the overall price could fall to the same extent.

2.6.2 Properties of Permanent Magnets

There are three classes of PMs currently used for electric motors: (i) Alnicos (Al, Ni, Co, Fe), Ceramics (ferrites), e.g., Barium Ferrite BaO X $6Fe_2O_3$ and Strontium Ferrite SrO X $6Fe_2O_3$ (ii) Rare-earth materials, i.e., Samarium-Cobalt SmCo and (iii) Neodymium-Iron-Boron NdFeB, Properties of PM Materials are given in Table 2.2

Table 2.2: Properties of PM Materials

Mes. Material	Br (T)	Hc (kA/m)	BHmax (KJ/m)	Temp. Coefficient Remanance	Coerisivity	Operating ((Tmax^{0}C)	Density
ALNICO (AL-NI-CO-Fe) (1930)	1.24	50	40	-0.02	0.02	500	7.3
Ferrite (1950)	0.4	295	29	- 0.02	0.04	250	4.9
Samarium Cobalt (Sm-Co) (1960)	0.92	70.5	170	-0.045	-0.25	250	8.4
Neodymium Iron Boron (Nd-Fe-B) (1989)	1.25	840	240	-0.1	-0.7	150	7.4

Note: * Maximum Energy Product and Minimum Volume (Neodymium Iron Boron)

2.6.3 Permanent Magnet Versus Electromagnetic Excitation

The use of permanent magnets (PMs) in construction of electrical machine brings the following benefits

- No electrical energy is absorbed by the field excitation system and thus there is no excitation losses which mean substantial increase in the efficiency,
- Higher torque and/or output power per unit volume than that for using electromagnetic excitation,
- Better dynamic performance than motors with electromagnetic excitation, (higher magnetic flux density in the air gap),
- Simplification of construction and maintenance,
- Reduction of prices for same types of machines.

2.6.4 Electric Motor Design with NdFeB: Problems and Advantages

The major problems for the designer working with ferrite are:

- The material is still very expensive,
- The working flux-density in the sintered magnet should be about 0.6T for minimum magnet volume, about 3 times higher than ferrite or 0.4T for bonded NdFeB,
- The maximum recommended operating temperature is 150^0C,
- The coercive force in some grades decreases with increasing temperature.

To achieve the advantages of NdFeB at low cost, careful innovative design is needed. The advantages possible with NdFeB, depending on the application, include:

- Higher torque/weight ratio,
- Easier manufacturing methods (no flux concentration),
- Higher torque/ inertia,
- Smaller current,
- Higher efficiency,
- Smaller variations with load,
- Higher peak torque without demagnetization,
- Better commutation (brushed machines),
- Lower armature Inductance,
- Faster electrical time constant,
- Lower torque ripple,
- Lower leakage flux,
- Lower noise,
- Magnetization before assembly,
- Larger air-gap, allowing toothless construction,
- No necessity for flux concentration constructions,
- Close pole spacing without demagnetization.

2.6.5 Applications of Permanent Magnet Brushless DC Motor

▶ Industry

Industrial drives, e.g., pumps, fans, blowers, compressors, centrifuges, mills, hoists, handling system, etc., Machine tools, Servo drives, Automation processes, Internal transportation systems, Robots.

▶ **Public life**

Air conditioning systems, Catering equipment, Coin laundry machines, Auto bank machines, Automatic vending machines, Money changing machines, Ticketing machines, Bar-code readers at supermarkets, Environmental control systems, Clocks, Amusement park equipment.

▶ **Domestic life**

Kitchen equipment (refrigerators, microwave ovens, mixers, dish washers), Bathroom equipment (shavers, hair dryers, tooth brushes, massage apparatus), Washing machines and clothes dryers, Heating and air conditioning systems, Vacuum cleaners, Lawn mowers, Swimming pool pumps, Toys, Vision and sound equipment, Security systems (automatic garage doors, automatic gates).

▶ **Information and office equipment**

Computers, Printers, Scanners, Facsimile machines, Photocopiers, Audiovisual aids

▶ **Transportation**

Elevators and escalators, People movers, Light railways and streetcars (trams), Electric road vehicles, Aircraft flight control surface actuation, Electric ships, Boats.

▶ **Defense forces**

Tanks, Missiles, Radar systems, Submarines, Torpedoes.

▶ **Aerospace**

Rockets, Space shuttles, Satellites

▶ **Medical and healthcare equipment**

Dentist's drills, Electric wheelchairs, Compressors, Trotters, Rehabilitation equipment, Artificial heart motors

▶ ***Power tools***

Drills, Hammers, Screwdrivers, Grinders, Polishers, Saws, Sanders, Sheep shearing hand pieces

- Renewable energy systems,
- Automobiles with combustion engines,
- Research and exploration equipment,
- Factory automation systems, computers and marine technology.

2.7 Source of Excitation

The choice of a suitable excitation source plays an important role in shaping the performance of the drive system. Since the main emphasis of the present research is on achieving a higher level of dynamic performance, the source should have a feature of fast regulation of stator currents. A current-controlled voltage-source inverter (CC-VSI) has normally been used in vector control induction motor drive and for similar reasons, this has also been found effective in case of PMBL motors. In the case (CC-VSI), the output currents of inverter do not involve any delay on account of motor parameters, unlike, the voltage-controlled voltage-source inverter (VC-VSI) in which case the output currents get delayed due to the non-linear behavior of the electrical circuit of the motor (Krishnanan, and Lee, 1997; Krishnanan, 1997; Kumar, Roy, Singh, 2002).

The CC-VSI supplying power to a drive motor is generally fed from a diode bridge rectifier. Although it has been considered as a versatile form of excitation source feeding power to the vector-controlled induction motor drive, it lacks in some desirable features at the front end converter and there is some scope for improvements in its performance in terms of energy conservation (Thakur and Singh, 2001; Singh, Kumar and Bordoloi, 2004; Singh and. Kumar, 2005), reactive-power management (power factor improvement) and suppression of harmonics in AC mains. This can be achieved by replacing the diode bridge rectifier with a current-controlled converter. The next logical step is to apply these modifications and examine their effects in the case of PMBLDC drives also. It becomes, therefore, desirable to study the performance of PMBL motor when this is fed from an improved excitation source consisting of an integrated current-controlled converter-inverter system.

2.8 Rotor Position Sensing of DC Brushless Motors

Rotor-position sensing in a dc motor is done by position sensors such as Hall elements, encoders, resolvers. In rotating machines position sensors provide feedback signals proportional to the rotor angular position.

2.8.1 Encoders

There are two types of optical encoders: absolute and incremental encoders. In optical encoders a light passes through the transparent areas of a grating and is sensed by a photo detector. To increase the resolution, a collimated light source is used and a

mask is placed between the grating and detector. The light is allowed to pass to the detector only when the transparent sections of the grating and mask are in alignment.

In an incremental encoder a pulse is generated for a given increment of shaft angular position which is determined by counting the encoder output pulses from a reference. The rotating disk (grating) has single track as shown in Figure 2.3. In the case of power failure an incremental encoder looses position information and must be reset to known zero point.

To provide information on direction of rotation a two-channel encoder is used. The output square signals of two channels are shifted by 90^0, i.e., channels are arranged to be in quadrature. Four pulse edges from channels A and B may be seen during the same period. By processing the two channel outputs to produce a separate pulse for each square wave edge the resolution of the encoder is quadrupled. The range of resolution of square wave output encoders is wide, up to a few thousand lines/rev.

The slew rate of an incremental encoder is the maximum speed determined by the maximum frequency at which it operates. If this speed is exceeded, the accuracy will significantly deteriorate making the output signals unreliable.

An absolute encoder is a position verification device that provides unique position information for each shaft angular location. Owing to a certain number of output channels, every shaft angular position is described by its own unique code. The number of channels increases as the required resolution increases. An absolute encoder is not a counting device like an incremental encoder and does not loose position information in the case of loss power.

The disk made of glass or metal of an absolute encoder has several concentric tracks to which independent light sources are assigned. The tracks vary in the slot size and pattern at the outer edge enlarging towards the center. A low state or "0" is created when the light passes through the disk. Pattern "1" and "0" provide information about the shaft position. The resolution or the amount of position information that can be obtained from the absolute encoder disk is determined by the number of tracks, i.e., for 10 tracks the resolution is usually 2^{10} =1024 positions per revolution. The disk pattern is in machine-readable code, i.e., binary or gray codes. Figure 2.4 shows a simple binary output with 4 bits of information. The indicated position corresponds to the decimal number 11 (1101 binary). The next position

moving to the right corresponds to 10 (0101 binary). The previous position moving to the left corresponds to 12 (0011 binary).

Multi-turn absolute encoders have additional disks geared to the main high-resolution disk with step up gear ratio. For Example, adding a second disk with 3 tracks and 8.1 gear ratio to main disk with 1024 positions per revolution, the absolute encoder will have 8 complete turns of the shaft equivalent to 8192 discrete positions.

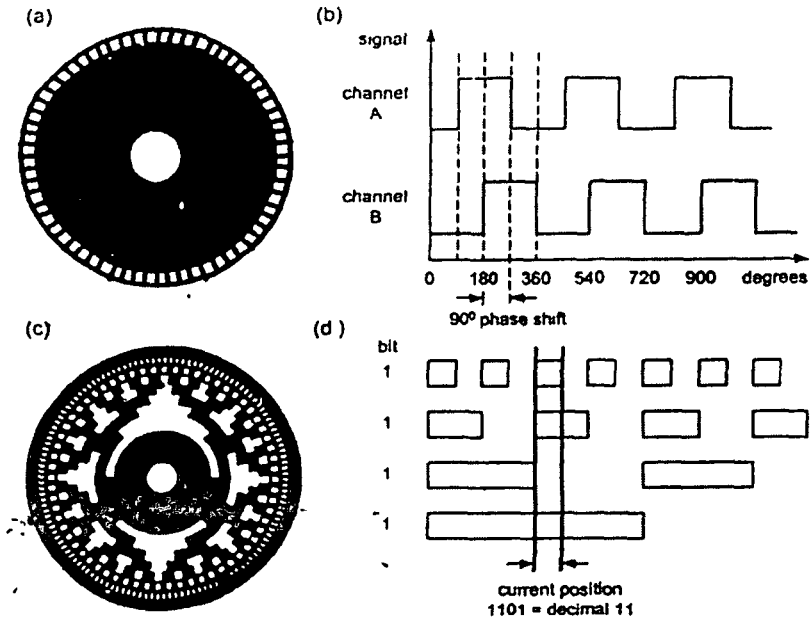

Figure 2.3: Incremental and absolute encoders (a) disk of an incremental encoder, (b) quadrature output signals, (c) disk of an absolute encoder, (d) absolute encoder output signals

2.8.2 Resolvers

A resolver is a rotary electromechanical transformer that provides outputs in the form of trigonometric functions of its inputs. For detecting the rotor position of brushless motors, the excitation or primary winding is mounted on the resolver rotor and the output or secondary windings are wound at right angles to each other on the stator core. As a result the output signals are sinusoidal waves in qudrature, i.e., one wave is a sinusoidal function of the angular displacement θ and the second wave is co-sinusoidal function of θ (Figure 2.4).

There is one electrical cycle for each revolution of the motor. The analog output signals are converted to digital form to be used in a digital positioning system.

The difference between the two waves reveals the position of the rotor. The speed of the motor is determined by the period of the waveforms and the direction of rotation is determined by the leading waveform.

Instead of delivering the excitation voltage to the rotor winding by brushes and slip rings, an inductive coupling system is frequently used. A brushless resolver with rotary transformer is shown in Figure 2.5.

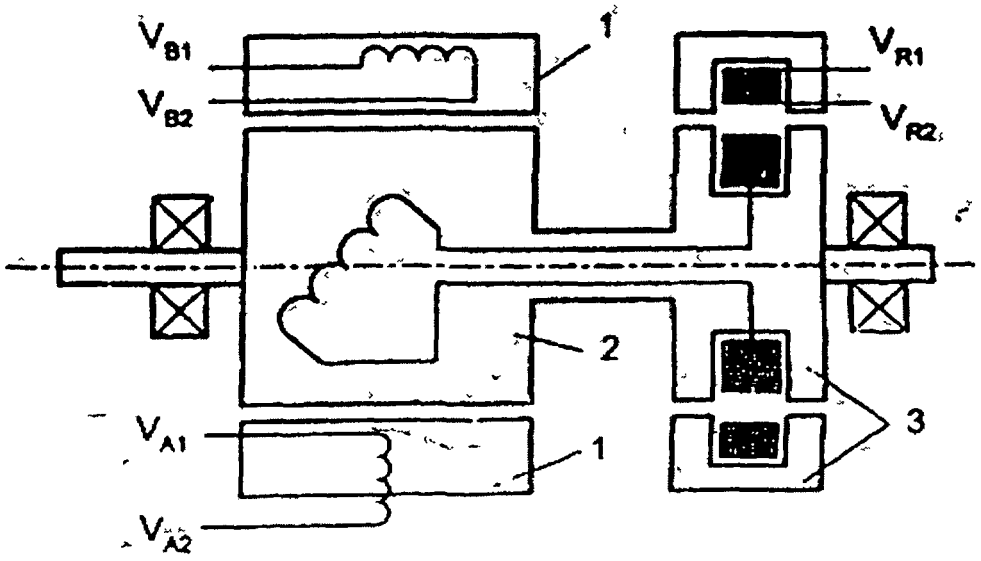

Figure 2.4: Brushless resolver.1-stator, 2-rotor, 3-rotary transformer

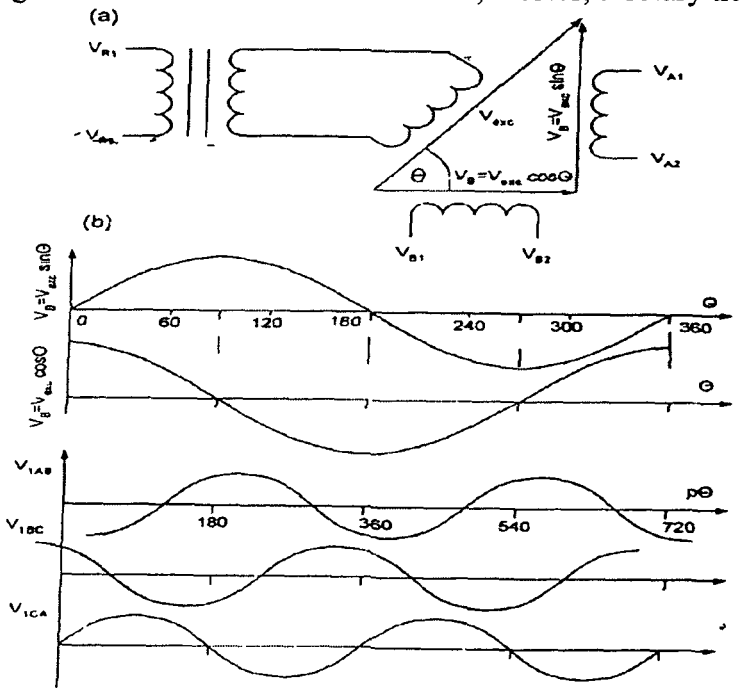

Figure 2.5: Principle of operation of a rotary resolver: (a) winding configuration, (b) resolver output waves and 4-pole voltages. The interval $0 \leq p\theta \leq 720^0$ corresponds to one revolution.

2.9 Different Types of Speed Controllers

After developing abc phase model of PMBLDC motor using circuit concepts, attempts have been made to use different types of speed controllers to obtain improved performance to suit a particular application. Among different speed controllers used in the closed-loop control are PI, PID, SMC, Fuzzy PI, Fuzzy PID, Fuzzy SMC, Gain Scheduling PI, Self-Organizing and Hybrid (FP+ID) controllers. Numerous research papers (Jespersen, 1981; Lee, 1990; Consoli and Testa, 1991; Carrara, Casini and Taponecco, 1991; Dote and Kano, 1992; Hwang and Lin, 1992; Zhang and Edmunds, 1992; Lee and Kim, 1992; Lu and Chen, 1994; Puttaswamy, 1994; Kim and Chong, 1994; Souza and Bose, 1994; Ceruto, Cosoli, Raciti and Testa, 1995; Cerrupto, Consoli and Raciti, 1997; Neto and Huy, 1997; Matavelli and Spiazzi, 1997; Panda, Lim and Dash, 1997; Lo and Kuo, 1998; Li, 1998; Singh et al, 1999; Yamamoto and Furuhashi, 2001; Han, Su and Murakami, 2003; Kumar, Singh, and Bordoloi, 2005; Uddin, Abido and Rahman, 2005) have been published on similar lines including the use of different speed controllers.

Consoli and Testa, 1991 have presented low-chattering sliding-mode control of a PM motor drive. Chern and Chang, 1991 and Zhang, Li and Zuo, 2000 have discussed DSP-based integral variable structure model for Brushless DC motor drives. Souza and Bose, 1994 have discussed the application of fuzzy logic in a speed-control system that uses a phase-controlled bridge converter and a separately-excited DC motor. They have used fuzzy logic in the design of current and speed controllers of the drive system and the performance is compared with that of PI controller system. Neto and Huy, 1997 and Uddin, Radwan and Rahman, 2002 have presented a very simple fuzzy logic adaptable strategy that can be readily implemented. It is composed by a fuzzy-logic controller and a fuzzy logic adaptation mechanism for PMSM. According to them (Neto and Huy, 1997; Matsui and Ohashi, 1992; Ehasani and Rahman, 1997; Butt, Hoque and Rahman, 2004) this mechanism has very fast learning features and very good tracking characteristics even under severe variations of the system parameters. The authors have tried to combine the knowledge-based controllers with the conventional controllers to acquire the advantages of both. Chang and Kuo, 1998 have presented a decoupled Fuzzy SMC. In this, the fuzzy control rules could be greatly reduced for higher-order systems. Dote and Kano, 1992 have discussed a DSP-based neuro-fuzzy position controller for servomotors. By taking advantages of neuro control and fuzzy control they have combined to construct a non-

linear self-tuning controller. This neuro-fuzzy controller proposed by them is robust and gives improved control performance than conventional PI controller. By changing the equation in a range, it is possible to control the system without any overshoot. Emanuse Cerruto, 1995 and 1997 have proposed fuzzy adaptive controller for PM motor drives. In this work, they have developed a theoretical and a practical implementation of an adaptive speed and position regulator based on model MARC approach. According to this work it is possible to reduce the complexity of the adaptive algorithm while increasing the robustness of the control. Because of the limitation of fuzzy controllers an effective approach to solving these limitations is provided by self-organizing fuzzy-logic controllers. Zhang and Edmunds, 1992 and Yamamoto and Furuhashi, 2001 have proposed a self-organizing fuzzy logic controller. Kim and Chang, 1994; Singh et al, 1999; Carvajal, Chen and Ogmen, 2000; Yamamoto and Furuhashi, 2001; Uddin, Abido and Rahman, 2005; Kumar, Singh and Bordoloi, 2005; Singh and kumar, 2005 have described Fuzzy precompensated PID controllers. This scheme is based on trying to compensate for overshoots and undershoots in transient response.

2.10 Sensorless Control of PMBL Motors

Rajashekara and Kawamura, 1994; Kumar and Singh, 2002; Zhu, Zhu, Ede and Howe, 2002 have presented a brief review of position sensorless strategies reported in the literature. The position sensorless schemes are based on the methods of position detection and control strategy. The schemes for both PM brushless DC motor and PM synchronous motor are also discussed in the literature (Hzuka, Uzuhashi, Endo and Mohri, 1985; Ogasawara and Akagi, 1991; Ertugal, 1992; Consoli, Musumeci, Raciti and Tesla, 1994; Ertugrul and Acarnley, 1994; Moreia, 1994; Rajeshekara and Kawannura, 1994). Hzuka, Uzuhashi, Endo and Mohri, 1985 and Bhowmik, Renespee and Enslin, 1997 have explained a method which permits the regulation of permanent-magnet rotor position by the back electromotive force (EMF) induced in the stator windings. They have also explained starting technique. The motor voltage is chopped by commutator transistors to change the motor speed. Ogasawara and Akagi, 1991 have proposed an approach to position sensorless drive based on detection of the conducting interval of free-wheeling diodes connected in anti-parallel with power transistors. This approach makes it possible to detect the rotor position over a wide range of speed, especially at a lower speed. Experimental

results obtained by them are shown in their work to confirm the validity of sensorless drive from 45 to 2300 r.p.m. A starting procedure of the motor is also discussed by Ogasawara. and Akagi, 1991 because it is not possible to detect the rotor position at standstill. Moreira, 1994 has described an indirect sensing method for the rotor-flux position in Permanent Magnet (PM) ac motors operating in a wide range of speed. The starting of the motor is also superior with this method since the third-harmonic signal can be detected and processed at lower speeds in comparison to for conventional method of back-EMF sensing. In this work the third- harmonic indirect sensing is implemented and compared to a conventional back-EMF sensing method.

Ertugrul and Acarnley, 1994 have investigated a new algorithm for shaft position sensorless operation of permanent-magnet motors, based on flux linkage and line-current estimation. Measurement of line current and terminal voltage is used to estimate flux linkage of the motor. This work presents a wide range of computed and experimental results, demonstrating the reliability of the method even during acceleration of the motor from rest. Cardoletti and Jufer, 1997 have described a methodology to control a motor from standstill to full speed without direct position and speed sensors. This scheme offers the possibility to start surely, without oscillation. This method has also presented a thorough analysis of the starting scheme with experimental measurements.

2.11 Design Optimization of PM Brushless Motor

The performance of PM motors over DC and induction motors can be improved by using integrated current-controlled-voltage-source inverter as a source of excitation along with feed forward controller etc. The PM motor drive is quite attractive performance-wise, but it has higher initial cost. This is due to the requirement of costly position and current sensors and high-energy PM material used in the motor. The main aim of this part of the investigation is to develop a computer-aided design methodology to reduce the cost of PM motors. Continuous attempts have been made in the past by designers to improve the design of electrical motors with a view to improve its performance characteristics and reducing cost. However, most of these attempts were basically of trial and error type in which improvements in design were not the result of any mathematical analysis but attributed solely to professional experience.

In most of the available literature, the stress is mainly on the minimization of manufacturing cost of active materials. However, with the increasing cost of electrical energy, the operating cost has now assumed a significant role in determining the overall system economy. A need is, therefore, felt to go in for the design optimization of high- efficiency and cost-effective machines using a proper mix of active material cost and operating cost as the objective functions. The advents of digital computers with tremendous computing capability and ability to carry out logical decisions have facilitated the use of well known optimization techniques in the design of electrical machines. Design optimization is generally aimed to a given quantity, which is to be optimized. For this purpose, one or more objective functions can be selected depending upon the specific requirements. Thus, the design optimization of PM motors has been carried out by considering three different objective functions, namely, the cost of active material, the cost of annual energy consumed and the total annual cost.

The optimization methods are mathematical programming techniques, which provide a means of finding the minimum or maximum of a function of several variables under the prescribed set of constraints. These optimization techniques may be broadly classified into two categories, namely, the gradient and non-gradient methods. However; the gradient methods are more cumbersome and time consuming for nonlinear multivariable constraint programming as they exhibit poor converging properties. In this investigation, the direct search method, namely, Rosen Brock's method of rotating coordinates in Sequential Unobstructed Minimization Technique (SUMT) has been employed in design optimization of PM motor for different objective functions.

Another aspect of design optimization of PM motor is the selection of their set of basic variables. In PM machine design, a large number of variables can be selected from the physical consideration. Some of these may be assigned fixed values as they have little influence either on the objective function or on the specified constraints. Usually, such assigned variables are the number of slots, winding factor, space factor, etc. An attempt should be made to identify a set of basic variables having a significant bearing on the cost and/or the performance of the motor. The variables considered in the design optimization are judiciously selected. In the process of design optimization, the used algorithm with programme description and flowchart summary are given. For simplicity, consideration in this investigation has been restricted to PM motors using

Nd-Fe-B magnets. However; the same approach can be adopted for other types of magnetic materials.

2.11.1 Formulation of PM Motor Design Optimization Problem

Mathematically, the general nonlinear multivariable-constrained optimization problem can be formulated as follows:

Find $X(x_1, x_2, \ldots\ldots x_n)$ such that

F(x) is optimum.

Subject to

$g_j(x) > 0$ for $j = 1, 2, 3\ldots..m$

and $x_{li} < x_i < x_{ui}$ for $i = 1, 2, 3\ldots..n$

Where, $(x_1, x_2\ldots..x_n)$ is a set of independent design variables with their lower and upper bounds as x_{li} and x_{ui}. F(X) is the objective function to be optimized. The gj(x) are the imposed constraints. There are m constraints out of them some are implicit constraints such as bounds on performance criteria and some are explicit constraints such as bounds on design variables.

2.11.2 Design variables

In the design of PM motor a number of physical parameters can be considered for design optimization. Fortunately, some of them may be assigned fixed values as they have little influence either on objective function or the specified constraints. In the present investigation eight design variables $X(x_1, x_2, x_3\ldots x_8)$ are considered with their upper and lower limits. The basis of selecting these variables depends upon the design of PM machine. The selected variables are outlined here under:

1. Stator radius (mm), x_1
2. Rotor length (mm), x_2
3. Linear current density (A/m^2), x_3
4. Ratio of yoke –depth- to-stator radius, x_4
5. Air-gap flux-density (Tesla), x_5
6. Air-gap length (mm), x_6
7. Depth of the slot (mm), x_7
8. Slot-width-to-slot-pitch ratio, x_8

2.11.3 Design constraints

To make the design feasible and practically acceptable, some constraints are imposed. These constraints are selected based on the manufacturing standards, customer specifications and also on properties of the materials available for the designing the machine. The imposed constraints on the design during the optimization process are:

1. Temperature rise of the motor,
2. Efficiency of the motor,
3. Temperature of the magnet,
4. Flux-density in the yoke,
5. Flux-density in the teeth,

2.11.4 Design objectives

To have the design practically acceptable, the following three different objective functions are considered separately while optimizing the design of the motor:

1. The first objective function considered here is the manufacturing cost of the active materials consisting of stator/rotor stampings, winding materials and magnetic materials. The cost of the iron stamping is considered at the rate of Rs.150/kg, Cost of the copper is used as Rs.350/kg and cost of high-energy permanent-magnet (Nd-Fe-B) is assumed to be Rs.5400/kg.This is in favour of manufacturer and will reduce the manufacturing cost of the machine.
2. The second objective function is the cost of annual energy consumed by the motor. The annual energy cost is considered for 4000 operating hrs in a year at the rate of Rs.3.00 per kWh. The justification for selecting this objective function lies on the point of view of consumers to account for the increasing cost of electrical energy.
3. The third objective function includes a certain part of manufacturing cost as well as the annual operating cost of the motor. It consists of 20% of active material cost, the annual operating cost and annual cost of energy consumed by the motor. This objective function gives due consideration to the advantages of consumers as well as the system economy.

2.11.5 Optimization Technique

The design optimization of PM motor is a highly nonlinear, multivariable, constrained optimization problem. It may be solved by using either direct or indirect search methods. Here indirect search method namely, Sequential Unconstrained Minimization Technique (SUMT) in association with Rosenbrock's method of rotating co-coordinates is used to achieve the optimized design. Some of these are explained here.

2.11.6 Sequential Unconstrained Minimization Technique (SUMT)

The Sequential Unconstrained Minimization Technique (SUMT) with interior penalty function approach was originally developed by Fiacco and Mccermic. In the present investigation, the SUMT in conjunction with Rosenbrock's method of direct search, in which the constrained optimization problem is converted into series of unconstrained problem, is used in the following manner:

An augmented objective function at K^{th} iteration is expressed in terms of objective function as follows:

$$P(X, б_k) = F(X) + б_k \sum_{J=1}^{m} (1/G(X))$$

where $P(X, б_k)$ is known as the augmented objective function. The sigma term, called the penalty term, is helpful to ensure the feasibility of design during the optimization process. In this, the scalar $б_k$ ($б_k > 0$) is called the penalty factor. $G_j(x)$ is the normalized form of all constraints $g_j(X)$ lying between -1 and 0 only. The process is started with initial feasible design X_0, i.e. with the design satisfying all constraints. The starting value of $б_k$ is considered so that the starting value of $P(X, б_k)$ is minimized with the help of a suitable unconstrained minimization technique to get a point, say X_k. Now the new augmented function $P(X_k, б_{k+1})$ is formed with $б_{k+1} < б_k$, ($б_{k+1} = c\ б_k$). Here, c has its limit as ($0<c<1$).In next step the augmented objective function $P(X, б_{k+1})$ is minimized with X_{k+1} as a variable. In the process of unconstrained minimization of $P(X, б_{k+1})$ for a decreasing sequence of values of $б_k$, it is necessary to use proper convergence criteria to identify the optimum point. The convergence criteria is such that the process is considered for either a predetermined number of iterations or until the progress in objective function(F) becomes less than a small specified quantity. In the present investigation, the value of c is selected as 0.25.

2.11.7 Algorithm

The algorithm for the PM motor design optimization using SUMT in conjunction with the Rosenbrock's method of direct search and interior penalty-function approach is illustrated with a flowchart on Figure 2.6 and is explained below:

1. Read the rating, initial design vector, step size, bounds of variables and constraints, the value of c, initial value of penalty parameter, characteristics data and number of iterations (M).
2. Set K=1, ie, set iteration number one
3. Formulate an augmented objective function
4. Find out the unconstrained minimum (X^*_k at P(X, бk)) using Rosenbrock's method of direct search.
5. Check convergence, whether number of iterations are greater than the predetermined number or the change in per-unit value of variables is smaller than a specified small quantity.
6. Set $б_{k+1}$=c $б_k$, (0<c<1), $Xb_i=X_k^*$, I and k=k+1, go to step-3.
7. Print optimum design result
8. Stop.

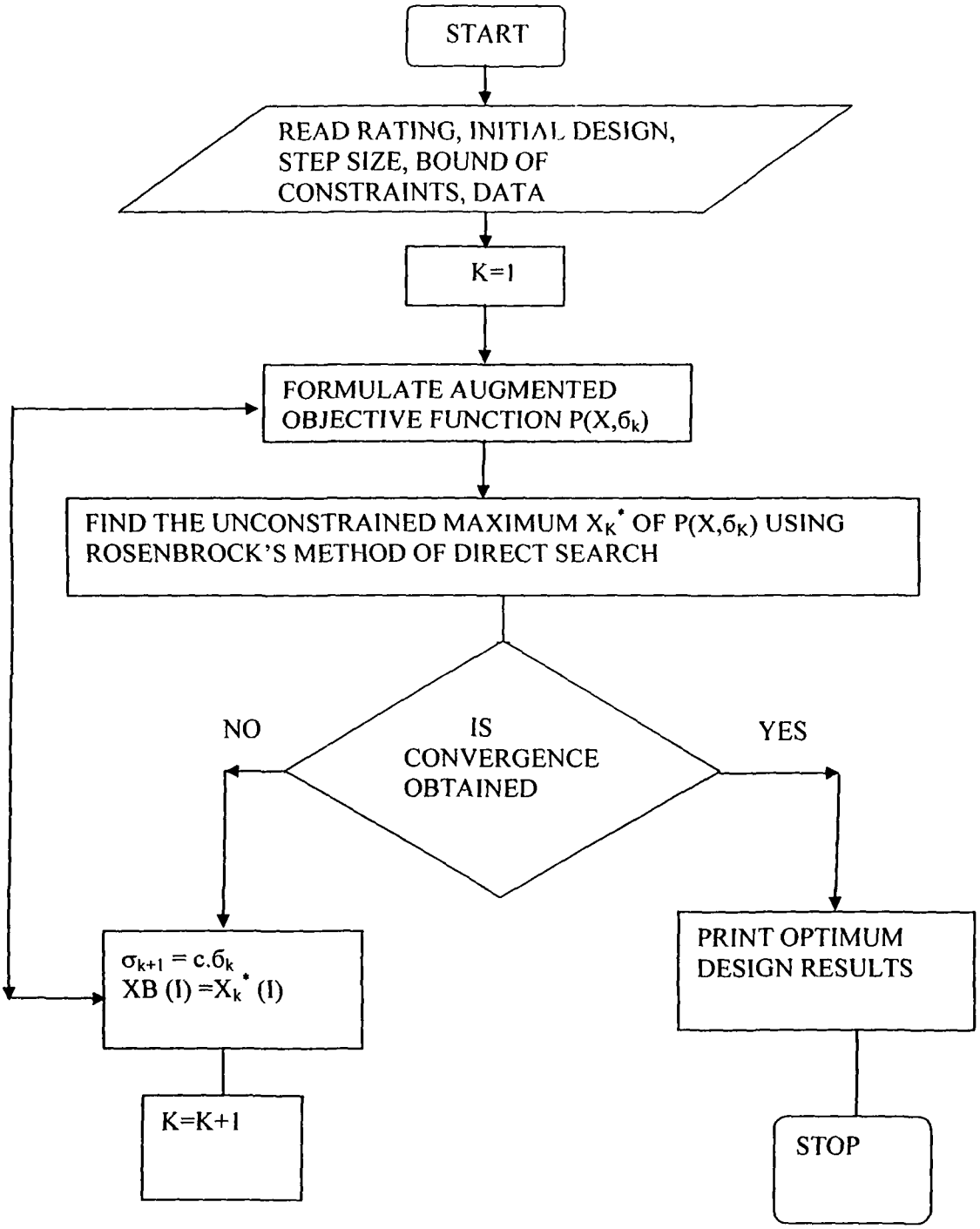

Figure 2.6: Flow Chart of 'SUMT' for PM Motor Design Optimization

2.11.8 RosenBrock's method

The method of rotating co-ordinates, given by Rosenbrock can be considered as a further development of Hook and Jeev's method and is being selected for present studies. Earlier this method was employed in many applications. This method is used in conjunction with SUMT to achieve unconstrained minimum in the SUMT. In this case, the co-ordinate

system is rotated in each stage of minimization in such a manner that the first axis is oriented towards the locally estimated direction of valley and all the other axes are made usually orthogonal and normal to the first one. The detailed description of RosenBrock's method is explained in stages as follows:

At the first stage of this method, the design variables are varied in sequence in both the directions parallel to the axes. When for a particular variable, there is an improvement in the value of objective function, that is success, the step length corresponding to this variable is magnified by an acceleration factor 'a' (a>1) in the search direction for the next cycle. If there is no improvement in the current value of the objective function, that is a failure, the step length of this variable is decreased by deceleration factor 'b'(0<b<1) in the reverse direction. The sequence is repeated until a success and a failure are encountered for all variables at this stage.

In the second stage the direction of search is given a rotation with respect to the original axis. For computing the appropriate direction, the co-ordinate system is rotated in such a manner that the first axis is oriented towards the locally estimated direction of the valley and all the other axes are made mutually orthogonal and normal to the first one. The procedure is continued for either a given number of stages or until the progress in the value of objective function becomes less than a specified small quantity.

The algorithm for the RosenBrock's method has been given below. The initial values of design variables (xb_i, i=1,n),their step size (SX_i, i=1,n),initial value of objective function (TF) and number of stages (M) are common to both the algorithms. The detailed flow chart which demonstrates the RosenBrock's method is shown in Figure 2.7.

1. Set number of stages=0, directions ($PS^J_{i=1}$ and i=1, n) parallel to their axes for the first stage $Sx1_i=S\,x_i$, for i=1, n
2. Set J=J+1, $T\,K^J_i = 0.0$ for i=1, n
3. Set k=1
4. Calculate the value of variables x_i using step size S_K1_k and directions $PS^J{}_{k,i}$ and initial design vector xb_i for i=1,n as

   $X_i=Xb_i+ PS^J_{kJ}\ SK1_k$ for i=1, n.
5. Check whether these variables (X_i, i=1, n) are within the specified limits. If not, go to step 10.
6. Calculate the objective function (F) and constraints.
7. Check whether the design satisfies the imposed constraints

   With improvements in the objective functions (F). If not, go to step 9.

8. Set initial values of variables ($xb_i = x_i$, i =1, n)

$T K^j_k = T K^j_k + Sk^1_k$ step size as $Sx^1_k = a\, SK^1_k$ (a>1)

TF=F, and store the design. Note a success and go to step 10.

9. Set steps size $SK1^1_k = - b\, S\, K1^1_k$, (0 < b< 1) and a failure

10. Check whether all variables have been considered (i.e. k = n). If not, set K= K+1 and go to step 3.

11. Check whether a success and failure have been encountered in all directions .If not, go to step 14.

12. Check convergence. If the number of stages (J) exceeds the pre-determined values (m) or change in per unit values of variables is smaller than the specified small quantity .If yes, go to step 15.

13. Set step size ($Sx1_i = Sx_i$, i =1, n), rotate axes and compute directions for the other stages as follows.

$PS^{J+1}_{i,1} = QS^J_{i,1} / \| QS^J_{i,1} \|$

Where $QS^J_{i,1} = PT^J_{i,1}$

and

$QS^J_{i,1} = PT^J_{i,1} - \Sigma [(\Sigma PT^{J+1}_{l,nJ} PS^{J+1}_{nJ,lm}) PSJ^{+1}_{i,lm}]$

For I = 1, 2, 3, 4.....n.

where

$$PK^J_{i,lm} = \begin{vmatrix} TK^J_1 & 0 & 0 \ldots\ldots & 0 \\ TK_2 & TK^J_2 & 0 \ldots\ldots & 0 \\ - & & & \\ - & & & \\ - & & & \\ TK^J_n & TK^J_n & 0 \ldots\ldots & TK^J_n \end{vmatrix}$$

Lm =1, 2, 3..... n

where

I = Variable index =1, 2.....n

L = Direction index 1, 2.....n

J = Stage index

TK^J_i = Sum of distance moved in the ith direction for J_{th} stage

Go to step 2.

14. Print stored optimum design result.

15. Stop.

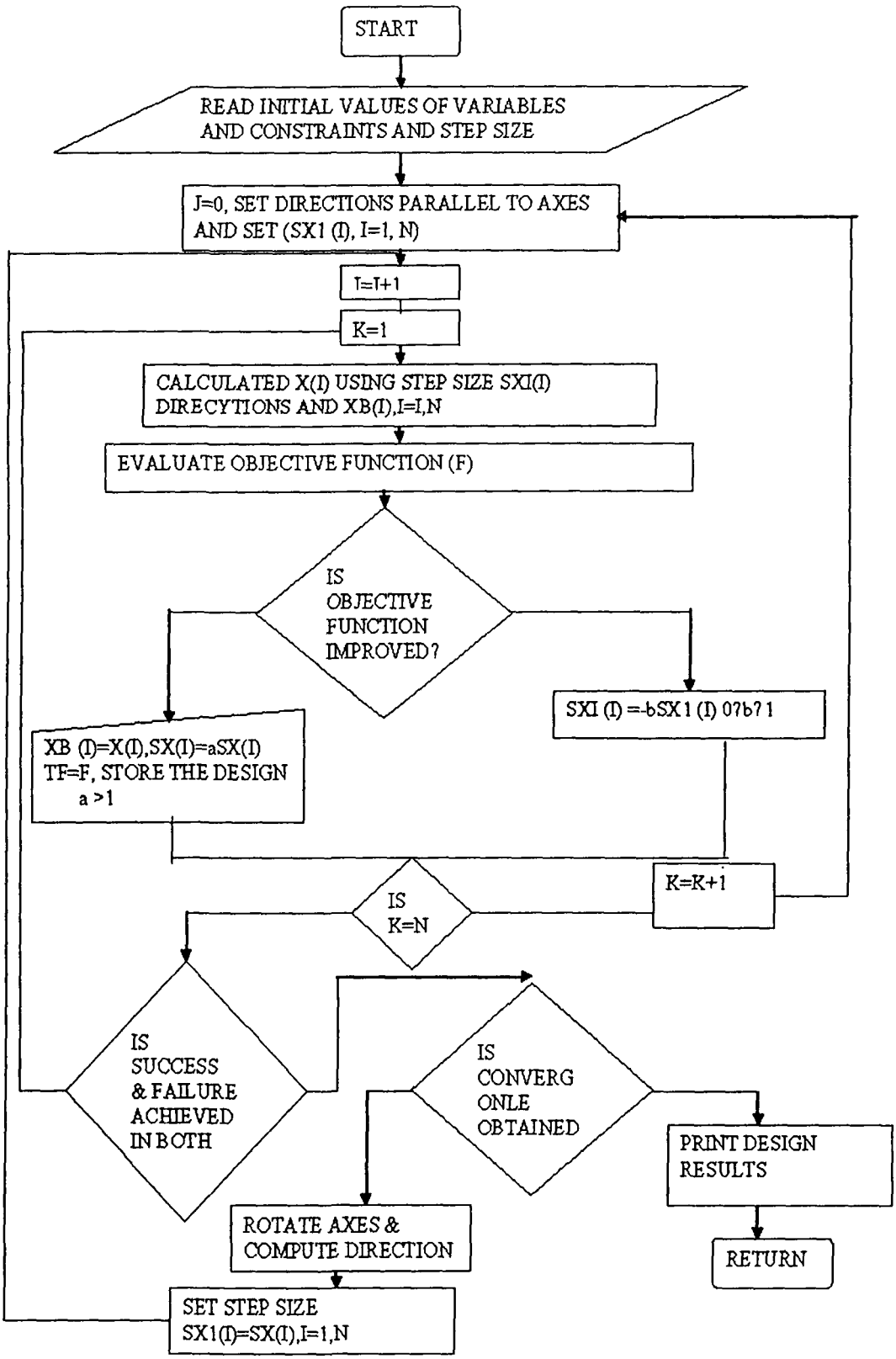

Fig: 2.7: Flow Chart of 'Rosen Brock's method' For PM Motor Design Optimization

2.12 Conclusion

The literature survey has revealed that the use of PMBL motor is gaining momentum in various applications. It has become a competitor to DC, induction motors and SRM. The PMBL motor drive system has been found to be suitable for high performance applications. However, it suffers from the disadvantage of higher initial cost. Thus, with the knowledge of past and present drive technologies, one can think of further improvements.

Active research is going on towards providing a suitable controller for PMBLDC drive. Many control theories have been proposed. Some of them have been simulated as well. The researchers find it difficult to compromise on the controllers already available. More advanced controllers are being reported in the literature. Still there is problem of developing simple tuning procedures working on a wide range of operating conditions. Considerable research is undertaken towards developing digital speed controllers. Simulations of this drive with fast processors have been reported in recent years. Furthermore the researchers are trying to make the drive sensorless such that it becomes cost effective. Considering all the research reported so far, the present efforts is on the simulation and control of PMBLDC drive with improved design of controllers. An attempt has also been made to have the drive sensorless.

The design optimization of a PM motor employing SUMT optimization technique forms the basis for further studies reported in chapters 3-6. Experience with the design optimization indicates that the optimization based on individual objective function leads to designs which are favourable to one or more of the following, namely, the consumer, the manufacturer and the suppliers of electrical energy.

CHAPTER 3

MATHEMATICAL MODELLING OF PMBLDC MOTOR DRIVE

3.1 General

The model of the drive system consists of a speed controller, reference current generator, PWM current controller, inverter and the PMBLDC motor. All these components are modelled and integrated for system identification and simulation. The performance of the closed-loop-controlled drive system depends on the choice of the controllers. As the model of the PMBLDC motor is nonlinear, a numerical technique namely Runge-Kutta method is used to get the solution of the system equations and all control functions are tested for several operating conditions such as starting, braking, speed reversal and load perturbation.

3.2 Description of the PMBLDC Motor Drive System

Figure 3.1 describes the basic building blocks of the PMBLDC motor drive. The drive consists of speed controller, reference current generator, PWM current controller, position sensor, brushless motor and MOSFET based inverter. The speed of the motor is compared with the reference value and the error in speed is processed in speed controller. The output of speed controller is considered to be the reference torque. A limit is put on the speed controller output depending on maximum winding currents. The reference- current-generator block generates the three-phase reference currents (i_a^*, i_b^*, i_c^*) using the limited peak current magnitude decided by the controller and the position sensor. The reference currents have the shape of quasi-square wave in phase with respective back emfs to develop constant unidirectional torque. The PWM current controller regulates the winding currents (i_a, i_b, i_c) within the small band around the reference currents (i_a^*, i_b^*, i_c^*). The motor winding currents are compared with the reference currents and the switching commands are generated to drive the inverter devices.

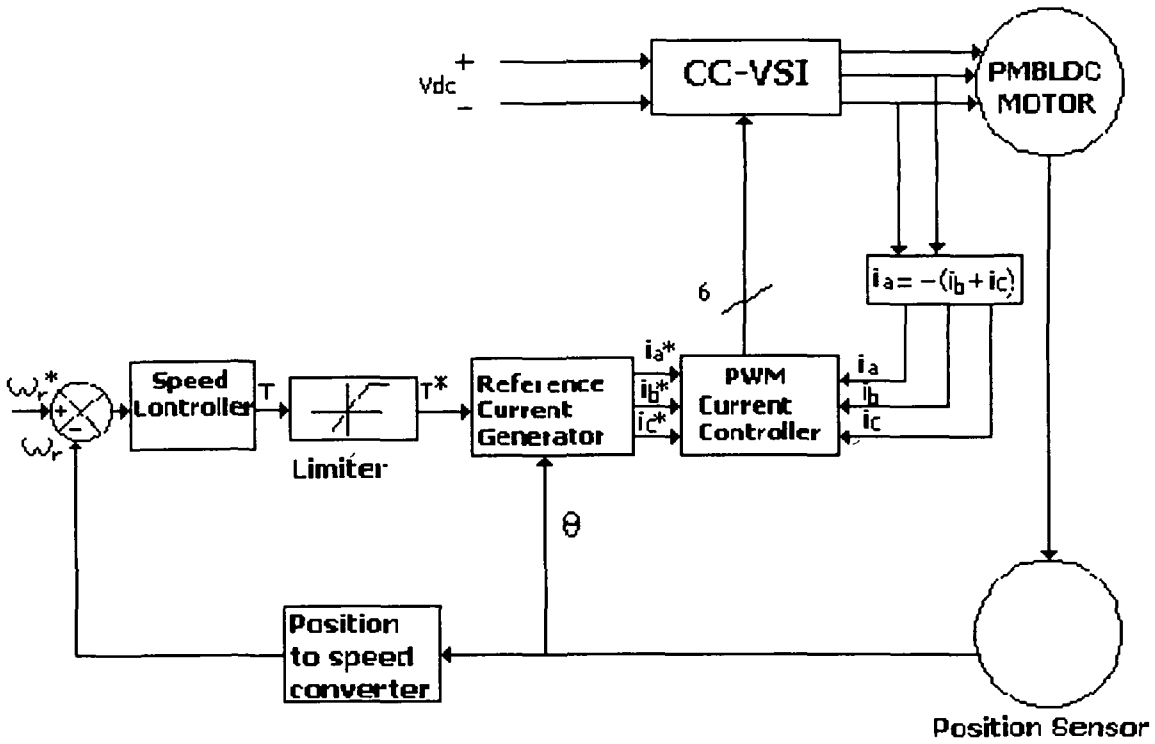

Figure 3.1; Schematic Block Diagram of PMBLDC Motor

3.3 Types of Speed Controllers

There has been tremendous research on different types of speed controllers to improve the dynamic performance of the drive. Closed-loop operation of digital speed controller is useful especially in applications such as in robots, aerospace and servo drives, where precise control is needed. Literature reveals that different types of speed controllers have been used for various applications. In this investigation, dynamic performance of the drive system is analyzed using different types of speed controllers and the simulated results are obtained for different operating conditions such as starting, speed reversal and load perturbations. A conventional PI controller is most widely used in industry due to its simple control structure, simple design and relatively lower cost. However, the control performance of PMBL drive is still influenced by uncertainties of the plant which features parametric variations, external load disturbances, unmodelled and nonlinear dynamics. This has boosted the use of nonlinear control schemes such as model reference adaptive control, variable structure control etc. Another type of controller based on fuzzy logic is being increasingly applied to systems with non linearity and uncertainty. Considering the above observations, a range of speed controllers starting from conventional controllers to the modern ones has been used for the simulation study of the PMBLDC drive. In this

investigation, the transient and steady-state responses of the drive are examined with different speed controllers like PI, PID, SMC and Fuzzy logic controllers. Of these, the PI, PID are conventional controllers and SMC, Fuzzy Logic Controllers are modern or very intelligent controllers.

The main objective is to compare the performance of the drive with different types of controllers thereby examining the effectiveness of the controllers for a given application and also to establish the viability of the proposed model and to demonstrate the versatility of applications.

3.3.1 PI Speed Controller

PI controller is widely used in industry due to easy design, simple structure and the flexibility it offers for implementation. A fixed-gain PI controller operates satisfactorily as long as the operating point does not change. Since the steady-state accuracy is of primary importance, the PI control is still the best choice. It can also be designed to have a fast transient response, but then it becomes very sensitive to parametric variations.

3.3.2 PID Speed Controller

Conventional PID controller is most widely used in industry due to its simple control structure, easy design and relatively lower cost. Moreover, it can be easily implemented in a closed-loop drive system. The PID controller mainly consists of three controller gains namely, the proportional, integral and derivative gains. Traditionally, a conventional fixed-gain PID controller with its proportional, integral and derivative gains tuned properly for given operating conditions provides satisfactory transient response so long as the operating point does not deviate too much from the initial position. Owing to its simplicity, it has also paid the price of not having an efficient and practical way of determining optimal gains. Generally, in response to an input signal, it is desirable for the drive system to have a fast response, reasonably small overshoots and zero steady-state error. Moreover the system should be insensitive to load-torque disturbances.

3.3.3 Sliding Mode Controller (SMC)

The problems of overshoot and oscillations associated with the use of PID controller can be overcome with SMC controller. Sliding-mode control has a distinct

feature of dealing with nonlinearities offering robust control. It does not require exact mathematical model. It is operates on second and fourth quadrants of the plot between speed error and acceleration of the drive system. The output of the sliding-mode controller is limited through a limiter and the signal obtained is used to determine torque (T^*). Since it is impossible to switch the control at infinite rate, chattering always occurs in the sliding mode control.

3.3.4 Fuzzy Logic Controller

Another type of controller based on Fuzzy logic is being increasingly applied to many systems with non-linearity and uncertainty. The concept was introduced about three decades ago, but recently its application has received increased attention. The development of fuzzy logic controllers is easier to learn and requires less skilled personal than the development of conventional controllers. Fuzzy logic controllers are represented by "if-then" rules and thus can provide a user friendly and understandable knowledge representation. Since the Fuzzy logic controller requires lesser complex mathematical operations than classical controllers, its implementation does not require a computationally sophisticated processor such as DSP. Standard Fuzzy logic method consists of three stages: fuzzification, decision-making logic or rule evaluation and defuzzification.

Fuzzification: The process of converting a numerical variable (real number) into a linguistic variable (Fuzzy member) is called fuzzification.

Rule evaluation: The first two linguistic values are associated with the input variables e(k) and Δe(k), while the third linguistic value is associated with the output. For example, if error in speed is zero (Z) and change in speed-error is negative small (NS), then output is negative medium (NM). There are 7×7 rules altogether. The rules are derived by using a combination of experience and the knowledge of the response of the drive system.

Defuzzification: The reverse of fuzzification is called defuzzification. The rules of FLC produce required output in a linguistic variable. Linguistic variables have to be transformed to crisp output. Center of gravity method is used in this work. Finally, crisp output is obtained by using the relationship

$$\text{FLC}\,[(e(k),\Delta e(k)] = \Sigma A_i * x_i / \Sigma A_i \qquad (3.1)$$

The crisp output of Fuzzy logic controller is taken as reference torque and is limited through a limiter. Fuzzy logic controllers often yield superior results to conventional control approaches. Moreover, Fuzzy logic controllers are inherently robust to load variations. Many advantages of Fuzzy logic controllers have been mentioned in the literature (Li, 1998). One relevant advantage is the possibility of converting a linguistic control strategy based on experience and expert knowledge of an automatic control strategy. Another advantage is that Fuzzy logic controllers can be easily implemented.

3.3.4.1 Fuzzy Precompensated PI Controller

Conventional PI controllers, though simple to implement and commonly used in practice, suffer from poor performance when applied to systems with significant nonlinearities. Fuzzy-logic concept can be used effectively to complement conventional controllers for improving performance and robustness. Kim and Chong, 1994; Kovacic and Bogdan, 1998; Singh et al, 1999; Kumar, Singh, and Bordoloi, 2005 have applied precompensation scheme for PID controllers. The scheme is based on efforts to compensate for overshoots and undershoots in transient responses. The purpose of the Fuzzy precompensator is to modify the command signal to compensate for the overshoots and undershoots present in the output response when the system has nonlinearities. The fuzzy precompensated controllers have superior performance compared to conventional PI controllers. Besides, this controller is robust to variations in load. Another advantage is that an existing PI controller can be easily modified into this control structure simply by adding Fuzzy precompensation.

3.3.4.2 Fuzzy PID Controller

In recent years, Fuzzy logic is finding increased use in numerous applications that include areas such as management, economics, medicine and more recently in closed- loop system applications. The objective of Fuzzy control is to design a system with an acceptable level of performance over a wide range of uncertainties (Carrara, Casini, Landi and Taponecco, 1991; Le-Huy, Viarouge and Kamwa, 1991; Sousa and Bose, 1994; Yamamoto and Furuhashi, 2001). This theory was introduced about three decades ago by Zadeh, 1973 but only recently its application has received increased attention. The essential part of the Fuzzy- logic control-rules are related by the dual concepts of fuzzy implication and the compositional rule of interference. The Fuzzy-

logic control also performs well for complex nonlinear multi-dimensional systems and systems with parameter variation or when the sensor signals are not precise. The Fuzzy control is basically nonlinear and is adaptive in nature, giving a robust performance in the face of parameter variation and/or load disturbance. Many researchers (Lee, 1990; Zhang and Edmunds, 1992; Kim and Chong, 1994; Kung and Liaw, 1994; Kovacic and Bogdan, 1998; Singh et al, 1999; Kumar, Singh and Bordoloi, 2005; Singh and Kumar, 2005) have reported that the Fuzzy- logic control yields results which are superior to those obtained using conventional control algorithms.

3.3.4.3 Fuzzy-Sliding-Mode Controller

To combine the attractive features of fuzzy control and the sliding-mode control, Hwang and Lin, 1992 have proposed a fuzzy-sliding-mode controller, which reduces the variable error in the conventional sliding-mode controller. An attractive approach to obtain the fuzzy control is provided by the fuzzy-self-organizing controller. The main objective of the fuzzy-sliding-mode controller is to remove the system uncertainties as well as to reduce chattering without sacrificing the level of system performance.

3.3.4.4 Self-Organizing-Fuzzy-Logic Controller

The idea of automated FLC was announced and elaborated by the groups of Procyk and Mamdani, 1982; Lee and Kim, 1992; Zhang and Edmunds, 1992; Yu-Sheng and Shiang, 1994; Butt, Hoque and Rahman, 2004. Since then, many researchers have attempted to improve the performance of Fuzzy-logic controllers using Self-organizing mechanisms. Self-organizing-Fuzzy-Logic Controllers (SFLCs) have been successfully applied to various controls such as pH-neutralization, inverted pendulum, robot drives, induction motor and many others (Jespersen, 1981; Lee and Kim, 1992; Kovacic and Bogdan, 1998; Uddin, Radwan and Rahman, 2002; Uddin, Abido .and Rahman, 2005). The objective of the SFLC is to change the rules definition in the FLC rule base-table, according to the comparison between the reference speed and the actual motor speed. The design of the Fuzzy adaptation strategy is based on the fact that each dynamical aspect of the system response is mainly influenced by a group of rules.

3.3.4.5 Gain Scheduled PI controller

The problem of developing a simple tuning procedure properly working over the wide range of operating conditions is still open. The present work considers the Gain Scheduling of PMBLDC motor as reported by Panda, Lim and Dash, 1997 and Kumar, Singh and Bordoloi, 2005. In this scheme, the PI gains are allowed to vary over a pre-determined range for varying operating conditions. It is well known that the proportional term is responsible for improving overshoots, rise-time, and the integral term reduces steady state error. When the speed-error is large, a large value of proportional gain is necessary for better control effort and similarly when the speed-error is small a large value of integral gain is necessary to overcome steady-state error. The key feature of the Gain scheduling control is the reduced amount of computation. An easy and low cost implementation is possible without employing expensive dedicated computing systems. An advantage of this approach is that an existing PI control system can be easily modified in to this control structure simply by adding the auto-tuning technique.

3.3.4.6 Hybrid Fuzzy Controller

In the hybrid controller (Li, 1998; Singh and Kumar, 2005), the output is decided by two controllers. One is conventional PI and the other one is Fuzzy. The output of the hybrid controller is also decided by the speed-error that will decide the membership function. The hybrid fuzzy logic with proportional plus conventional integral-derivative controller is used for the speed control of PMBLDC motor. Although the conventional PID controllers are widely used in the industry due to its simple control structure and ease of implementation, these controllers pose difficulties under the conditions of nonlinearity, load disturbances and parametric variations. In this Thesis, the performance of the PMBLDC motor drive is examined with the aid of the hybrid controller. The hybrid controller shows improved performance compared to the conventional PID speed controller.

3.4 Modelling of The PMBLDC Motor Drive System

3.4.1 Modelling of speed controllers

Different components of the drive system identified in the preceding subsection are modelled separately and then these are integrated for the purpose of system identification and simulation.

3.4.2 PI Speed Controller Modelling

This system utilizes the digital PI speed controller. Figure 3.2 shows the block diagram of PI speed controller. The rotor speed $\omega_{r(n)}$ is compared with the reference speed $\omega_{r(n)}^*$ and the resulting error in speed is estimated at the nth sampling instant as:

$$\omega_{e(n)} = \omega_{r(n)}^* - \omega_{r(n)} \tag{3.2}$$

The magnitude and sign of the speed-error may be positive or negative depending upon the rotor speed and its reference value. The speed-error is processed in a PI speed controller. The output of the PI speed controller at the nth sampling instant

$$T_{(n)} = T_{(n-1)} + K_P\{\omega_{e(n)} - \omega_{e(n-1)}\} + K_I\,\omega_{e(n)} \tag{3.3}$$

where K_P, and K_I are the proportional and integral gains of the speed controller respectively. The signal $T_{(n)}$ is the input to the limiter while T^* is the output of the limiter which is considered as reference torque. This reference torque decides the peak value of reference currents.

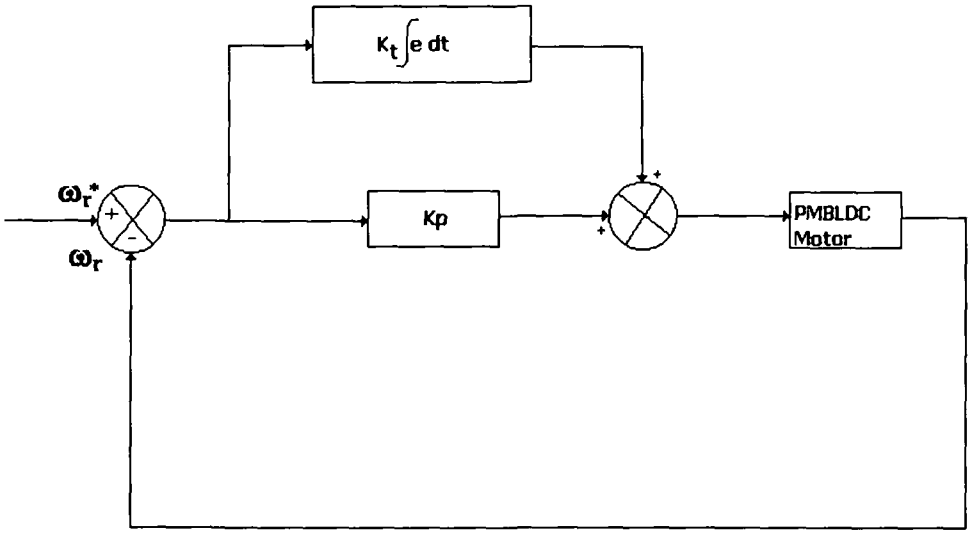

Fig. 3.2: Block Diagram representation of PI Speed controller

3.4.3 PID Speed Controller Modelling

Figure 3.3 shows the block diagram of PID speed controller used in this investigation. This system utilizes the digital PID speed controller. The rotor speed $\omega_{r(n)}$ is compared with the reference speed $\omega_{r(n)}^*$ and the resulting error in speed is estimated at the nth sampling instant as:

$$\omega_{e(n)} = \omega_{r(n)}^{*} - \omega_{r(n)}$$

The magnitude and sign of the speed-error may be positive or negative depending upon the rotor speed and its reference value. The speed error is processed in a PID speed controller. The output of PID speed controller at the nth sampling instant as:

$$T_{(n)} = T_{(n-1)} + K_P\{\omega_{e(n)} - \omega_{e(n-1)}\} + K_I\,\omega_{e(n)} + K_D\,\{\omega_{e(n)} - 2\,\omega_{e(n-1)} + \omega_{e(n-2)}\} \quad (3.4)$$

where K_P, K_I and K_D are the proportional, integral and derivative gains of the speed controller respectively. The signal $T_{(n)}$ is the input to the limiter while T^* is the output of the limiter which is considered as reference torque. The reference torque decides the peak value of the reference current.

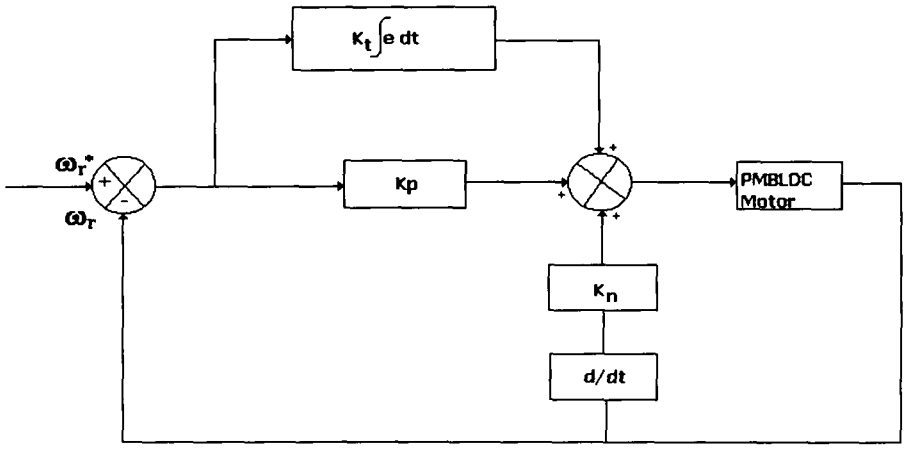

Figure 3.3: Block Diagram representation of PID Speed Controller

3.4.4 Modelling of Sliding Mode Controller

The block diagram of sliding mode controller (variable structure controller) is shown in Figure3.4. This block decides the switching of the structure of the system. Here S_1 and S_2 are the switching functions whose values are decided as:

$S_1 = +1$, if $\sigma x_1 > 0$

-1, if $\sigma x_1 < 0$

$S_2 = +1$, if $\sigma x_2 > 0$

-1 if $\sigma x_2 < 0$

where, x_1 is the speed error $(\omega_r^* - \omega_r)$ and x_2 is the derivative of the speed error dx_1/dt The output of the sliding mode controller (SMC) is given below:

$$V = K_1\,x_1\,S_1 + K_2\,x_2\,S_2 \quad (3.5)$$

where, K_1 and K_2 are controller gains on speed locus. The switching hyper plane function is expressed as:

$$\sigma = K x_1 + x_2 \tag{3.6}$$

Here K is an adjustable parameter.

The limiter limits the output of the sliding-mode controller and output of limiter is considered as the reference torque (T^*).

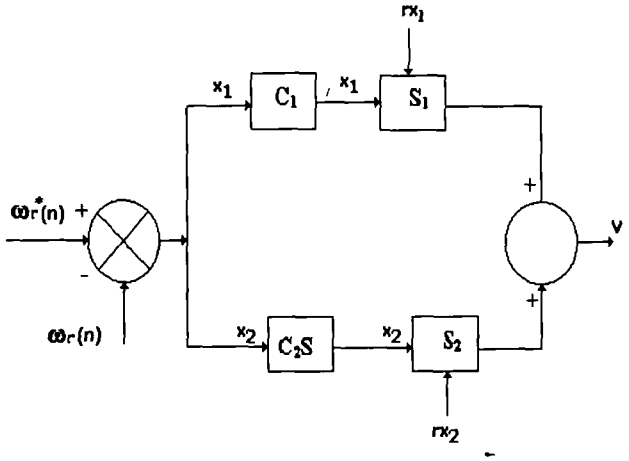

Figure 3.4: Block Diagram representation of Sliding Mode Controller

3.4.5 Modelling of Fuzzy Logic Controller

The Fuzzy Logic Control (FLC) is applied to the speed loop, replacing the conventional PI controllers. The objective is to explore the control robustness with the presence of parameter variation and load disturbances. Figure 3.5 shows the internal structure of Fuzzy-logic controller. The functional blocks in fuzzy logic are: (1) Fuzzification. (2) Rule evaluation and (3) Defuzzification.

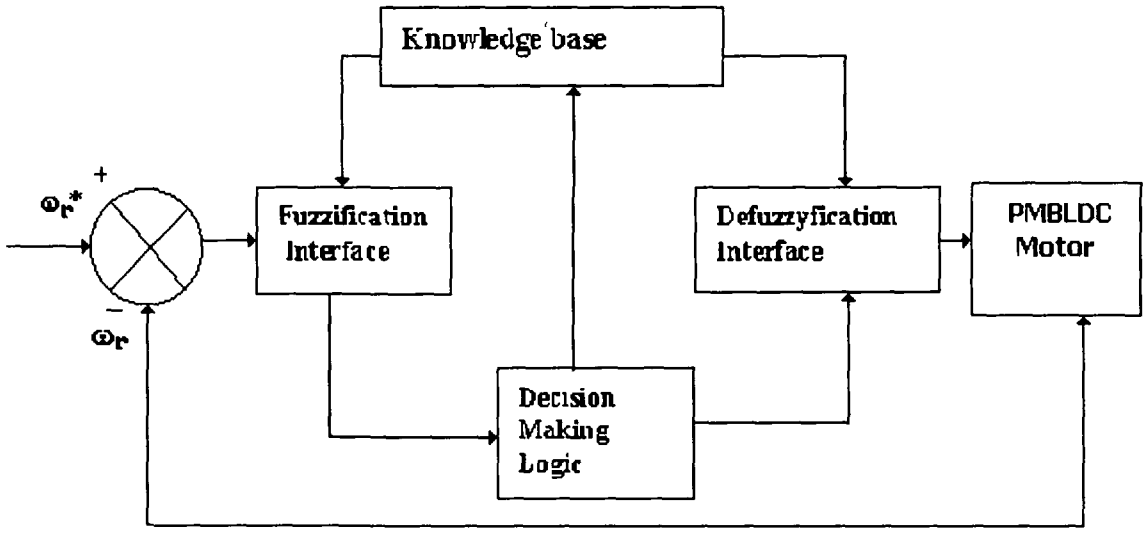

Figure 3.5: Basic diagram of Fuzzy Logic Controller

Fuzzification: Fuzzy logic uses linguistic variables instead of numerical variables. In a closed-loop control system, the speed error $\omega_{e(n)} = \omega_{r(n)}^{*} - \omega_{r(n)}$ can be labeled as zero(ZO), positive small (PS), negative small (NS) etc. In real world, measured quantities are real numbers (crisp). Similarly, change in speed-error is also labeled as ZO, PS, NS, NM, PM, NB and PB. This process of converting a numerical variable in to a linguistic variable (fuzzy member) is called fuzzification. Figure 3.6 shows the triangular membership functions used in fuzzification. The two inputs to the fuzzy logic controller are

$E_1 = \omega_{e(n)}$, where $\omega_{e(n)} = \omega_{r(n)}^{*} - \omega_{r(n)}$

$E_2 = \omega_{e(n)} - \omega_{e(n-1)}$

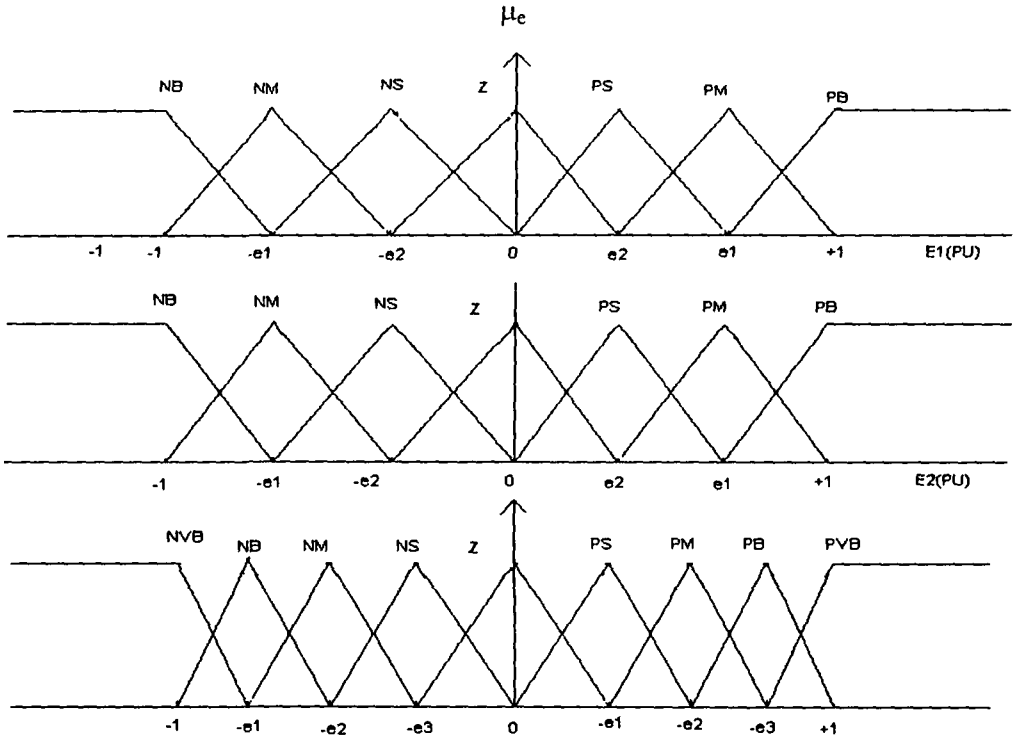

Figure 3.6: Membership functions used in fuzzy-logic controller

Rule evaluation: In FLC, the rules are linguistic in nature. A typical rule can be written as follows:

If E_1 is A and E_2 is B then output is C;

where A, B and C are the labels of linguistic variables. The linguistic rule table is shown in Table 3.1.

Table 3.1: Rule base Table for the Fuzzy Logic based speed Controller

E1/E2	NB	NM	NS	Z	PS	PM	PB
NB	NVB	NVB	NVB	NB	NM	NS	Z
NM	NVB	NVB	NB	NM	NB	Z	PS
NS	NVB	NB	NM	NS	Z	PS	PM
Z	NB	NM	NS	Z	PS	PM	PB
PB	NM	NS	Z	PB	PM	PB	PVB
PM	NS	Z	PS	PM	PS	PVB	PVB
PB	Z	PS	PM	PB	PVB	PVB	PVB

Defuzzification: The reverse of fuzzification is called defuzzification. The rules of FLC produce required output in a linguistic variable (fuzzy member). According to real world requirements, linguistic variables have to be transformed to crisp output (real number). The crisp output is obtained as:

Output = $\Sigma A_i \; x_i \; / \Sigma A_i$, i = 1 to n, where n is number of rules.

The steps for speed control can be summarized as follows:

1. Sample ω_r^* and ω_r.
2. Compute speed error and change of speed error and their per unit values.
3. Identify the interval index I and J for the two inputs.
4. Compute the degree of membership of two inputs for the relevant fuzzy subsets.
5. Identify the four valid rules in rule table and calculate the degree of membership using MIN (minimum) operator.
6. Retrieve dU_i for each rule from rule table. I =1.....n, n is the number of rules.
7. Calculate the resultant crisp value of dU by height defuzzification method.
8. Compute the next control signal as

$$U_{(k)} = U_{(k-1)} + GU \; dU(pu)$$

3.4.5.1 Modelling of Fuzzy Precompensated PI Controller

Figure 3.7 illustrates the basic control structure. This scheme consists of PI controller together with fuzzy precompensator. The fuzzy precompensator uses the reference speed command ω_r^* and the speed ω_r of the motor to generate a precompensated command signal ω_r^{**} described below.

$$E_1 = \omega_{c(n)} = \omega_{r(n)}^* - \omega_{r(n)}.$$

$$E_2 = \omega_{e(n)} - \omega_{e(n-1)}$$

$$\hat{u}(k) = FLC[E_1, E_2] \quad (3.7)$$

$$\omega_{r(n)}^{**} = \omega_{r(n)}^{*} + \hat{u}(k) \quad (3.8)$$

where E_1 is the error between reference speed and speed of the motor and E_2 is the change in speed error. The term FLC $[E_1, E_2]$ is nonlinear mapping of e (k) and $\Delta e(k)$ based on Fuzzy logic and represents a compensation or correction term, so that the compensated command signal $\omega_{r(n)}^{**}$ is simply the sum of the external command $\omega_{r(n)}^{*}$ and $\hat{u}(k)$. Then the compensated speed signal $\omega_{r(n)}^{**}$ is applied to a conventional PI scheme as shown in Figure 3.7(a) & 3.7(b).

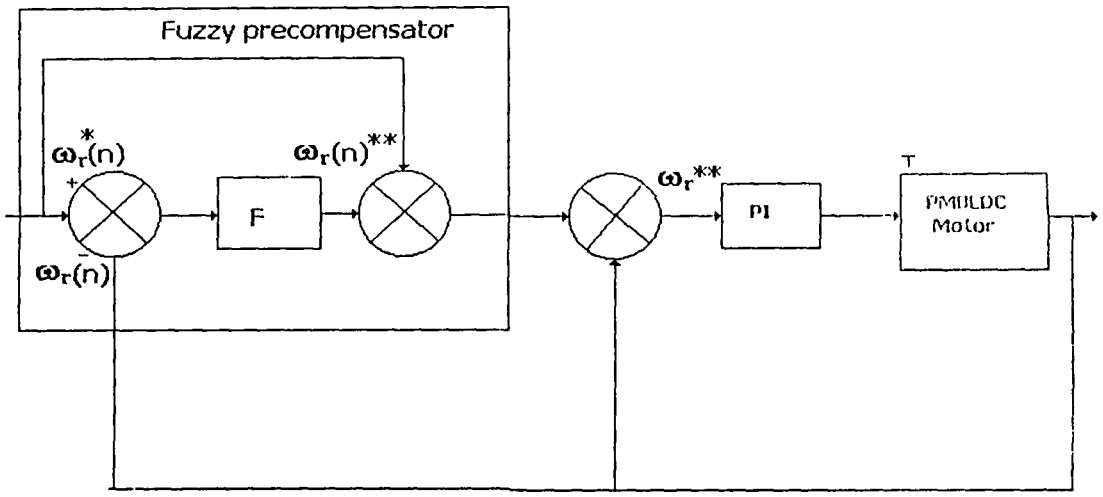

Figure 3.7(a): Basic control structure of the fuzzy Precompensated PI controller

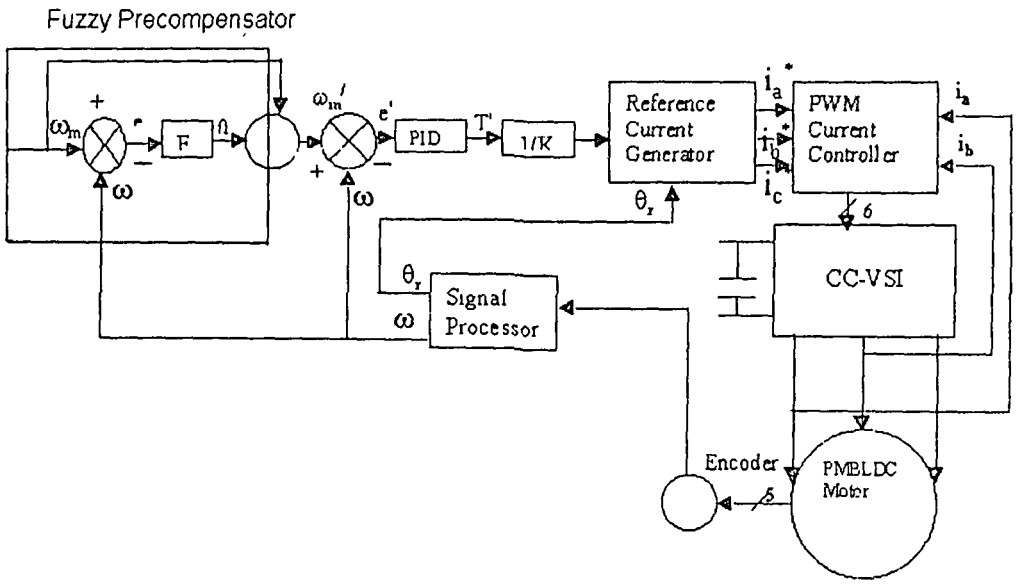

Figure 3.7(b): Basic control structure of the fuzzy Precompensated PI controller

The equations governing the PI controller are as follows.

$$E_1' = \omega'_{e(n)} = \omega_{r(n)}^{**} - \omega_{i(n)}. \quad (3.9)$$

$$E_2' = \omega'_{e(n)} - \omega'_{e(n-1)} \quad (3.10)$$

$$T^*_{(n)} = T^*_{(n-1)} + K_P [\omega'_{e(n)} - \omega'_{e(n-1)}] + K_I \omega'_{e(n)} \quad (3.11)$$

The output of the above equation T^* is considered as the reference torque of the PMBLDC motor. Now we describe the fuzzy logic term $\hat{u}$ (k) = FLC [E_1, E_2]. E_1 and E_2 are the inputs to the fuzzy logic controller and $\hat{u}$(k) is the output. In this investigation, we have used seven linguistic values namely NB, NM, NS, ZO, PS, PM and PB. The height of the membership functions in this case is one, which occurs at the points –1, -0.57, -0.27, 0, 0.27, 0.57,1. The realization of the function FLC [E_1, E_2] based on the standard fuzzy method consists of three stages: fuzzification, rule evaluation, and defuzzification.

Fuzzification: The process of converting a numerical variable (real number) into a linguistic variable (fuzzy member) is called fuzzification. Fig 3.8 explains this process.

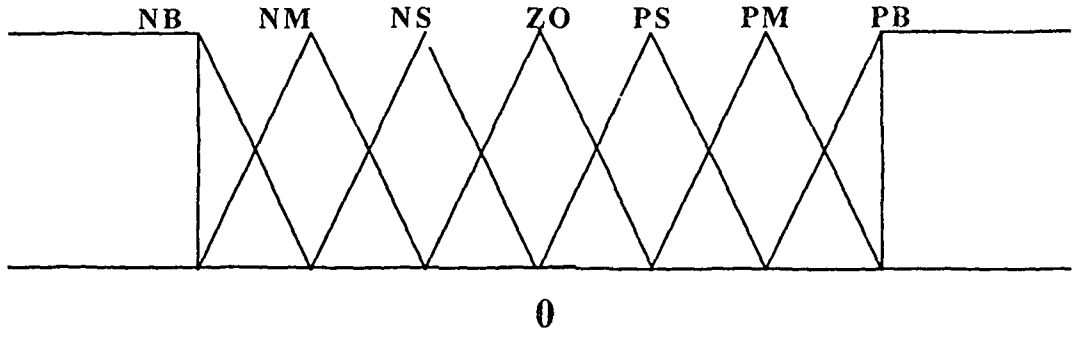

Figure 3.8: Membership function for speed error

Rule evaluation: The set of rules of fuzzy precompensator is given in Table 3.2. The first two linguistic values are associated with the input variables E_1 and E_2, while the third linguistic value is associated with the output. For example, if error in speed is ZO and change in speed error is NS, then output is NM. The rules are derived by using a combination of experience and the knowledge of the response of the drive system.

Defuzzification: The reverse of fuzzification is called defuzzification. The rules of FLC produce required output in a linguistic variable. Linguistic variables have to be transformed to crisp output. Center of gravity method is used in this work. Finally, crisp output is obtained by using

FLC $[E_1, E_2] = \Sigma A_i x_i / \Sigma A_i$, i = 1 to n, where n is number of rules.

This ends the description of the term $\hat{u}(k)$ = FLC $[E_1, E_2]$.

Table 3.2: Rule base Table for Fuzzy Precompensated PI controller

E_1 / E_2	NB	NM	NS	ZO	PS	PM	PM
NB				NB	NB		
NM	NB			NB	NB		
NS	NB			NM	NM	NM	NM
ZO	NB	NM	NS	ZO	PS	PM	PB
PS	NM			PS	PS		
PM				PM	PB	PB	
PB			PM	PM	PB		

3.4.5.2 Modelling of Self-organizing Fuzzy Logic Controller

The idea of self-organization of FLC was first announced and elaborated by the group of Mamdani et al, 1982. Since then, many researchers have attempted to improve designing and tuning the fuzzy controller. SFLCs have been applied to many control processes. Silva Neto and Huy, 1997 have proposed a Self-organizing controller for the speed control of PMSM. In this work, the effectiveness of the Self-organizing controller is examined by applying it to PMBLDC motor drive system. The objective of the SFLC is to change the rules structure in the FLC rule base-table, based on comparison between the reference speed and motor speed. The design of the fuzzy adaptation strategy is based on the fact that each dynamical aspect of the system response is mainly influenced by a group of rules. Changing the consequent of a given rule that has just been evaluated may affect the system rise-time, overshoot, steady-state error and other dynamical indices. The block-diagram representation of SFLC is shown in Figure 3.9. The inputs to the FLC is defined as

$$E_1 = \omega_{e(n)} = \omega_{r(n)}^{*} - \omega_{r(n)}$$

$$E_2 = \omega_{e(n)} - \omega_{e(n-1)} \qquad (3.12)$$

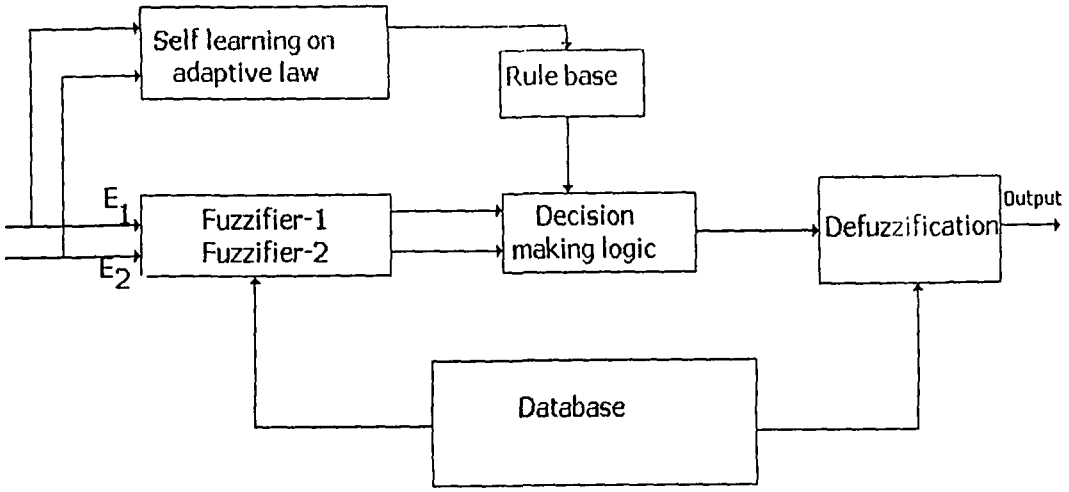

Figure 3.9: Block diagram representation of Self-Organizing Fuzzy Logic Controller

Table 3.3: Rule base table for the Self-organizing fuzzy logic controller

E1/E2	NB	NN	NS	ZO	PS	PM	PB
NB	NB	NB	NB	NB	NM	NS	ZO
NM	NB	NB	NB	NM	NS	ZO	PS
NS	NB	NB	NM	NS	ZO	PS	PM
ZO	NB	NM	NS	ZO	PS	PM	PB
PB	NM	NS	ZO	PS	PM	PB	PB
PM	NS	ZO	PS	PM	PB	PB	PB
PB	ZO	PS	PM	PB	PB	PB	PB

If the speed-error is positive, the control effort must be increased so that ω_r can reach ω_r^*. In order that the change in the current should be positive with a higher magnitude, the consequent of the rule defined by the linguistic values of E_1 and E_2 must be submitted for another "more positive value". The expected actions of adaptation mechanism can then be expressed by a group of linguistic rules. From the idea presented above, and using the same linguistic values defined for the FLC, the rule base-table of the SLFLC is constructed as shown in Table 3.3. The forms of the membership functions are the same as those used on the FLC. Rules have the form described as:

IF E_1 = PB and E_2 = NB THEN the output = ZO

If it is an active rule, the SLFLC will eventually have major changes in the current linguistic value of the consequent. To realize the adaptive strategy, the membership functions of the output are decided by a sequence of integer numbers, where higher the magnitude of the code, higher is the magnitude of the correspondent fuzzy region. The values of E_1 and E_2 are applied to the SLFLC which computes a small increment to be added to the code of the consequents related to the rules. The inference mechanism of the FLC however will take only the integer parts of the codes.

C_{NB}, C_{ZO}, C_{PB} are defined as the integer sequence for the linguistic values NB, ZO, PB respectively. Suppose that $O^{(i)}_{(n-1)}$ is the code stored in the rule base table associated with the ith rule at sampling instant n. The learning strategy is then:

$$O^{(i)}_{(n)} = O^{(i)}_{(n-1)} + \Delta O_{(n)} \tag{3.13}$$

where $\Delta O_{(n)}$ is the output of the SLFLC. The inference mechanism will take only the integer part of $O^{(i)}_{(n)}$ to calculate the output as

$$C^{(i)} = \text{int}[O^{(i)}_{(n)}] \tag{3.14}$$

The integer parts of the codes stored in the rule base-table are obviously the original codes defined above. According to those values the consequents of the active rules will jump to the required linguistic values.

3.4.5.3 Modelling of Gain Scheduled PI Speed Controller

The basic control structure of the Gain-Scheduled PI controller is shown in Fig.3.10. The gain scheduled PI controller output, which is considered as the reference torque of the motor can be described by Eqn (3.20).

$$T^* = K_P(t) \times e(t) + K_I(t) \int e(t)\ dt \tag{3.15}$$

where $e(t) = \omega_r^*(t) - \omega_r(t)$, $K_P(t)$ is the proportional gain, $K_I(t)$ is the integral gain. These gains are the functions of the speed error e(t).

$K_P(t)$ is expressed as a function of speed error as follows.

$$K_P(t) = K_{P(max)} - (K_{P(max)} - K_{P(min)}) \exp^{-(k\,|e(t)|)} \tag{3.16}$$

where k is a constant which decides the rate at which $K_P(t)$ varies between maximum and minimum values of the proportional gain.

A large proportional gain, $K_{P\,(max)}$ is used to speed up the transient response when the speed error e(t) is large and when the error e(t) becomes small, a minimum proportional gain $K_{P(min)}$ is used to eliminate overshoots and oscillations.

The integral gain $K_I(t)$ is expressed as a function of speed error signal e(t) as shown below.

$$K_I(t) = [1 - \alpha(t)]\, K_{I(max)} \quad (3.17)$$

where $0 < \alpha(t) < 1$. Then integral gain varies in the range of $0 \leq K_I(t) \leq K_{I(max)}$. Under steady state condition when the speed error e(t) is small, large integral gain is used to overcome the steady state error. When the speed error is large, a small integral gain, i.e. $K_{I(max)} = 0$ is used in order to eliminate the undesirable oscillations and overshoot.

$\alpha(t)$ takes a value either 1 or 0 as $|e(t)|$ approaches infinity (or) enters the range $0 \leq |e(t)| \leq \epsilon$.

Hence, it can be stated that,

$$\alpha(t) = 1 \quad \text{if } |e(t)| >> \epsilon \quad (3.18)$$

$$= 0 \quad \text{if } |e(t)| \leq \epsilon$$

Instead of abrupt change from 0 to 1, the integral gain K_I is expressed as

$$K_I(t) = K_{I(max)} \times \exp^{-(k|e(t)|)} \quad (3.19)$$

The value of ϵ is a fractional part of $\omega_r(t)$. In transient condition, a large control signal is used to accelerate or decelerate the motor to the reference value with in shortest possible time. During this period, $K_P(t)$ is at its maximum value and $K_I(t)$ is maintained at its minimum value. Under steady-state operating condition, the integral gain $K_I(t)$ is increased to its maximum value. These two gains are varied on line as a function of speed error, e(t).

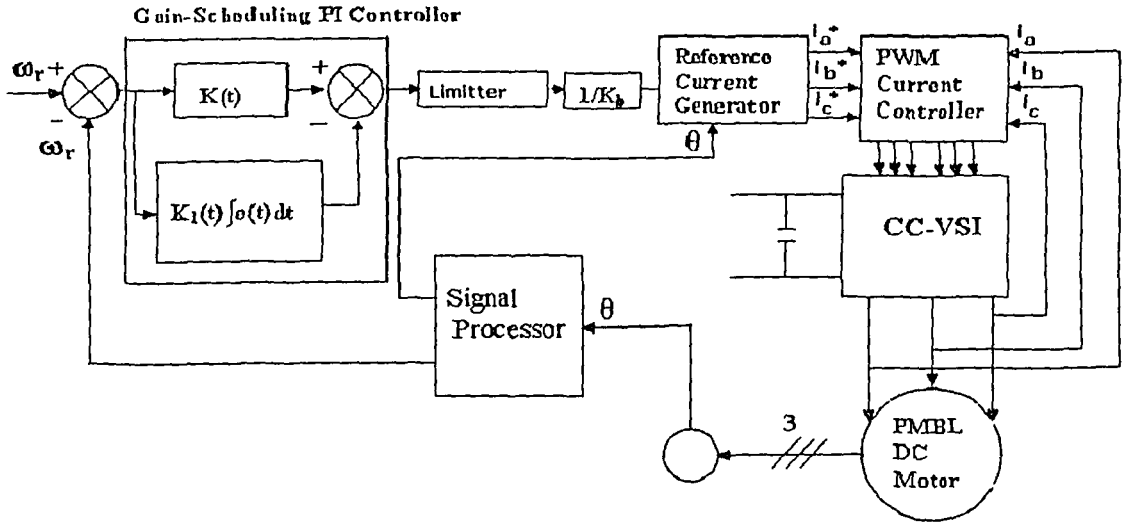

Figure 3.10 Basic Diagram of Gain Scheduling Speed Controller for PMBLDC Motor

3.4.5.4 Modelling of Hybrid FP+ID controller structure

Figure 3.11 illustrates the basic control structure of FP+ID speed controller. The hybrid fuzzy controller has the advantages of classical action. The control signal of conventional PID speed is described below:

$$\omega_{e(n)} = \omega_{r(n)}^{*} - \omega_{r(n)}.$$

$$\Delta\omega_{e(n)} = \omega_{e(n)} - \omega_{e(n-1)}$$

$$T^{*}_{(n)} = T^{*}_{(n-1)} + K_P\{\omega_{e(n)} - \omega_{e(n-1)}\} + K_I\,\omega_{e(n)} + K_D\,\{\omega_{e(n)} - 2\,\omega_{e(n-1)} + \omega_{e(n-2)}\} \quad (3.20)$$

where K_P, K_I and K_D are the proportional, integral and derivative gains of the speed controller and n is the sampling index

$$T^{*}_{(n)} = T^{*}_{(n-1)} + K_P \times \Delta\hat{u}(k) + K_I\,\omega_{e(n)} + K_D\{\omega_{e(n)} - 2\,\omega_{e(n-1)} + \omega_{e(n-2)}\} \quad (3.21)$$

where K_P, K_I and K_D are identical to the fixed gain PID speed controller, $\Delta\hat{u}$ (k) is the output of the fuzzy logic controller. The output of the above equation T^{*} is considered as the reference torque of the PMBLDC motor. The dominating term in the hybrid FP+ID controller is the proportional gain which is the responsible for reduce of overshoot and rise time. The fuzzy logic control output $\Delta\hat{u}$ (k) is a function is the function of $w_{e(n)}$ and $\Delta\omega_{e(n)}$ and is expressed as

$$\Delta\hat{u}(k) = \text{FLC}\,[w_{e(n)} \text{and}\ \Delta\omega_{e(n)}] \quad (3.22)$$

where $w_{e(n)}$ is the error between reference speed and speed of the motor and $\Delta\omega_{e(n)}$ is the change in speed error.

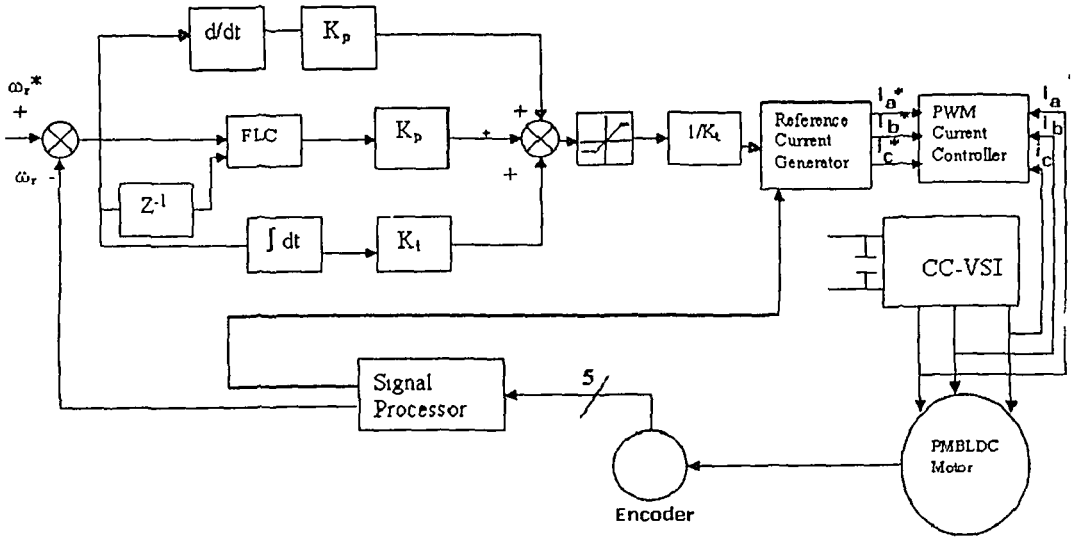

Figure 3.11 Block diagram hybrid FP+ID of PMBLDC motor

Fuzzy members are chosen as per Table 3.4.

Table 3.4: Fuzzy members

PB	PM	PS	Z or Z0	NB	NM	NS
Positive Big	Positive medium	Positive Small	Zero	Negative Big	Negative Medium	Negative Small

The triangular shaped functions are chosen as the membership functions due to the resulting control performance and simplicity. The height of the membership functions in this case is one, which occurs at the points –1, -0.57, -0.27, 0, 0.27, 0.57, 1 respectively as shown in Fig.3.8. An overlap of 50% is provided for neighboring fuzzy subsets. Therefore, at any point of the universe of discourse, no more than two fuzzy subsets will have non-zero degrees of membership. The realization of the function FLC [$w_{e(n)}$ and $\Delta\omega_{e(n)}$], based on the standard fuzzy method, consists of three stages: fuzzification, interference and defuzzification.

Fuzzification: This converts point-wise (crisp) data into fuzzy sets (linguistic variable), making it compatible with fuzzy representation.

Interference method: A linguistic rule according to the dynamic performance of the drive is tabulated in Table 3.4. The first two linguistic values are associated with the input variables $\omega_{e(n)}$ and $\omega_{e(n-1)}$, while the third linguistic value is associated with the output. For example, if error in speed is ZO and change in speed error is NS, then output is NM.

Defuzzification: The reverse of fuzzification is called defuzzification. The rules of FLC produce required output in a linguistic variable. Linguistic variables have to be transformed to crisp output. By using the center-of-gravity defuzzification method, crisp output is obtained.

Table 3.5: Fuzzy Logic Rules for hybrid (FP+ID) controller

e\ce	NB	NM	NS	ZO	PS	PM	PL
NB	NB	NB	NB	NB	NM	NS	ZO
NM	NB	NB	NB	NM	NS	ZO	PS
NS	NB	NB	NM	NS	ZO	PS	PM
ZO	NB	NM	NS	ZO	PS	PM	PB
PS	NM	NS	ZO	PS	PM	PB	PB
PM	NS	ZO	PS	PM	PB	PB	PB
PB	ZO	PS	PM	PB	PB	PB	PB

3.4.6 Modelling of Reference-Current Generator

The input to the reference current generator are reference torque (T^*) and the rotor position signal (θ_r). The magnitude of the three-phase current (I^*) is determined by using reference torque (T^*) and the back-emf constant (K_b) is as:

$$I^* = T^* / K_b \tag{3.23}$$

Depending on the rotor position, the reference-current generator generates the reference currents (i_a^*, i_b^*, i_c^*) by taking the value of reference current magnitude as I^*, $-I^*$ and zero.

Table 3.6: Reference currents corresponding to the Position Signals

Rotor Position Signal	**Reference Currents**		
θ_r	i_a^*	i_b^*	i_c^*
0° – 60°	I^*	$-I^*$	0
60° – 120°	I^*	0	$-I^*$
120° – 180°	0	I^*	$-I^*$
180° – 240°	$-I^*$	I^*	0
240° – 300°	$-I^*$	0	I^*
300° – 360°	0	$-I^*$	I^*

These reference currents are fed to the PWM current controller.

3.4.7 Modelling of PWM Current Controller

The switching logic is formulated as given below.

If $i_a < (i_a^* - h_b)$ switch 1 ON and switch 4 OFF

If $i_a > (i_a^* + h_b)$ switch 1 OFF and switch 4 ON

If $i_b < (i_b^* - h_b)$ switch 3 ON and switch 6 OFF

If $i_b > (i_b^* + h_b)$ switch 3 OFF and switch 6 ON

If $i_c < (i_c^* - h_b)$ switch 5 ON and switch 2 OFF

If $i_c > (i_c^* + h_b)$ switch 5 OFF and switch 2 ON (3.24)

where h_b is the hysteresis band around the three phase reference currents.

3.4.8 Modelling of back EMF using rotor position

The per-phase back emf's in the PMBLDC motor is trapezoidal in nature as shown in Figure 3.12 and are functions of the speed and rotor position angle (θ_r).

The normalized function of back-emf's are shown in Fig.3.12. From this, the phase back- emf's e_{an} can be expressed as:

$$e_{an} = E \qquad 0° < \theta_r < 120°$$

$$e_{an} = (6E/\pi)(\pi-\theta_r) - E \qquad 120° < \theta_r < 180°$$

$$e_{an} = -E \qquad 180° < \theta_r < 300°$$

$$e_{an} = (6E/\pi)(\theta_r-2\pi) + E \qquad 300° < \theta_r < 360° \qquad (3.25)$$

where $E = K_b \omega_r$ and e_{an} can be described by E and normalized back-emf function $f_a(\theta_r)$ which is shown in Figure 3.12 as $e_{an} = E f_a(\theta_r)$. The back emf's function of other two phases e_{bn} and e_{cn} are defined in similar way using E and the normalized back emf's function $f_b(\theta_r)$ and $f_c(\theta_r)$ as shown in Fig.3.12.

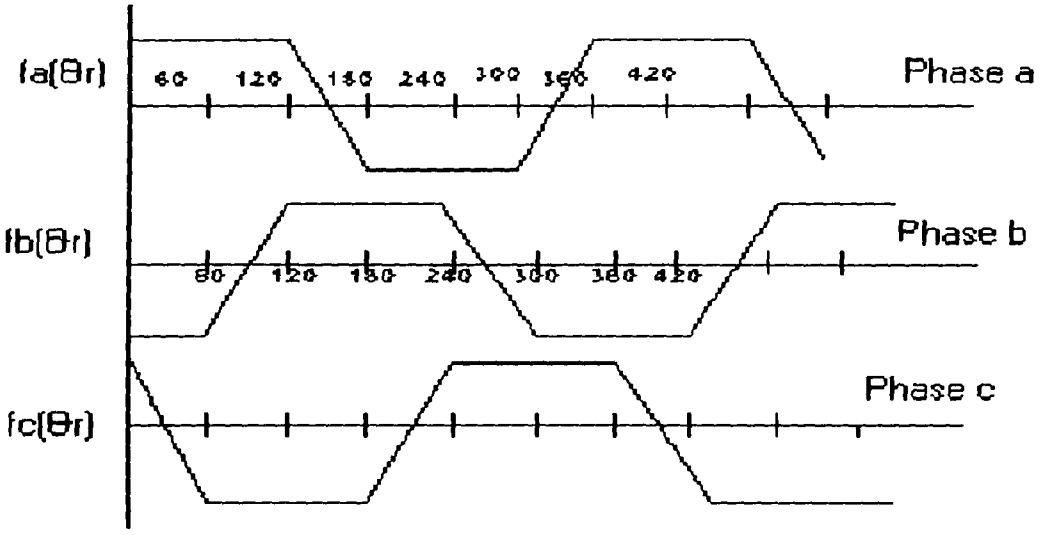

Figure 3.12: Back-EMF of PMBLDC Motor drive

3.4.9 Modelling of PMBLDC Motor and Inverter

The PMBLDC motor is modelled in the 3-phase abc variables. The general volt -ampere equation for the circuit shown in the Figure 3.13 can be expressed as:

$$v_{an} = Ri_a + p\lambda_a + e_{an} \qquad (3.26)$$

$$v_{bn} = Ri_b + p\lambda_b + e_{bn} \qquad (3.27)$$

$$v_{cn} = Ri_c + p\lambda_c + e_{cn} \qquad (3.28)$$

where v_{an}, v_{bn} and v_{cn} are phase voltages and may be designed as:

$$v_{an} = v_{ao} - v_{no},\ v_{bn} = v_{bo} - v_{no} \text{ and } v_{cn} = v_{co} - v_{no}. \qquad (3.29)$$

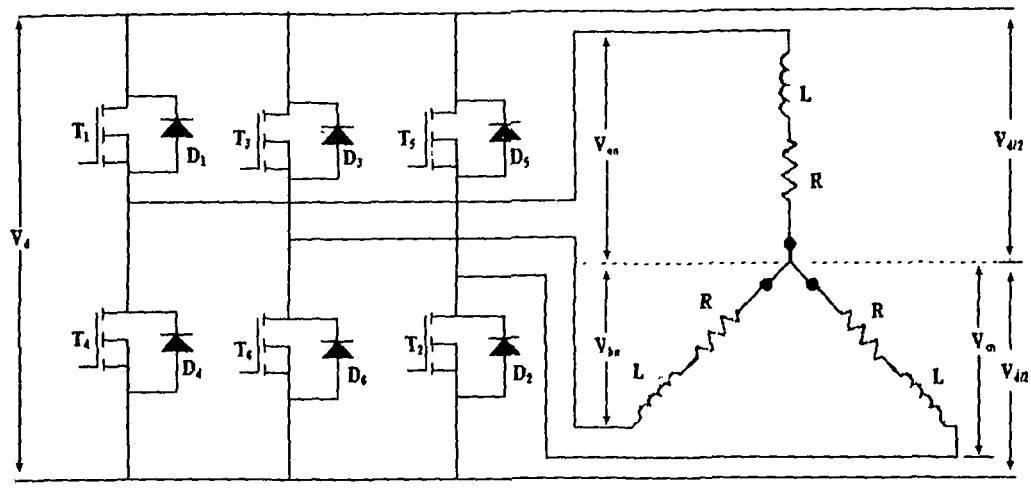

Figure 3.13: Inverter Circuit of PMBLDC Motor drive

where v_{ao}, v_{bo}, v_{co} and v_{no} are three-phase and neutral voltages referred to the zero- reference potential at the mid- point of DC link (o) shown in the Fig.3.13. R is the resistance per phase of the stator winding, p is the time differential operator and e_{an}, e_{bn} and e_{cn} are phase to neutral back emf's. The λ_a, λ_b and λ_c are total flux linkages of phase windings a, b and c respectively. These values can be expressed as:

$$\lambda_a = L_s i_a - M (i_b + i_c) \quad (3.30)$$

$$\lambda_b = L_s i_b - M (i_a + i_c) \quad (3.31)$$

$$\lambda_c = L_s i_c - M (i_a + i_b) \quad (3.32)$$

where L_s and M are the self and mutual inductance, respectively

The PMBLDC motor has no neutral connection and hence this results in:

$$i_a + i_b + i_c = 0 \quad (3.33)$$

Substituting equation (3.33) into equations (3.30), (3.31) and (3.32) the flux linkages are given as:

$$\lambda_a = i_a(L_s + M),\ \lambda_b = i_b(L_s + M) \text{ and } \lambda_c = i_c(L_s + M) \quad (3.34)$$

By substituting Eqn. (3.34) in volt-ampere eqns. (3.26) – (3.28) and rearranging these equations in a current derivative of state-space form, one gets

$$pi_a = 1/(L_s+M) [v_{an} - Ri_a - e_{an}] \quad (3.35)$$

$$pi_b = 1/(L_s+M) [v_{an} - Ri_b - e_{bn}] \quad (3.36)$$

$$pi_c = 1/(L_s+M) [v_{cn} - Ri_c - e_{cn}] \quad (3.37)$$

The developed electromagnetic torque may be expressed as:

$$T_e = [e_{an} i_a + e_{bn} i_b + e_{cn} i_c] / \omega_r \quad (3.38)$$

where ω_r is the rotor speed in electrical rad/sec.

This expression for the torque runs into the computational difficulty at zero speed as the induced emf's are zeros. The back-emf's are expressed as functions of position θ_r, which can be written as:

$$e_{an} = k_b\, f_a(\theta_r)\, \omega_r \tag{3.39}$$

$$e_{bn} = k_b\, f_b(\theta_r)\, \omega_r \tag{3.40}$$

$$e_{cn} = k_b\, f_c(\theta_r)\, \omega_r \tag{3.41}$$

where $f_a(\theta_r)$, $f_b(\theta_r)$ and $f_c(\theta_r)$ are function of rotor position with a maximum of plus or minus 1 are identical to induced emf in shape.

Substituting equations (3.39) – (3.41) into equation (3.38), the torque expression becomes:

$$T_e = k_b\{ f_a(\theta_r)\, i_a + f_b(\theta_r)\, i_b + f_c(\theta_r)\, i_c\} \tag{3.42}$$

The mechanical equation of motion in speed derivative form can be expressed as:

$$p\omega_r = (P/2)\,(T_e - T_l - B\,\omega_r)\,/J \tag{3.43}$$

where P is the number of poles, T_l is the load torque in N-m, B is the frictional coefficient in N-ms/rad, and J is the moment of inertia, kg-m^2.

The derivative of the rotor position (θ_r) in state-space form is expressed as:

$$p\theta_r = \omega_r \tag{3.44}$$

The potential of the neutral point with respect to the zero potential (v_{no}) is required to be considered in order to avoid imbalance in the applied voltage and simulate the performance of the drive.

This can be obtained as follows:

Substituting equation (3.29) in the volt-ampere equations (3.26) – (3.28) and adding them together gives:

$$v_{ao} + v_{bo} + v_{co} - 3\, v_{no} = R(i_a + i_b + i_c) + (L_s + M)(pi_a + pi_b + pi_c) + (e_{an} + e_{bn} + e_{cn}) \tag{3.45}$$

Substituting equation (3.33) in equation (3.45) we get:

$$v_{ao} + v_{bo} + v_{co} - 3v_{no} = (e_{an} + e_{bn} + e_{cn})$$

Thus,

$$v_{no} = [v_{ao} + v_{bo} + v_{co} - (e_{an} + e_{bn} + e_{cn})] / 3 \tag{3.46}$$

The set of differential Equations mentioned in Eqns. (3.35), (3.36), (3.37), (3.43) and (3.44) defines the developed model in terms of the variables i_a, i_b, i_c, ω_r, θ_r and time as an independent variable.

3.5 Sensorless Control of PMBLDCM Drive System

3.5.1 General

Permanent-magnet brushless motors have wide applications due to their high power-density and ease of control. The motor requires a rotor-position sensor for starting and for providing proper commutation sequence to turn on the switches in the inverter. The position sensors such as resolvers, absolute position encoders and Hall sensors increase cost and size of the motor. Furthermore, the Hall sensors need at least eight signal wires. These sensors, particularly Hall sensors, are temperature sensitive, limiting the operation of the motor to below 75°. The position sensors also limit the speed to about 6000 rpm. In some cases, it may not be possible to mount any position sensor on the shaft of the motor. Because of these limitations of the motor operation with position sensors, sensorless operation of PM brushless motors is receiving significant attention in recent years.

Permanent-magnet motors are generally classified as permanent-magnet-brushless DC motors with trapezoidal back emf and permanent-magnet-synchronous motors with sinusoidal back emf. Several schemes for sensorless operation of PM motors are reported in recent years (Hzuka, Uzuhashi, Rano, Endo and Mohri, 1985; Rajeshekara and Kawannura, 1994; Moreia, 1994; Bhownik, 1991 & 1997; Song, Rahman and Lim, 1997; Ertugrul and Acarnley, 1994; Kumar and Singh, 2002). This chapter describes the simulation of sensorless control by using direct back-emf method. As the PM motor is not self-starting, starting strategies without using position sensors are also briefly discussed. The section summarizes different schemes of position sensorless-operation for the speed control of PMBLDC motor. Also simulation details of sensorless operation based on back-emf sensing are explained.

3.5.2 Different Sensorless Schemes of PMBLDC Motor

3.5.2.1 Terminal Voltage Sensing

In this method, the three terminal voltages v_a, v_b, v_c are measured. At the instants of the zero crossing of the back-emf waveform, the terminal voltage is equal to the neutral voltage. When the back-emf of phase A crosses zero, then $v_a=v_n=(1/2)\,v_{dc}$. In order to use this zero-crossing point to drive the switching sequence, this point has to be phase-shifted by 30°. Also to achieve this, the terminal voltages are first

converted to triangle waveforms and then compared with the neutral voltage. The output of the comparators determines the switching sequence. The position detection scheme based on terminal voltage sensing is simple for steady-state operation (Hzuka, Uzuhashi, Rano, Endo and Mohri, 1985; Ertugal, 1992; Rajeshekara and Kawannura, 1994; Hu Dawson and Anderson, 1995; Kim and Yoon, 2002).

3.5.2.2 Third Harmonic Voltage Integration

The rotor position is determined based on the third-harmonic voltage component (Ogasawara and Akagi, 1991; Rajeshekara and Kawannura, 1994; Ertugrul and Acarnley, 1994; Rajasekhara, Kawamura and Matsuse, 1996; Kumar and Singh, 2002). To detect the third-harmonic voltage, a set of three resistances is connected across the motor windings. The voltage across the two neutrals V_{NM} determines the third-harmonic voltage. This voltage is integrated and fed to a zero-crossing detector to determine the switching sequence for turning on the devices. The main disadvantage is the relatively low value of the third-harmonic voltage at low speed. It is difficult to detect the right relative phase position between the third harmonic and the corresponding phase. If the sequence is lost, the system has to be restarted again. The amplitude and phase of the third harmonic is directly related to the saturation.

3.5.2.3 Method Based on Monitoring Switching States in the Inverter

It involves detection of ON/OFF state of the switching devices of the inverter to determine a commutation instant. The method is based on the motor with a trapezoidal back emf (Ogasawara and Akagi, 1991; Ertugal, 1992). The position information is given on the basis of the conducting state of freewheeling diodes in an open-phase over wide speed-range. This method is suitable for medium and high - speed applications.

3.5.2.4 Position Detection Using Phase Current Sensing

The magnetic flux of the motor is in phase with the stator current. Therefore, near exact rotor position signals can be obtained just by detecting and processing the phase current waveforms. Using a signal processing circuit, the phase-current signals can be converted into the required rotor-position signals (Ertugal, 1992; Ertugrul and Acarnley, 1994). Establishing the starting strategy could be a problem. The system can be noise sensitive. It also depends on the arbitrary reference level for comparing the current signals.

3.5.2.5 Observer Methods

An observer reconstructs a physical variable (such as position) which is not directly measurable. The observer method proposed by Dhauadi and Mohan uses a Kalman Filter technique to estimate the speed and position from measurements of stator voltage and currents. The method needs a motor, which is dq transformable.

3.5.2.6 By Using a Special Windings

The method proposed by Binns et al requires modification by the addition of search coils on the stator teeth of the motor, and suitable additional cabling is required between the motor and the controller. Induced voltages in the special windings are in phase with back emf and have no commutation transients.

Some of the above methods need neutral point of the motor and some of them need special types of windings for position detection. In this investigation, position sensing from back-emf of the motor without accessing neutral point is considered. Moreover back-emf sensing method is simple and cost effective.

3.5.3 Different Starting Strategies of PMBL Motor

The Table 3.9 presents a glimpse of the various starting strategies concerning the PMBL motor as follows.

Table 3.7 Summary of indirect position sensing methods in brushless PM motors

METHODS	MOTOR TYPES	LIMITATIONS
Evaluation or estimation of back emf: (a) direct back emf detection. (b) Estimation of back emf	Discontinuous current controlled drives. PMBLDC and PMSM motors.	Sensitive to switching transients. Needs a special starting method. Method is sensitive to change of winding resistance and measurement noise.
Third-harmonic Voltage Detection.	Star-connected PMBLDC Motor.	The method needs a motor, which has reasonable amount of third-harmonic voltage. Requires reference back-emf zero-crossings. It is difficult to sense the third-harmonic voltage at low speeds.
Monitoring Current or Calculation Method of the Phase Inductance.	PMSM and PMBLDC Motors.	Requires a starting method from standstill. Limitation at higher currents and speeds. Motors which have variable winding inductance.
Observer Methods.	PMSM and PMBLDC Motors.	Need starting method from standstill. Motor d-q transferable mainly suffer from complex estimation techniques.
Monitoring Switching States in the Inverter	PMBLDC motors	Requires a starting method from rest.
Using a Special Winding	PMBLDC motors	Requires modification in the motor. Number of connection increases between the motor and the controller.

The sensorless schemes are not self-starting. In order to sense the back-emf or to calculate the position based on measured voltages and currents, the motor must be first started and brought up to a certain speed where the terminal quantities can be detected. Most of the starting strategies presented are based on arbitrarily energizing the two or three windings and expecting the rotor to align to a certain definite position.

To start the motor, the currents in the motor phases are injected corresponding to a certain increasing frequency-profile. Then at some instant, the rotor aligns itself to the desired position to provide accelerating torque capability. Once the speed of the motor reaches a threshold value, the developed back-emf is used for position information and the required switching sequence is established. The motor can also be started by applying a specific PWM pattern (say, devices T1 and T2 are turned ON

and OFF, Figure 3.13) to the inverter. This is repeated several times to align the rotor in the direction of a particular phase winding. The regular sensorless control strategy is then followed.

The above strategies have poor dynamic responses and the rotor can be in the hunting mode. Besides, the above techniques do not give position information at standstill. If the electrical drive system has been switched off, it is not possible to know the actual rotor position in one period with respect to the stator phases.

3.6 Mathematical Modelling of Sensorless Speed Controller

Algorithm per sensorless operation, which is based on back emfs of the motor, has been presented in this work. The model of the drive system consists of speed controller, reference current generator based on rotor position detection, current controller etc. Runge-Kutta method is used for solving differential equations of the drive model. The model of the sensorless drive is similar to that already explained in sections 3.4.6 – 3.4.9 excepting speed and position sensing scheme. The entire model of the sensorless drive system is described below.

3.6.1 Modelling of Speed Controller

Speed is detected by measuring the time elapsed between two successive pulses that are deducted from the zero crossings of back-emf. After measuring the magnitude of the motor speed, it is compared with the reference speed. The error in speed is processed through the PI speed controller to get the torque command. The zero-crossing instants of the back-emf and the corresponding position signal are shown in Figure 3.14.

The rotor speed $\omega_{r(n)}$ is compared with the reference speed $\omega_{r(n)}^{*}$ and the resulting error in speed is estimated at the nth sampling instant as:

$$\omega_{e(n)} = \omega_{r(n)}^{*} - \omega_{r(n)} \tag{3.47}$$

The magnitude and direction of the speed-error may be positive or negative depending upon the rotor-speed and its reference value. The speed-error is processed in a PI speed controller.

The output of the speed controller at the nth sampling instant is

$$T_{(n)} = T_{(n-1)} + K_P\{\omega_{e(n)} - \omega_{e(n-1)}\} + K_I\,\omega_{e(n)}. \tag{3.48}$$

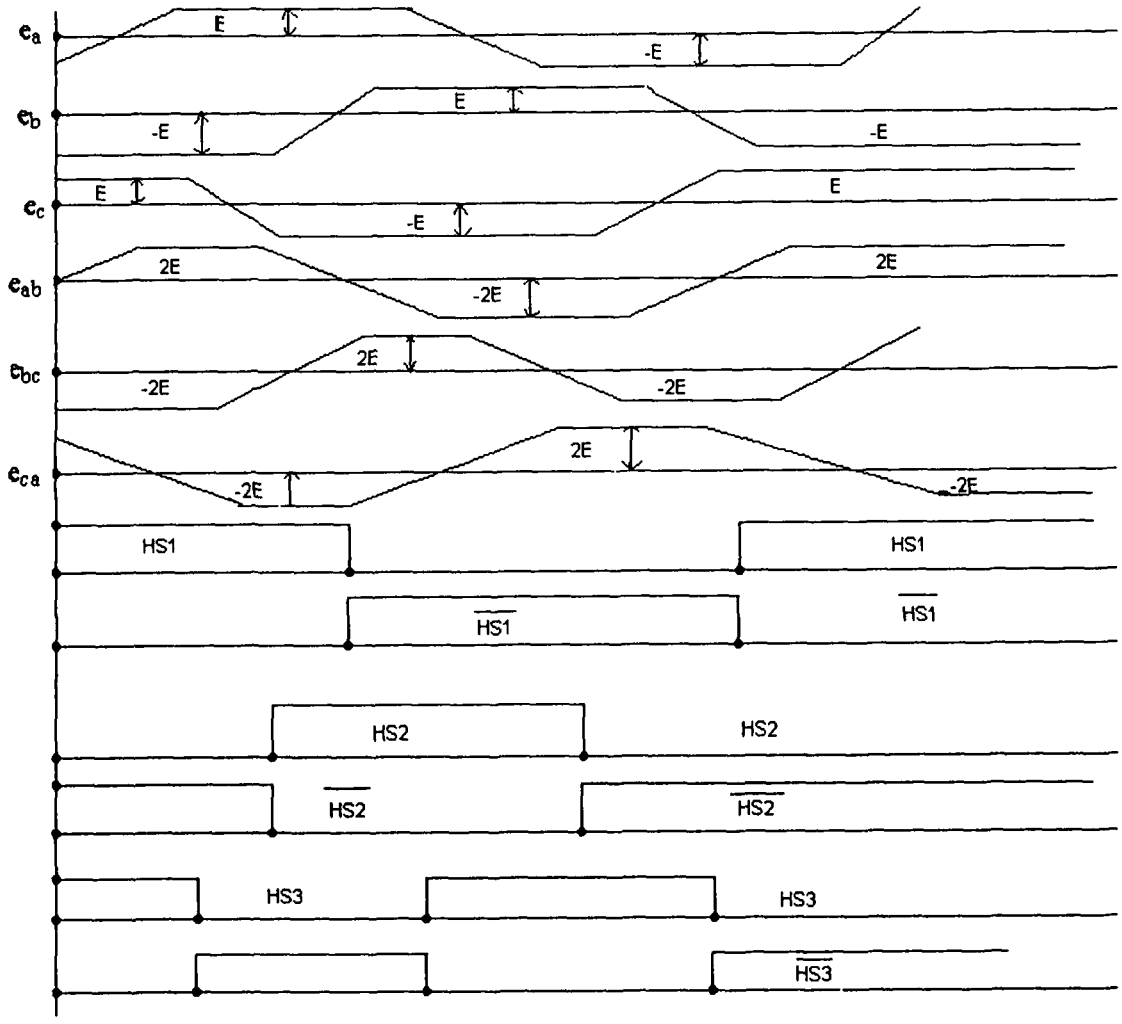

Figure 3.14: Zero-crossing instants of the back-emf and the corresponding position signals

3.6.2 Modelling of position detection using Back EMF

e_a, e_b, e_c are the induced emf's in the phase windings and are trapezoidal in shape as shown in Figure 3.15. The line voltages of the PMBLDC motor e_{ab}, e_{bc}, e_{ca} are derived from the induced phase voltages as $e_{ab}= e_a- e_b$, $e_{bc}= e_b- e_c$, $e_{ca}= e_c - e_a$. From these three line voltages, the three position signals namely (HS1, HS2 and HS3) are deducted by zero-crossing detector. By logically ANDing these 180-degree pulse signals, the commutation signals are derived and used in simulation. The modelling of switches is carried out in the following way.

Table 3.8: Conduction period

Rotor position in degrees	Switch position
0-60	Switch 5 & 6 are ON/OFF
60-120	Switch 6 & 1 are ON/OFF
120-180	Switch 1 & 2 are ON/OFF
180-240	Switch 2 & 3 are ON/OFF
240-300	Switch 3 & 4 are ON/OFF
300-360	Switch 4 & 5 are ON/OFF

3.7 Conclusion

Chapter 3 introduces the various models of controllers used for simulation. The different types of control structures presented in this work are capable of taking care of transients in speed, current and torque variations during starting, reversal and load perturbations. Since the transient currents drawn by the motor never exceed the maximum permissible limits, it can be concluded that the motor control structure takes care of the over-current protection. The dynamic responses of the drive are observed to be improved with SMC and Fuzzy based controllers. It is also observed from this investigation that all the speed controllers used have their own advantages and disadvantages and the choice depends upon the requirements of a particular application. It has been observed that PI and PID controllers are simple and easy to implement, but they exhibit poor performance under load disturbances and nonlinearities. SMC is observed to suffer from chattering problems. FP-PI, FP-PID and FSMC controllers are observed to be more robust to load variations than PI, PID and SMC respectively. FP-PI controller also shows significant improvement in transient and steady state responses of the PMBLDC drive. Compared to PI and PID speed controllers, the Gain-Scheduled PI, Self-Organizing Fuzzy Logic and Hybrid (FP+ID) controllers show better performances with respect to overshoot, rise time and load disturbances.

The speed control of PMBLDC drive without a shaft-positioning sensor has been simulated. The method employed sensing of the motor. The starting of the motor at standstill has been realized by applying a specific PWM pattern. This method of starting needs no extra hardware. The method of sensing position from back-emf is observed to be more practical and suitable for steady state operation. The method can be applied to any winding connection, either star with or without accessible neutral point or delta.

CHAPTER 4

MATHEMATICAL MODELLING OF PMSM MOTOR DRIVE

4.1 General

Similar to PMBLDC motors Permanent Magnet Synchronous Motors (PMSM) have higher torque-to-weight ratio as compared to other AC motors. At higher speeds permanent-magnet machines also retain higher efficiency because of reduced iron losses. Hence these machines have been quite useful for high performance and high-speed applications. However, the extremely high unit cost has restricted their use in larger numbers in industrial applications. A cost-effective design will make the use of the motor more expensive (Dhaoudi and Mohan, 1991).

The PMSM is a rotating electric machine where the stator has a classical three-phase winding like that of an induction motor and the rotor has surface-mounted permanent magnets (Chaaban., Mellor and Binns, 1990). In this respect, the PMSM is equivalent to an induction motor where the air-gap magnetic field is produced by permanent magnets. The use of permanent magnets to generate a substantial air-gap magnetic flux makes it possible to design highly-efficient PM motors (Thomas, 1987).

Among AC motors, the PMSM has high power-density and torque-to-inertia ratio that makes it the most promising for replacing DC motors for servo applications (Slemon. and Gumaste, 1983). The PMSM with sinusoidal flux distribution is preferred over the one with trapezoidal flux distribution due to lower torque ripple. For a PMSM the rotor position information is fed back to the controller which generates the stator voltages according to the rotor-position. So the rotor is always in synchronism with the rotating magnetic field. The rotor and stator fluxes are always at right angles under normal operating conditions, thus giving maximum torque. Such an arrangement is called the self-synchronous motor.

The PMSM has a wound stator, a permanent magnet rotor assembly and internal or external devices to sense roto-position. The sensing devices provide logic signals for electronic switching of the stator windings in the proper sequence to maintain rotation of the magnet assembly. The combination of an inner permanent-

magnet rotor and outer windings offers the advantages of low rotor inertia, efficient heat dissipation, and reduction of the motor size. Moreover, the elimination of brushes reduces noise vibration, EMI generation and suppresses the need for brush maintenance. Two configurations of permanent magnet motor are usually considered: the trapezoidal type and the sinusoidal type. Depending on how the stator is wound, the back-emf will have a different shape. To obtain the maximum performance from each type of permanent magnet synchronous motor, an appropriate control strategy has to be implemented (Jahns, Kliman and Neuman, 1980). The trapezoidal motor called brushless DC motor (BLDC) uses a "two phases on" strategy, whereas the sinusoidal motor offers its best performances when driven by sinusoidal currents. The sinusoidal voltage waveform applied to this motor is created by using the space vector modulation technique.

Several control algorithms (Slemon and Gumaste, 1983; Kenjo and Nagamori, 1985; Ostovic, 1987; Miller, 1989; Verster and Enslin, 1990; Ziyad and Lynch, 1991; Johns, 1994; Zhou, Rahman and Jabbar, 1994; Gieras and Wing, 1996; Singh and Kumar, 2005) have evolved for achieving high-performance vector-control of the PMSM. These are based on linear control techniques like PI/PID compensation. Improvement for better rejection of disturbances by using back-emf compensation techniques has been suggested. However, the PMSM is non-linear and exhibits coupled dynamics. As a result, PI controllers are inadequate in applications where good transient performance under all motor operating conditions is desired. This has prompted the application of modern control techniques for PMSM control.

The Permanent Magnet Synchronous Motor (PMSM) is also one of the types of brushless PM motor, where, the windings of the motor are sinusoidally distributed and generate sinusoidal induced emfs or back emfs. The salient features of PMSM are already explained in Chapter-1.

4.2 Principle of PMSM Motor Drive

The rotor excitation field in a synchronous motor can be obtained by replacing the electromagnet field-poles of Figure 4.1 by permanent magnets. Magnetically hard materials such as ceramic ferrites or alloys of iron, nickel and cobalt may be used (Irdand, 1968; Rahman and Slemon, 1985; Ritchter, Miller, Neumann and Hudson, 1985; Low and Binns, 1986; Mellor, Ramsden, and Nguyen, 1987; Chaaban and.Binns, 1991). The modern trend is to use samarium-cobalt rare-earth materials

(Sawyer and Edge, 1977) because their high remanance and high coercive force permit reductions of magnet size and weight.

An inherent problem with permanent-magnet motors is that the field current and the field flux are not adjustable. The internal e.m.f remains proportional to speed, even in the overspeed (constant horsepower) range. With conventional fixed-frequency operation this does not matter since the speed is constant In adjustable speed (i e. adjustable frequency) applications, calling for overspeed, high terminal voltages may be required, necessitating increased rating of the drive inverter.

A permanent-magnet motor eliminates the need for a d.c. supply and avoids excitation winding copper losses (Mecrow, Jack and Masterman, 1993). Because the excitation-flux is constant, the motor cannot be used for power-factor control. Also, the constant excitation flux tends to inhibit the induction action starting torque, which is lower than for a wound-field motor. Because of their high power/weight ratio the permanent-magnet synchronous motors are used in high-speed, 400Hz aerospace applications

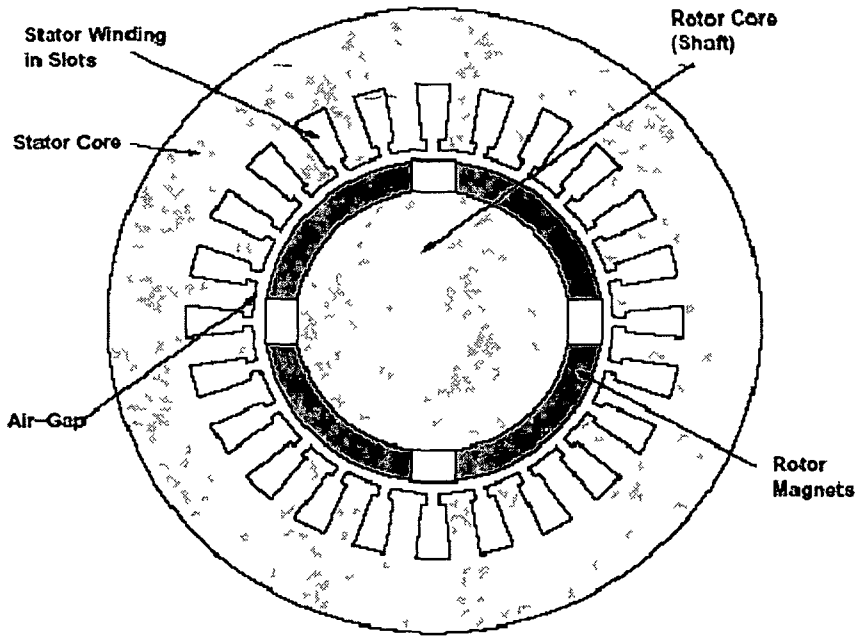

Figure 4 1 Schematic Diagram of PMSM motor Drive

4.3 Description of the PMSM Motor Drive System

Figure 4.2 illustrates the basic building blocks of the PMSM drive considered in this investigation The PMSM drive (Slemon and Gumaste, 1983, Sebastian, Slemon and Rahman, 1986, Chaaban, Mellor and Binns, 1990; Chaaban, Mellor and

Binns, 1995; PuttaSwamy, 1996; Soulard and Nee, 2000; Bernal-Fernandez, Garcia-Cerrada and Faure, 2001; Barakat, El-meslouhi and Dakyo, 2001; Singh and Kumar, 2005) system consists of discrete speed controller, reference current generator, PWM current controller, position sensor, a MOSFET based current controlled VSI and the PMSM (Kliman and Neuman, 1980; Dote, 1990; Jahns, Johns, 1994; Kim and Yoon, 2002; Rahman, Vilathgamuwa, Uddin and Tseng, 2003; Uddin, Abido and Rahman, 2004). The rotor speed ω_r is compared with the reference speed ω_r^* and the error in motor speed is processed in the PID speed controller for each sampling interval. The output of this is considered to be the reference torque T^*. The quadrature-axis reference I_q^* is obtained by using the reference torque T^* and the torque-constant K_t. For low-speed operation of PM motors, the flux weakening (Jahns, 1987; Parviainen, Pyrhönen, and Niemelä, 2001) effect is not considered in this investigation, however, the effect of flux weakening is employed for high-speed operation of the PMSM drive. Hence in this investigation, the direct-axis reference current (i_d^*) is considered to be zero for low-speed operation. The d-q axis reference currents i_d^* and i_q^* are used to generate the reference currents i_a^*, i_b^* and i_c^* in the reference current generator. The reference currents have the shape of the sinusoidal wave in phase with respective back-emfs to develop constant unidirectional torque. In PWM current regulating block, the motor winding currents i_a, i_b and i_c are compared with the reference currents i_a^*, i_b^* and i_c^* and the switching commands are generated for the inverter devices to drive the PMSM.

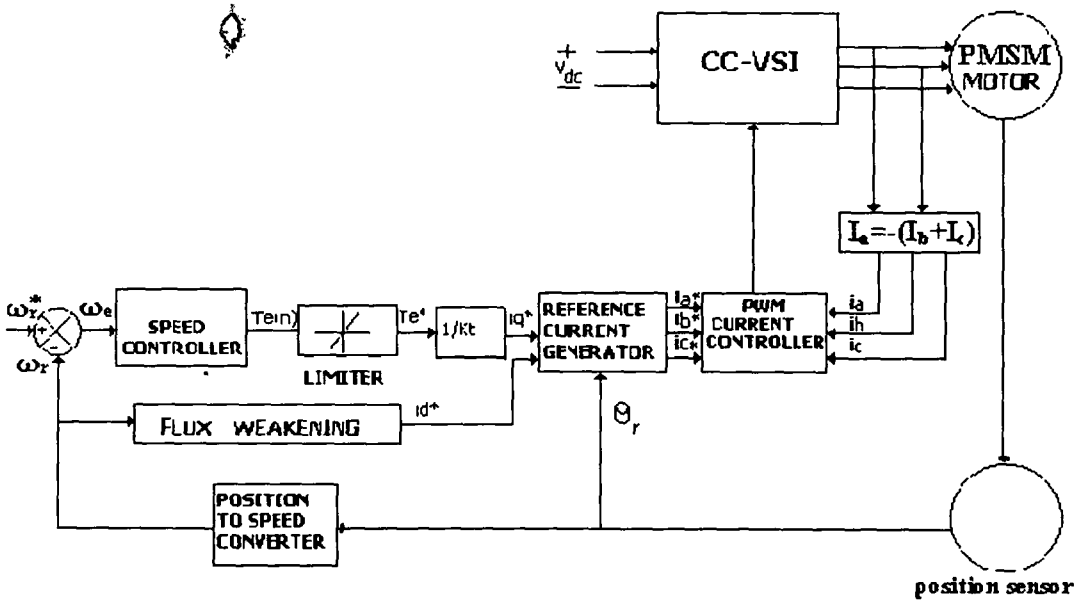

Figure 4.2: Schematic Block Diagram of PMSM Drive

4.4 Types of Speed Controllers

The speed controller forms the most important section of the motion control system which helps in controlling the motor performances. There are four different types of speed controllers which are considered in the present studies. These are the Proportional plus Integral (PI), the Proportional plus Integral plus Derivative (PID), the Sliding Mode (SM) and the Fuzzy Logic controllers which are more advanced ones belonging to the intelligent type of the controllers. There has been tremendous research towards different types of speed controllers to improve the dynamic performance of the drive (Ostovic, 1987; Consoli and Testa, 1991; Le-Huy, Viarouge and Kamwa, 1995; Cerrupto, Consoli and Raciti, 1997; Uddin, Radwan and Rahman, 2002). Closed-loop operation of digital speed controller is useful especially in applications such as in robots, aerospace and servo drives, where precise control is needed (Gieras and Wing, 1996; Friedrich and Kant, 1998; Yang, 2001; Rahman, Vilathgamuwa, Uddin and Tseng, 2003). Literature reveals (Sebastian, Slemon and Rahman, 1986; Pillay and Krishnan, 1987; Quian and Rahman, 1993; Morimoto, Sanada and Takeda, 1994; Kim, Cheng and Moon, 1995) that different types of speed controllers have been used for various applications. In this investigation, the dynamic performance of the drive system is analyzed using different types of speed controllers and the simulated results are obtained for different operating conditions such as starting, speed reversal and load perturbations. The control performance of PMSM drive is influenced by uncertainties of the plant which features parametric variations, external load disturbances, unmodelled and nonlinear dynamics. This has boosted the use of nonlinear control schemes such as model reference adaptive control, variable structure control etc. In this investigation, the transient and steady-state responses of the drive are examined with different speed controllers like PI, PID, SMC and Fuzzy logic controllers for the simulation of the PMSM drive system. Of these, the PI and PID are conventional controllers whereas the SMC, Fuzzy Logic Controllers are modern controllers.

The main objective is to compare the performance of the drive with different types of controllers and to examine the effectiveness of different controllers for a given application; and further to establish the viability of the proposed model to demonstrate the versatility of applications in different conditions.

4.4.1 Different Types of Speed Controllers

In proportional control the actuating signal for the control action is proportional to the error signal. The error signal is the difference between the reference input signal and the feedback signal obtained from the output. For the system shown in Figure 4.3, the actuating signal is proportional to the error signal. Therefore the system is called proportional control system. It is desirable that the control system be underdamped from the point of view of quick response. An underdmped control system exhibits exponentially decaying oscillations of the output response with respect to time during the transient period. Without sacrificing the steady-state accuracy the maximum overshoot can be reduced to the same extent by modifying the actuating signal.

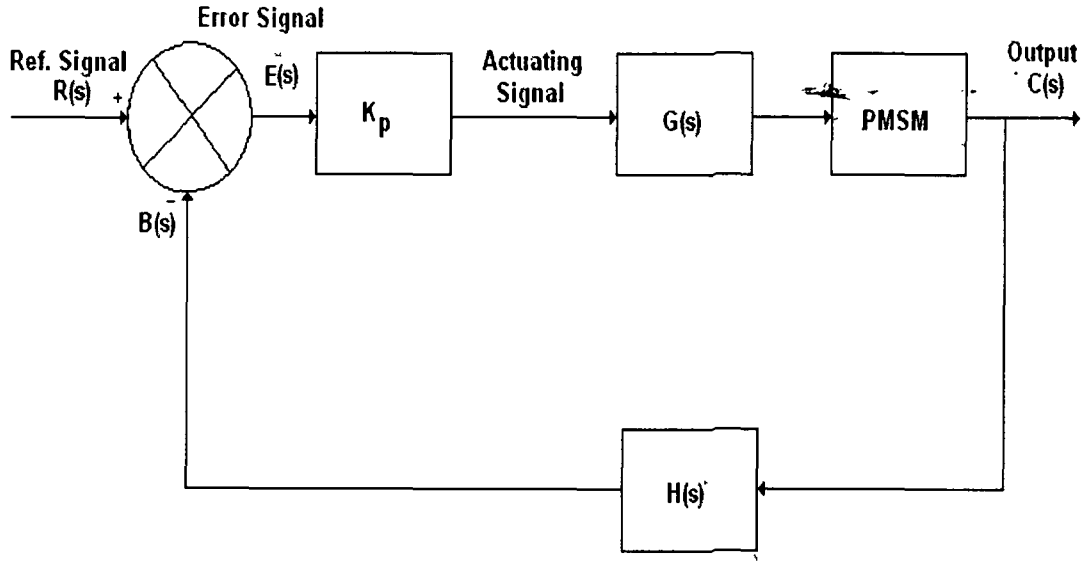

Figure 4.3: Proportional type of controller

4.4.2 Proportional and Derivative Controller

For the derivative control action the actuating signal consists of proportional error-signal added with derivative of the error signal (Figure 4.4). Therefore the actuating signal for the derivative control action is given by

$$Ea(s) = e(s) + s.\ T_d\ E(s)$$

So the transfer function of the system is obtained as:

$$C(s) / R(s) = (1+sT_d)\ \omega_n^2 / s^2 + (2\ \xi\ \omega_n + \omega_n^2\ T_d)\ s + \omega n^2)$$

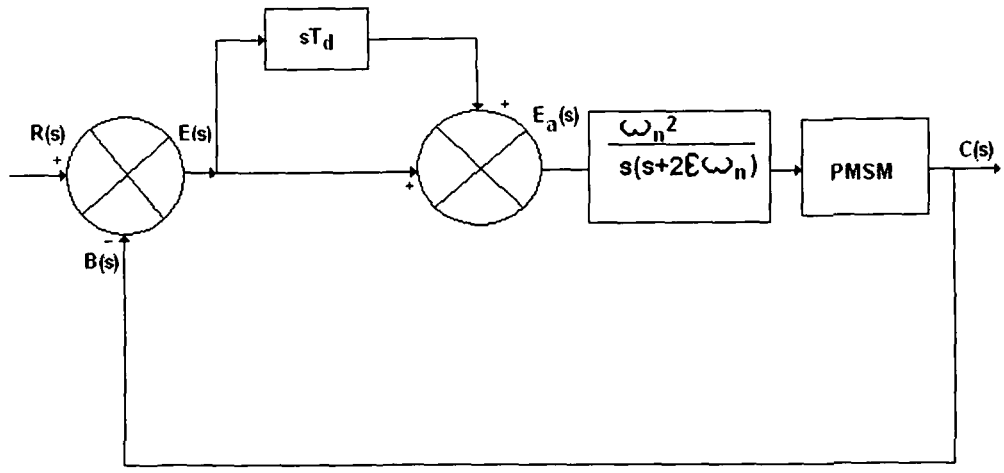

Figure 4.4: Proportional and Derivative controller

4.4.3 Proportional and Integral Controller

PI controller is widely used in industry due to its easy design, simple structure and ease of implementation. A fixed gain PI controller operates satisfactionary as long as the operating point does not change. Its steady-state accuracy is of primary importance. The PI control is still the best choice in terms of cost effectiveness. It can also be designed to have a faster transient response, but then it becomes very sensitive to parametric variations. For integral control action the actuating signal consists of proportional error signal added with integral of the error signal (Figure 4.5) .Therefore the actuating signal for integral control action is given by

$$Ea(s) = E(s) + K_i E(s)/ s$$

So the transfer function of the system is obtained as:

$$C(s) / R(s) = (s+ K_i)\, \omega n^2 / s^3 + 2\, \xi\, \omega_n\, s^2 + \omega n^2\, s + Ki\, \omega_n^2$$

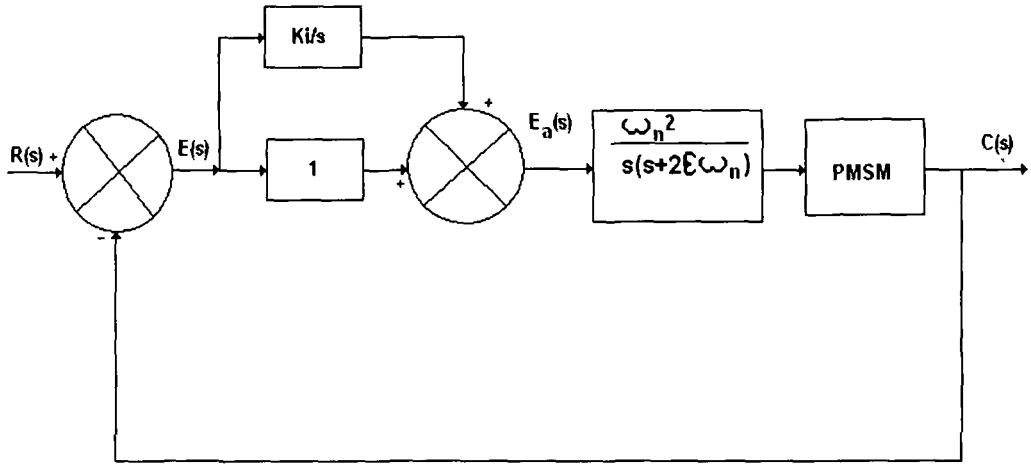

Figure 4.5: Proportional and Integral controller

4.4.4 Proportional Plus Derivative Plus Integral (PID) controller

Conventional PID controller is extensively used in industry for its simple control structure, ease of design and comparatively lower cost. Moreover, it can be easily implemented in a closed-loop operation of the drive system. The PID controller mainly consists of three controller gains namely, the proportional, integral and derivative gains. Traditionally, a conventional fixed gain PID controller with its proportional, integral and derivative gains tuned properly for given operating condition, provides satisfactionary transient response so long as the operating point does not deviate too much from initial position. Generally, in response to an input signal, it is desirable for the drive system to have a fast response, reasonably small overshoots and zero steady-state error. Moreover the system should be insensitive to load-torque disturbances. For PID control the actuating signal consists of proportional error signal added with derivative and integral of the error signal (Figure 4.6). Therefore the actuating signal for PID control is

$$Ea(s) = E(s)\,[1+sT_d+K_i / s]$$

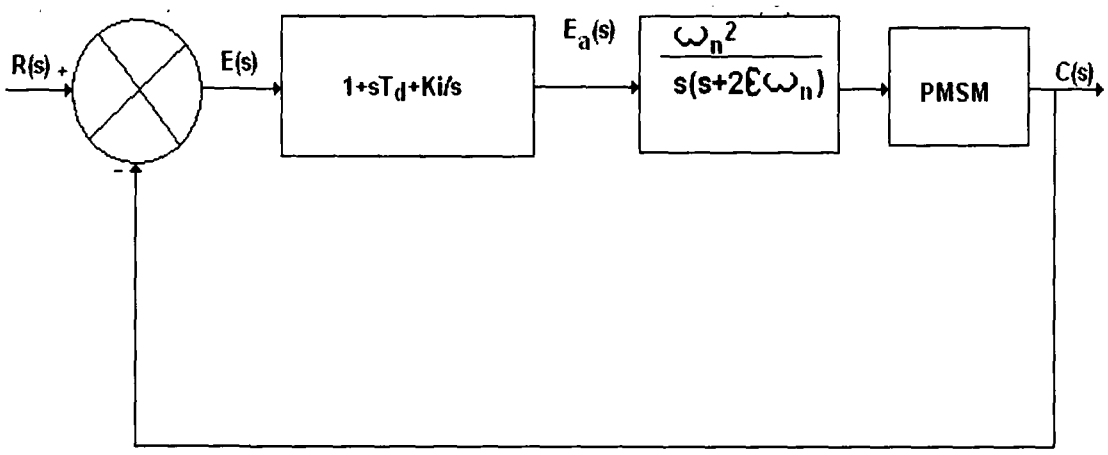

Figure 4.6: Proportional Plus Derivative plus Integral (PID) controller

4.5 Modelling of a Drive System

The PMSM drive system consists of speed controller, vector controller, hystresis controller/ PWM controller, current-controlled inverter and the motor. All the components of the drive system are modelled independently and integrated together in order to obtain complete method used for the purpose of motor performance simulation.

4.5.1 Modelling of Speed Controller

This system utilizes the digital PID speed controller. The rotor speed Wr(n) is compared with the reference speed Wr*(n) and the resulting error in speed is estimated at the nth sampling instant as:

$$We(n) = Wr^*(n) - Wr(n) \tag{4.1}$$

The magnitude and direction of the speed-error may be positive or negative depending upon the rotor speed and its reference counterpart. The speed-error is processed in a PID speed controller. The output of the speed controller is considered as torque signal at (n-1) th sampling instant

$$T(n-1) = Kp\ We(n-1) + Ki\Sigma We(j) + Kd\ \{We(n-1) - We(n-2)\} \tag{4.2}$$

The output of the speed controller at the nth sampling instant is given as

$$T(n) = Kp\ We(n) + Kd\ \{We(n) - We(n-1)\} \tag{4.3}$$

Subtracting Equation (4.2) from Equation (4.3) one gets:

$$T(n) - T(n-1) = Kp\{We(n) - We(n-1)\} + Ki\ We(n) + Kd\ \{We(n) - 2\,We(n-1) + We(n-2)\} \tag{4.4}$$

Hence, the output of the speed controller at the nth sampling instant

$$T(n) = T(n-1) + Kp\{We(n) - We(n-1)\} + Ki\ We(n) + Kd\ \{We(n) - 2\ We(n-1) + We(n-2)\} \tag{4.5}$$

where Kp, Ki and Kd are the proportional, integral and derivative gains of the speed controller respectively.

4.5.2 Modelling of Vector Control

The rotor flux revolves at rotor speed W_r and is positioned away from stationary reference by the rotor angular position (θ_r). The PMSM is usually controlled in the brushless DC motor mode where the stator current is orthogonally aligned to vector control using an absolute-rotor-position encoder. Vector control in this type of machine is simpler because of decoupling between the stator current and the magnet flux in comparison to what happens in a DC machine. By neglecting the flux weakening effect for low-speed operation of the PMSM motor, the reference direct-axis current (I_d^*) becomes zero and the direct-axis flux is considered equal to flux set by the excitation of the magnet as:

$$\lambda_d = \lambda_{af} \tag{4.6}$$

and

$$T_e = 3\ P\lambda_{af}\ i_q/2 \tag{4.7}$$

Since the magnetic flux-linkage is a constant, the torque is directly proportional to the q-axis current I_q. Hence the torque is represented as:

$$T_e = K_t\, i_q \tag{4.8}$$

where $K_t = 3\, P\, \lambda_{af} / 2$ (4.9)

P = Number of poles of the motor.

4.5.3 Reference Current Generator Modelling

The inputs to the reference current generator are quadrature and direct-axis reference currents i_q^* and i_d^* respectively and the rotor position signal (θ_r). The q-axis reference current i_q^* is obtained from Equation (4.8) as:

$$i_q^* = T_e / K_t \tag{4.10}$$

where, T^* is the reference torque which is the output of the PID speed controller and K_t is the torque constant.

The value of i_d^* is considered zero due to the absence of flux weakening in low- speed operation. However, the effect of i_d^* is significant in high-speed operation. Three stator winding reference currents i_a^* i_b^* and i_c^* are related to reference currents i_q^* and i_d^* and rotor position θ_r in the following way:

$$i_a = i_q^* \cos(\theta_r) + i_d^* \sin(\theta_r) \tag{4.11}$$

$$i_b = i_q^* \cos(\theta_r - 120^0) + i_d^* \sin(\theta_r - 120^0) \tag{4.12}$$

$$i_c = i_q^* \cos(\theta_r + 120^0) + i_d^* \sin(\theta_r + 120^0) \tag{4.13}$$

The reference currents are fed to the hysteresis current controller and are considered as 3-phase reference current signals.

4.5.4 Modelling of PWM Current Controller

In the basic PWM scheme, the stator winding currents are sensed and compared with the reference currents using a hystresis comparator. The PWM current controller contributes the switching pattern to the inverter devices. The switching logic is all ready explained in section 3.4.7.

Pulse-Width-Modulation (PWM) controller can provide very fast transient response and they are more robust than linear controllers. The stator-winding currents i_a, i_b and i_c are regulated in a sine-wave pattern of varying frequency and magnitude as per their reference counterparts.

4.5.5 Motor and Inverter Modelling

In this investigation, the d-q model is considered for PMSM motor, because, in vector control of PMSM the components of i_d and i_q are necessary for proper control of flux and torque components. Hence, in this scheme, the model is developed in d-q axes rather than the abc reference frame.

The general form of volt-ampere stator d-q equations of the PMSM in the rotor reference frame are:

$$V_q = R\, i_q + p\lambda q + \omega_r \lambda_d \tag{4.14}$$

$$V_d = R\, i_d + p\lambda q + \omega_r \lambda_q \tag{4.15}$$

and

$$\lambda_q = L_q\, i_q \tag{4.16}$$

$$\lambda_d = L_d\, i_d + \lambda_{af} \tag{4.17}$$

Where, V_d and V_q are the d- and q- axis voltages respectively,

i_d and i_q are the d-and q- axis currents respectively,

L_d and L_q are the d-and q- axis inductances respectively,

λ_d and λ_q are the d- and q- axis fluxes respectively,

R is the stator resistance per phase,

$\dot{\omega}_r$ is the rotor speed,

λ_{af} is the flux linkage due to the rotor magnets.

The developed electromagnetic torque is given as:

$$T_e = 3P\, [\lambda_{af} i_q + (L_d - L_q)\, i_d\, i_q\,] / 2 \tag{4.18}$$

where, P is the number of poles.

The torque balance equation for the motor is as:

$$T_e = T_l + B\, \omega_r + J\, p\omega_r \tag{4.19}$$

Where, T_l is the load torque, B is the damping coefficients and J is the moment of inertia.

For dynamic simulation, the model equations of PMSM are presented in Equations (4.6), (4.14), (4.15) and (4.19) must be expressed in the state space derivative form as:

$$P\, i_d = (V_d - Ri_d + \omega_r L_q\, i_q) / L_d \tag{4.20}$$

$$P\, i_q = (V_q - Ri_q + \omega_r L_d\, i_d - \omega_r \lambda_{af}) / L_q \tag{4.21}$$

$$P\, \omega_r = (T_e - T_l - B\, \omega_r) / J \tag{4.22}$$

$$p\, \theta_r = \omega_r \tag{4.23}$$

where V_d and V_q are the forcing function to decide the currents in d-q axes model which may be obtained from 3-phase voltages (V_{as},V_{bs} and V_{cs}) through the park transformation technique as:

$$V_q = (2/3)\,[V_{as}\cos(\theta_r) + V_{bs}\cos(\theta_r - 120^0) + V_{cs}\cos(\theta_r + 120^0)] \quad (4.24)$$

$$V_d = (2/3)\,[V_{as}\sin(\theta_r) + V_{bs}\sin(\theta_r - 120^0) + V_{cs}\sin(\theta_r + 120^0)] \quad (4.25)$$

where V_{as},V_{bs} and V_{cs} are the instantaneous phase voltages impressed across the phase windings and are decided by the inverter.

4.5.6 Phase Voltage Reconstruction from DC Link Voltage

The switching function (SF) is defined for each phase to represent the switching state of the devices and for the phase A it is given as:

SFA = 1 if upper device of the phase A is on:

SFA = 0 if lower device of the phase A is on:

Similarly, the device switching functions of the phase B and phase C are also defined. The phase voltages are expressed in terms of the switching functions SFs and DC link voltage V_{dc} as follows:

$$V_{as} = (V_{dc}/3)^{*}(+2*SFA-SFB-SFC) \quad (4.26)$$

$$V_{bs} = (V_{dc}/3)\,(-SFA+2*SFB-SFC) \quad (4.27)$$

$$V_{cs} = (V_{dc}/3)\,(-SFA-SFB+2*SFC) \quad (4.28)$$

The set of differential equations (Equations 4.20 – 4.23) defines the developed model in terms of four dependent variables I_d, I_q, ω_r and θ_r and time as an independent variable. Since these model equations are nonlinear in nature and cannot be solved in the closed form solution, hence a numerical technique, namely, fourth order Runge Kutta method is used to obtain the solution of these equations.

4.5.7 PI Speed Controller Modelling

The PI speed controller modeling is already described in section 3.4.2.

4.5.8 PID Speed Controller.

The working of the PID controller and the output of the speed controller are explained in section 3.3.2 & 3.4.3 respectively.

4.6 Conclusion

The mathematical models are developed for simulating and analyzing the dynamic performance of the PMSM drive. The PI and PID speed controllers as used in the closed-loop control of PMSM have been found to be capable of maintaining the accurate control of speed in either directions of rotation of the drive. It has also been confirmed that the control structure of the drive takes care of the transients. It is observed that the transient currents drawn by the motor never exceed the permissible values. Therefore, it is concluded that the motor-control scheme takes care of the over-current problems of inverter devices. However, the superiority of advanced controllers (SMC/FLC) in handling the quick and instantaneous changes in the motor currents in response to any disturbances within the set operating parameters of the drive system will make them popular in the years to come provided the cost effectiveness is justified. The results on the performance of these models are illustrated in Chapter 6.

CHAPTER 5

SIMULATION RESULTS FOR PMBLDC MOTOR

5.1 General

The performance of the closed-loop speed-controlled drive system depends on the choice of controllers. The equations governing the model of a drive system are presented in the chapter 3. As the model of the PMBLDC motor is nonlinear, a numerical technique, namely, Runge-Kutta method is used to get the solution of these equations for the variables such as i_a, i_b, i_c, ω_r and θ_r. The motor torque, winding currents, reference speed, reference currents and rotor speed were simulated for studying the dynamic responses of the drive. The control performance of the PMBLDC motor drive is influenced by parameter variations and external load disturbances. This has resulted in continuous thrust in recent years on exploring the use of modern control schemes such as adaptive control and sliding-mode control. Another type of controller based on fuzzy logic is being increasingly applied to systems with non-linearity and uncertainty. In the light of the above observations, a range of speed controllers starting from conventional controllers to the modern ones has been tried for simulation of the PMBLDC drive. In this investigation, the transient and steady- state responses of the drive are examined with different speed controllers like PI, PID, SMC, Fuzzy Precompensated PI, Self-Organizing Fuzzy Logic controllers and Hybrid FP+ID. The PWM current controller has been found to be best among currents controllers. An algorithm is also developed for the simulation in real-time operating conditions. The PMBLDC motor used for this simulation is a prototype motor of 0.5 H.P, 4 pole, 3- phase, 1500 rpm, star-connected motor. The specification of the motor is listed in Table-A.1 and Table-A.2 and the gain parameters of different speed controllers are given in Table- C.1 to Table-C.9. The specifications of the electronic components used in the research work are given in Table-D.1 and D.2.

The results of several simulation runs have been compiled for the comprehensive study of the performance of the PMBLDC motor under deployment of a wide range of controllers. Figures 5.1 to 5.162 illustrate the simulation results.

5.2 Simulation Results of PMBLDC Motor with PI Controller

The simulation results have been obtained separately for all the speed controllers used. For each of these cases results pertaining to three modes of dynamic operations namely, the starting, speed reversal and load perturbation have been obtained. The simulated responses of the drive under PI controller, thus obtained are shown in Figures 5.1 to 5.18. The Figures 5.1 to 5.6 illustrate the starting response of the drive with PI controllers. The reference speed is set at 157 rad/sec.

5.2.1 Responses of PMBLDC Motor Current with PI Controller During Starting

Figures 5.1 – 5.3 show the motor currents (i_a, i_b and i_c) which increases to 5.0 A (peak) at the time of starting without any load and reduces to a 1.05 A (peak) during the steady-state condition. The current (in each phase) reaches steady state very fast which is indicative of motor's sensitivity and suitability for practical applications.

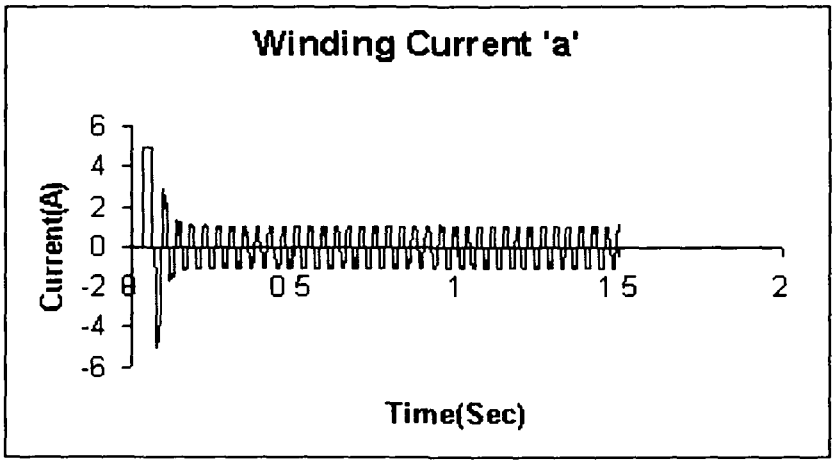

Figure 5.1: Motor Current 'i_a'

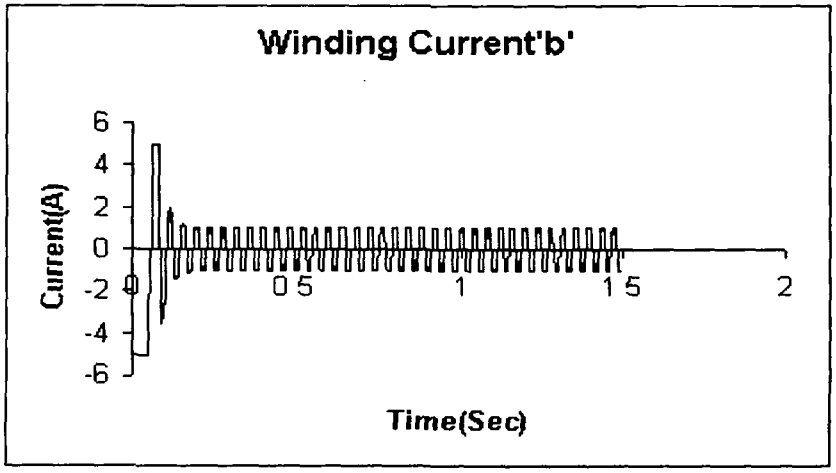

Figure 5.2: Motor Current 'i_b'

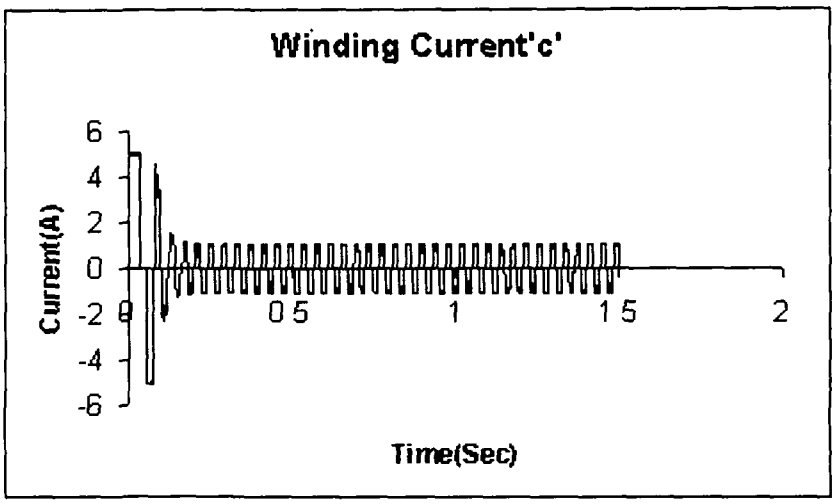

Figure 5.3: Motor Current 'i_c'

5.2.1.1 Response of PMBLDC Motor Speed with PI Controller During Starting

Figure 5.4 shows the rotor speed developed during starting of PMBLDC motor from standstill up to the rated speed of 1500 rpm (157 rad/sec) with PI controller. The gains used for the controller are Kp = 0.3, K_I = 0.0005. The drive takes 160 msec to reach the reference speed. The developed torque rises to maximum permissible value to start the motor from standstill.

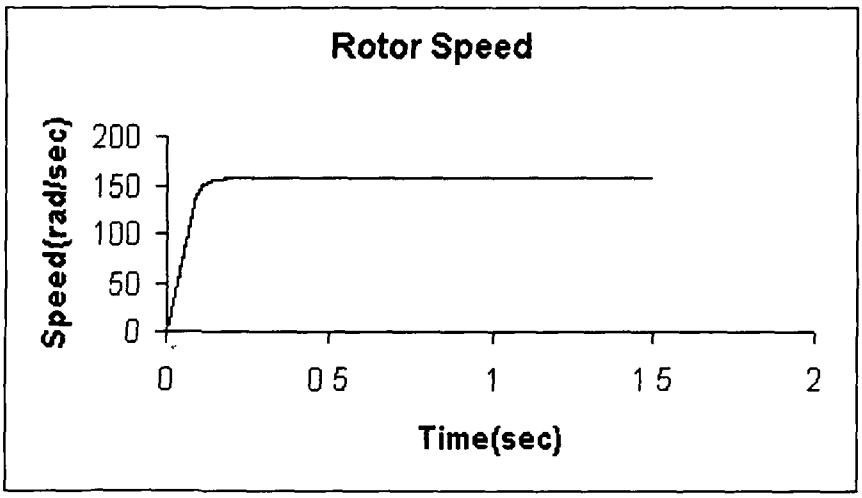

Figure 5.4: Rotor speed Vs time plot during starting

5.2.1.2 Response of PMBLDC Motor Torque with PI Controller During Starting

Figure 5.5 shows the motor electromagnetic torque which rises to 12 Nm (maximum permissible value) during starting of the motor from standstill condition. The electromagnetic torque rises instantaneously to 12 Nm to start the motor from

standstill and by the time the motor reaches the steady-state condition, the torque also undergoes a quick transient decrease and settles down to the steady-state level of 2.5 Nm and maintains the same level over the remaining period of time. The value of electromagnetic torque under steady-state is decided by the extent of the load torque on the shaft.

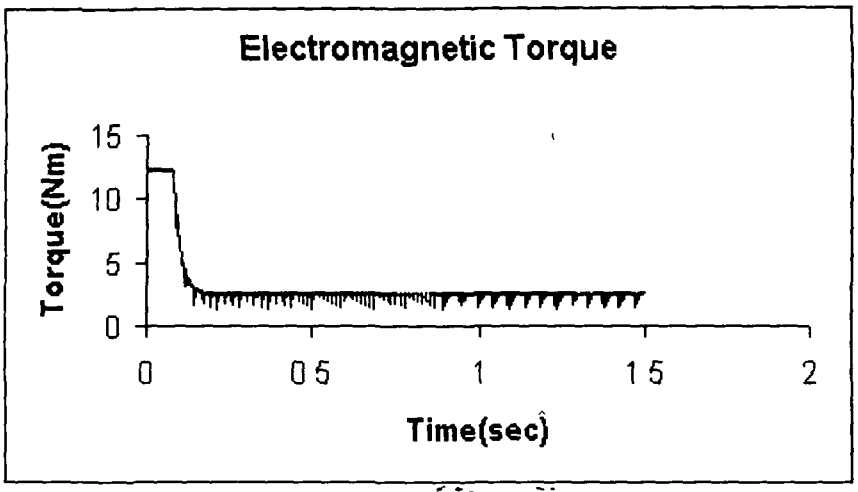

Figure 5.5: Electromagnetic Torque Vs time plot during starting

5.2.1.3 Response of PMBLDC Motor Voltage with PI Controller During Starting

Figure 5.6 shows the motor winding voltage of phases. Each winding voltage increases up to 300 V / 305 V (peak).

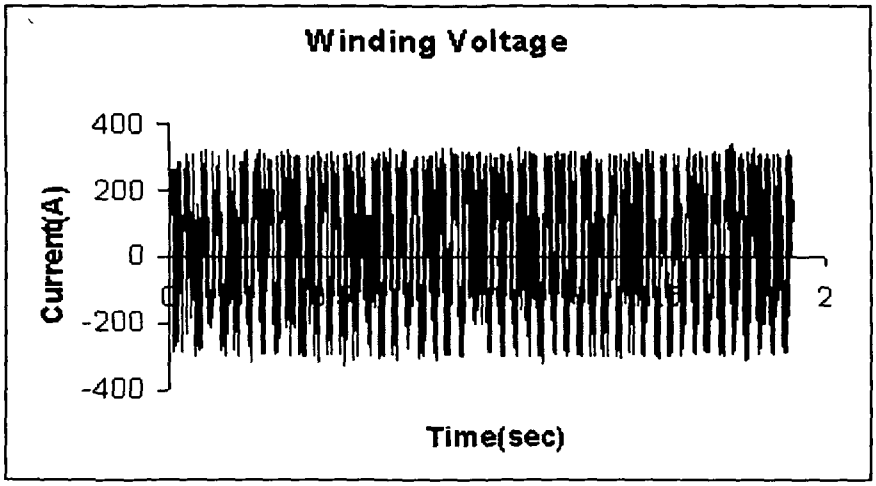

Figure 5.6: Motor winding Voltage Vs time plot during starting

5.2.2 Response of PMBLDC Motor Current with PI Controller During Speed Reversal

Figures 5.7 – 5.9 show the motor currents (i_a, i_b and i_c) which increase to 5.0 A (peak) at the time of starting without any load and reduces to a 1.05 A (peak) during the steady-state condition and then after 780 msec currents again rise up to 5.0

A due to the speed reversal. The drive takes 280 msec for a reversal of speed and currents come in the original value of 1.05 A (peak).

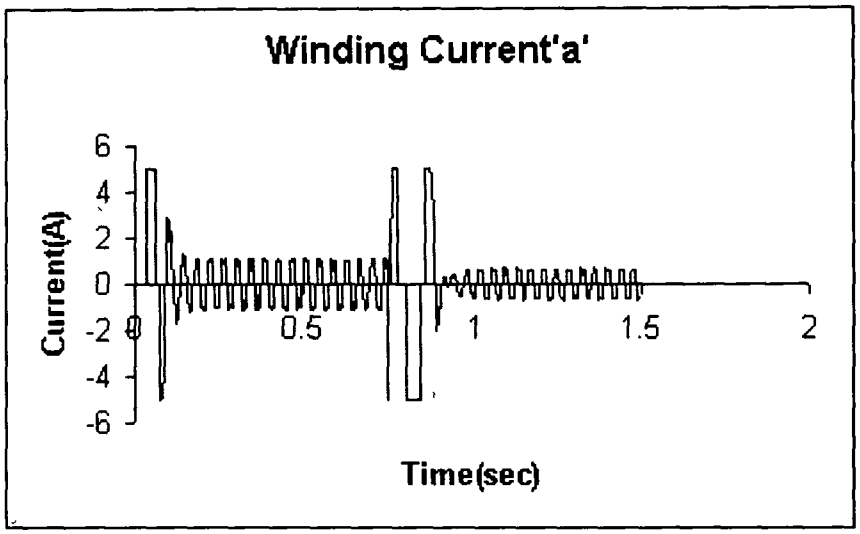

Figure 5.7: Motor Current 'i_a'

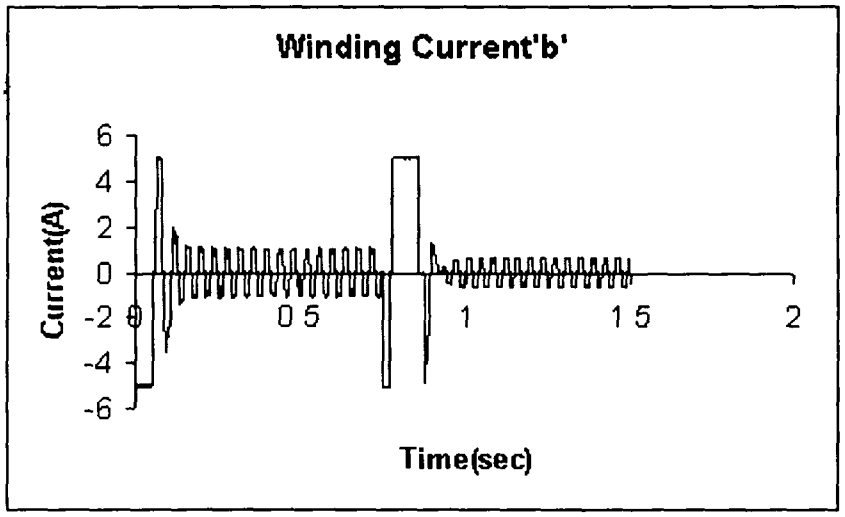

Figure 5.8: Motor Current 'i_b'

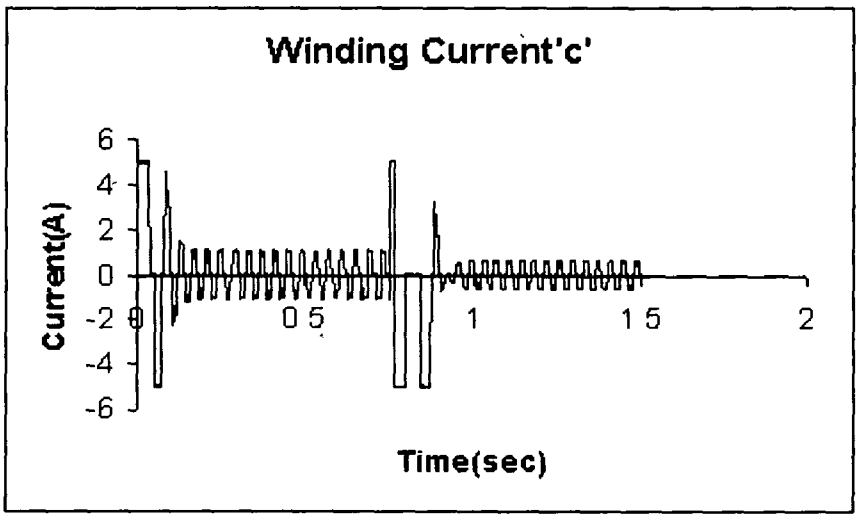

Figure 5.9: Motor Current 'i_c'

5.2.2.1 Response of PMBLDC Motor Speed with PI Controller During Speed Reversal

Figure 5.10 shows the speed reversal dynamics of the PMBLDC motor with PI speed controller. When the set speed is changed to –157 rad/sec (speed reversal), the PI controller becomes active and makes the motor reach the reference speed. The drive takes 280 msec for the speed reversal.

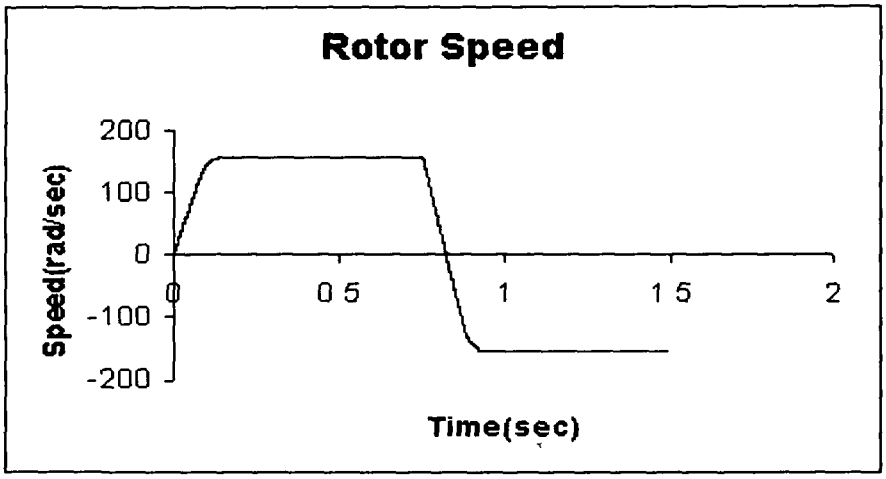

Figure 5.10: Rotor speed Vs time plot during Reversal

5.2.2.2 Response of PMBLDC Motor Torque with PI Controller During Speed Reversal

Figure 5.11 shows the electromagnetic torque which rises instantaneously to 12 Nm (Maximum permissible value) during starting of the motor from the standstill condition, and by the time the motor reaches the steady state condition, the torque also undergoes a quick transient decrease to settle down to the steady state level of 2.5 Nm. On speed reversal, the torque attains the negative value (-12 Nm) almost instantaneously and the motor speeds up in the reverse direction till it reaches the steady state (-ve) value with torque being maintained at its original value.

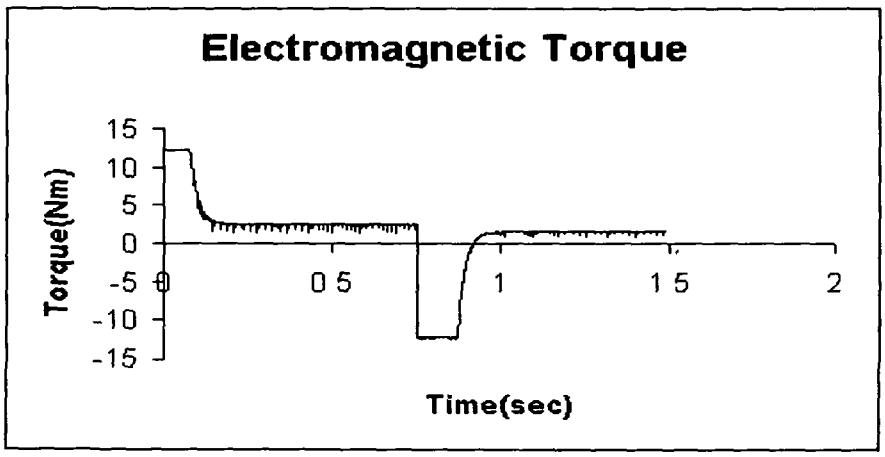

Figure 5.11: Electromagnetic Torque Vs time plot during Reversal

5.2.2.3 Response of PMBLDC Motor Voltage with PI Controller During Speed Reversal

Figure 5.12 shows the motor winding voltages. Winding voltage increases upto 300 V / 305 V (peak) in all the three phases.

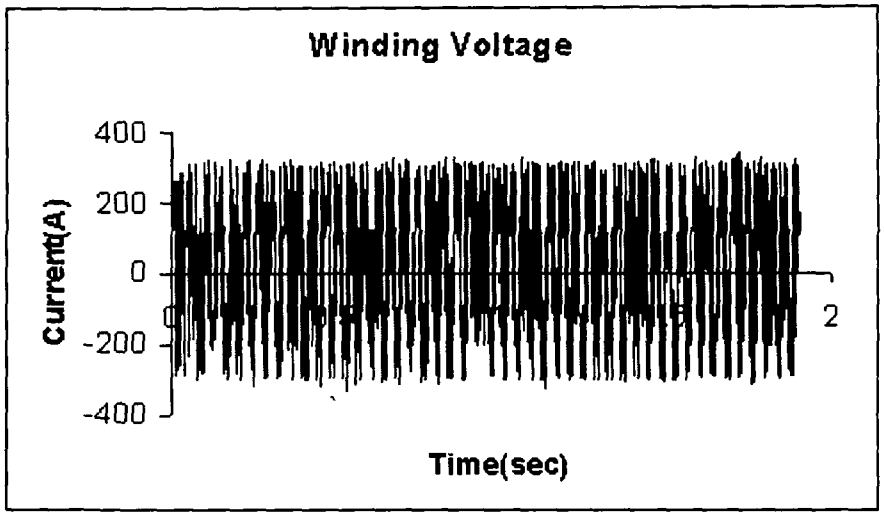

Figure 5.12: Motor winding Voltage Vs time plot during Reversal

5.2.3 Response of PMBLDC Motor Current with PI Controller During Load Perturbations

Figures 5.13 – 5.15 show the motor currents (i_a, i_b and i_c) increasing upto 5.0A (peak) at the time of starting without any load and settling down to the steady-state value of 1.15 A (peak). The increase in current to 3.75 A is due to the load perturbation to meet the increased demand of load. The winding currents are found to follow the reference currents even during the conditions of load perturbation.

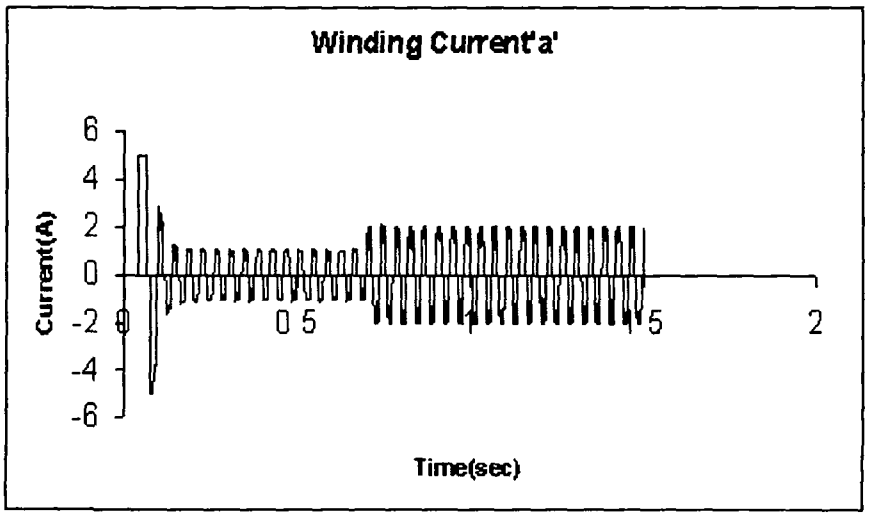

Figure 5.13: Motor Current 'i_a'

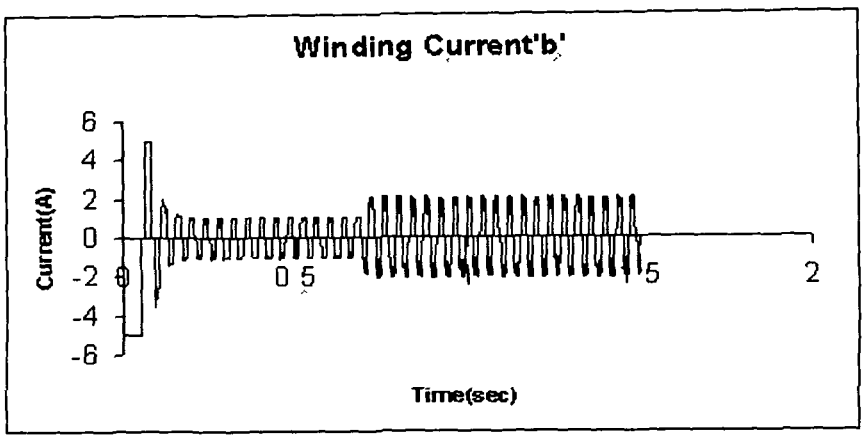

Figure 5.14: Motor Current 'i_b'

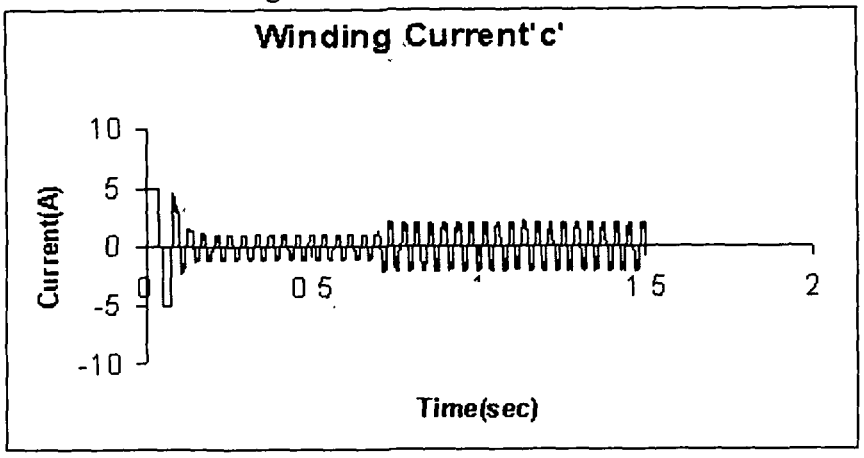

Figure 5.15: Motor Current 'i_c

5.2.3.1 Response of PMBLDC Motor Speed with PI Controller during Load Perturbations

Figure 5.16 shows the performance of the drive with the PI speed controller under load perturbations. The sudden application of the load on the motor causes a very small dip in the motor speed, which recovers very quickly under the fast controller action. Due to the load perturbation, the dip in speed is around 4 rad/sec and the drive takes 100 msec to regain the rated speed after sudden removal of load.

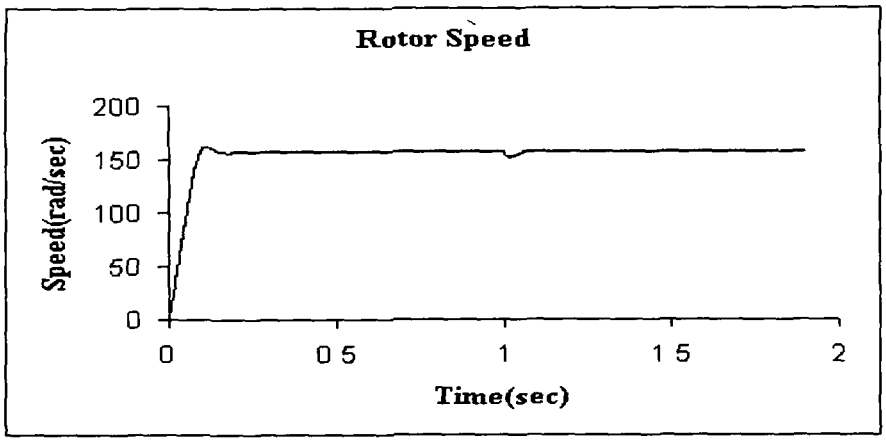

Figure 5.16: Rotor speed Vs time plot during Load Perturbations

5.2.3.2 Response of PMBLDC Motor Torque with PI Controller During Load Perturbations

Figure 5.17 shows the electromagnetic torque which increases to 5.0 Nm and maintains the higher value till the load is removed.

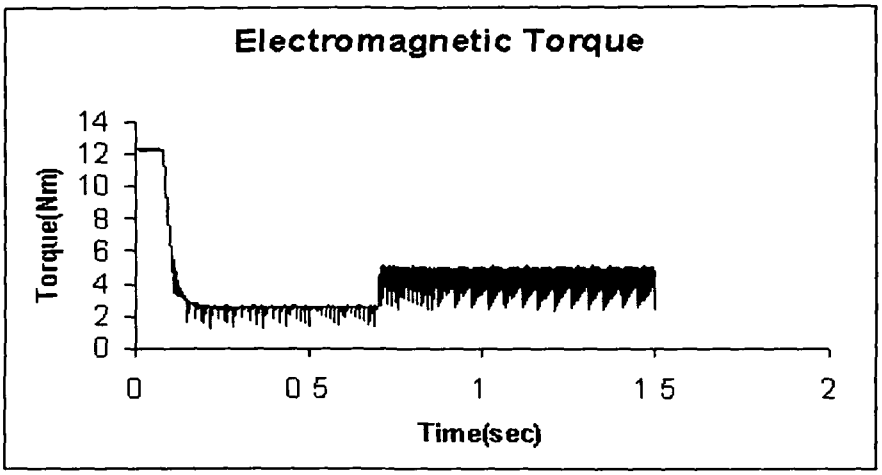

Figure 5.17: Electromagnetic Torque Vs time plot during Load Perturbations

5.2.3.3 Response of PMBLDC Motor Voltage with PI Controller During Load Perturbations

The response of the motor winding voltage is shown in the Figure 5.18. Winding voltage increases up to 300V / 305V (peak) in all the three phases. The voltage does not show any perceptible change during load perturbations.

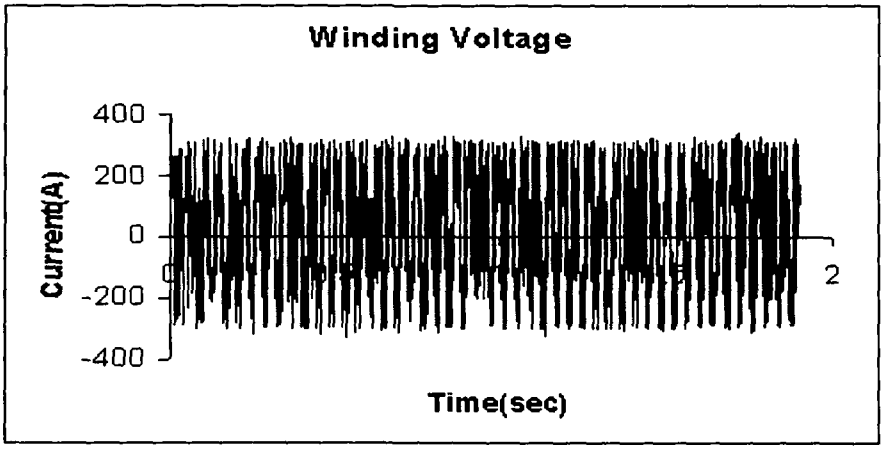

Figure 5.18: Motor winding Voltage Vs time plot during Load Perturbations

5.3 PID Speed controller

The simulated dynamic responses of winding current, speed, torque and winding voltage characteristics of a 3-phase, 4-pole, 0.5 HP PMBLDC motor with its reference speed set at 1500 rpm (157 rad/sec) are shown in Figure 5.19 to 5.36.

5.3.1 Response of PMBLDC Motor Current with PID Controller during Starting

Figures 5.19 – 5.21 show the motor currents (i_a, i_b and i_c) which increase to 5.0 A (peak) at the time of starting without any load and settle down at 0.125A(peak) during the steady state condition. The steady state current is 125 mA which is reached in about 170 msec after its start on no load. The current in each phase reaches steady state very fast which is indicative of motor's sensitivity and its suitability for practical applications.

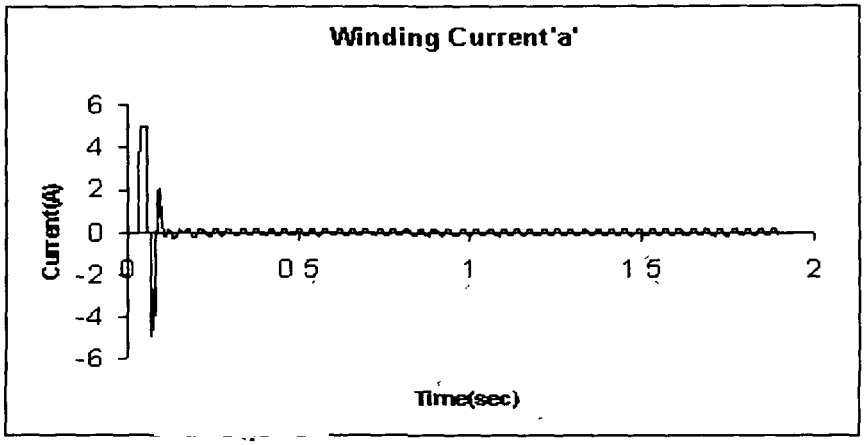

Figure 5.19: Motor Current 'i_a'

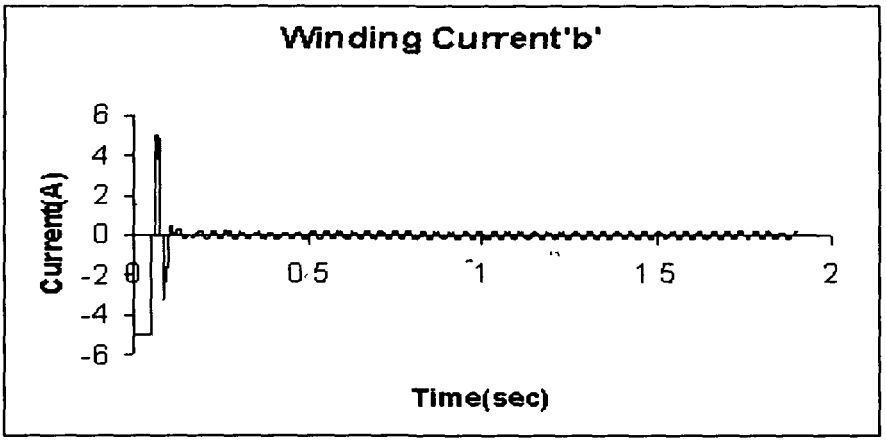

Figure 5.20: Motor Current 'i_b'

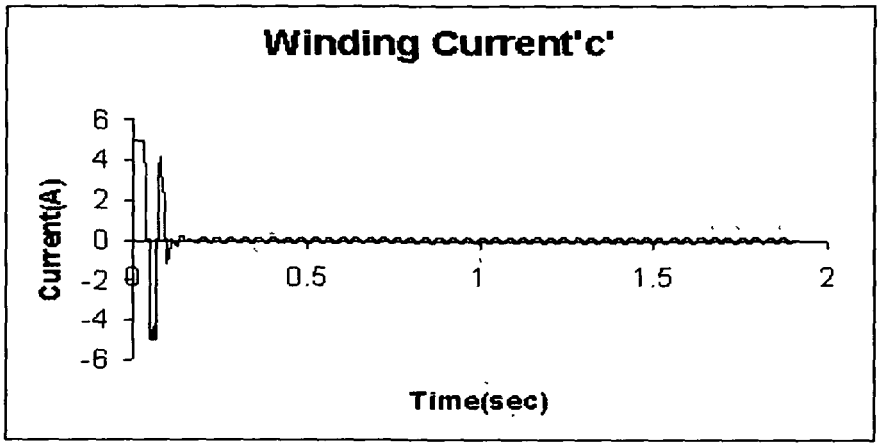

Figure 5.21: Motor Current 'i_c'

5.3.1.1 Response of PMBLDC Motor Speed with PID Controller During Starting

Figure 5.22 shows the rise in rotor speed during starting of PMBLDC motor from standstill up to rated speed of 1500 rpm (157 rad/sec) with PID controller. The of gains used for the controller are Kp = 0.3, K_I= 0.0005 and K_I= 0.12. The drive takes 170 msec to reach the reference speed. The developed torque rises to maximum permissible value to start the motor from standstill.

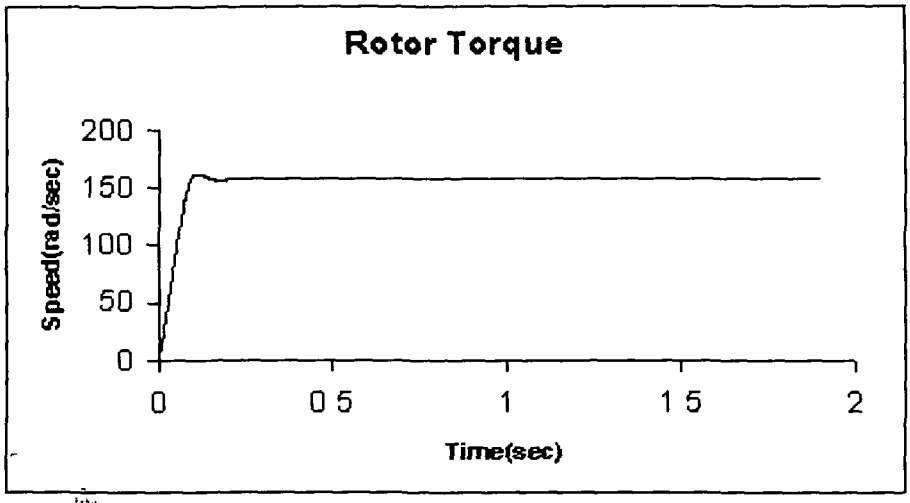

Figure 5.22: Rotor Speed Vs time plot during Starting

5.3.1.2 Response of PMBLDC Motor Torque with PID Controller During Starting

Figure 5.23 shows the motor electromagnetic torque which rises instantaneously to 12 Nm (maximum permissible value) during the starting of the motor from standstill condition. The torque also undergoes a quick transient decrease and settles down to the steady-state level of 0.35 Nm and maintains the same level over the remaining period of time.

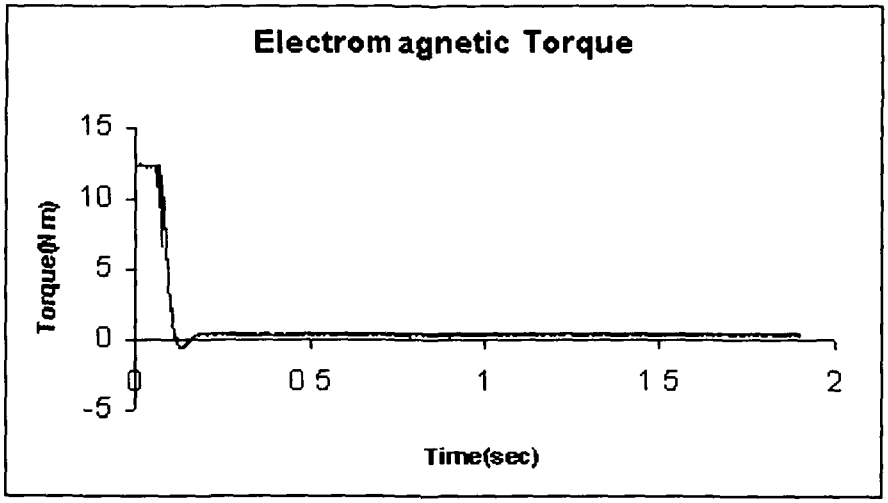

Figure 5.23: Electromagnetic Torque Vs time plot during Starting

5.3.1.3 Response of PMBLDC Motor Voltage with PID Controller During Starting

The response of the motor winding voltage is shown in the Figure 5.24. Winding voltage increases up to 300V / 305V (peak) in all the three phases.

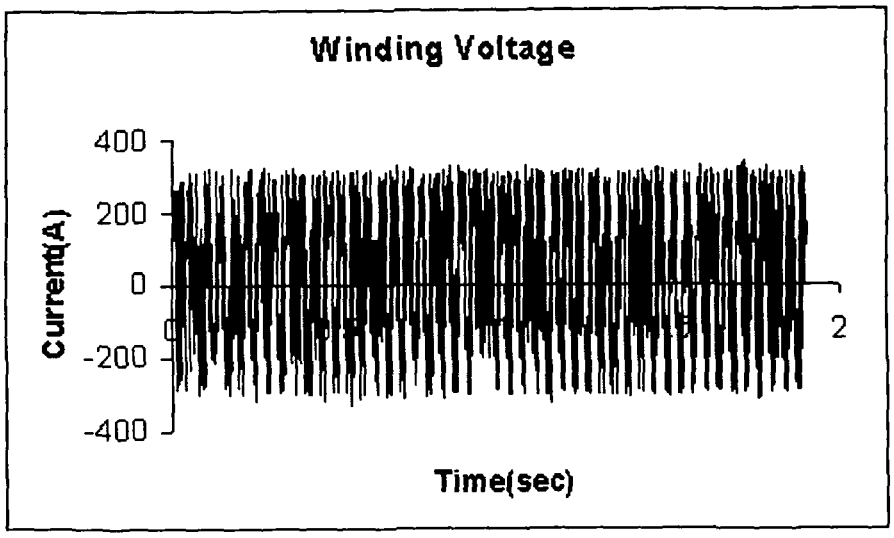

Figure 5.24: Motor winding Voltage Vs time plot during Starting

5.3.2 Response of PMBLDC Motor Current with PID Controller During Speed Reversal

Figures 5.25 –5.27 show the motor currents (i_a, i_b and i_c) which increase to 5.0 A (peak) at the time of starting without any load and drop to a 0.125 (peak) during the steady-state condition. After 750 msec currents again rise to 5.0A due to the speed reversal. The drive takes 260 msec for reversal of speed and the currents reach the original value of 0.125A.

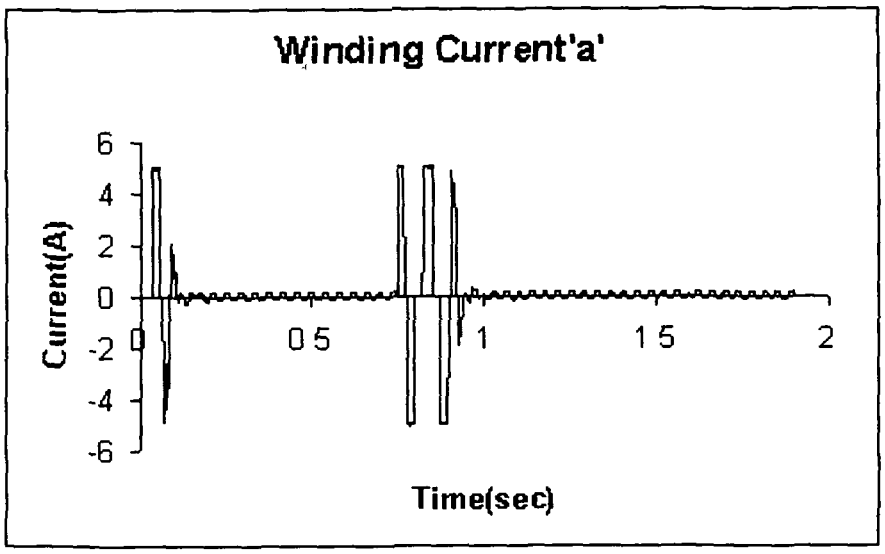

Figure 5.25: Motor Current 'i_a'

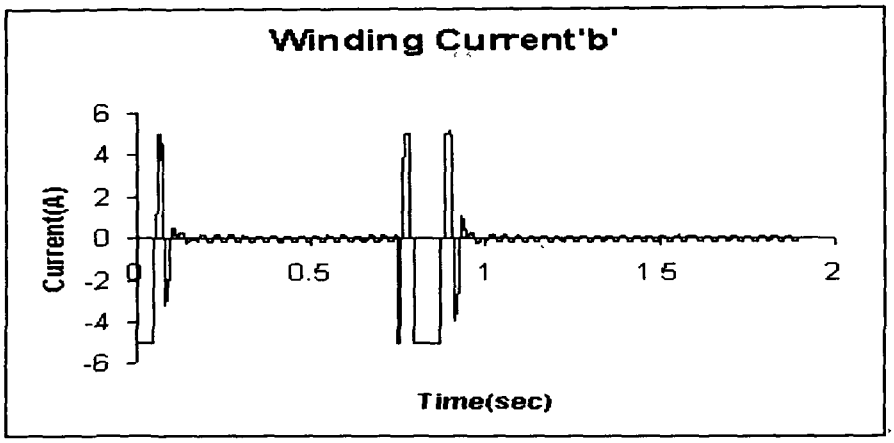

Figure 5.26: Motor Current 'i_b'

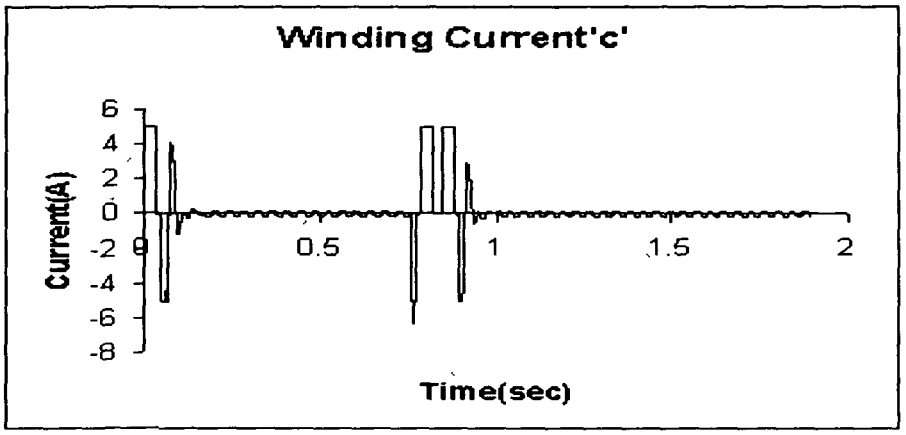

Figure 5.27: Motor Current 'i_c'

5.3.2.1 Response of PMBLDC Motor Speed with PID Controller During Speed Reversal

Figure 5.28 shows the dynamics of speed reversal of the PMBLDC motor under the action PID speed controller. When the set speed is changed to –157 rad/sec (speed reversal), the PID controller becomes active and brings the motor speed equal to the reference speed. The drive takes 260 msec for the speed reversal, which is an improvement over the PI Controller.

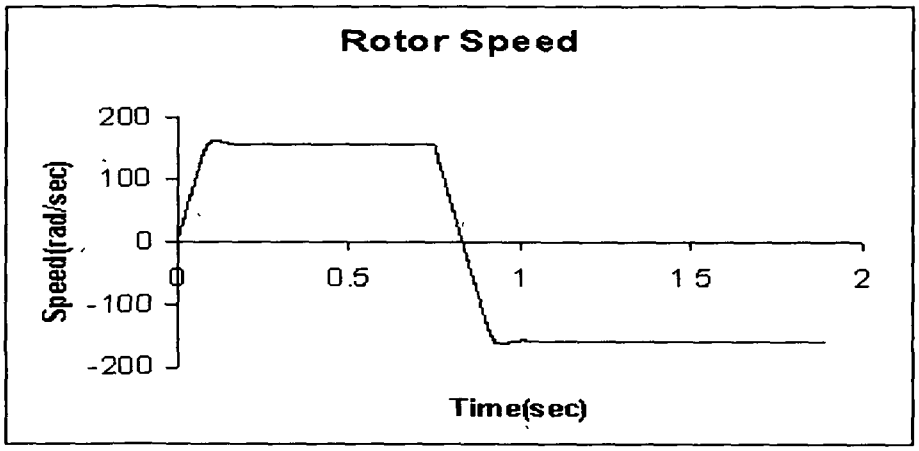

Figure 5.28: Rotor speed Vs time plot during Reversal

5.3.2.2 Response of PMBLDC Motor Torque with PID Controller During Speed Reversal

Figure 5.29 shows the electromagnetic torque which rises instantaneously to 12 Nm (Maximum permissible value) to start the motor from the standstill and by the time the motor reaches the steady-state condition, the torque also undergoes a quick transient decrease to settle down to the steady-state level of 0.3 Nm and is maintained there of. When the speed reversal occurs, the torque becomes maximum with negative value (-12 Nm) and the motor speeds up in the reverse direction. Once the motor speed reaches the steady-state in the negative direction, the torque is again settles down to the steady-state value.

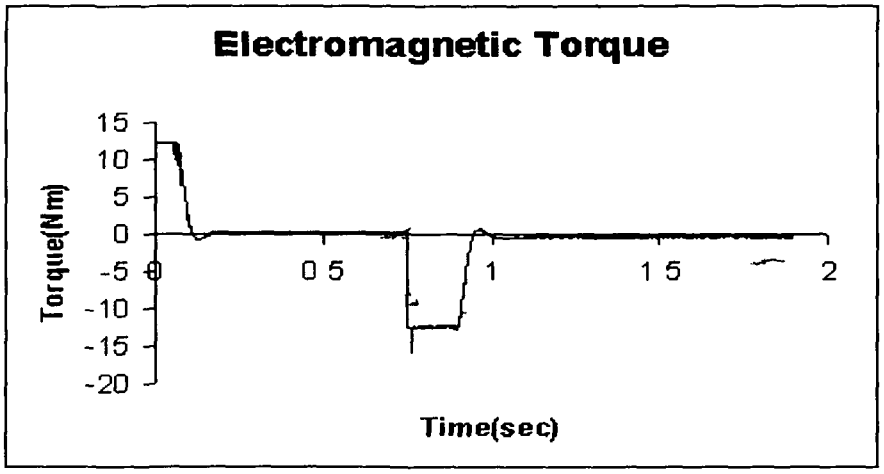

Figure 5.29: Electromagnetic Torque Vs time plot during Reversal

5.3.2.3 Response of PMBLDC Motor Voltage with PID Controller During Speed Reversal

Figure 5.30 shows the motor winding voltage response of one of the phases. Winding voltage increases up to 300V to 305V in all the three phases.

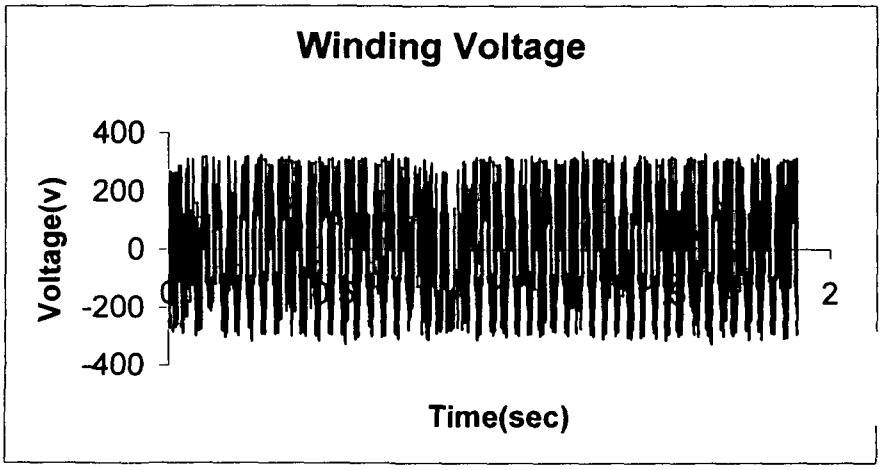

Figure 5.30: Motor winding Voltage Vs time plot during Reversal

5.3.3 Response of PMBLDC Motor Current with PID Controller During Load Perturbations

Figures 5.31 – 5.33 show the motor currents (i_a, i_b and i_c) which increase upto 5.0 A (peak) at the time of starting without any load and drop to 0.13 A (peak) during the steady-state condition. During the load perturbation, the current increases to 1.85 A to meet the increased demand due to extra load. When the load is removed, the current returns to the original steady-state value. The winding currents are found to follow the reference currents even during the conditions of load perturbations.

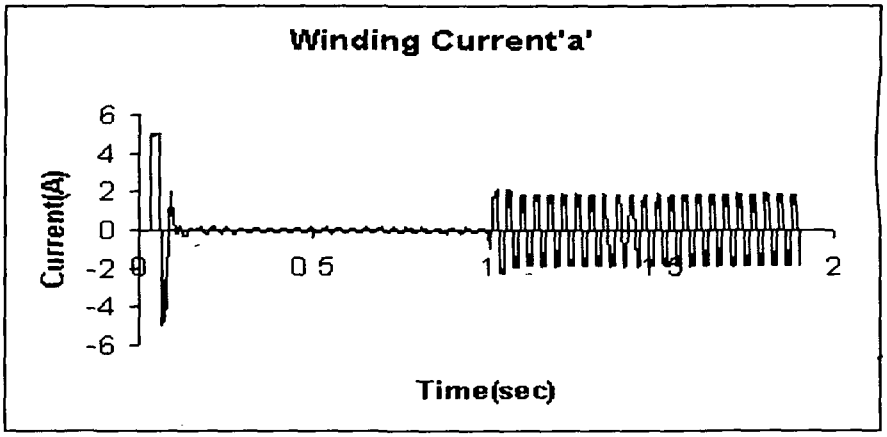

Figure 5.31: Motor Current 'i_a'

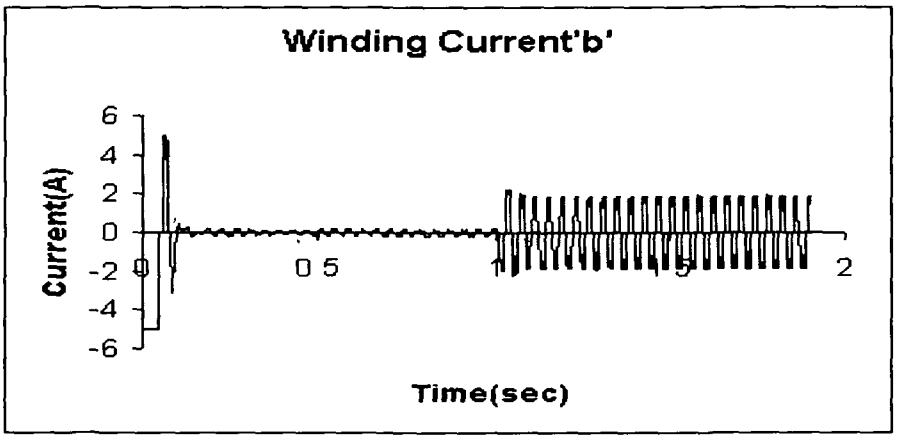

Figure 5.32: Motor Current 'i_b'

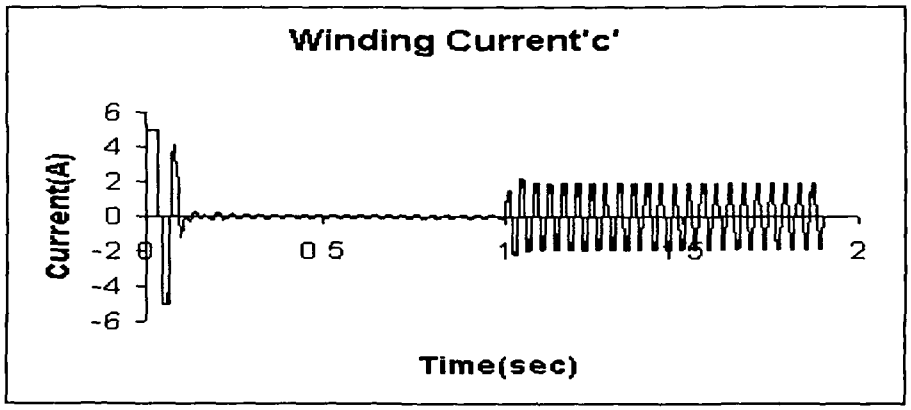

Figure 5.33: Motor Current 'i_c'

5.3.3.1 Response of PMBLDC Motor Speed with PID Controller During Load Perturbations

Figure 5.34 shows the performance of the drive with the PID speed controller under load perturbations. The sudden application of load on the motor causes a small dip in the motor speed, which needs quick recovery for high performance applications under the fast acting PID controller action within a short period. Due to the load perturbation, the dip in speed is around 4 rad/sec and the drive takes 100 msec to recover the rated speed.

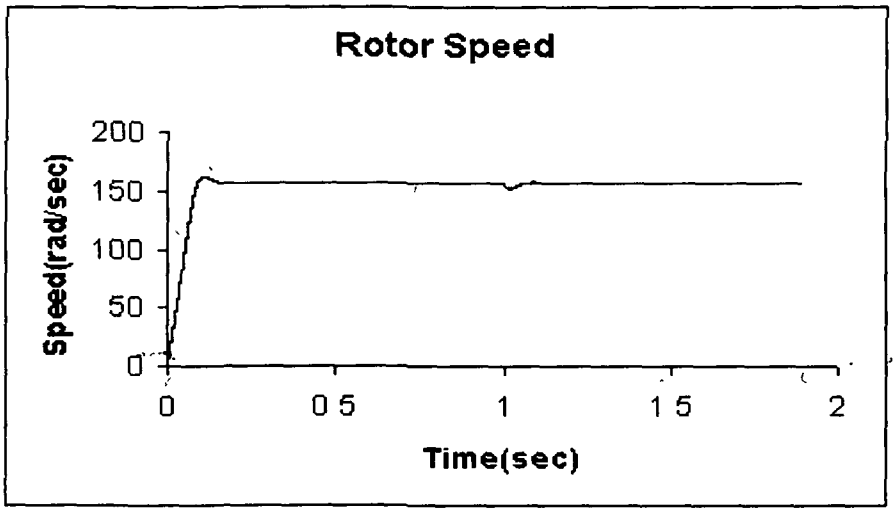

Figure 5.34: Rotor speed Vs time plot during Load Perturbations

5.3.3.2 Response of PMBLDC Motor Torque with PID Controller During Load Perturbations

Figure 5.35 shows the electromagnetic torque which increases to 4.55 Nm and is maintained at the higher value till the load is removed. The sudden applications of the load torque results in the small dip in motor speed. The electromagnetic torque which rises corresponding to the load torque retains the same value.

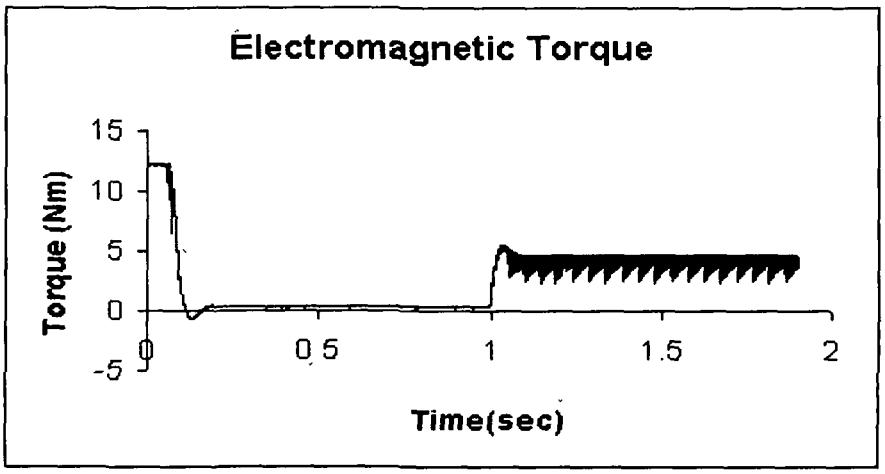

Figure 5.35: Electromagnetic Torque Vs time plot during Load Perturbations

5.3.3.3 Response of PMBLDC Motor Voltage with PID Controller During Load Perturbations

The response of the motor voltage with reference to one of the phases is shown in the Figure 5.36. Winding voltage increases up to 300V to 305V in all the three phases.

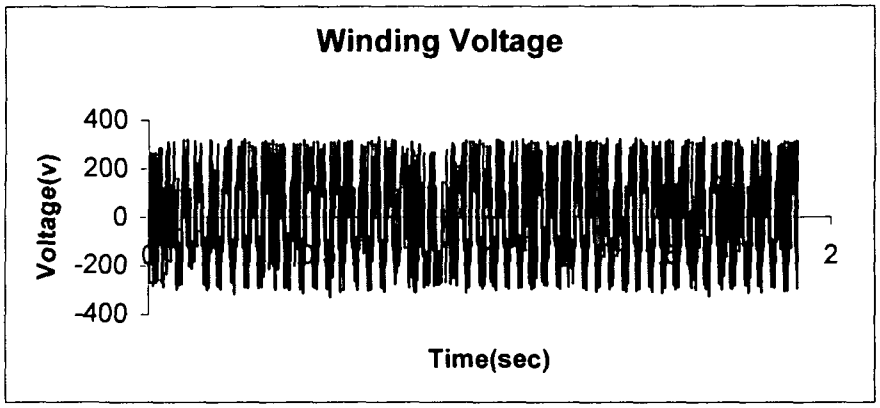

Figure 5.36: Motor winding Voltage Vs time plot during Load Perturbations

5.4 SMC Speed controller

The simulated dynamic responses of torque and speed of a 3-phase, 4-pole, 0.5 HP PMBLDC motor with its reference speed set at 1500 rpm (157 rad/sec) are shown in Figures 5.37 to 5.54.

5.4.1 Response of PMBLDC Motor Current with SMC Controller during Starting

Figures 5.37 – 5.39 show the motor currents (i_a, i_b and i_c) which increase upto 6.5 A (peak) at the time of starting without any load and settle down at 0.185 A during the steady-state condition. However, the steady-state current is reached in about 205 msec after its start on no-load. There appears to be a transition period before the current settles down to the steady-state value.

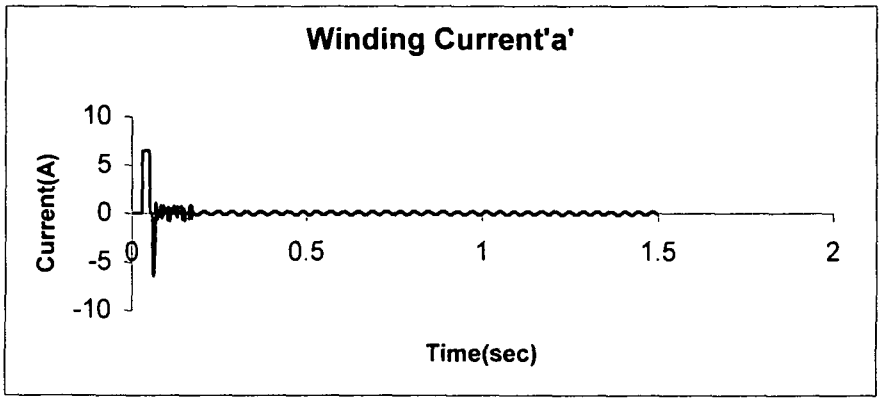

Figure 5.37: Motor Current 'i_a'

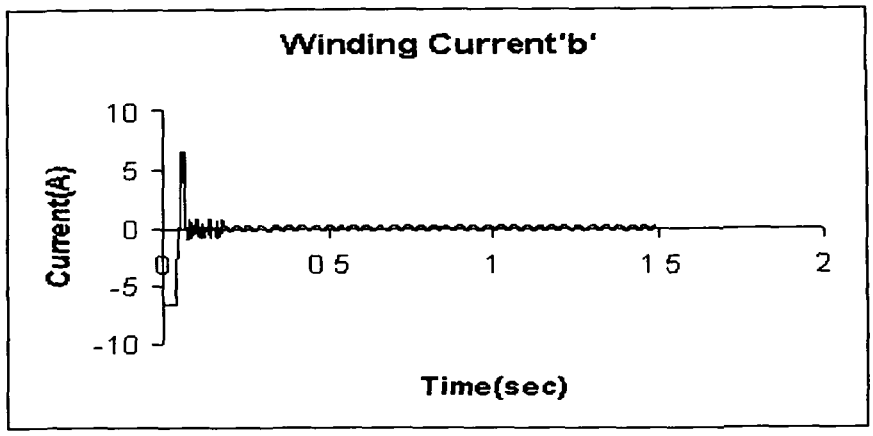

Figure 5.38: Motor Current 'i_b'

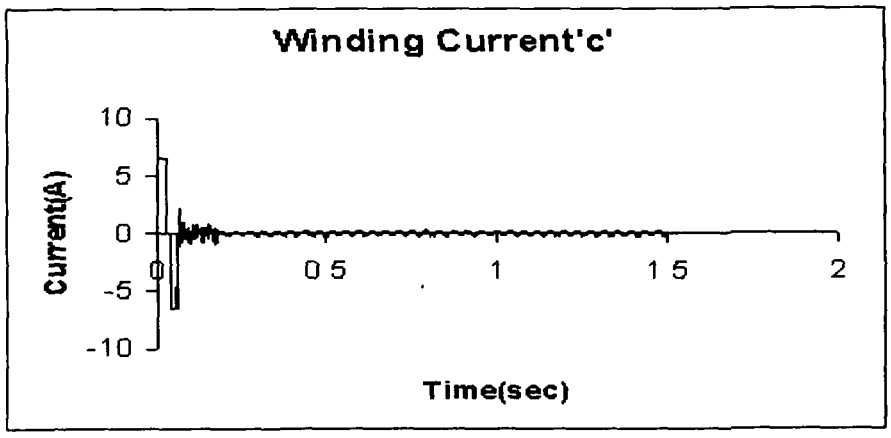

Figure 5.39: Motor Current 'i_c'

5.4.1.1 Response of PMBLDC Motor Speed with SMC Controller During Starting

Figure 5.40 shows the rotor speed during starting of PMBLDC motor from standstill up to rated speed of 1500 rpm (157 rad/sec) with SMC controller. The controller gains are K=2.0, K_1= 10.0 and K_2= 10.0. The drive takes 140 msec to reach the reference speed. The developed torque rises to maximum permissible value to start the motor from standstill.

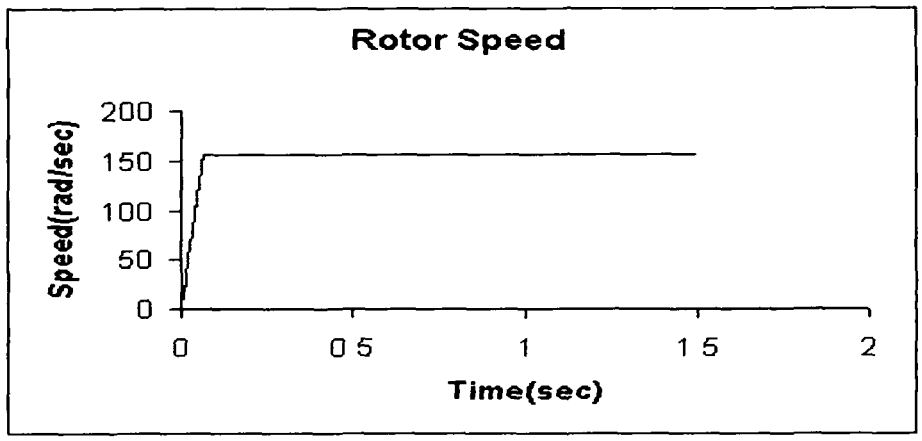

Figure 5.40: Rotor speed Vs time plot during Starting

5.4.1.2 Response of PMBLDC Motor Torque with SMC Controller During Starting

Figure 5.41 shows the motor electromagnetic torque which rises instantaneously to 16 Nm during the starting of the motor from standstill condition. The rise in torque is almost instantaneous. By the time the motor reaches the steady-state, the torque undergoes a quick transient decrease to settle down to the steady-state level of 0.185 Nm after 205 msec and maintains the same level over the remaining period of time. The level of electromagnetic torque under steady-state is decided by the extent of the load torque on the motor shaft.

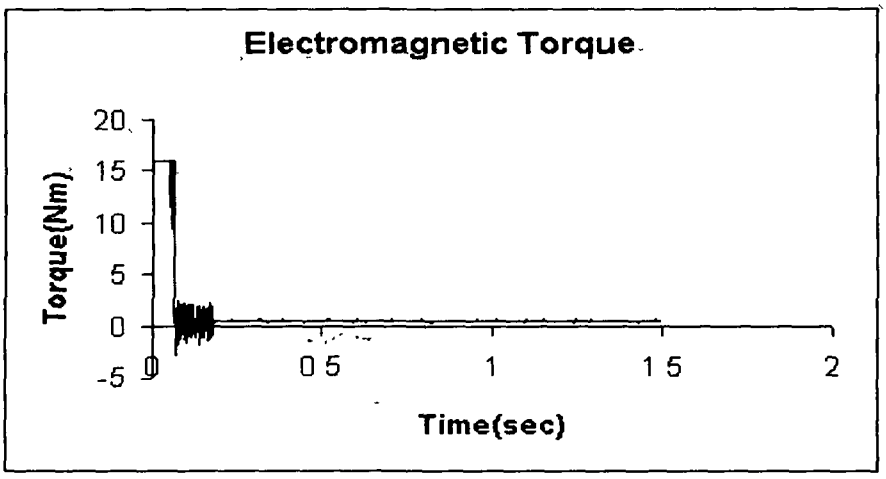

Figure 5.41: Electromagnetic Torque Vs time plot during Starting

5.4.1.3 Response of PMBLDC Motor Voltage with SMC Controller During Starting

Figure 5.42 shows the motor voltage response of one of the phases. Winding voltage increases up to 300 V / 305 V in all the three phases.

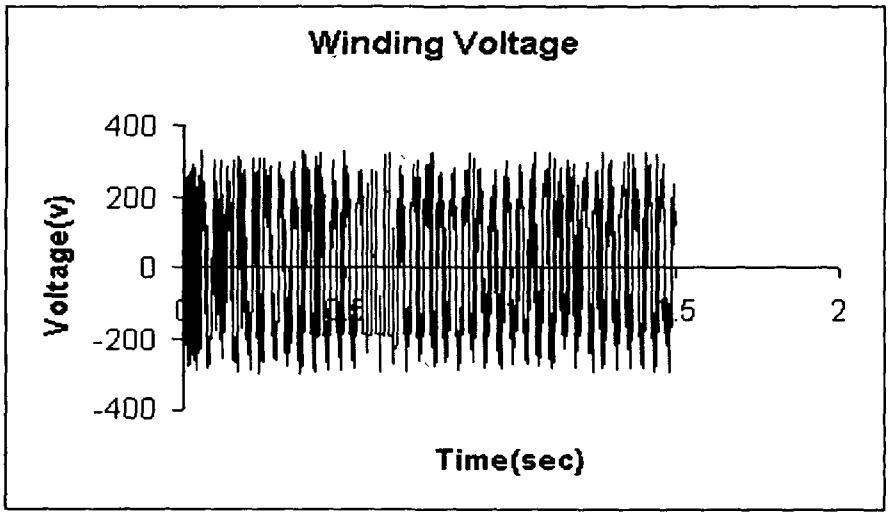

Figure 5.42: Motor winding Voltage Vs time plot during Starting

5.4.2 Response of PMBLDC Motor Current with SMC Controller During speed Reversal

Figures 5.43–5.45 show the motor currents (i_a, i_b and i_c) which increase upto 6.5 A (peak) at the time of starting without any load and drop to 0.185A (peak) at the steady- state condition. After 760 msec currents again rises up to 6.5A (peak) due to the speed reversal. The drive takes 205 msec for reversal of the speed and currents come to the steady-state values.

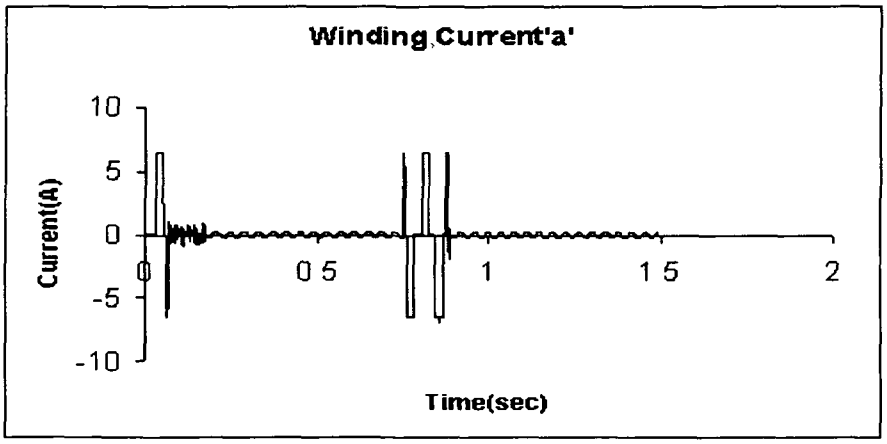

Figure 5.43: Motor Current 'i_a'

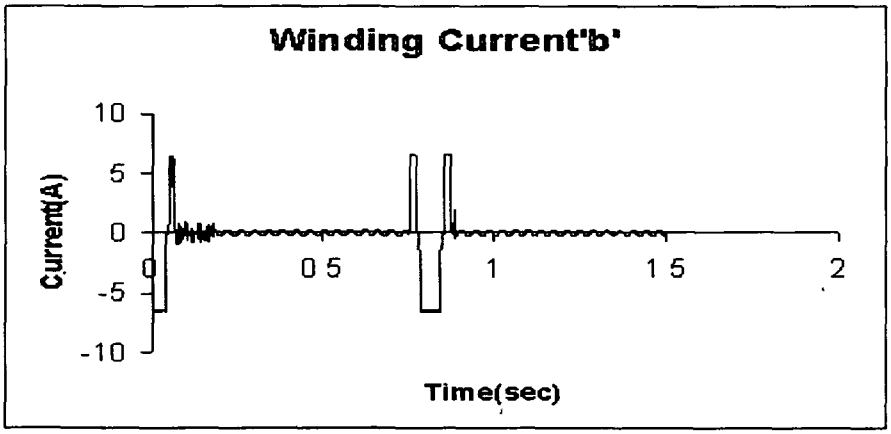

Figure 5.44: Motor Current 'i_b'

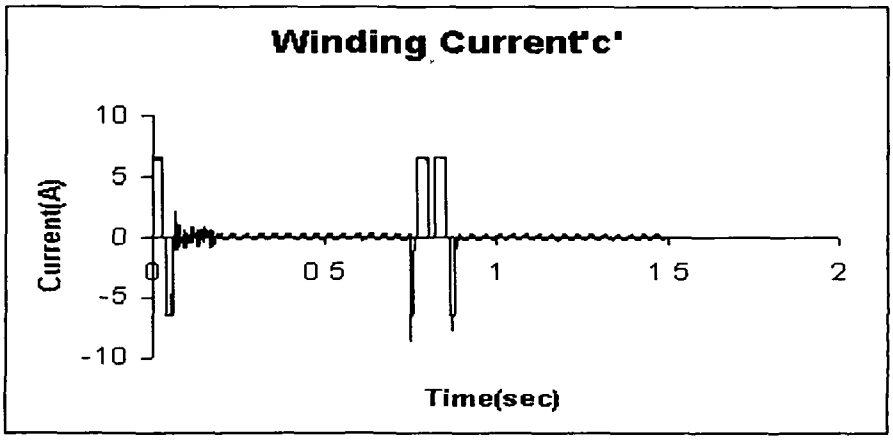

Figure 5.45: Motor Current 'i_c'

5.4.2.1 Response of PMBLDC Motor Speed with SMC Controller During Speed Reversal

Figure 5.46 shows the speed reversal dynamics of the PMBLDC motor with SMC speed controller. When the set speed is changed to –157 rad/sec (speed reversal), the SMC controller becomes active and brings the motor speed equal to the reference speed. The drive takes 205 msec for the speed reversal, which is an improvement over PI and PID controllers.

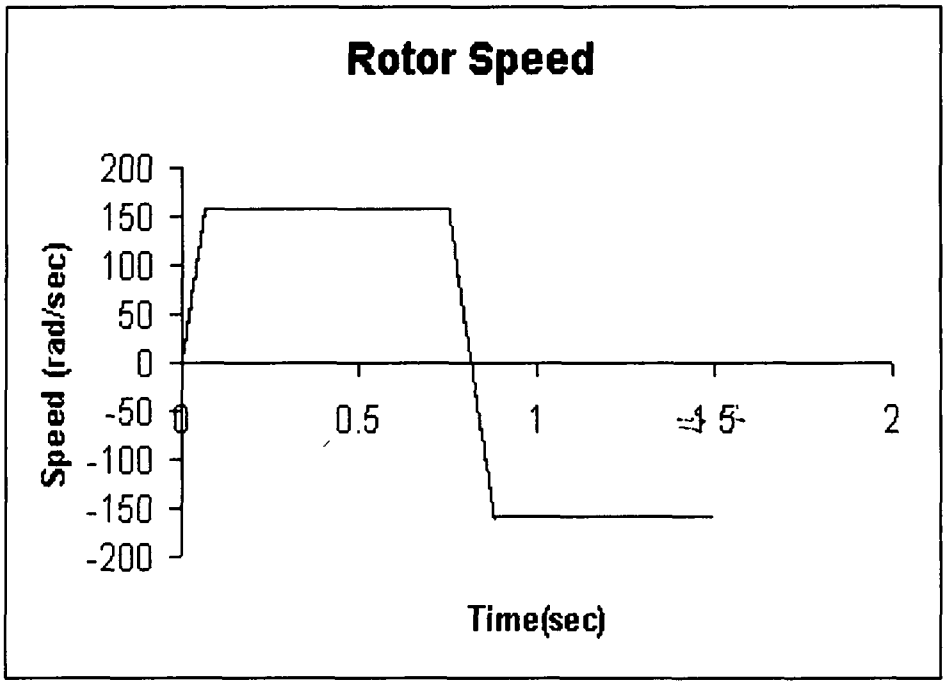

Figure 5.46: Rotor speed Vs time plot during Reversal

5.4.2.2 Response of PMBLDC Motor Torque with SMC Controller During Speed Reversal

Figure 5.47 shows the electromagnetic torque which rises instantaneously 16 Nm (Maximum permissible value) to start the motor from standstill. By the time of the motor reaches the steady-state condition, the torque also undergoes a quick transient decrease to settle down at the steady-state level of 0.185 Nm and is maintained there of before the reversal condition. When the speed is changed suddenly, the torque becomes maximum with negative value (-16 Nm) and the motor speeds up in reverse direction. Once the motor reaches the steady state in (-ve) direction, again torque is maintained at the steady-state.

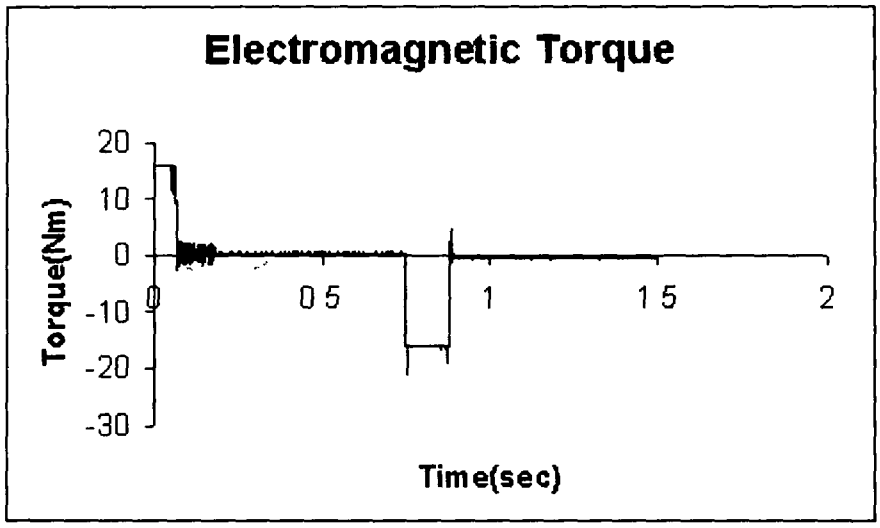

Figure 5.47: Electromagnetic Torque Vs time plot during Reversal

5.4.2.3 Response of PMBLDC Motor Voltage with SMC Controller During Speed Reversal

Figure 5.48 shows the motor voltage in one of the phases. Winding voltage increases up to 300 V / 305 V in all the three phases. The voltage does not show any perceptible change during speed reversal.

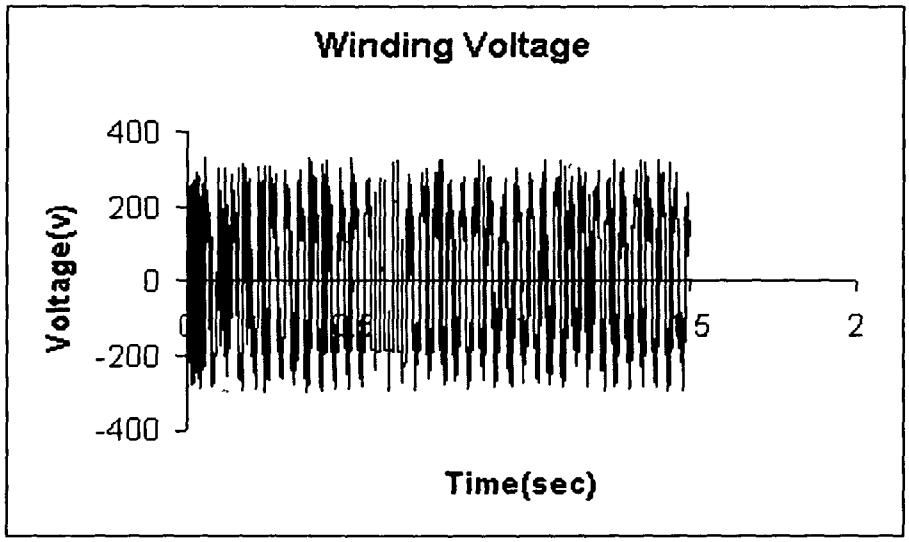

Figure 5.48: Motor winding Voltage Vs time plot during reversal

5.4.3 Response of PMBLDC Motor Current with SMC Controller during Load Perturbation

Figures 5.49 – 5.51 show the motor currents (i_a, i_b and i_c) which increase upto 6.5 A (peak) at the time of starting without any load and drop to 0.185 A (peak) during the steady-state condition. During the load perturbation, the current increases

to 4.35A to meet the increased demand of load. When the load is removed, the current returns to the original steady-state value. The winding currents are found to follow the reference currents even during the conditions of load perturbations.

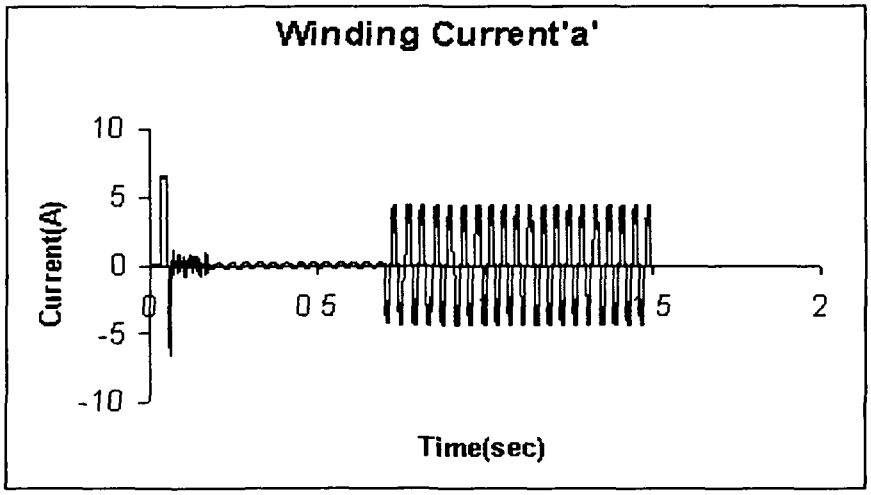

Figure 5.49: Motor Current 'i_a'

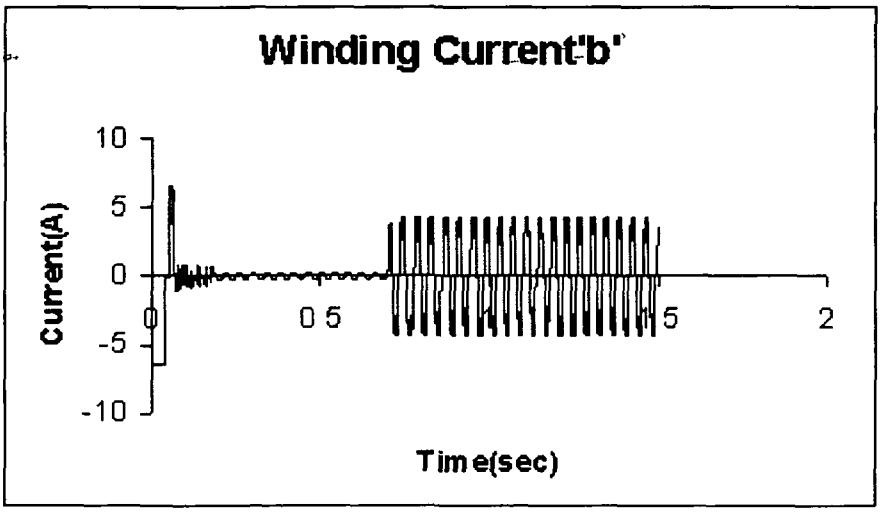

Figure 5.50: Motor Current 'i_b'

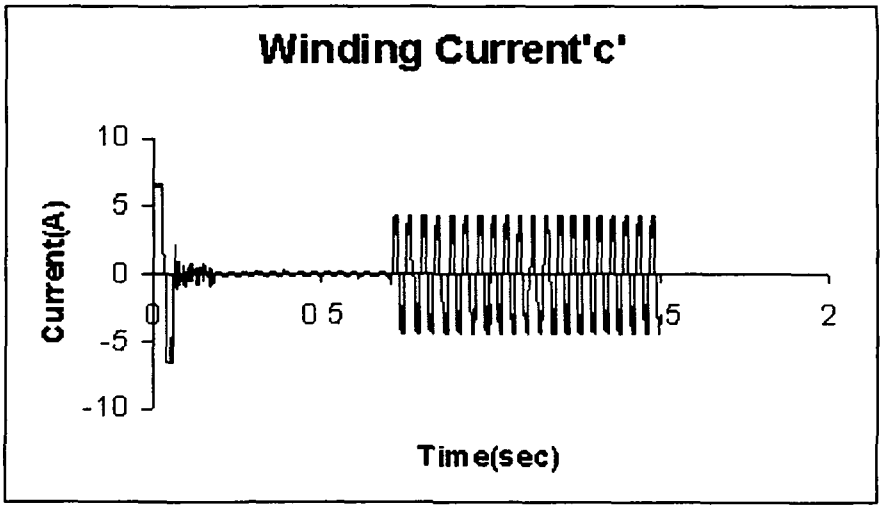

Figure 5.51: Motor Current 'i_c'

5.4.3.1 Response of PMBLDC Motor Speed with SMC Controller During Load Perturbation

Figure 5.52 shows the performance of the drive with the SMC speed controller under load perturbations. The sudden application of the load on the motor causes a small dip (4 rad/sec) in the motor speed, which persists for the period of low perturbation indicating speed-error and drive takes 205 msec to recover the rated speed.

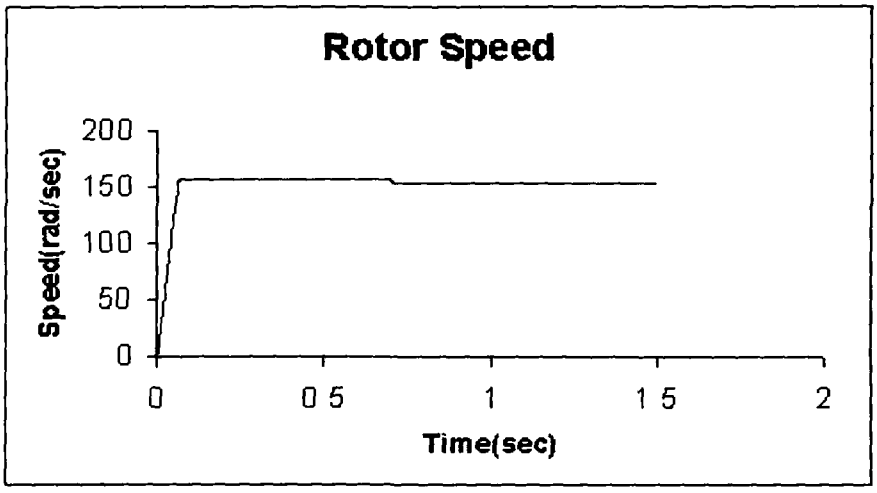

Figure 5.52: Rotor speed Vs time plot during Load Perturbation

5.4.3.2 Response of PMBLDC Motor Torque with SMC Controller during Load Perturbation

Figure 5.53 shows the electromagnetic torque which increases to 10.65 Nm and is maintained at the higher value till the load is removed. The sudden applications of the load torque results in a small and continuous drop in motor speed. The electromagnetic torque which rises to value equal to load torque applied retains the same value.

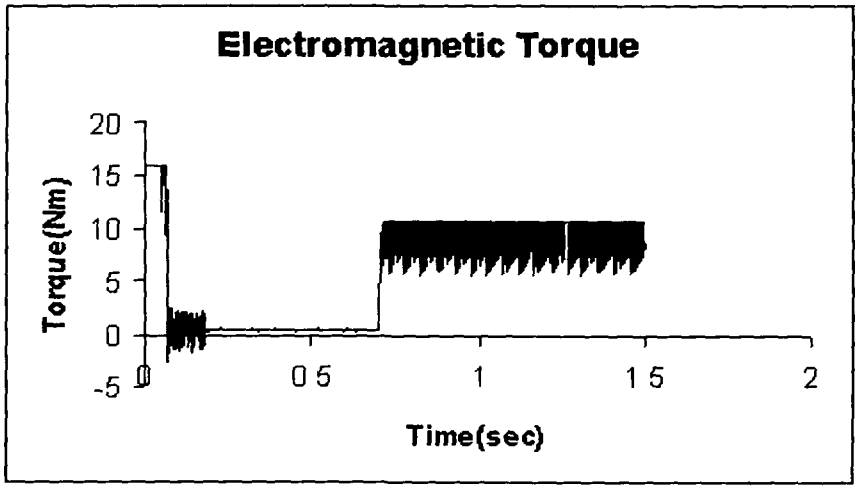

Fig. 5.53: Electromagnetic Torque Vs time plot during Load Perturbation

5.4.3.3 Response of PMBLDC Motor Voltage with SMC Controller during Load Perturbation

Figure 5.54 the motor voltage response of one of the phases. Winding voltage increases up to 300 V / 305 V in all the three phases. The voltage does not appear to be affected by low perturbation.

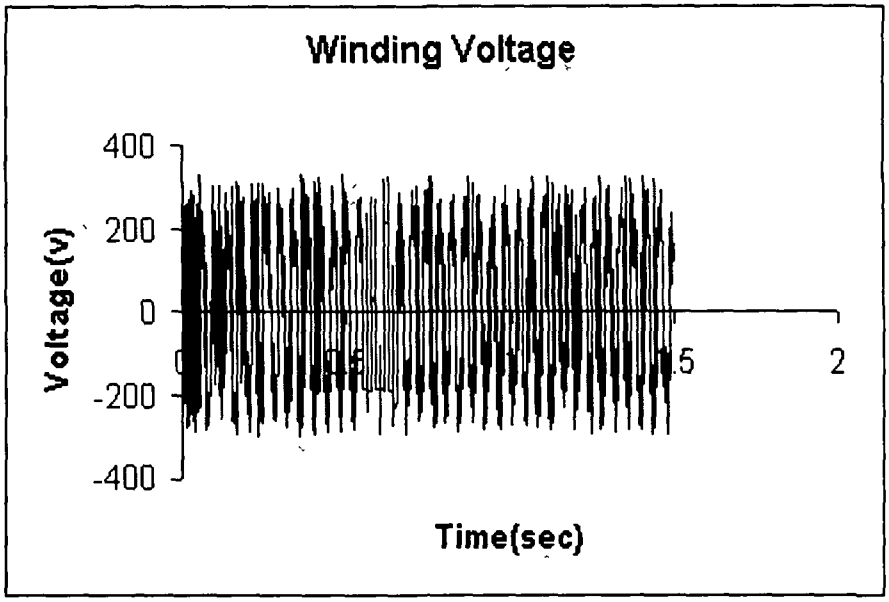

Figure 5.54: Motor winding Voltage Vs time plot during load Perturbation

5.5 Fuzzy Precompensated PI Speed Controller

The simulated dynamic responses of torque and speed of a 3-phase, 4-pole, 0.5 HP PMBLDC motor with its reference speed set at 1500 rpm (157rad/sec) are shown in Figures 5.55 to 5.72.

5.5.1 Response of PMBLDC Motor Current with Fuzzy Precompensated PI Controller During Starting

Figures 5.55 – 5.57 show the motor currents (i_a, i_b and i_c) which increase up to 3.65 A (peak) at the time of starting without any load and settle down to the steady-state of 0.08A (peak). The steady-state current is 80 mA is reached in about 130 msec after its start. The current in each phase reaches steady-state very fast which is indicative of motor's sensitivity and suitability for industrial applications. The starting current is smaller compared to PI, PID and SMC controllers which means that starting loss will be less.

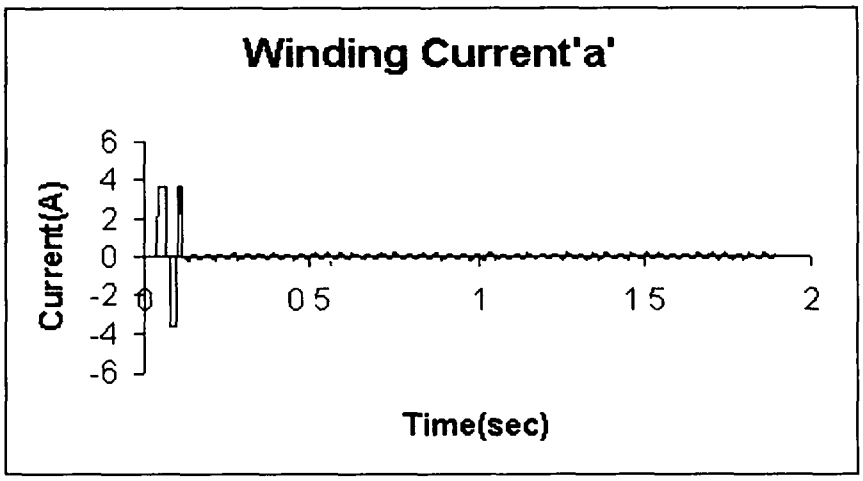

Figure 5.55: Motor Current 'i_a'

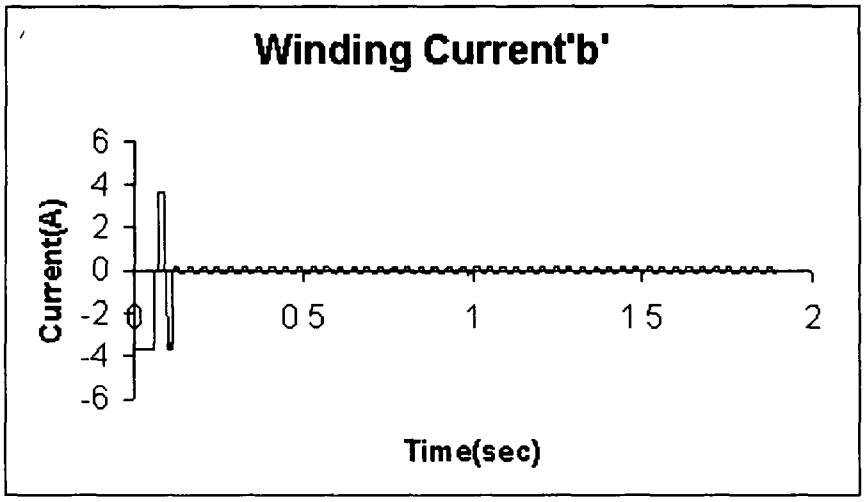

Figure 5.56: Motor Current 'i_b'

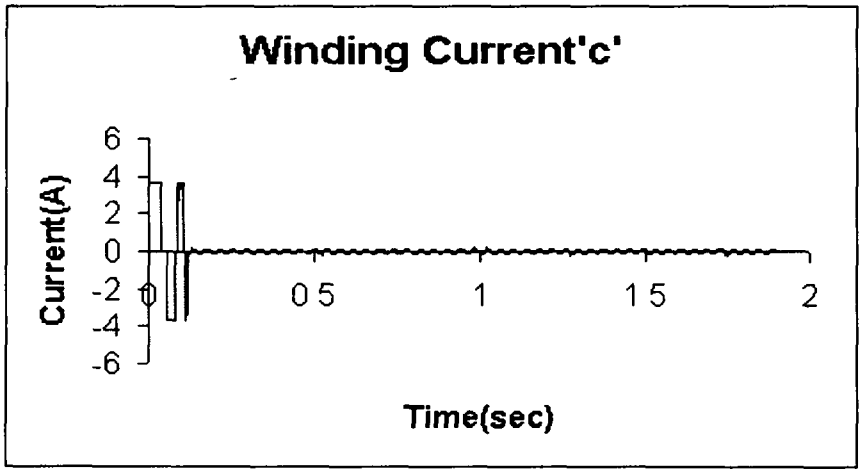

Figure 5.57: Motor Current 'i_c'

5.5.1.1 Response of PMBLDC Motor Speed with FP- PI Controller During Starting

Figure 5.58 shows the rotor speed during starting of PMBLDC motor from standstill up to rated speed of 1500 rpm (157 rad/sec) with Fuzzy PI Controller. The

controller gains are K_p= 0.09 and K_I = 0.025. The drive takes 130 msec to reach the reference speed. The developed torque rises to maximum permissible value to start the motor from standstill. From the Figure it is clear that the response has no overshoot and oscillations due the robust control structure and this illustrates a faster dynamic response to speed.

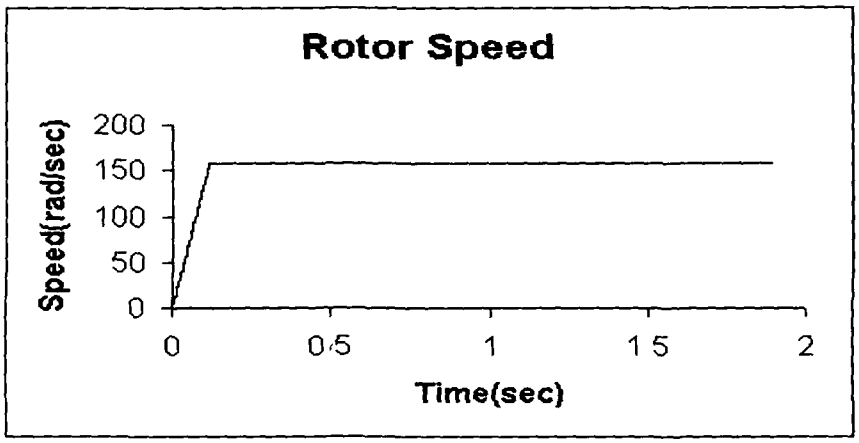

Figure 5.58: Rotor speed Vs time plot during Starting

5.5.1.2 Response of PMBLDC Motor Torque with FP-PI Controller During Starting

Figure 5.59 shows the motor electromagnetic torque which rises to 9.0 Nm (maximum permissible value) during the starting of the motor from standstill. The electromagnetic torque rises instantaneously to 9 Nm to start the motor from the standstill condition and by the time the motor reaches the steady state, the torque also undergoes a quick transient decrease and settles down to the steady-state level of 0.30 Nm and maintains the same level over the remaining period of time. The level of electromagnetic torque under steady-state is decided by the load torque on the motor shaft.

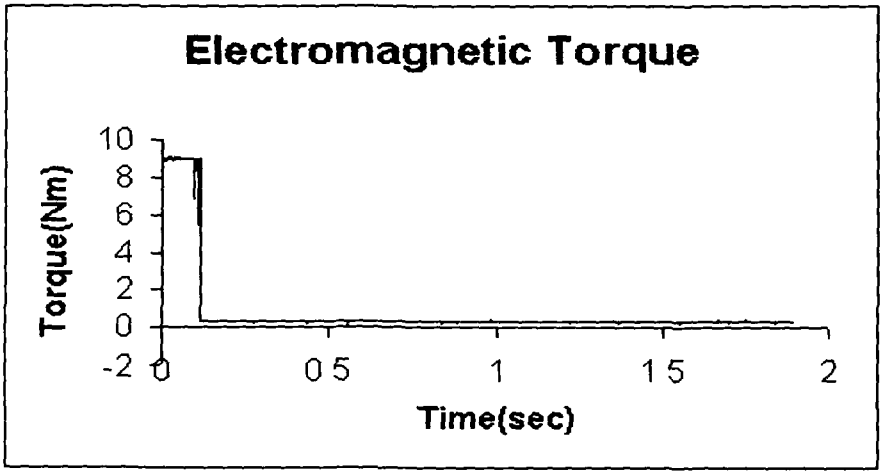

Figure 5.59: Electromagnetic Torque Vs time plot during Starting

5.5.1.3 Response of PMBLDC Motor Voltage with (FP- PI) Controller During Starting

Figure 5.60 shows the motor voltage response of one of the phases. Winding voltage increases up to 300 V / 305 V in all the three phases.

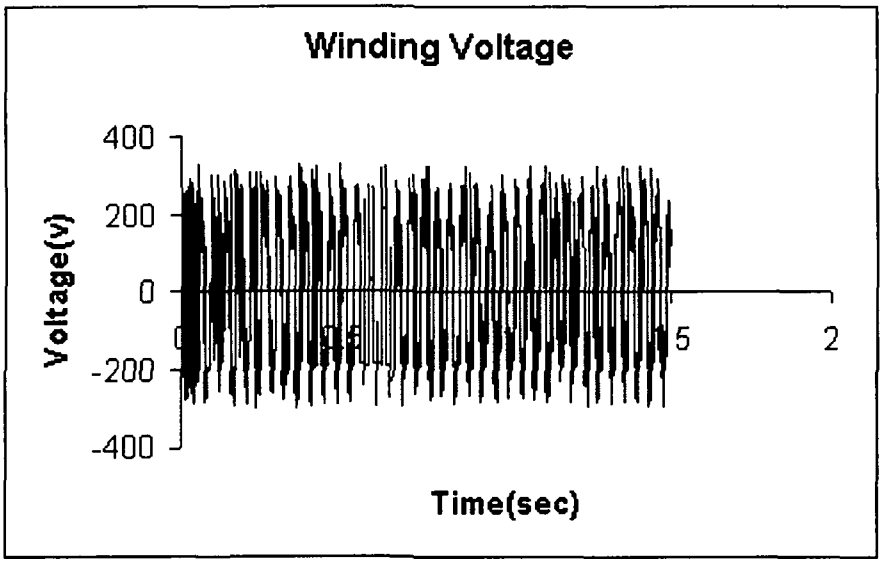

Figure 5.60: Motor winding Voltage Vs time plot during Starting

5.5.2 Response of PMBLDC Motor Current with (FP- PI) Controller During Speed Reversal

Figures 5.61–5.63 show the motor currents (i_a, i_b and i_c) which increase to 3.65 A (peak) at the time of starting at no-load and drop to the steady-state level of 0.125 A (peak). After 850 msec currents again rise up to 3.65A (peak) due to the speed reversal. The drive takes 230 msec for a reversal of speed and the currents reach in the original value of 0.125 A.

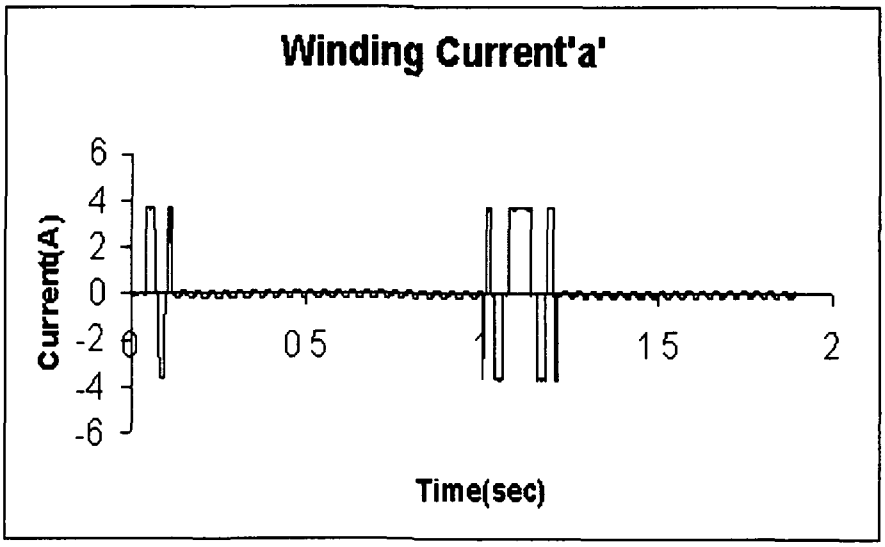

Figure 5.61: Motor Current 'i_a'

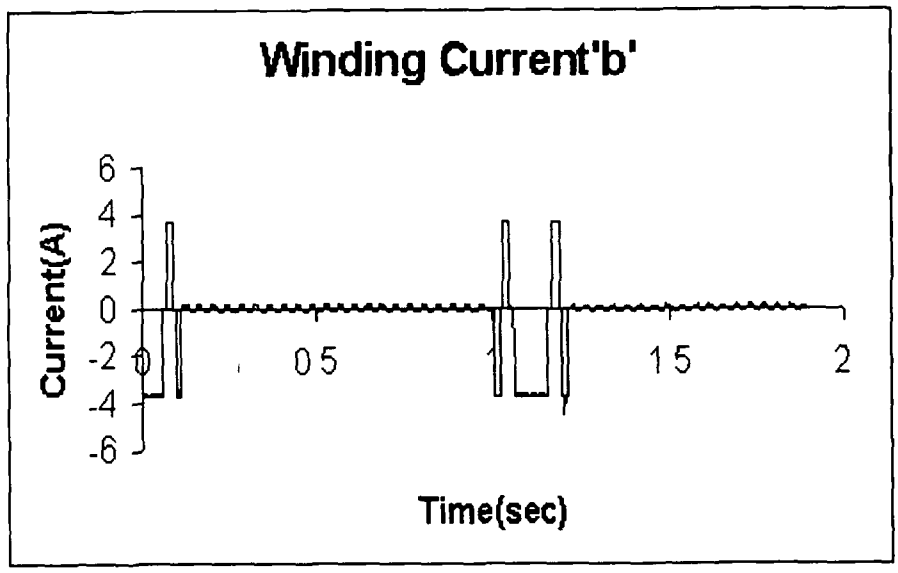

Figure 5.62: Motor Current 'i_b'

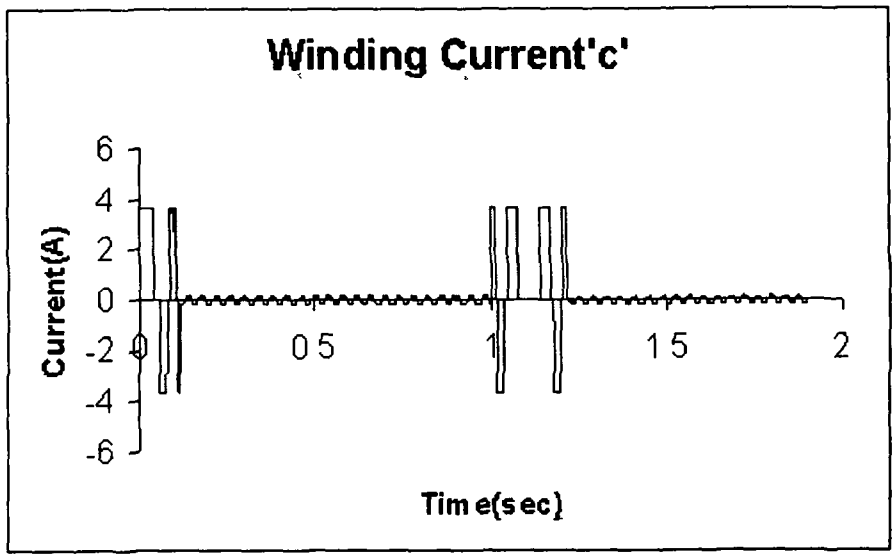

Figure 5.63: Motor Current 'i_c'

5.5.2.1 Response of PMBLDC Motor Speed with (FP- PI) Controller During Speed Reversal

Figure 5.64 shows the speed reversal dynamics of the PMBLDC motor with Fuzzy-PI speed controller. When the set speed is changed to –157 rad/sec (speed reversal), the Fuzzy-PI controller becomes active and brings the motor speed equal to the reference speed. The drive takes 230 msec for the speed reversal. The drive is simulated with different controller gains. It is quite interesting to observe that the Fuzzy-PI speed controller results in improved performance of the drive irrespective of the values of the gain parameters (K_p, K_I). This offers the advantage of avoiding the problem of tuning the gains of the PI controller.

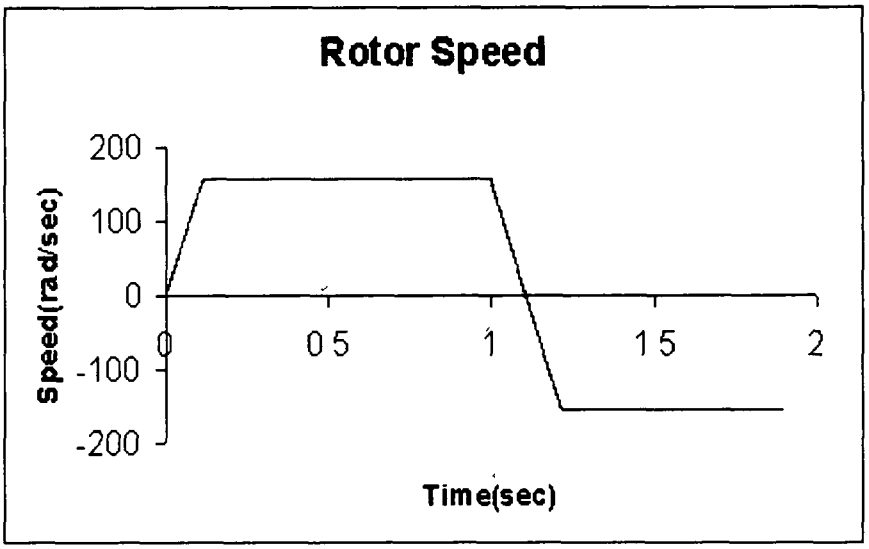

Figure 5.64: Rotor speed Vs time plot during Reversal

5.5.2.2 Response of PMBLDC Motor Torque with FP-PI Controller During Speed Reversal

Figure 5.65 shows the electromagnetic torque which rises instantaneously to 9 Nm (Maximum permissible value) to start the motor from the standstill. By the time the motor reaches the steady-state condition, the torque also undergoes a quick transient decrease to settle down at the steady-state level of 0.35 Nm and is maintained there. When the speed is changed suddenly, the torque becomes maximum with negative value (-9 Nm) and the motor speeds up in reverse direction. Once the motor reaches the steady- state (-ve) the torque also attains the final steady-state value.

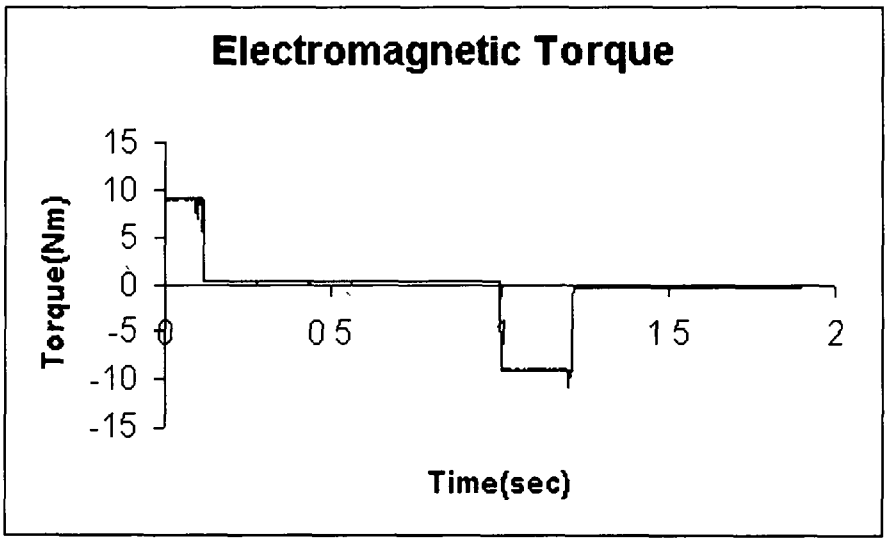

Figure 5.65: Electromagnetic Torque Vs time plot during Reversal

5.5.2.3 Response of PMBLDC Motor Voltage with Fuzzy PI Controller During Speed Reversal

Figure 5.66 shows the motor voltage response of one of the phases. Winding voltage increases up to 300 V / 305V (peak) in all the three phases. There is no appearant change in voltage during speed reversal.

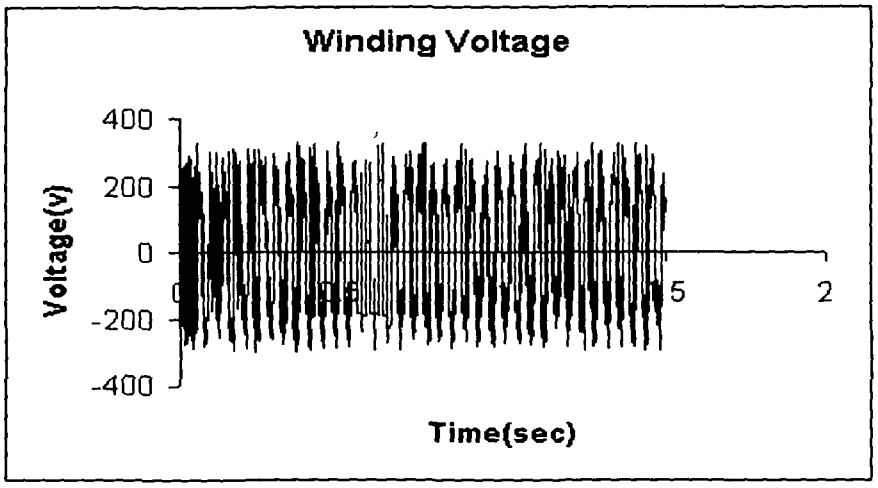

Figure 5.66: Motor winding Voltage Vs time plot during Reversal

5.5.3 Response of PMBLDC Motor Current with Fuzzy PI Controller During Load Perturbations

Figures 5.67 – 5.69 show the motor currents (i_a, i_b and i_c) which increase up to 3.65 A(peak) at the time of starting without any load and settle down at 0.15 A during the steady-state condition. During the load perturbation, the current increases to 2.25A to meet the demand of load. When the load is removed, the current returns the original value 0.15A. The winding currents are found to follow the reference currents even during the conditions of load perturbations.

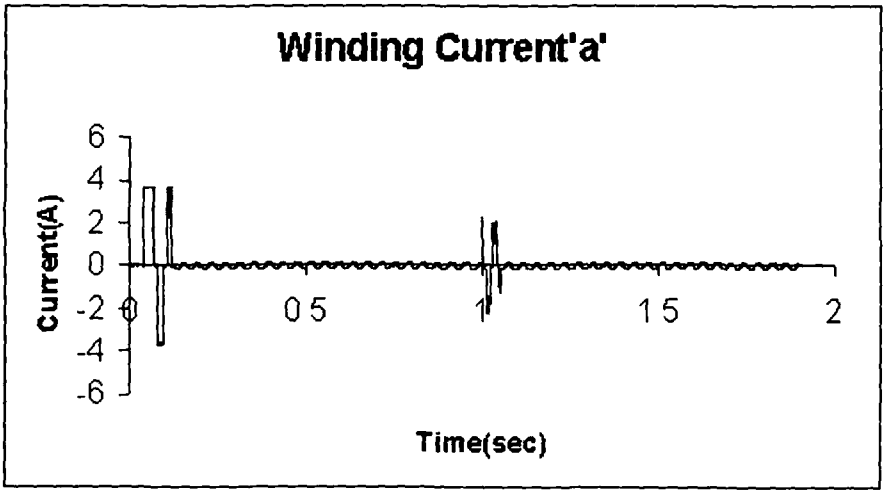

Figure 5.67: Motor Current 'i_a'

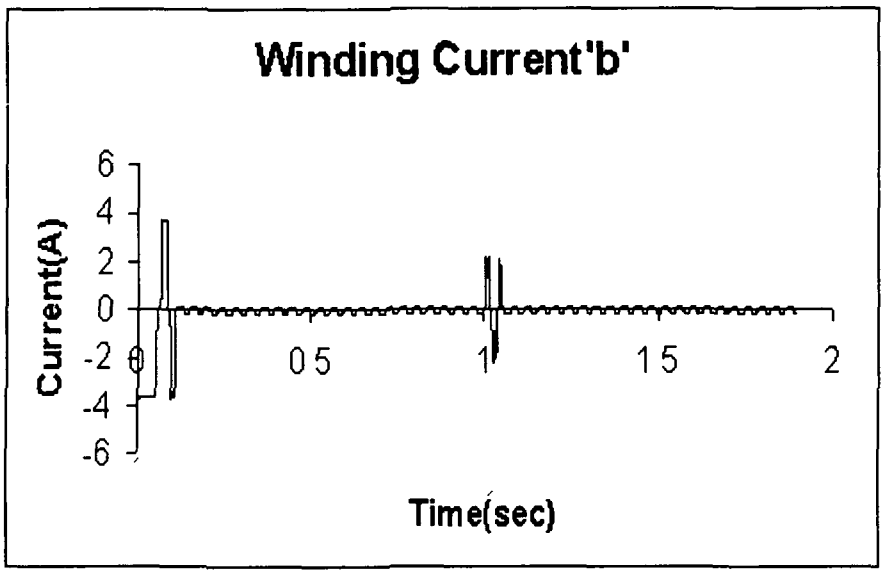

Figure 5.68: Motor Current 'i_b'

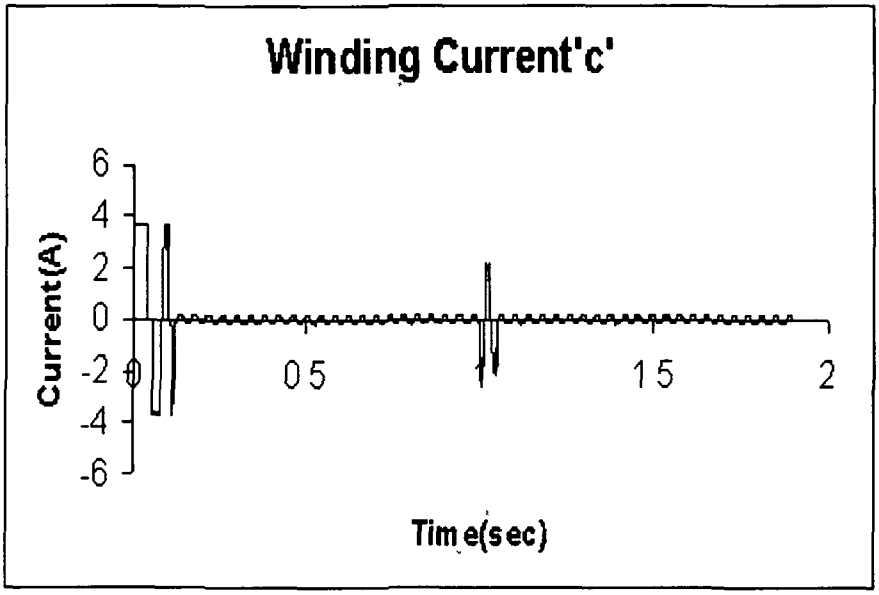

Figure 5.69: Motor Current 'i_c'

5.5.3.1 Response of PMBLDC Motor Speed with Fuzzy PI Controller During Load Perturbations

Figure (5.70) shows the performance of the drive with the Fuzzy-PI speed controller under load perturbations. The sudden application of full load at t=1.0 sec and sudden removal of full load at t=1.05 sec on the shaft cause a negligible variation in speed. It takes no time (about 5msec) to reach the reference speed. The Fuzzy-PI speed controller offers smooth action and makes the drive highly robust under the action of load perturbations.

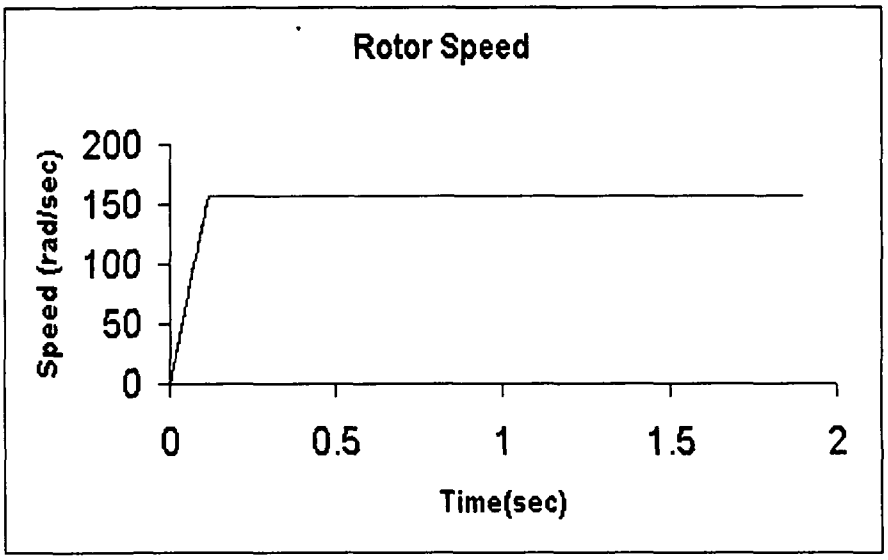

Figure 5.70: Rotor speed Vs time plot during Load Perturbations

5.5.3.2 Response of PMBLDC Motor Torque with Fuzzy PI Controller during Load Perturbations

Figure 5.71 shows the electromagnetic torque which increases to 4.8 Nm and is maintained at the higher value till the load is removed. It is observed that the Fuzzy-PI controller shows the superior response over PI controller in terms of the dynamics under load perturbations

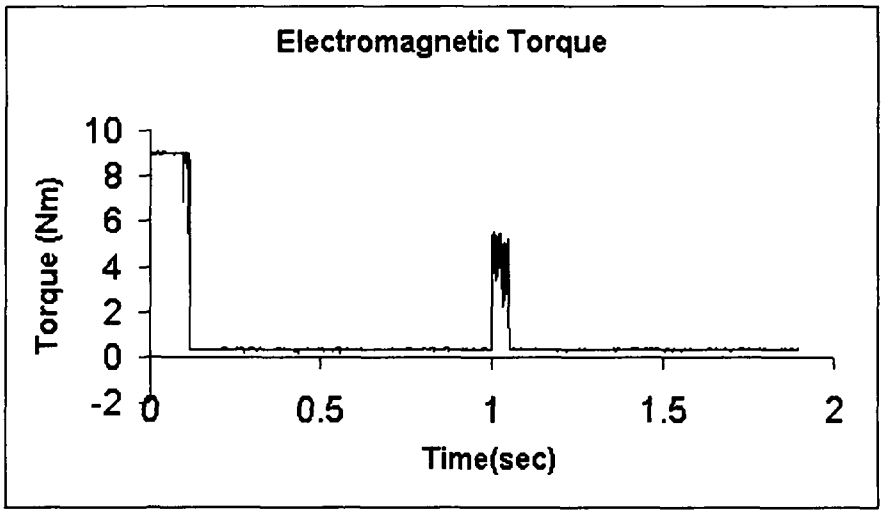

Figure 5.71: Electromagnetic Torque Vs time plot during Load Perturbations

5.5.3.3 Response of PMBLDC Motor Voltage with Fuzzy PI Controller During Load Perturbations

Figure 5.72 shows the motor voltage in one of the phases. Winding voltage is increases up to 300 V / 305 V (peak) in all the three phases. The load perturbation seems to have no effect on the motor voltage.

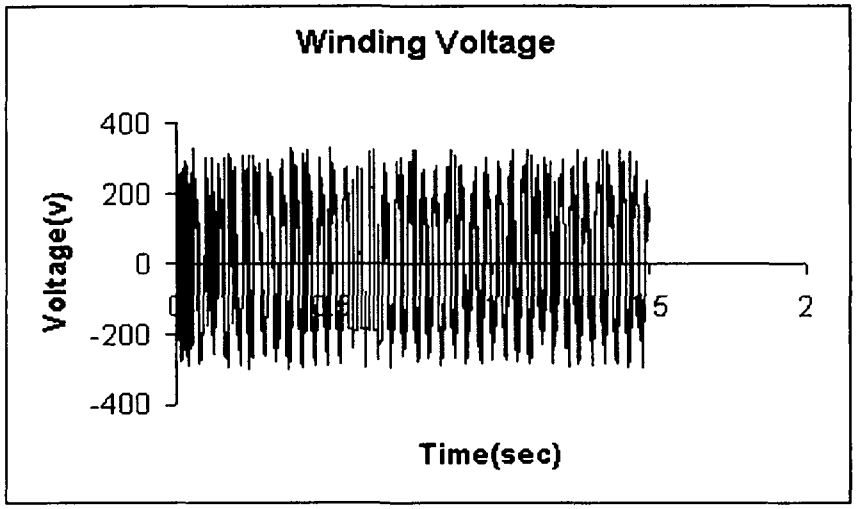

Figure 5.72: Motor winding Voltage Vs time plot during Load Perturbations

5.6 Fuzzy PID Speed Controller

The simulated dynamic responses of currents, rotor speed, torque and winding voltages of a 3-phase, 4-pole, 0.5 HP PMBLDC motor with its reference speed set at 157 rad/sec are shown in Figures 5.73 to 5.90.

5.6.1 Response of PMBLDC Motor Current with Fuzzy PID Controller During Starting

Figures 5.73– 5.75 show the motor currents (i_a, i_b and i_c) increasing up to 3.25 A (peak) at the time of starting at no-load and settling down at 0.20A (peak) during the steady-state condition. The steady-state current is reached in about 150 msec after its start on no-load.

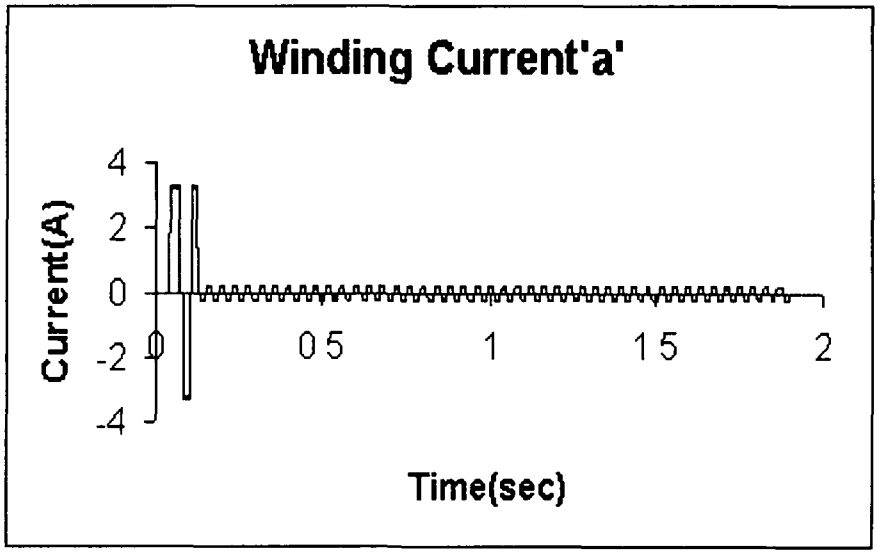

Figure 5.73: Motor Current 'i_a'

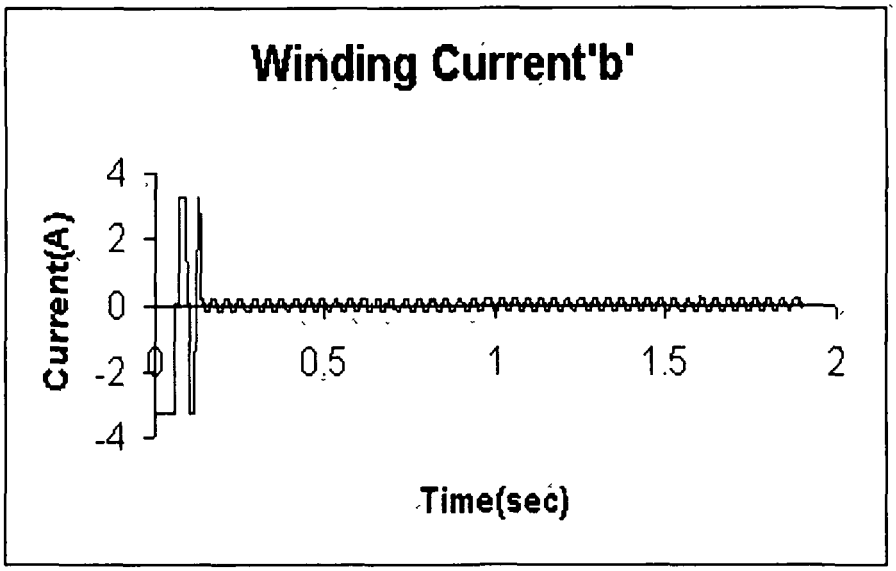

Figure 5.74: Motor Current 'i_b'

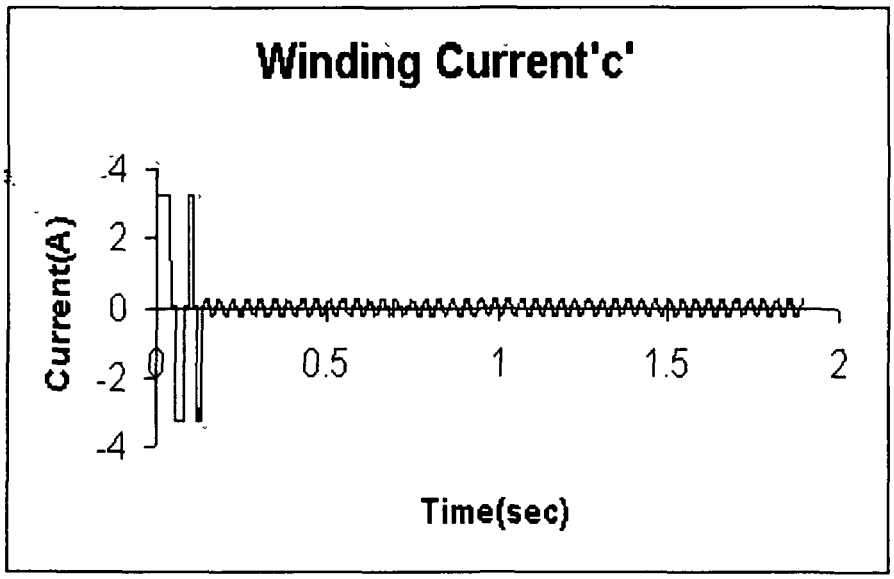

Figure 5.75: Motor Current 'i_c'

5.6.1.1 Response of PMBLDC Motor Speed with Fuzzy PID Controller During Starting

Figure 5.76 shows the rotor speed during starting of PMBLDC motor from standstill up to rated speed of 1500 rpm (157 rad/sec) with the Fuzzy-PID controller. The controller gains are K_p=0.09 and K_I= 0.0125 and K_D= 1.01. The drive takes 150 msec to reach the reference speed. It is clear that the response is free from overshoots and oscillations. Only during starting, the speed shows oscillations with marginal values. This illustrates the faster dynamic response of the proposed controller.

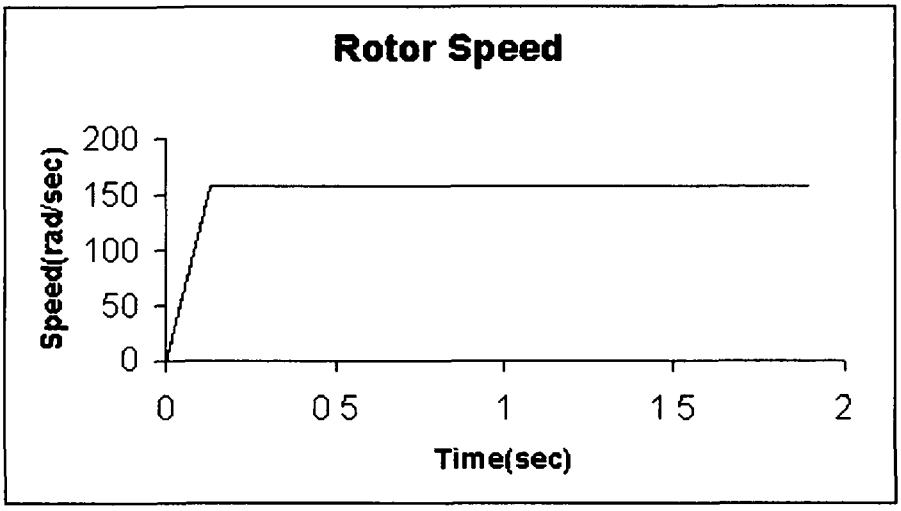

Figure 5.76: Rotor speed Vs time plot during Starting

5.6.1.2 Response of PMBLDC Motor Torque with Fuzzy PID Controller During Starting

Figure 5.77 shows the developed electromagnetic torque which rises to 8.0 Nm (maximum permissible value) during the starting of the motor from stand still condition. The rise in torque is almost instantaneous. By the time the motor reaches the steady state, the torque also undergoes a quick decrease and settles down to the steady-state level of 0.50 Nm and is maintained at the same level over the remaining period of time.

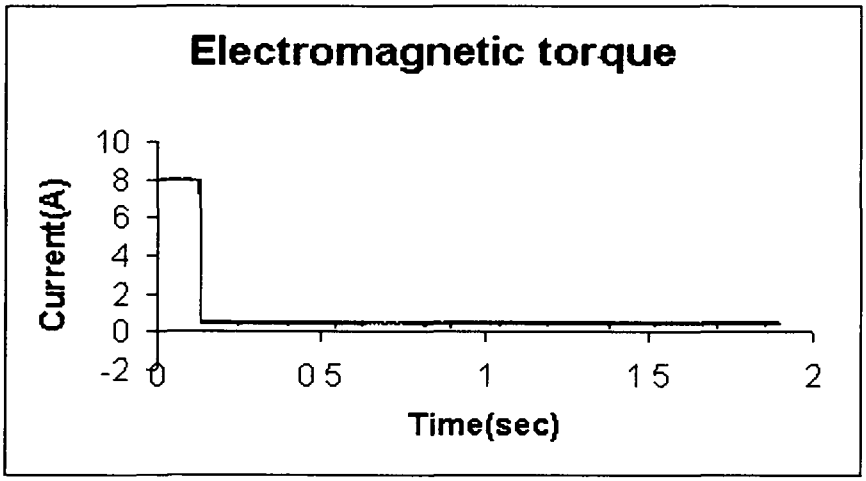

Figure 5.77: Electromagnetic Torque Vs time plot during Starting

5.6.1.3 Response of PMBLDC Motor Voltage with Fuzzy PID Controller During Starting

Figure 5.78 shows the motor voltage response of one of the phases. Winding voltage is increases up to 300 V / 305V (peak) in all the three phases.

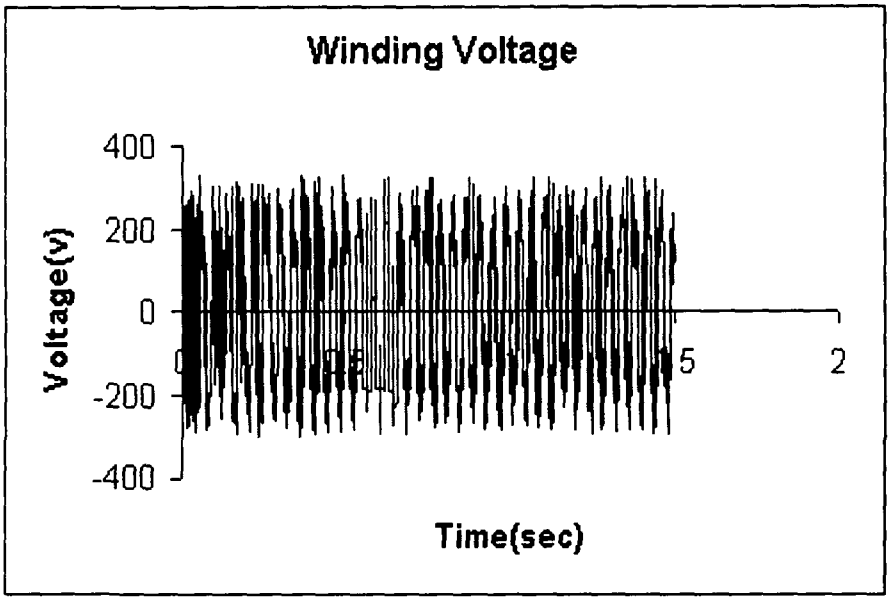

Figure 5.78: Motor winding Voltage Vs time plot during Starting

5.6.2 Response of PMBLDC Motor Current with Fuzzy PID Controller During Speed Reversal

igures 5.79–5.81 show the motor currents (i_a, i_b and i_c) which increase up to 4.0 A (peak) at the time of starting without any load and drop to 0.20 A(peak) at the steady state and then after 715 msec currents again rise up to 4.0 A due to the speed reversal. The drive takes 230 msec for a reversal of speed and the currents reach the original value of 0.20A.

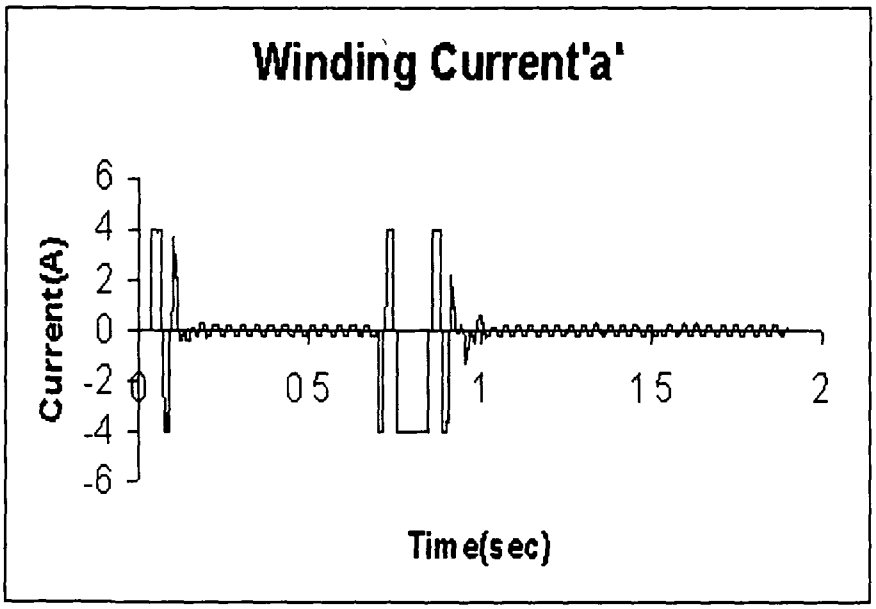

Figure 5.79: Motor Current 'i_a'

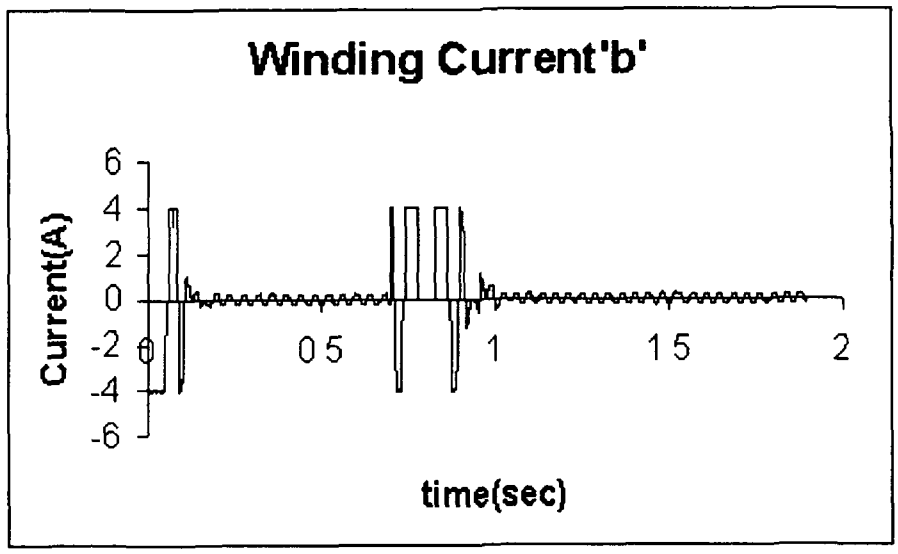

Figure 5.80: Motor Current 'i_b'

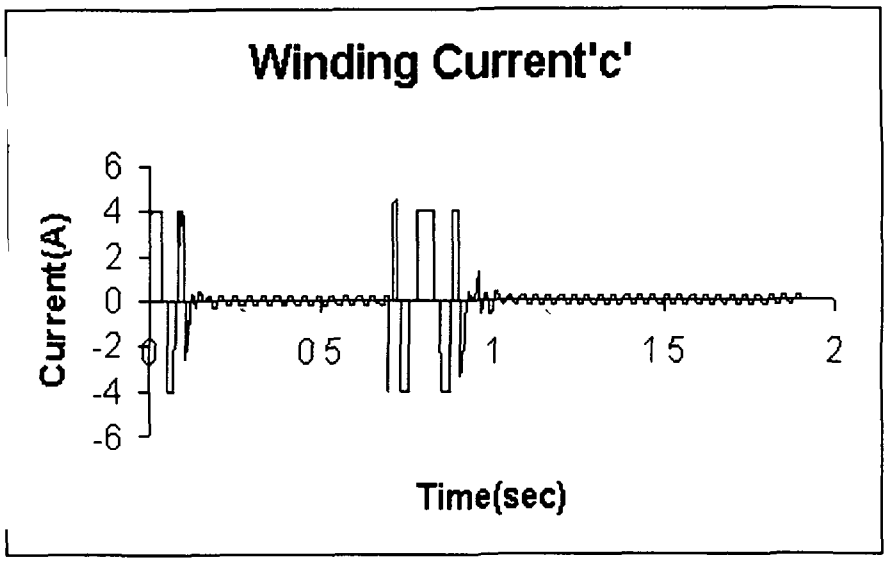

Figure 5.81: Motor Current 'i_c'

5.6.2.1 Response of PMBLDC Motor Speed with Fuzzy PID Controller During Speed Reversal

Figure 5.82 shows the speed reversal dynamics of the PMBLDC motor with Fuzzy-PID speed controller. When the set speed is changed to –157 rad/sec (speed reversal), the Fuzzy-PID controller becomes active and brings the motor speed equal to the reference speed. The drive takes 230 msec for the speed reversal. The drive is simulated with different controller gains. It is quite interesting to observe that the Fuzzy- PID speed controller results in improved performance of the drive irrespective of the values of the gain parameters (K_p, K_I and K_D). This offers the advantage of avoiding the problem of tuning the gains of the PID controller.

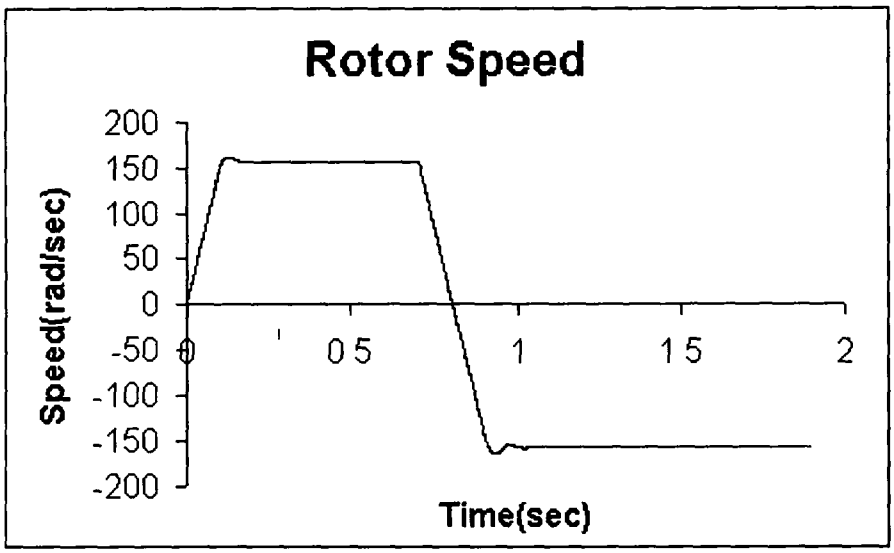

Figure 5.82: Rotor speed Vs time plot during Reversal

5.6.2.2 Response of PMBLDC Motor Torque with Fuzzy PID Controller During Speed Reversal

Figure 5.83 shows the electromagnetic torque which rises instantaneously to 10 Nm (Maximum permissible value) to start the motor from the standstill. By the time the motor reaches the steady-state condition, the torque also undergoes a transient decrease to settle down at the steady-state level of 0.45 Nm and is maintained there of before the reversal condition. When the speed is changed suddenly, the torque becomes maximum with negative value (-10 Nm) and the motor speeds up in reverse direction. Once the motor reaches the steady- state speed in the (-ve) direction, the torque drops down to the value of 0.45 Nm. It may be notes that the decrease in torque is oscillatory.

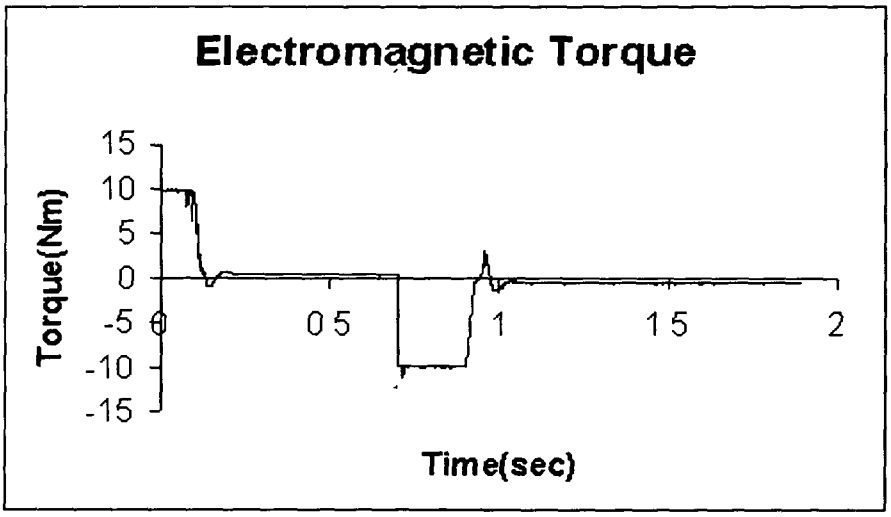

Figure 5.83: Electromagnetic Torque Vs time plot during Reversal

5.6.2.3 Response of PMBLDC Motor Voltage with Fuzzy PID Controller During Speed Reversal

Figure 5.84 shows the motor voltage response of one of the phases. Winding voltage is increases up to 300 V / 305 V in all the three phases.

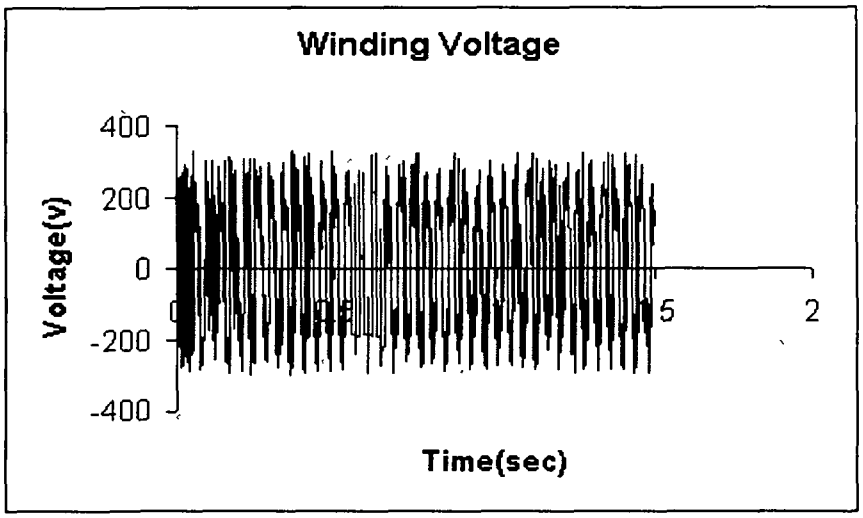

Figure 5.84: Motor winding Voltage Vs time plot during Reversal

5.6.3 Response of PMBLDC Motor Current with Fuzzy PID Controller during Load Perturbations

Figures 5.85–5.87 show the motor currents (i_a, i_b and i_c) which increase up to 4.0 A (peak) at the time of starting without any load and settle down at 0.01A (peak) at the steady-state condition. During the load perturbation, the current increases to 1.15A to meet the increased demand of load. The winding currents are found to follow the reference currents even during the conditions of load perturbations.

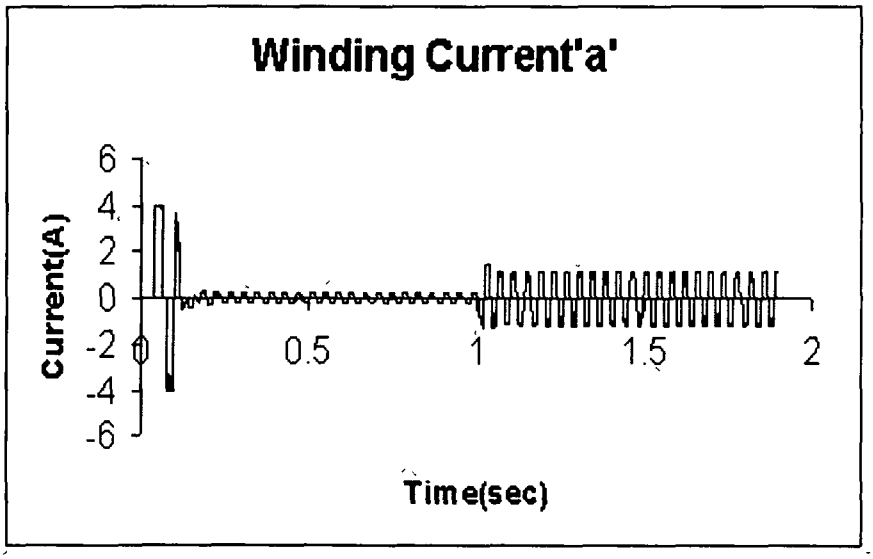

Figure 5.85: Motor Current 'i_a'

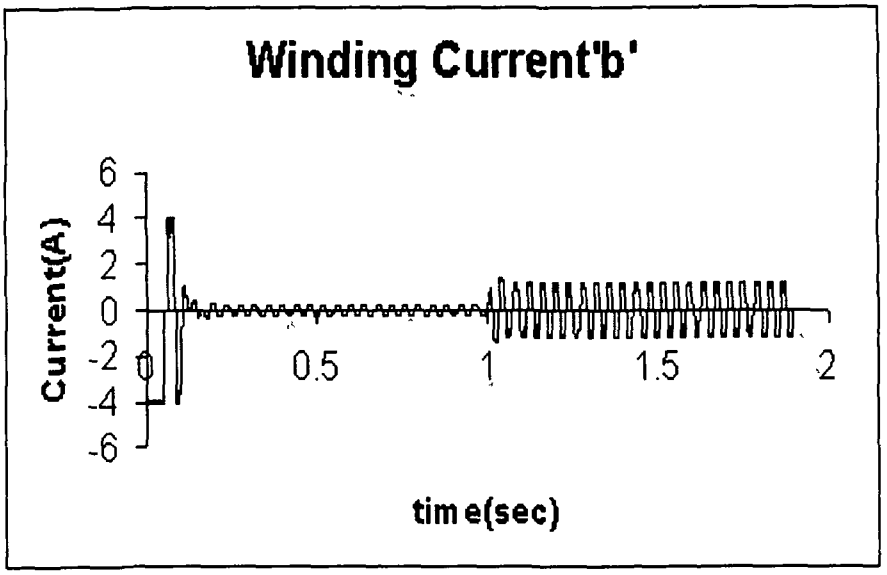

Figure 5.86: Motor Current 'i_b'

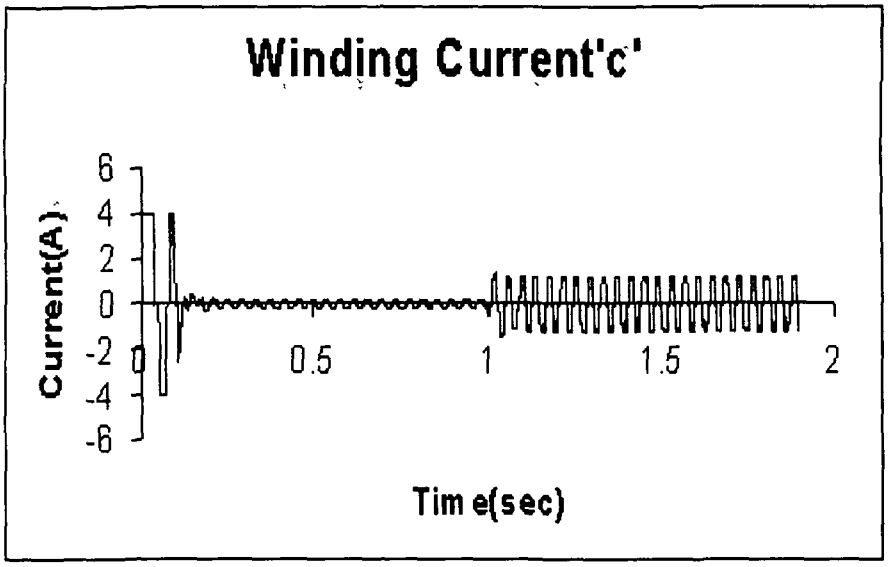

Figure 5.87: Motor Current 'i_c'

5.6.3.1 Response of PMBLDC Motor Speed with Fuzzy PID Controller During Load Perturbations

Figure 5.88 shows the performance of the drive with the Fuzzy-PID speed controller under load perturbations. The sudden application of full load at t = 1.0 sec and sudden removal of full load at t=1.05 sec on the shaft cause a negligible variation in speed. It takes negligible time(about 5 msec) to reach the reference speed. The Fuzzy- PID speed controller offers smooth action and makes the drive highly robust under load perturbations; however, a few ripples in the speed response are present.

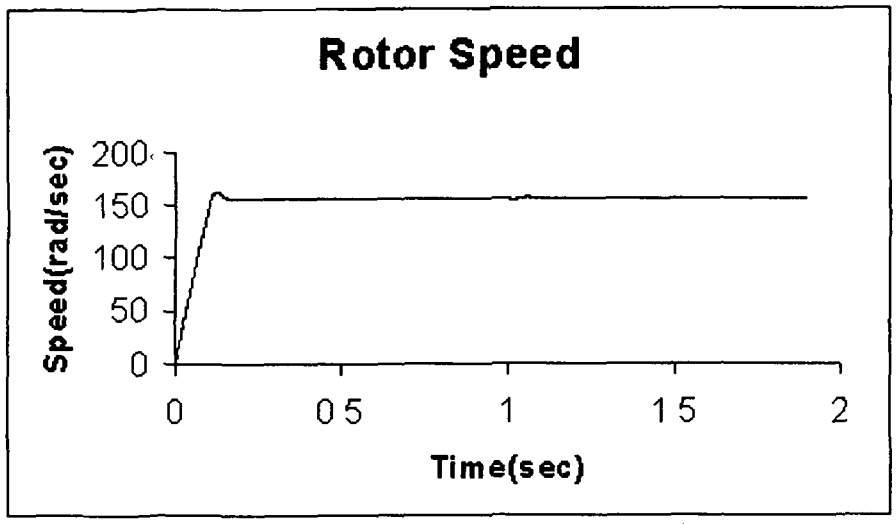

Figure 5.88: Rotor speed Vs time plot during Load Perturbations

5.6.3.2 Response of PMBLDC Motor Torque with Fuzzy PID Controller During Load Perturbations

Figure 5.89 shows the electromagnetic torque which increases to 2.85 Nm on application of load and is maintained at the higher value till the load is removed. It is observed that the Fuzzy PID controller shows the superior response over PID controller in terms of dynamics under load perturbations.

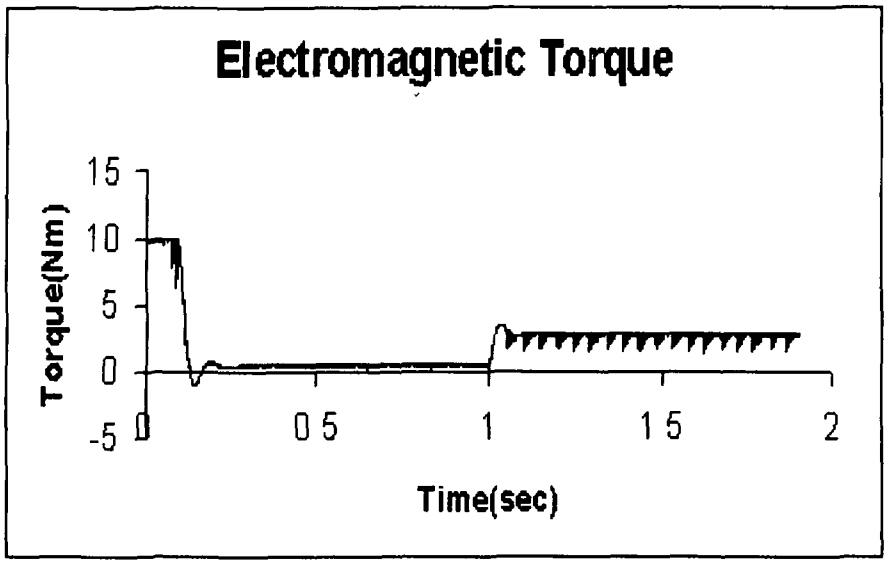

Fig. 5.89: Electromagnetic Torque Vs time plot during Load Perturbations

5.6.3.3 Response of PMBLDC Motor Voltage with Fuzzy PID Controller During Load Perturbations

Figure 5.90 shows the motor voltage response of one of the phases. Winding voltage is increases up to 300 V / 305 V (peak) in all the three phases. There is no apparent change in voltage due to load perturbations.

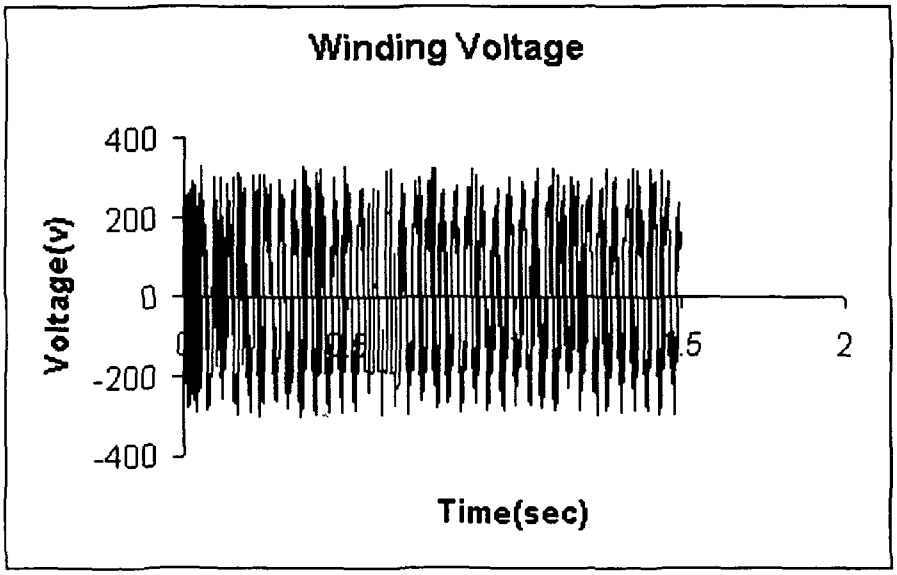

Fig. 5.90: Motor winding Voltage Vs time plot during Load Perturbations

5.7 Fuzzy SMC Speed Controller

The simulated dynamics responses of winding currents of three phases, speed, torque and winding voltages of a 3-phase, 4-pole and 0.5HP PMBLDC motor with its reference speed set at 157 rad/sec are presented in this section. For each of these cases, results pertaining to three modes of dynamic operations, namely, the starting, the speed reversal and the load perturbation have been obtained. The simulated responses of the drive, thus obtained, are shown in Figures 5.91 to 5.108. Figures 5.91 to 5.96 illustrate the starting response of the drive with each of speed controllers considered in this investigation. Figures 5.97 to 5.102 refer to speed reversal while Figures 5.103 to 5.108 refer to the load perturbations.

5.7.1 Response of PMBLDC Motor Current with Fuzzy SMC Controller During Starting

Figures 5.91–5.93 show the motor currents (i_a, i_b and i_c) which increase up to 4.05 A (peak) at the time of starting without any load and settle down at 0.08 A(peak) at the steady-state condition. The steady-state current is about 80 mA which is reached in about 125 msec after its start on no-load. The current response in each phase reaches steady- state very fast which is indicative of motor's sensitivity towards its suitability for particular industrial application.

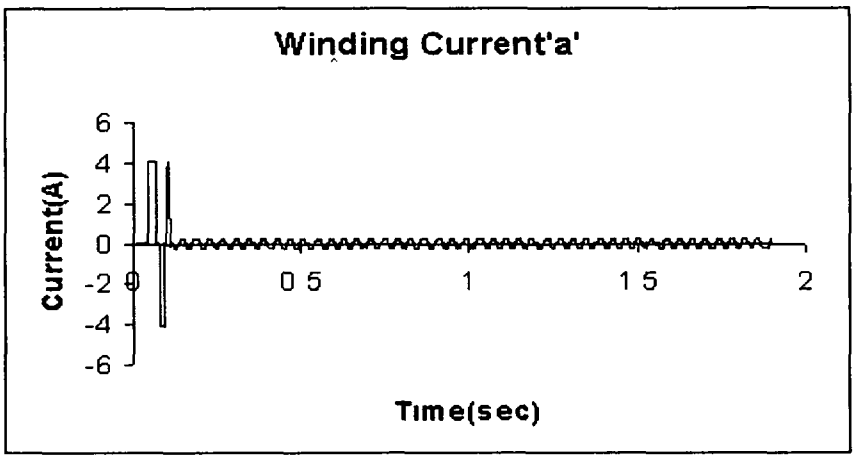

Figure 5.91: Motor Current 'i_a'

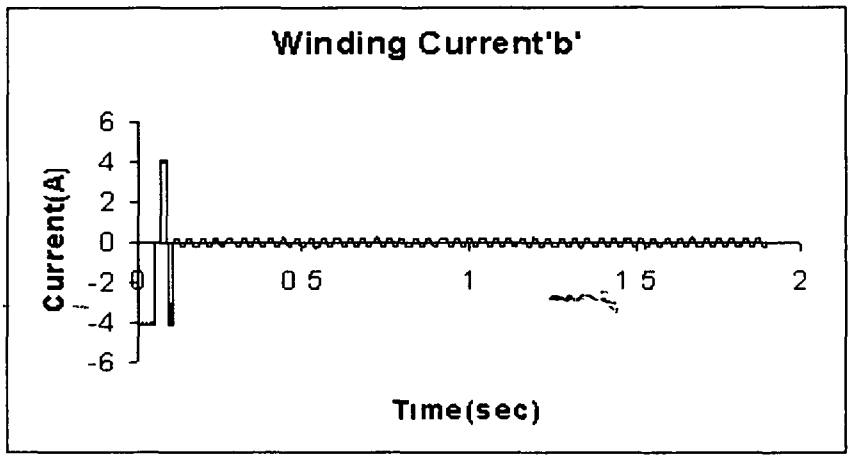

Figure 5.92: Motor Current 'i_b'

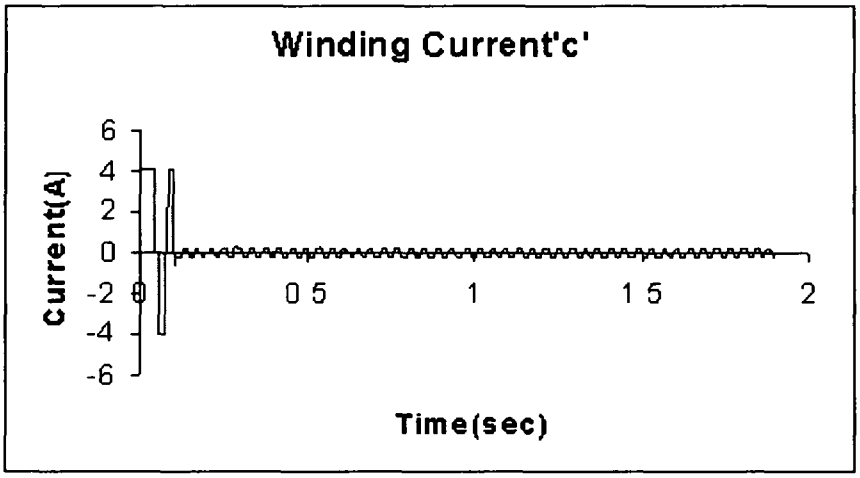

Figure 5.93: Motor Current 'i_c'

5.7.1.1 Response of PMBLDC Motor Speed with Fuzzy SMC Controller During Starting

Figure 5.94 shows the rotor speed during starting of PMBLDC motor from standstill up to rated speed of 1500 rpm (157 rad/sec) with the Fuzzy-SMC Controller. The controller gains are K_p=1.5, K_I= 0.001, and K_I= 2.0. The drive takes 125 msec to

reach the reference speed. It is clear that the response is free from overshoots and oscillations.

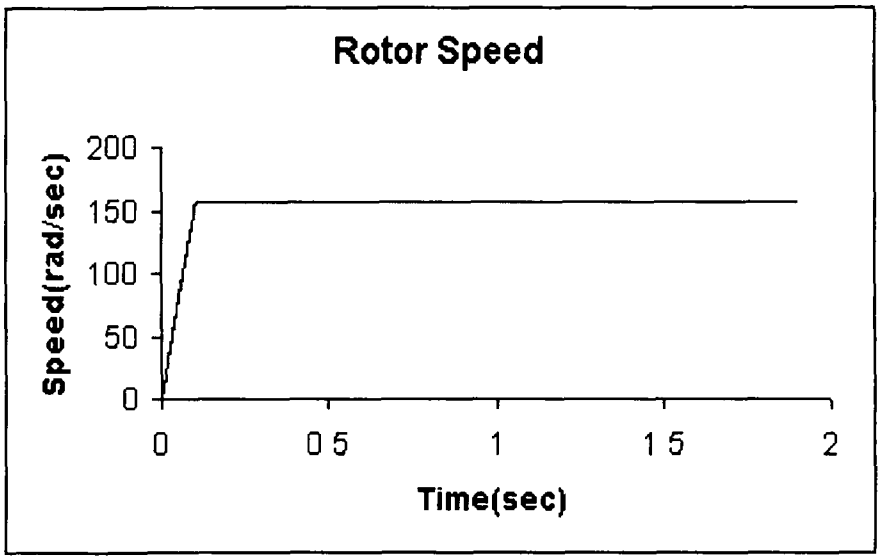

Figure 5.94: Rotor speed Vs time plot during Starting

5.7.1.2 Response of PMBLDC Motor Torque with Fuzzy SMC Controller During Starting

Figure 5.95 shows the motor electromagnetic torque which rises to 10 Nm (maximum permissible value) during the starting of the motor from standstill. The rise in torque is almost instantaneous. By the time the motor reaches the steady-state condition, the torque also undergoes a quick decrease and settles down to the steady-state value of 0.45 Nm and maintains the same level over the remaining period of time.

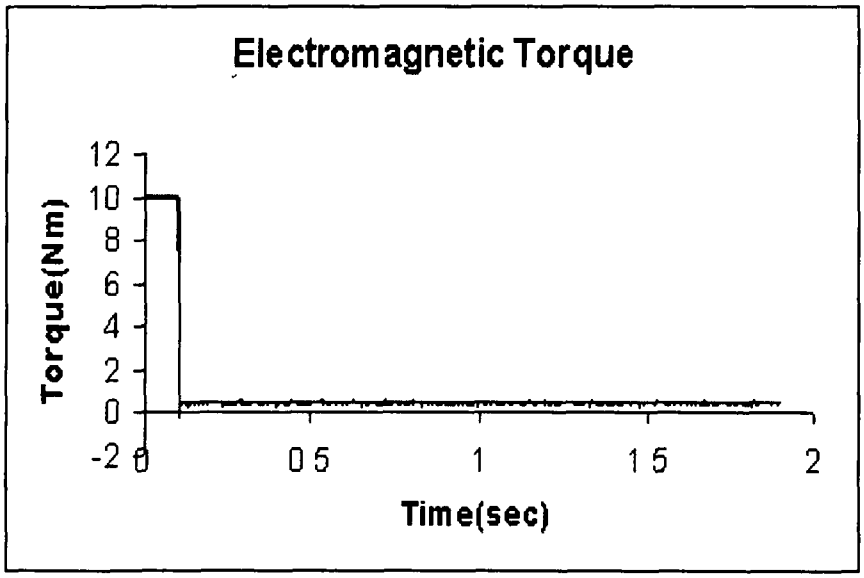

Figure 5.95: Electromagnetic Torque Vs time plot during Starting

5.7.1.3 Response of PMBLDC Motor Voltage with Fuzzy SMC Controller During Starting

Figure 5.96 shows the motor voltage response of one of the phases. Winding voltage is increases up to 300 V/ 305V (peak) in all the three phases.

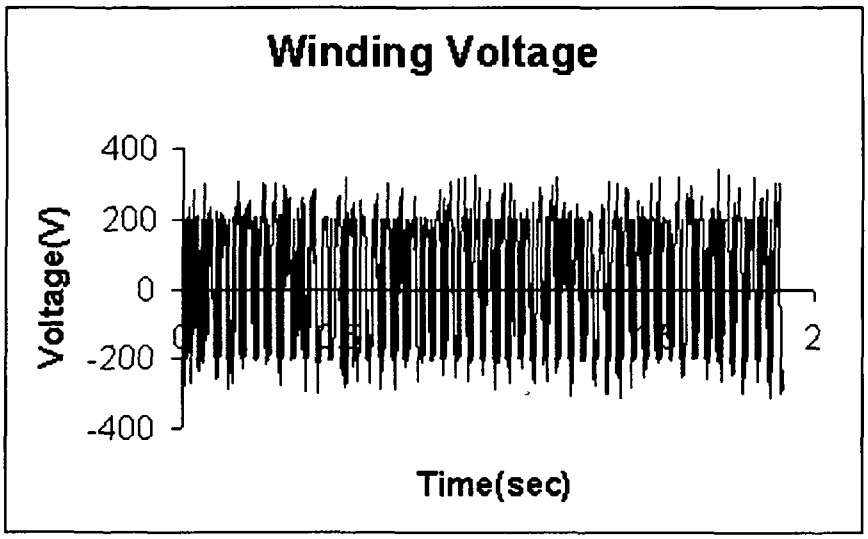

Figure 5.96: Motor winding Voltage Vs time plot during Starting

5.7.2 Response of PMBLDC Motor Current with Fuzzy SMC Controller During Speed Reversal

Figures 5.97 –5.99 shows the motor currents (i_a, i_b and i_c) which increase up to 4.05 A(peak) at the time of starting without any load and drop to 0.45 A(peak) during the steady-state condition. At 850 msec currents again rise up to 4.05 A due to the speed reversal. The drive takes 215 msec for a reversal of speed and the currents reach the original value of 0.45 A.

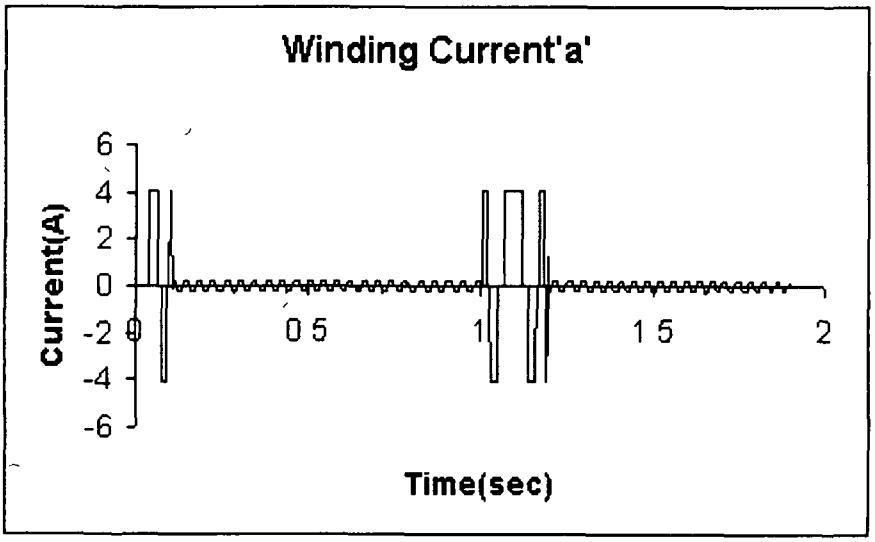

Figure 5.97: Motor Current 'i_a'

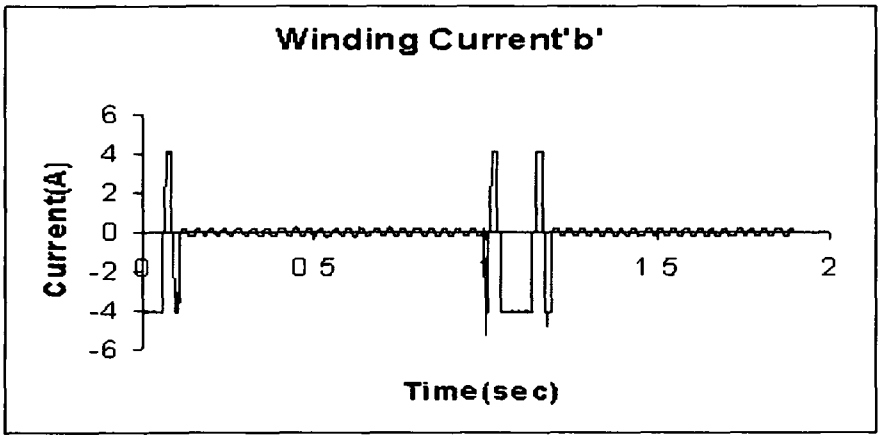

Figure 5.98: Motor Current 'i_b'

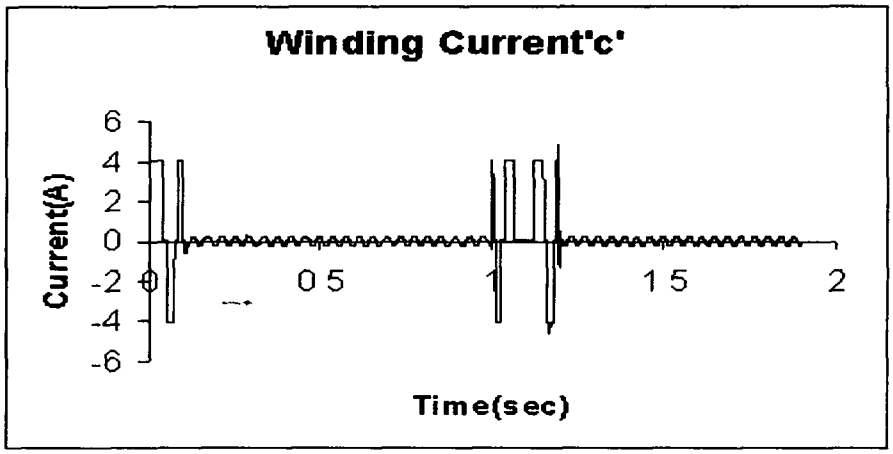

Figure 5.99: Motor Current 'i_c'

5.7.2.1 Response of PMBLDC Motor Speed with Fuzzy SMC Controller During Speed Reversal

Figure 5.100 shows the speed reversal dynamics of the PMBLDC motor-with Fuzzy-SMC speed controller. When the set speed is changed to –157 rad/sec (speed reversal), the SMC controller becomes active and makes the motor speed equal to the reference speed. The drive takes 215 msec for the speed reversal.

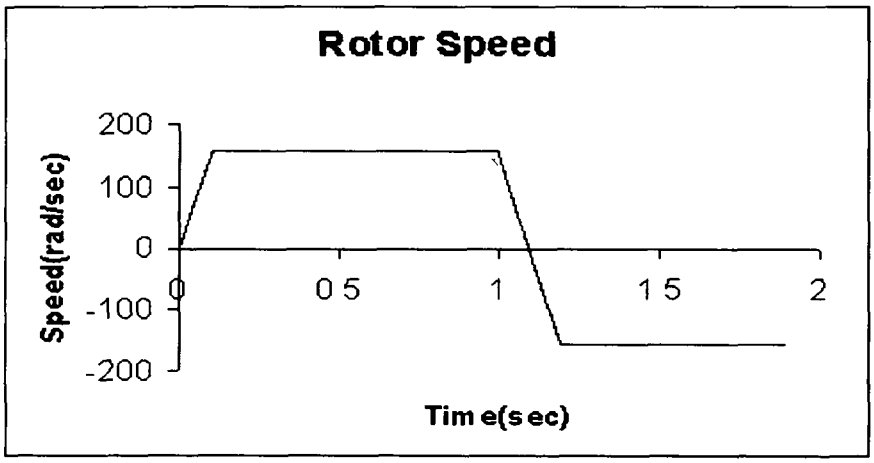

Figure 5.100: Rotor speed Vs time plot during Reversal

5.7.2.2 Response of PMBLDC Motor Torque with Fuzzy SMC Controller During Speed Reversal

Figure 5.101 shows the electromagnetic torque which rises instantaneously to 10 Nm (Maximum permissible value) to start the motor from the standstill condition. By the time the motor reaches the steady-state condition, the torque undergoes a quick decrease to settle down at the steady-state level of 0.45 Nm and is maintained there. When the speed is changed suddenly, the torque becomes maximum with negative value (-10 Nm) and the motor speeds up in the reverse direction. Once the motor reaches the steady-state in (-ve) direction, again the torque is maintained at the initial value.

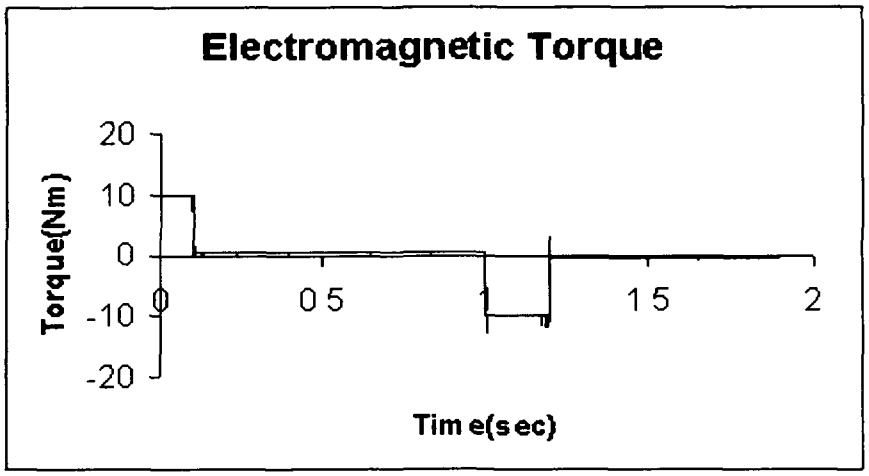

Figure 5.101: Electromagnetic Torque Vs time plot during Reversal

5.7.2.3 Response of PMBLDC Motor Voltage with Fuzzy SMC Controller During Speed Reversal

Figure 5.102 shows the motor voltage response of one of the phases. Winding voltage is increases up to 300 V / 305V (peak) in all the three phases. The voltage does not show any perceptible change during speed reversal.

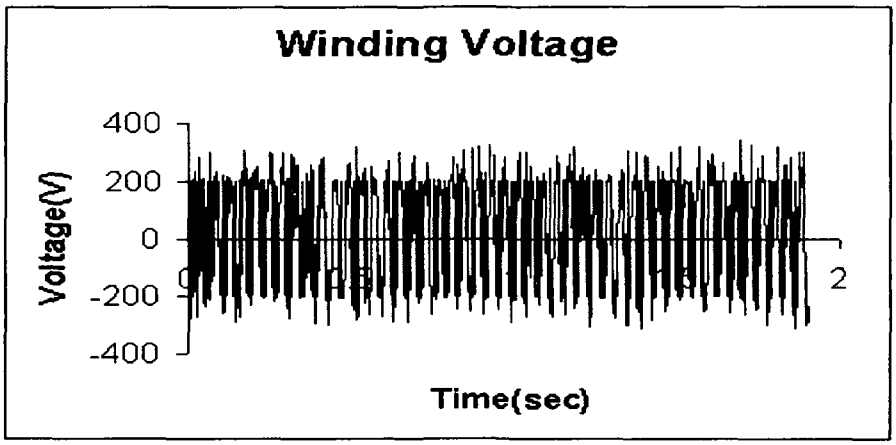

Figure 5.102: Motor winding Voltage Vs time plot during Reversal

5.7.3 Response of PMBLDC Motor Current with Fuzzy-SMC Controller During Load perturbations

Figures 5.103–5.105 show the motor currents (i_a, i_b and i_c) which increase up to 4.05 A (peak) at the time of starting without any load and settle down at 0.08A (peak) during the steady-state condition. During the load perturbation, the current increases to 2.20 A to meet the demand load. When the load is removed, the current returns to the original value. The winding currents are found to follow the reference currents even during the conditions of load perturbations.

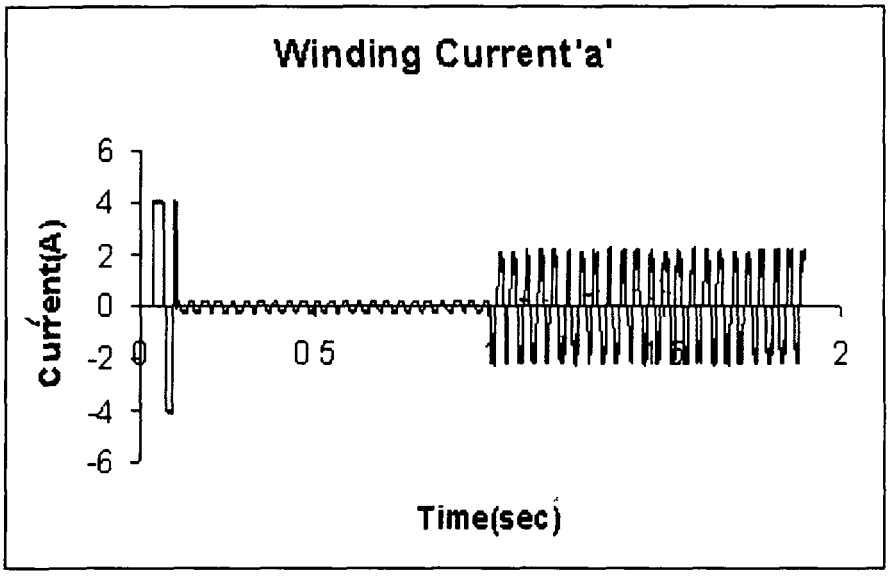

Figure 5.103: Motor Current 'i_a'

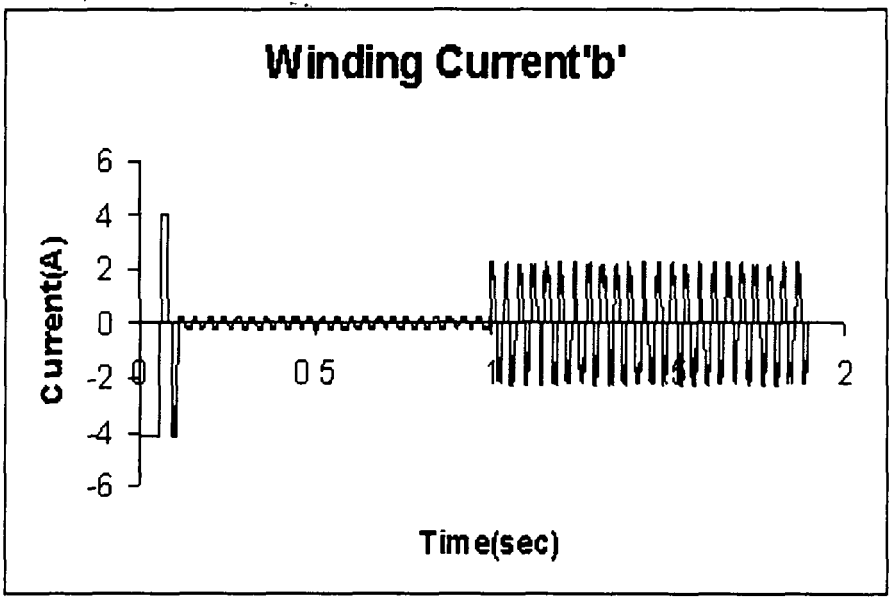

Figure 5.104: Motor Current 'i_b'

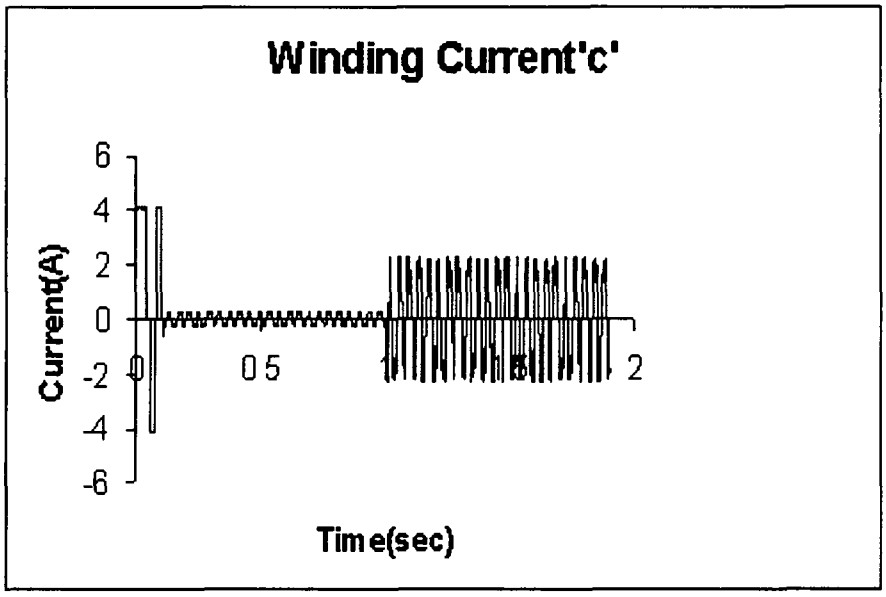

Figure 5.105: Motor Current 'i_c'

5.7.3.1 Response of PMBLDC Motor Speed with Fuzzy-SMC Controller during Load perturbations

Figure 5.106 shows the performance of the drive with the Fuzzy-SMC speed controller under load perturbations. The sudden application of full load at t = 1.0 sec and sudden removal of full load at t=1.05 sec on the shaft cause a negligible variation in speed response. It takes negligible time(about 10 msec) to reach the reference speed. The Fuzzy-SMC speed controller offers smooth action and makes the drive highly robust under load perturbations.

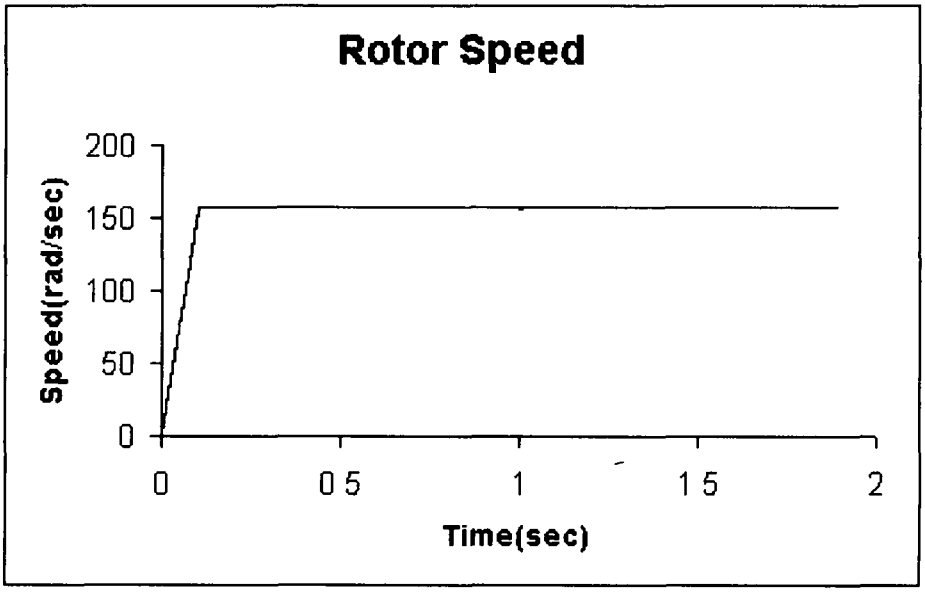

Figure 5.106: Rotor speed Vs time plot during Load perturbations

5.7.3.2 Response of PMBLDC Motor Torque with Fuzzy-SMC Controller During Load perturbations

Figure 5.107 shows the electromagnetic torque which increases to 5.5 Nm on application of load and is maintained at the value till the load is removed. It is observed that the Fuzzy-SMC controller shows the superior response over SMC controller in terms of the improved dynamics under load perturbations.

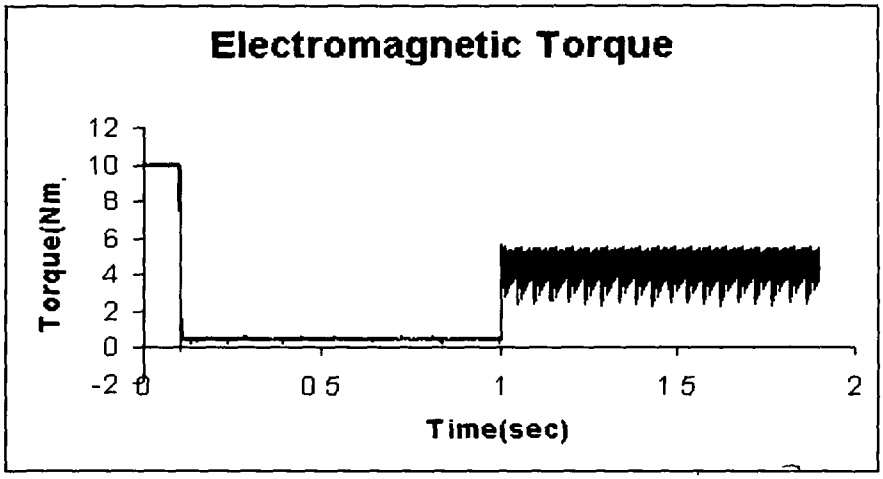

Figure 5.107: Electromagnetic Torque Vs time plot during Load perturbations

5.7.3.3 Response of PMBLDC Motor Voltage with Fuzzy SMC Controller During Load perturbations

Figure 5.108 shows the motor voltage response of one of the phases. Winding voltage is increases up to 300 V / 305 V (peak) in all the three phases.

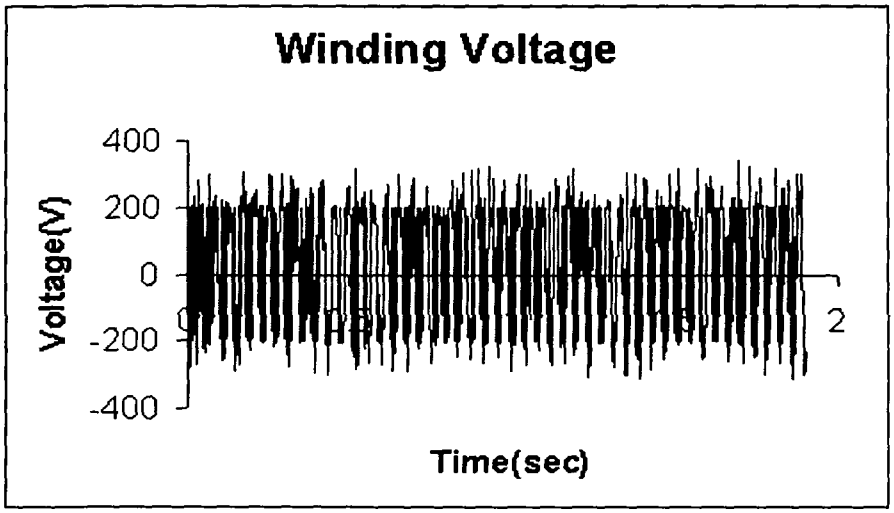

Figure 5.108: Motor winding Voltage Vs time plot during Load perturbations

5.8 Self–Organizing Fuzzy Logic Speed controller

The simulated dynamic responses of winding currents of three phases, speed, torque and winding voltage characteristics of a 3-phase, 4-pole, 0.5 HP PMBLDC

motor with its reference speed set at 157 rad/sec are presented in this section. For each of these cases, results pertaining to three modes of dynamic operations, namely, the starting, the speed reversal and the load perturbations have been obtained. The simulated responses of the drive, thus obtained, are shown in Figures 5.109 to 5.126. Figures 5.109 to 5.114 illustrate the starting response of the drive with each of speed controllers considered in this investigation. Figures 5.115 to 5.120 refer to speed reversal while Figures 5.121 to 5.126 refer to the load perturbations.

5.8.1 Response of PMBLDC Motor Current with Self-Organizing Fuzzy Controller During Starting

Figures 5.109–5.111 shows the motor currents (i_a, i_b and i_c) which increase up to 3.25 A (peak) at the time of starting without any load and settle down at 0.02A (peak) during the steady-state condition. The steady-state current is 20 mA which is reached in 145 msec after its start on no load.

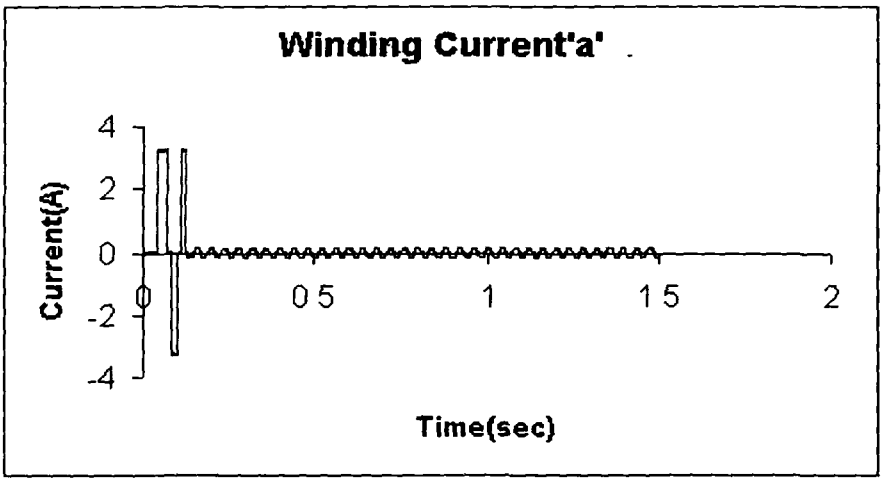

Figure 5.109: Motor Current 'i_a'

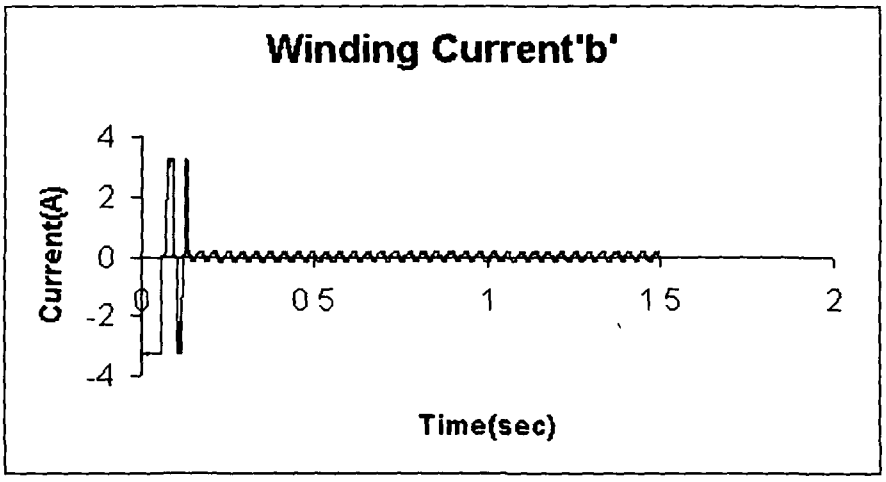

Figure 5.110: Motor Current 'i_b'

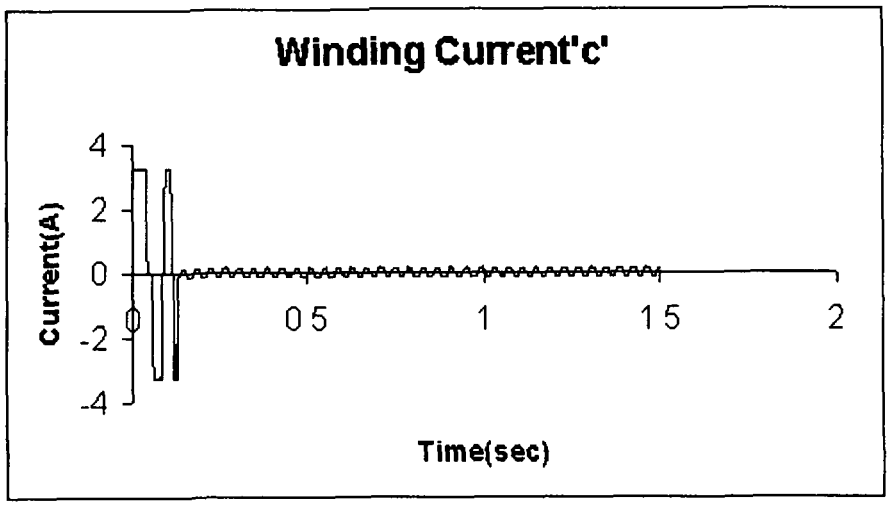

Figure 5.111: Motor Current 'i_c'

5.8.1.1 Response of PMBLDC Motor Speed with Self-Organizing Fuzzy Controller During Starting

Figure 5.112 shows the transient and steady state responses of the drive with Self-Organizing Fuzzy-Logic controller. This controller gives fast response similar to the fuzzy logic controller. For reaching the reference speed of 157 rad/sec the drive takes 145 msec.

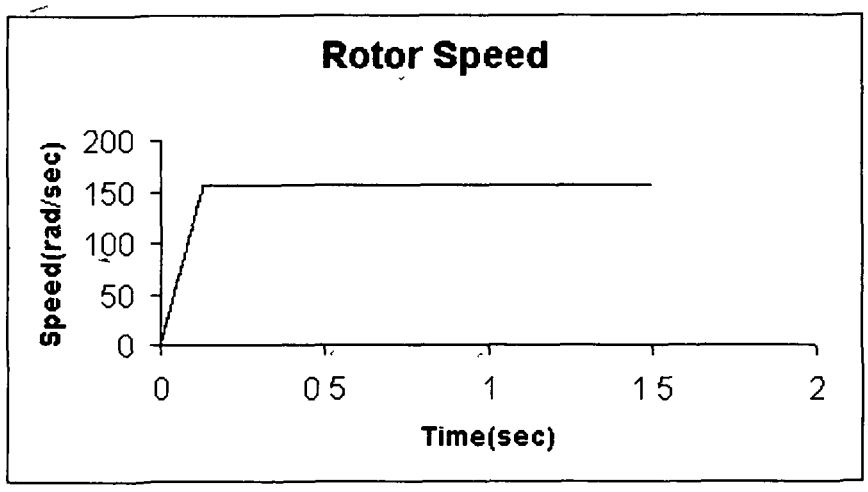

Figure 5.112: Rotor speed Vs time plot during Starting

5.8.1.2 Response of PMBLDC Motor Torque with Self-Organizing Fuzzy Controller During Starting

Figure 5.113 shows the motor electromagnetic torque which rises to 8 Nm (maximum permissible value) during the starting of the motor from standstill. The rise in torque is almost instantaneous. By the time the motor reaches the steady-state condition, the torque undergoes a quick decrease and settles down to the steady-state level of 0.30 Nm and maintains the same level over the remaining period of time.

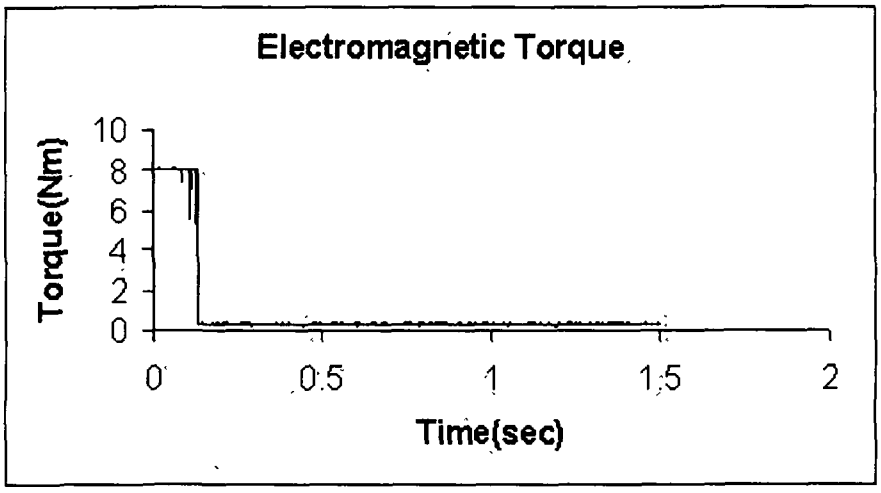

Figure 5.113: Electromagnetic Torque Vs time plot during Starting

5.8.1.3 Response of PMBLDC Motor Voltage with Self-Organizing Fuzzy Controller During Starting

Figure 5.114 shows the motor voltage response of one of the phases. Winding voltage is increases up to 300 V / 305V (peak) in all the three phases.

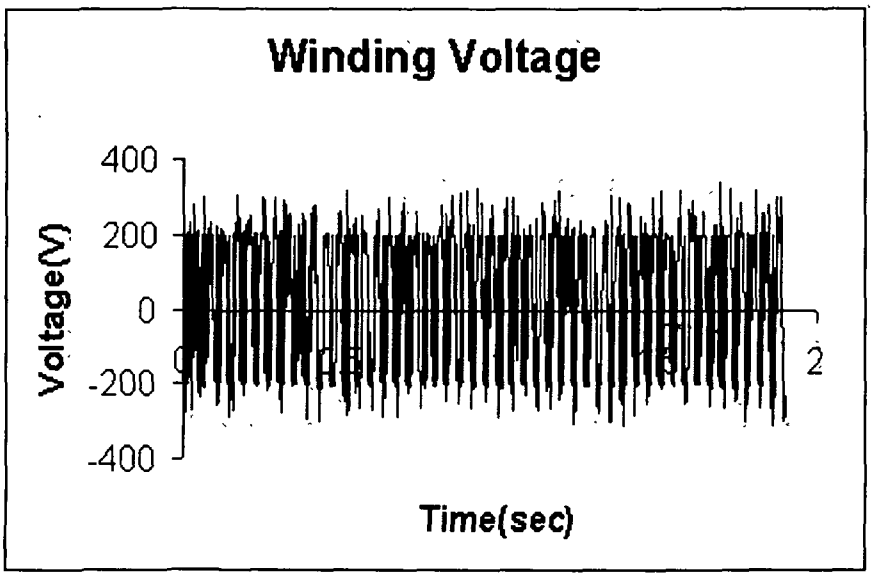

Figure 5.114: Motor winding Voltage Vs time plot during Starting

5.8.2 Response of PMBLDC Motor Current with Self-Organizing Fuzzy Controller During Speed Reversal

Figures 5.115 –5.117 shows the motor currents (i_a, i_b and i_c) which increase up to 3.25 A (peak) at the time of starting without any load and drop to 0.02A (peak) during the steady-state condition. At 800 msec currents again rise up to 3.25 A due to the speed reversal. The drive takes 240 msec for a reversal of speed and the currents reach the original value of 0.02A.

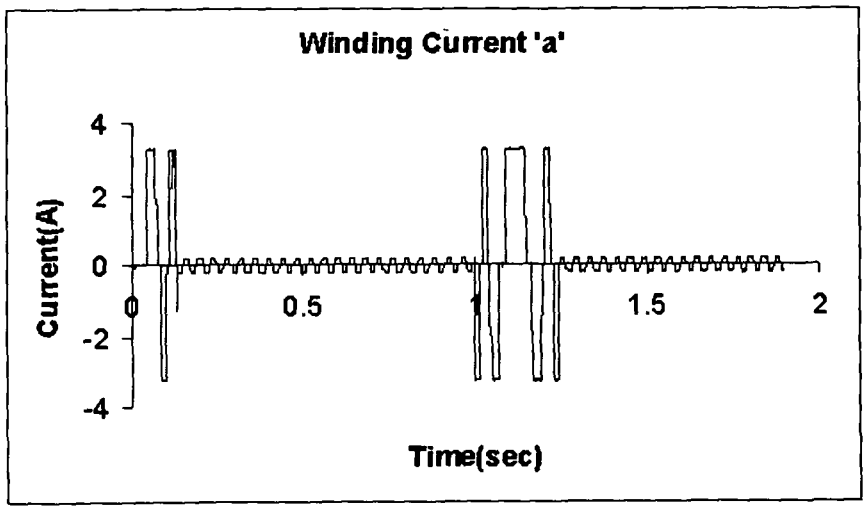

Figure 5.115: Motor Current 'i_a'

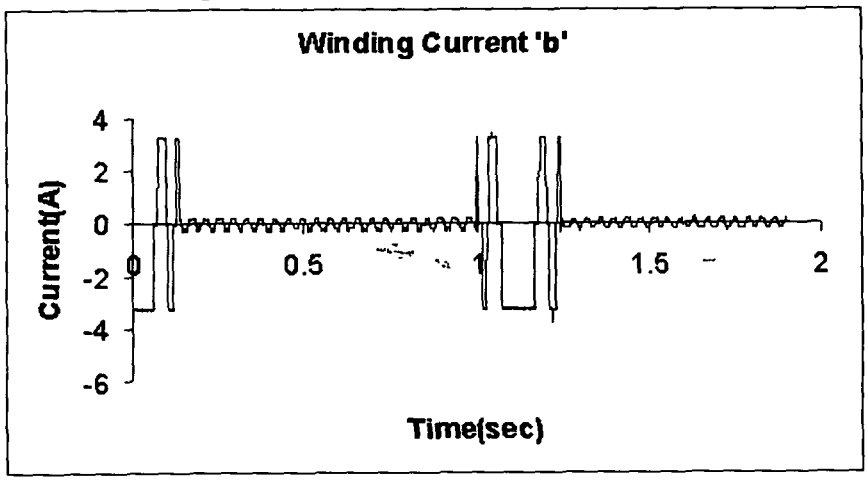

Figure 5.116: Motor Current 'i_b'

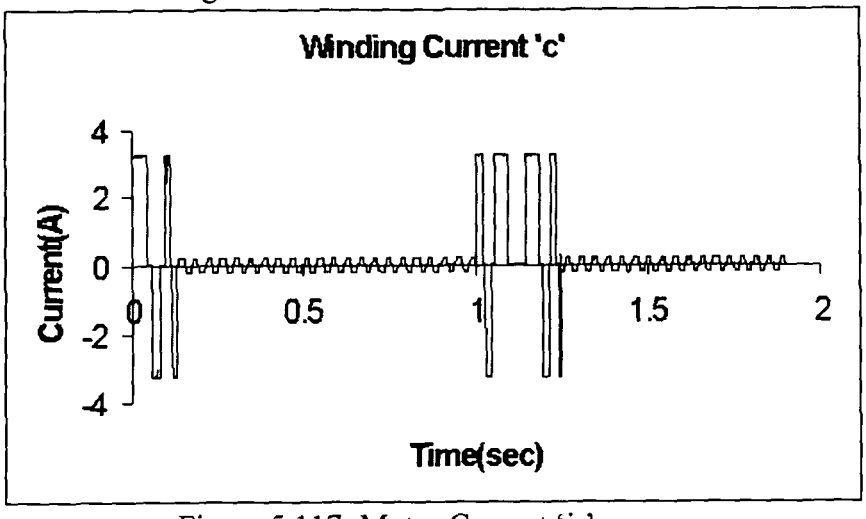

Figure 5.117: Motor Current 'i_c'

5.8.2.1 Response of PMBLDC Motor Speed with Self-Organizing Fuzzy Controller During Speed Reversal

Figure 5.118 shows the speed-reversal dynamics of the PMBLDC motor with Self-Organizing Fuzzy speed controller. When the set speed is changed to –157

rad/sec (speed reversal), the Self-Organizing Fuzzy controller becomes active and makes the motor speed equal to the reference speed. The drive takes 240 msec for the speed reversal.

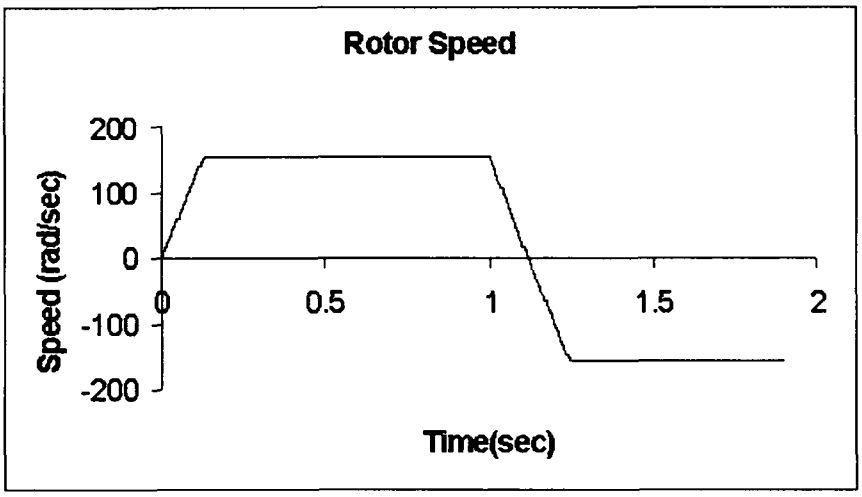

Figure 5.118: Rotor speed Vs time plot during Reversal

5.8.2.2 Response of PMBLDC Motor Torque with Self-Organizing Fuzzy Controller During Speed Reversal

Figure 5.119 shows the electromagnetic torque which rises instantaneously to 8 Nm (Maximum permissible value) to start the motor from the standstill condition. By the time the motor reaches the steady-state condition, the torque also undergoes a quick decrease to settle down at the steady-state level of 0.45 Nm and is maintained there. When the speed is changed suddenly, the torque becomes maximum with negative value (-8 Nm) and the motor speeds up in the reverse direction. Once the motor speed reaches the steady state in (-ve) direction, the torque is maintained at the initial value 0.45 Nm.

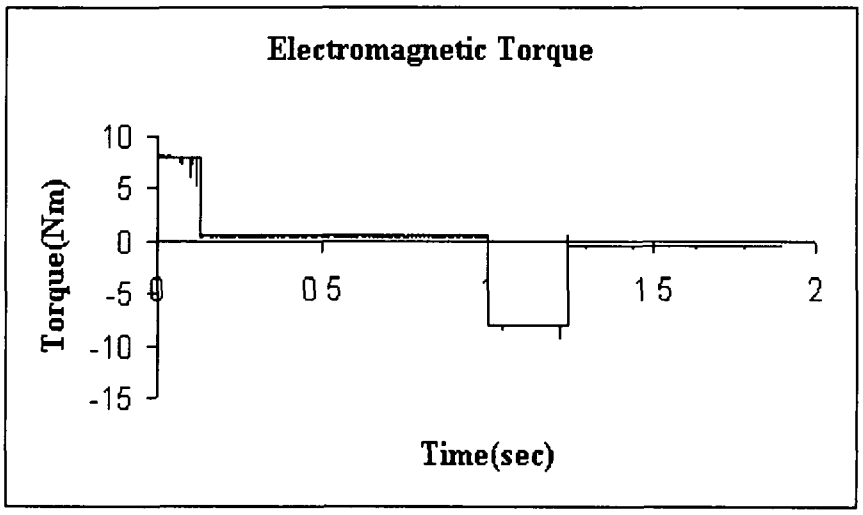

Figure 5.119: Electromagnetic Torque Vs time plot during Reversal

5.8.2.3 Response of PMBLDC Motor Voltage with Self-Organizing Fuzzy Controller During Speed Reversal

Figure 5.120 shows the motor voltage response of one of the phases. Winding voltage is increases up to 300 V / 305 V in all the three phases. The does not seem tobe affected by speed reversal.

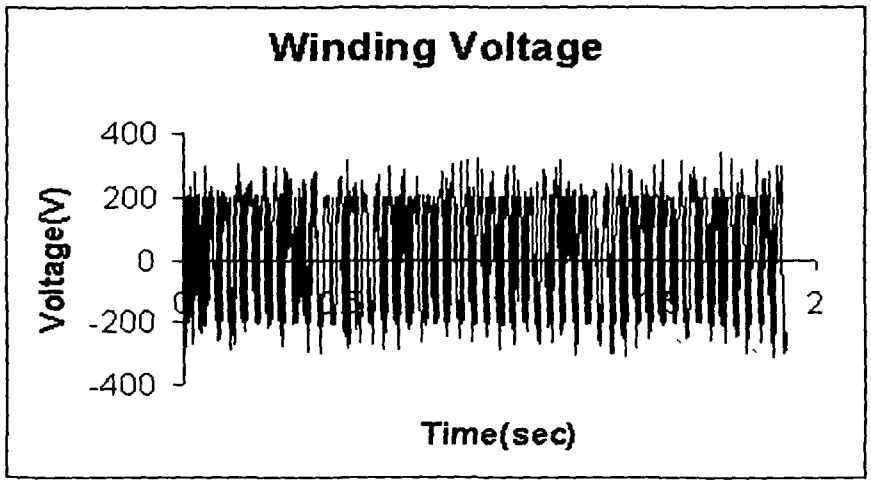

Fig. 5.120: Motor winding Voltage Vs time plot during Reversal

5.8.3 Response of PMBLDC Motor Current with Self-Organizing Fuzzy Controller During Load perturbations

Figures 5.121 – 5.123 show the motor currents (i_a, i_b and i_c) which increase up to 3.25 A (peak) at the time of starting without any load and settle down to 0.02A (peak) during the steady-state condition. During the load perturbation, the current increases to 2.20 A to meet the increased demand due to extra load. When the load is removed, the current returns to its the original value 0.02A. The winding currents are found to follow the reference currents even during the conditions of load perturbations.

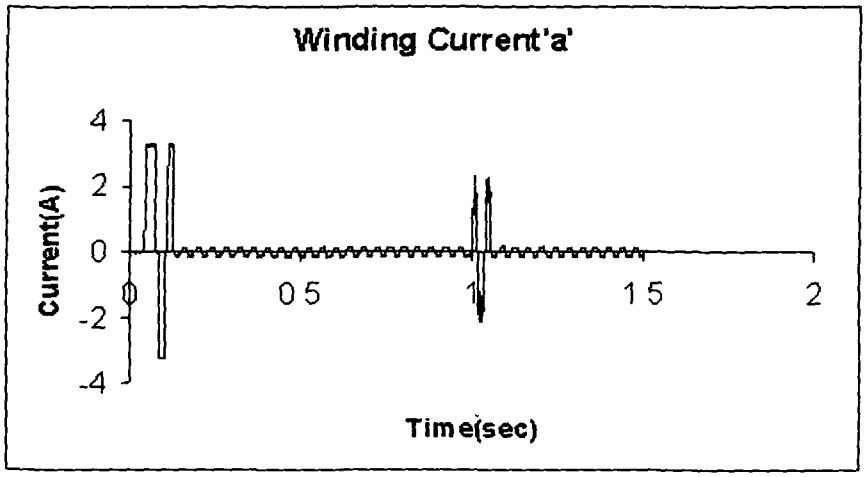

Figure 5.121: Motor Current 'i_a'

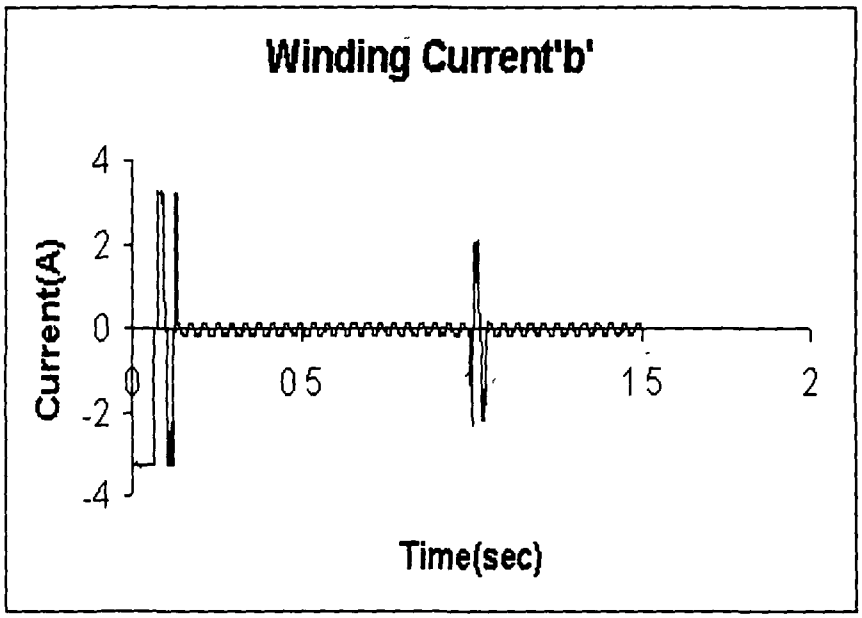

Figure 5.122: Motor Current 'i_b'

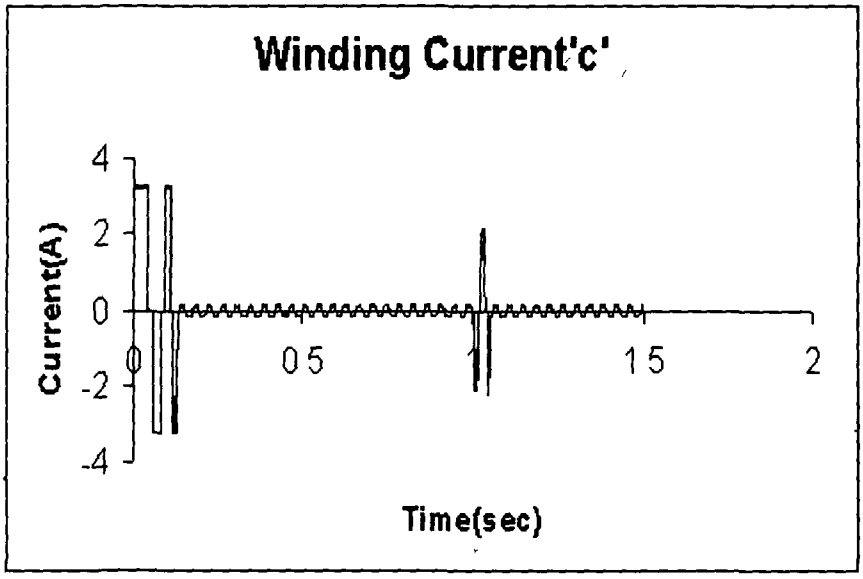

Figure 5.123: Motor Current 'i_c'

5.8.3.1 Response of PMBLDC Motor Speed with Self-Organizing Fuzzy Controller During Load perturbations

Figure 5.124 shows the performance of the drive with the Self-Organizing Fuzzy speed controller under load perturbations. The sudden application of full load at t = 1.0 sec and sudden removal of full load at t = 1.05 sec on the shaft cause a negligible variation in speed response. It takes time 10 msec to reach the reference speed. The Self-Organizing Fuzzy speed controller offers smooth action and makes the drive highly robust under the conditions of load perturbations.

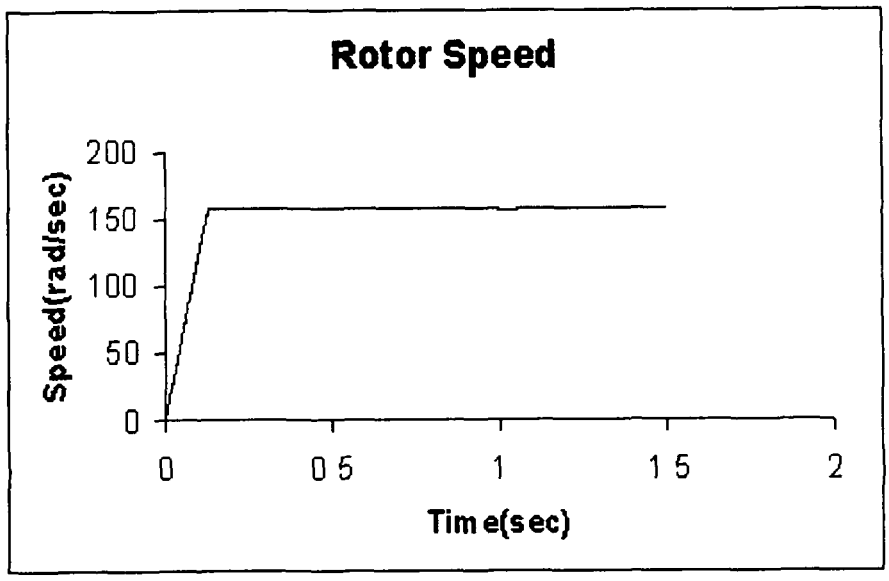

Figure 5.124: Rotor speed Vs time plot during Load perturbations

5.8.3.2 Response of PMBLDC Motor Torque with Self-Organizing Fuzzy Controller During Load perturbations

Figure 5.125 shows the electromagnetic torque which increases up to 5.25 Nm and maintained at the higher value till the load is removed.

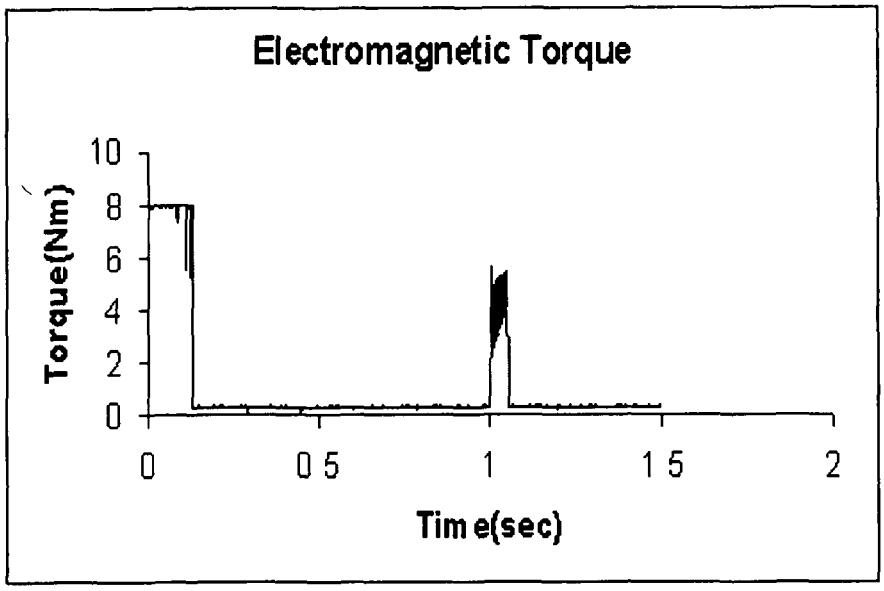

Figure 5.125: Electromagnetic Torque Vs time plot during Load perturbations

5.8.3.3 Response of PMBLDC Motor Voltage with Self-Organizing Fuzzy Controller During Load perturbations

Figure 5.126 shows the motor voltage response of one of the phases. Winding voltage is increases up to 300 V / 305 V in all the three phases.

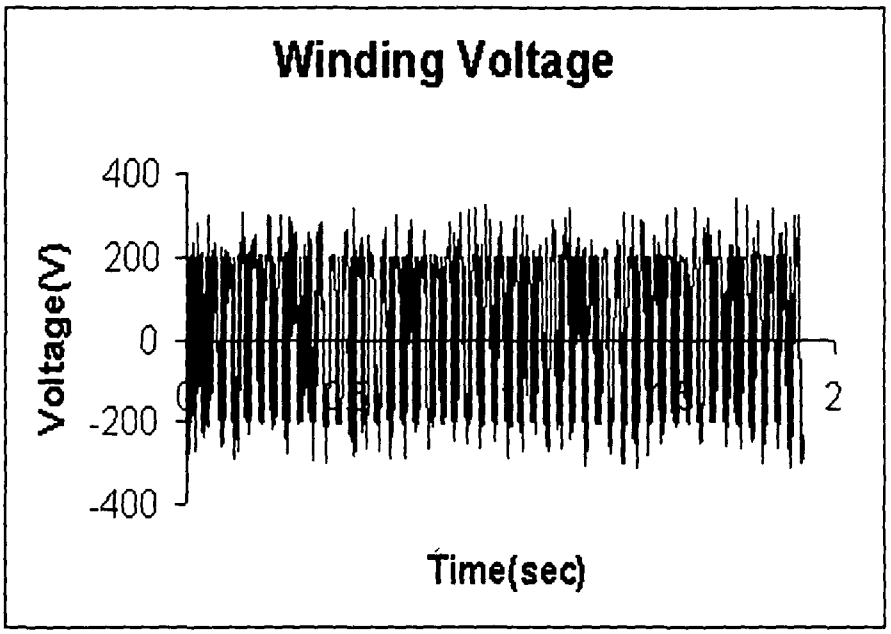

Figure 5.126: Motor winding Voltage Vs time plot during Load perturbations

5.9 Gain Scheduling PI Speed controller

The simulated dynamic responses of winding currents of three phases, speed, torque and winding voltages of a 3-phase, 4-pole, 0.5 HP PMBLDC motor with its reference speed set at 157 rad/sec are presented in this section. For each of these cases, results pertaining to three modes of dynamic operations, namely, the starting, the speed reversal and the load perturbations have been obtained. The simulated responses of the drive, thus obtained are shown in Figures 5.127 to 5.144. Figures 5.127 to 5.132 illustrate the starting responses of the drive with each of speed controllers considered in this investigation. Figures 5.133 to 5.138 refer to speed reversal while Figures 5.139 to 5.144 refer to the load perturbations.

5.9.1 Response of PMBLDC Motor Current with Gain-Scheduling PI Controller During Starting

Figures 5.127 – 5.129 show the motor currents (i_a, i_b and i_c) which increase up to 4.0 A (peak) at the time of starting without any load and settle down at 0.04A (peak) during the steady state condition. The steady-state current is about 40 mA which reached in about 125 msec after its start on no-load.

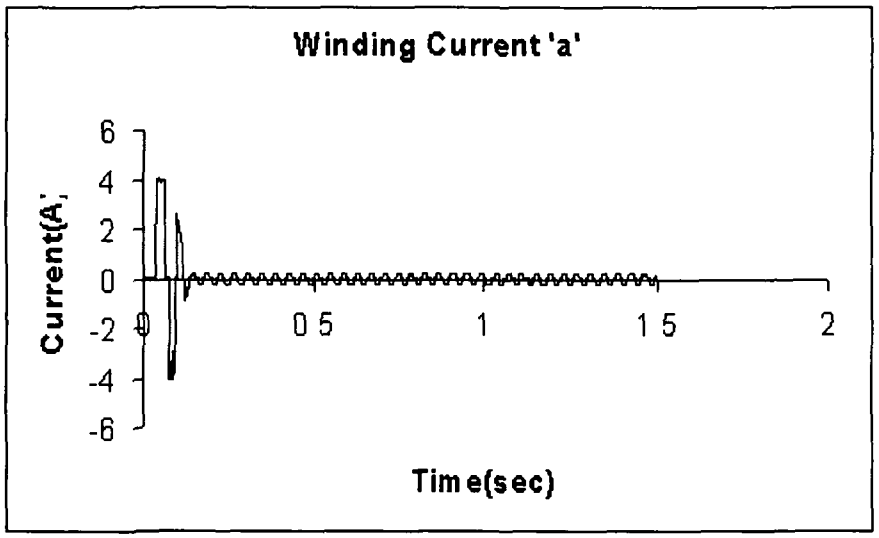

Figure 5.127: Motor Current 'i_a'

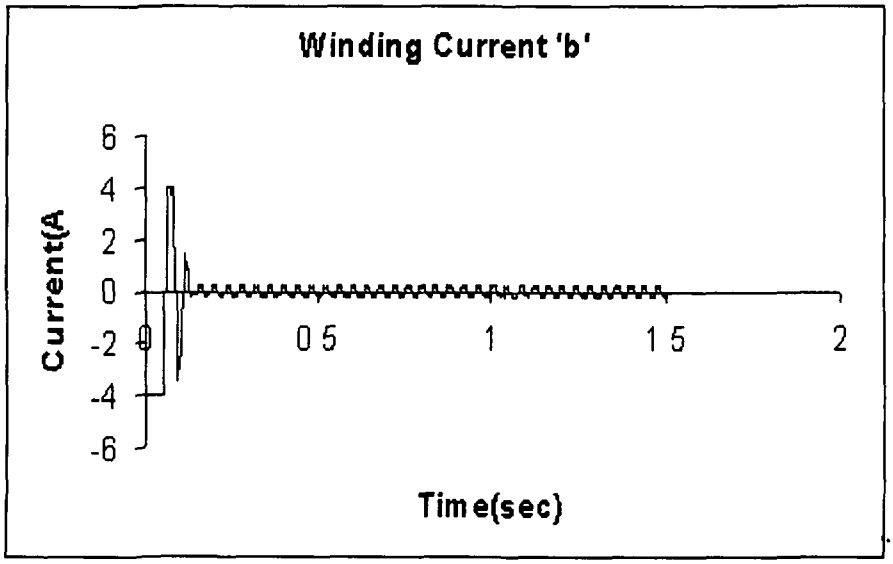

Figure 5.128: Motor Current 'i_b'

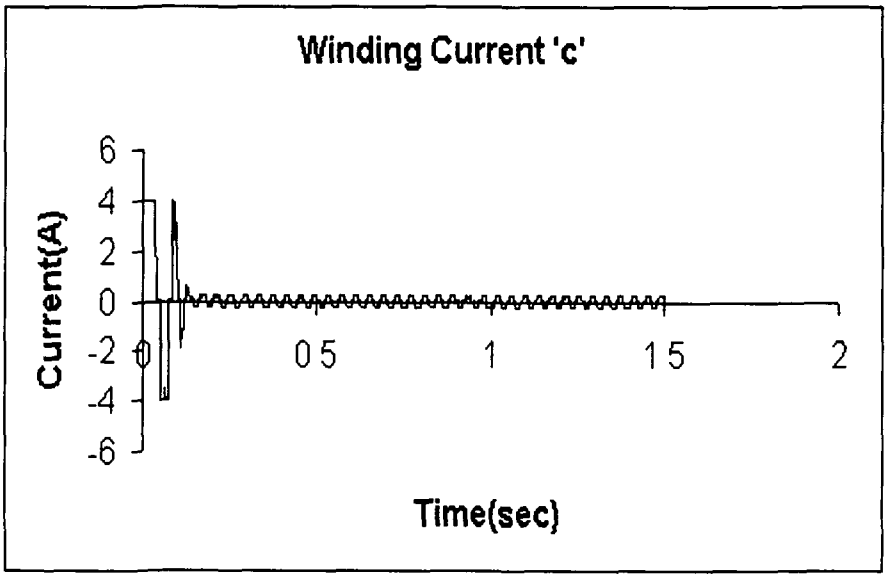

Figure 5.129: Motor Current 'i_c'

5.9.1.1 Response of PMBLDC Motor Speed with Gain-Scheduling PI Controller During Starting

Figure 5.130 shows the rotor speed during starting of PMBLDC motor from standstill up to rated speed of 1500 rpm (157 rad/sec) with the Gain Scheduling PI controller. The controller gains the controller are K_p (max) = 2.0, K_p (min) = 0.5, K_I (max) = 0.0008. The drive takes 125 msec to reach the reference speed of 157rad/sec. The controller gains are allowed to vary within a predefined range which eliminates the problem of manual tuning.

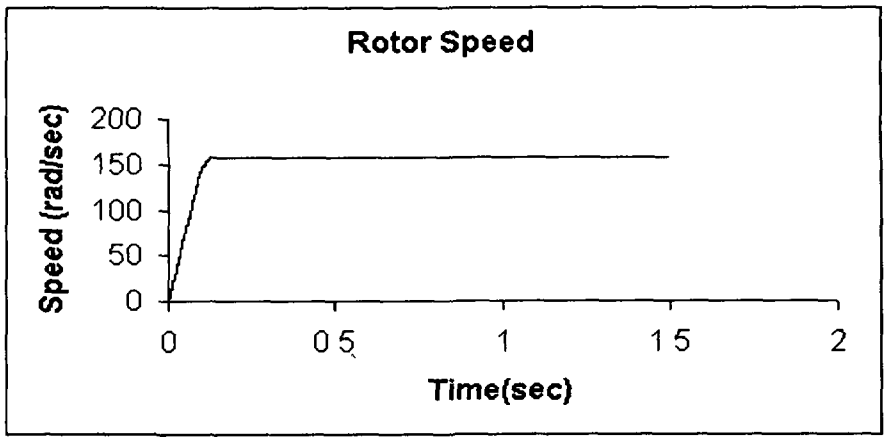

Figure 5.130: Rotor speed Vs time plot during Starting

5.9.1..2 Response of PMBLDC Motor Torque with Gain-Scheduling PI Controller During Starting

Figure 5.131 shows the motor electromagnetic torque which rises to 10 Nm (maximum permissible value) during the starting of the motor from standstill. The rise in torque is almost instantaneous. By the time the motor reaches the steady-state condition, the torque also undergoes a quick decrease and settles down to the stead-state level of 0.45 Nm and maintains the same level over the remaining period of time.

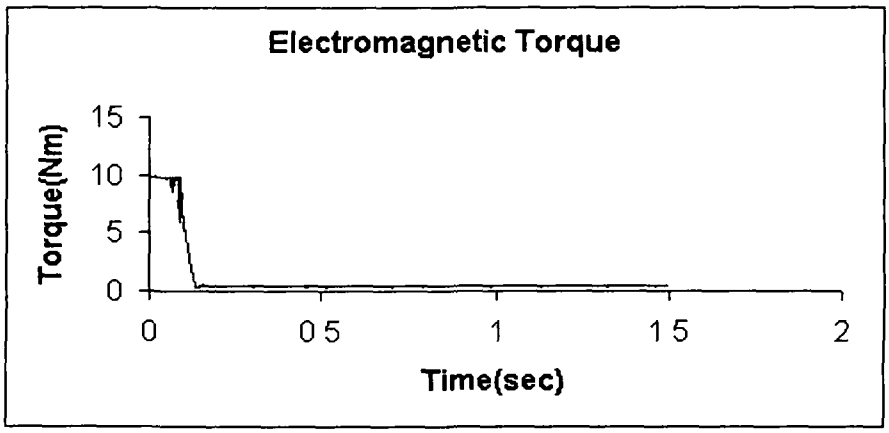

Figure 5.131: Electromagnetic Torque Vs time plot during Starting

5.9.1.3 Response of PMBLDC Motor Voltage with Gain-Scheduling PI Controller During Starting

Figure 5.132 shows the motor voltage response of one of the phases. Winding voltage is increases up to 300 V / 305V (peak) in all the three phases.

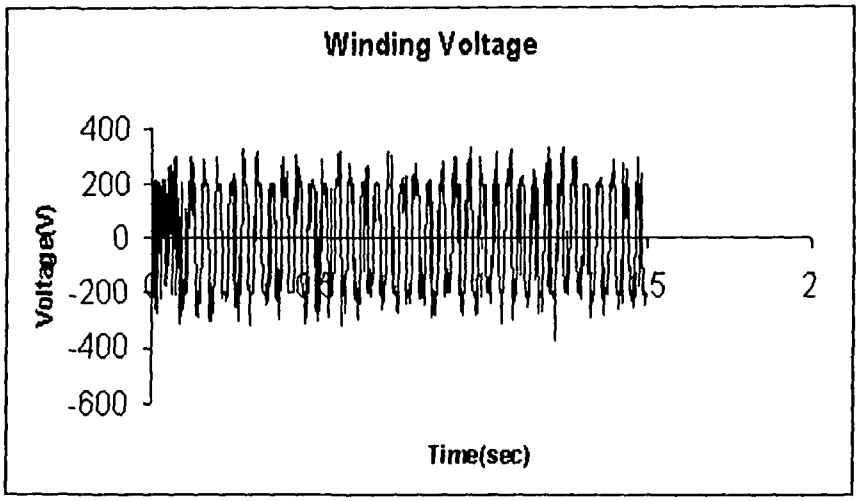

Figure 5.132: Motor winding Voltage Vs time plot during Starting

5.9.2 Response of PMBLDC Motor Current with Gain Scheduling PI Controller During Speed Reversal

Figures 5.133–5.135 show the motor currents (i_a, i_b and i_c) which increase up to 4.0 A (peak) at the time of starting without any load and drop to 0.04 A (peak) during the steady-state condition. At 750 msec currents again rise up to 4.0 A due to the speed reversal. The drive takes 240 msec for a reversal of speed and the currents reach the original value of 0.04 A.

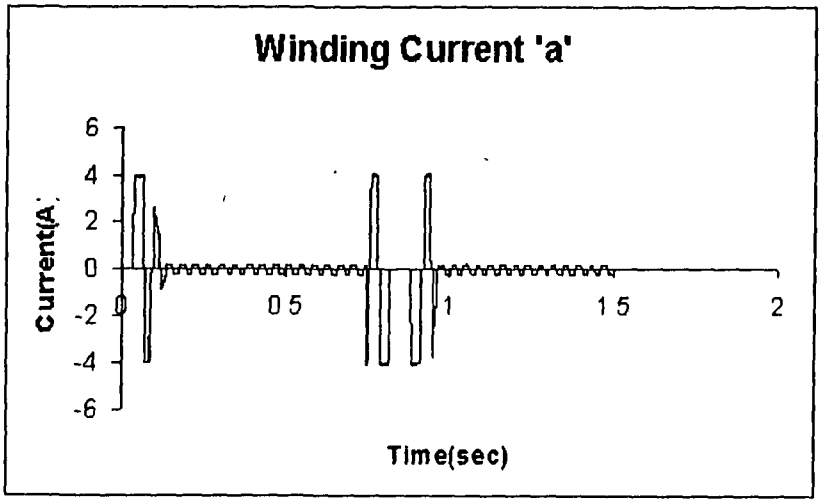

Figure 5.133: Motor Current 'i_a'

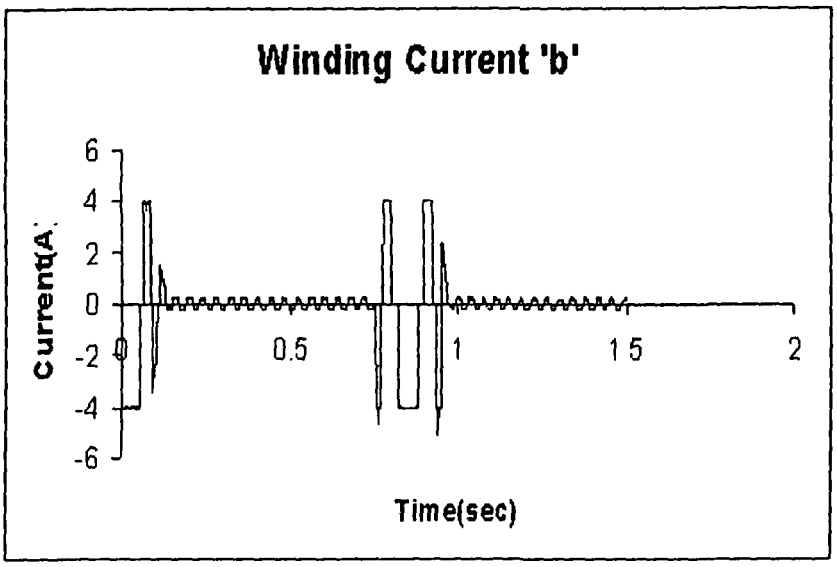

Figure 5.134: Motor Current 'i_b'

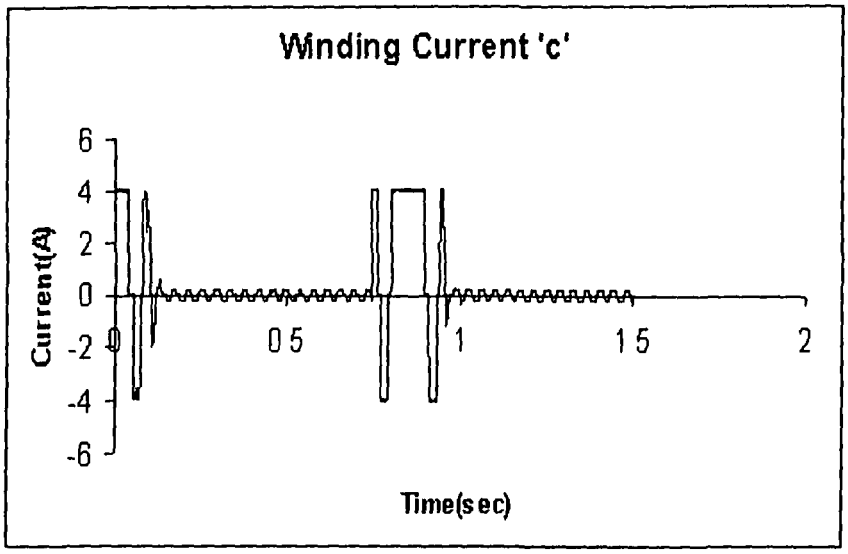

Figure 5.135: Motor Current 'i_c'

5.9.2.1 Response of PMBLDC Motor Speed with Gain-Scheduling PI Controller During Speed Reversal

Fig. 5.136 shows the speed-reversal dynamics of the PMBLDC motor with Gain- Scheduling PI speed controller. When the set speed is changed to −157 rad/sec (speed reversal), the Gain-Scheduling PI controller becomes active and brings the motor speed equal to the reference speed. The drive takes 240 msec for the speed reversal.

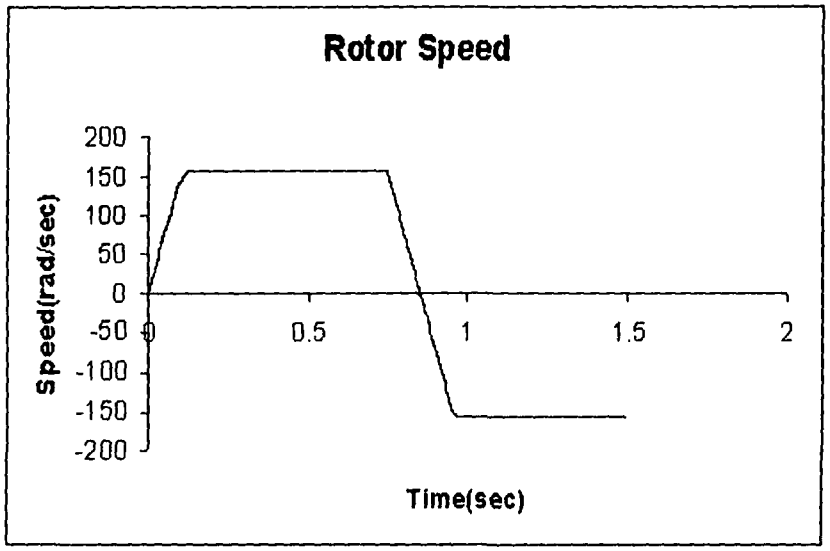

Figure 5.136: Rotor speed Vs time plot during Reversal

5.9.2.2 Response of PMBLDC Motor Torque with Gain Scheduling PI Controller During Speed Reversal

Figure 5.137 shows the electromagnetic torque which rises instantaneously to 10 Nm (Maximum permissible value) to start the motor from the standstill condition. By the time of the motor reaches the steady-state condition, the torque also undergoes a transient decrease to settle down at the steady-state level of 0.50 Nm and is maintained till the reversal. When the speed reversal occurs the torque becomes maximum with negative value (-10 Nm) and the motor speeds up in the reverse direction. Once the motor reaches the steady state is (-ve) direction, again the torque is maintained at the initial value of 0.50 Nm.

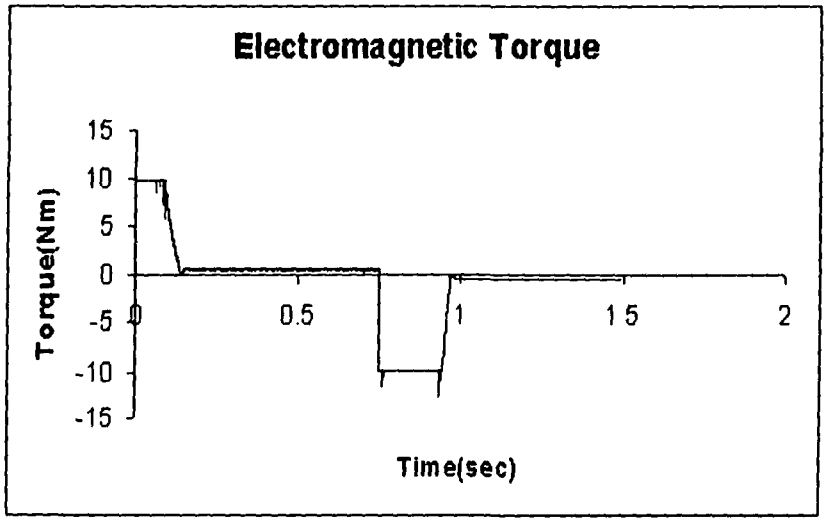

Figure 5.137: Electromagnetic Torque Vs time plot during Reversal

5.9.2.3 Response of PMBLDC Motor Voltage with Gain-Scheduling PI Controller During Speed Reversal

Figure 5.138 shows the motor voltage response of one of the phases. Winding voltage is increases up to 300 V / 305V (peak) in all the three phases. The voltage does not seem to be affected by speed reversal.

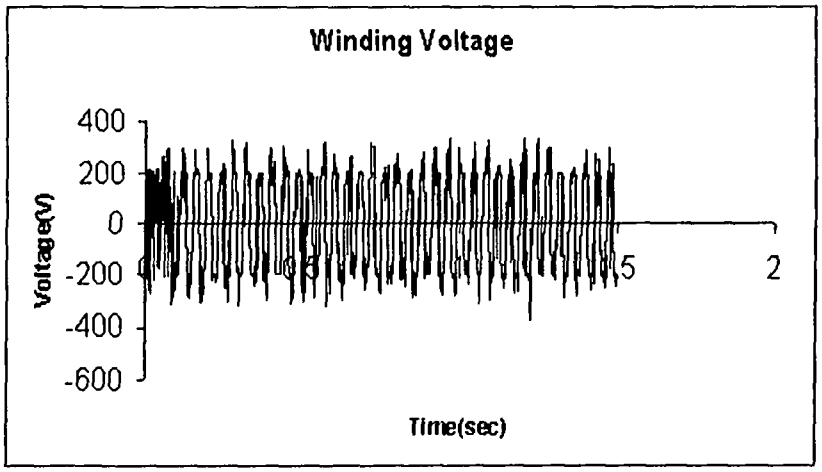

Figure 5.138: Motor winding Voltage Vs time plot during Reversal

5.9.3 Response of PMBLDC Motor Current with Gain-Scheduling PI Controller During Load perturbations

Figures 5.139–5.141 show the motor currents (i_a, i_b and i_c) which increase up to 4.0 A (peak) at the time of starting without any load and settle down at 0.04 A (peak) during the steady-state condition. During the load perturbation, the current increases to 4.0 A to meet the demand of the load. When the load is removed the current returns to the original value. The winding currents are found to follow the reference currents even during the load perturbations.

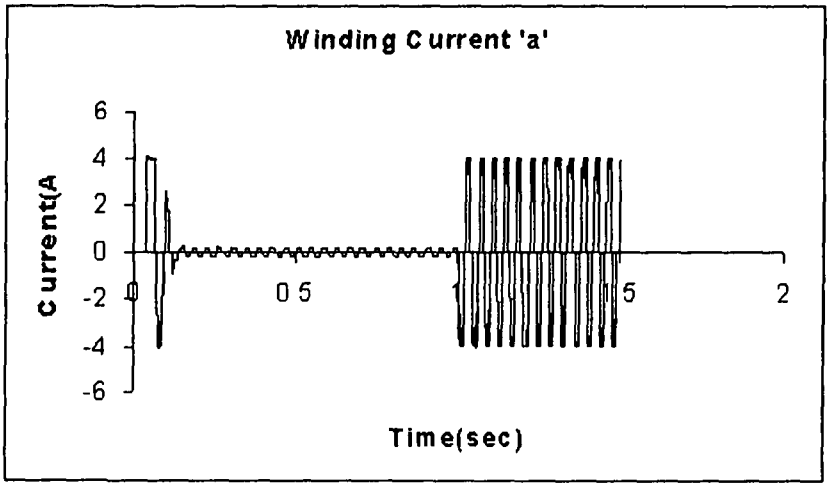

Figure 5.139: Motor Current 'i_a'

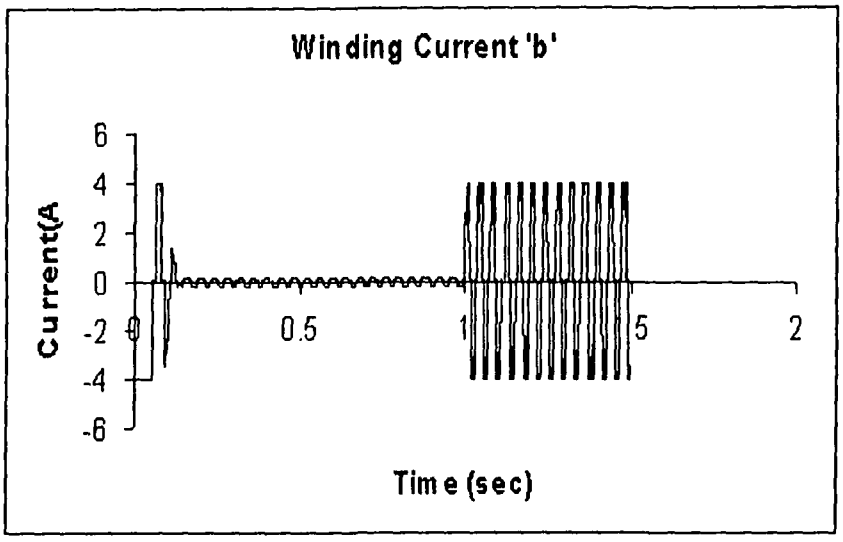

Figure 5.140: Motor Current 'i_b'

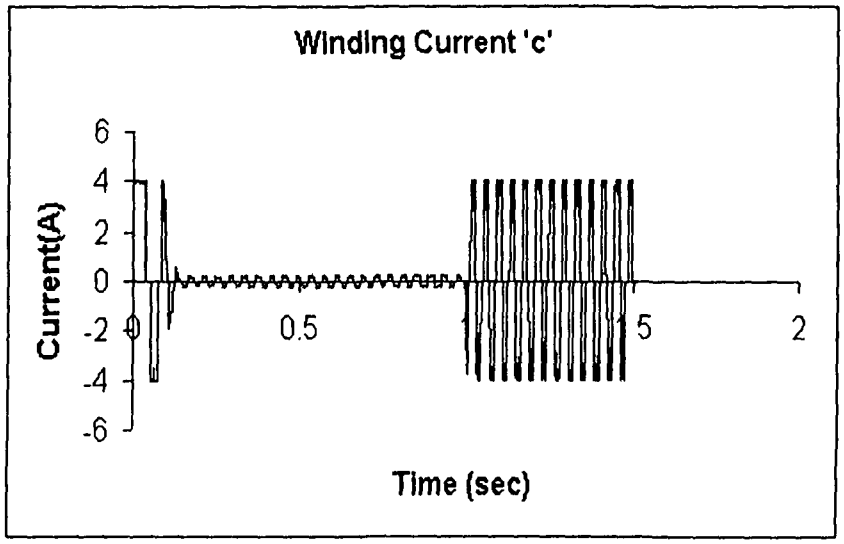

Figure 5.141: Motor Current 'i_c'

5.9.3.1 Response of PMBLDC Motor Speed with Gain-Scheduling PI Controller During Load perturbations

Figure 5.142 shows the performance of the drive with the Gain-Scheduling PI controller under load perturbations. The sudden application of full load at t = 0.70 sec and sudden removal at t=0.75 sec on the shaft cause a negligible variation in speed. It takes 25 msec time to reach the reference speed. The Gain-Scheduling PI speed controller is quite effective and makes the drive highly robust under the actions of load perturbations.

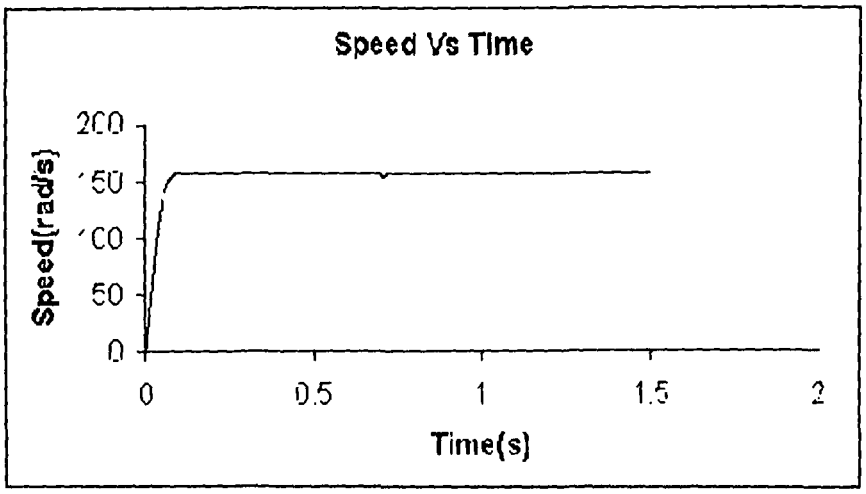

Figure 5.142: Rotor speed Vs time plot during load perturbations

5.9.3.2 Response of PMBLDC Motor Torque with Gain-Scheduling PI Controller During load perturbations

Figure 5.143 shows the electromagnetic torque which increase to 9.80 Nm on application of load and is maintained at that value till the load is removed. It is observed that the Gain-Scheduling PI controller shows the superior response over that of PI controller in terms of the improved dynamics under load perturbations.

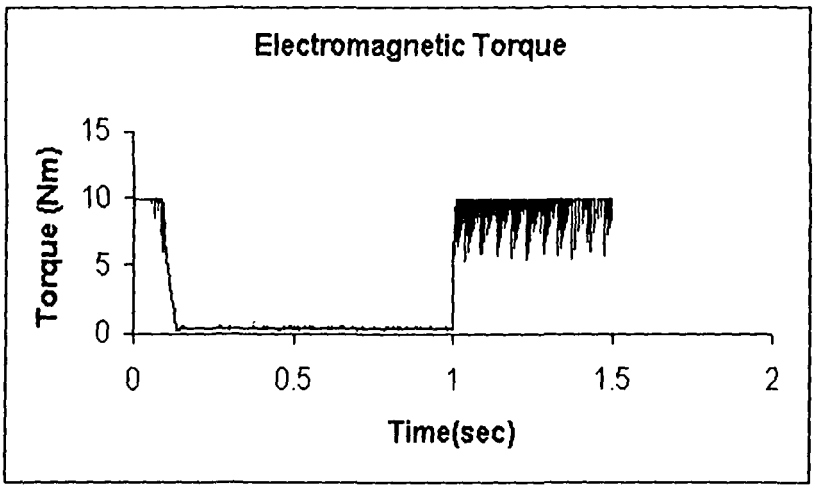

Figure 5.143: Electromagnetic Torque Vs time plot during load perturbations

5.9.3.3 Response of PMBLDC Motor Voltage with Gain Scheduling PI Controller During Load perturbations

Figure 5.144 shows the motor voltage response of one of the phases. Winding voltage is increases up to 300 V / 305V (peak) in all the three phases.

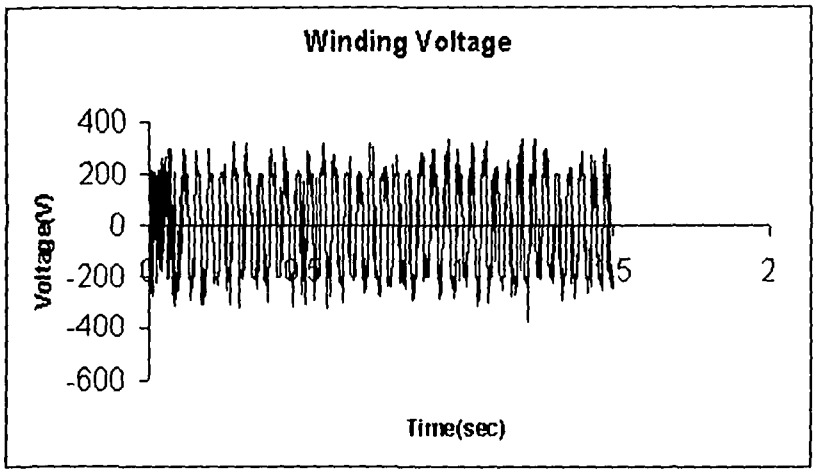

Figure 5.144: Motor winding Voltage Vs time plot during load perturbations

5.10 Hybrid FP+ID Speed Controller

The speed controller and switching logic of current controller are used in this simulation. The performance of the FP+ID controller for speed control of PMBLDC motor is judged during different operating conditions. The simulated dynamic responses of winding currents of three phases, speed, torque and winding voltage characteristics of a 3-phase, 4-pole, 0.5 HP PMBLDC motor with its reference speed set at 157 rad/sec are presented in this section. For each of these cases, results pertaining to three modes of dynamic operations, namely, the starting, the speed reversal and the load perturbations have been obtained. The simulated responses of the drive, thus obtained are shown in Figures 5.145 to 5.162. Figures 5.145 to 5.150 illustrate the starting responses of the drive with each of speed controllers considered in this investigation. Figures 5.151 to 5.156 refer to speed reversal while Figures 5.157 to 5.162 refer to the load perturbations.

5.10.1 Responses of PMBLDC Motor Current with Hybrid FP+ID Controller During Starting

Figures 5.145 –5.147 show the motor currents (i_a, i_b and i_c) which increase up to 4.06 A (peak) at the time of starting without any load and settle down at 0.15 A at the steady-state condition. The steady- state current is 15 mA which is reached 140 msec after its start on no-load.

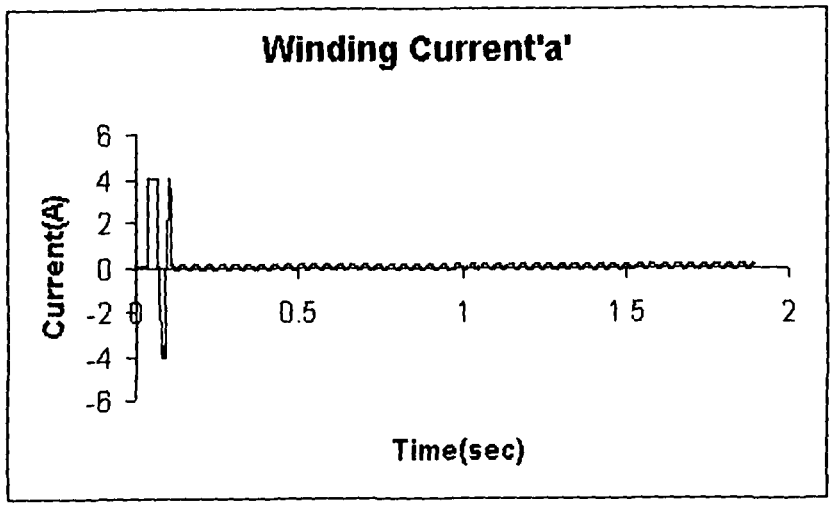

Figure 5.145: Motor Current 'i_a'

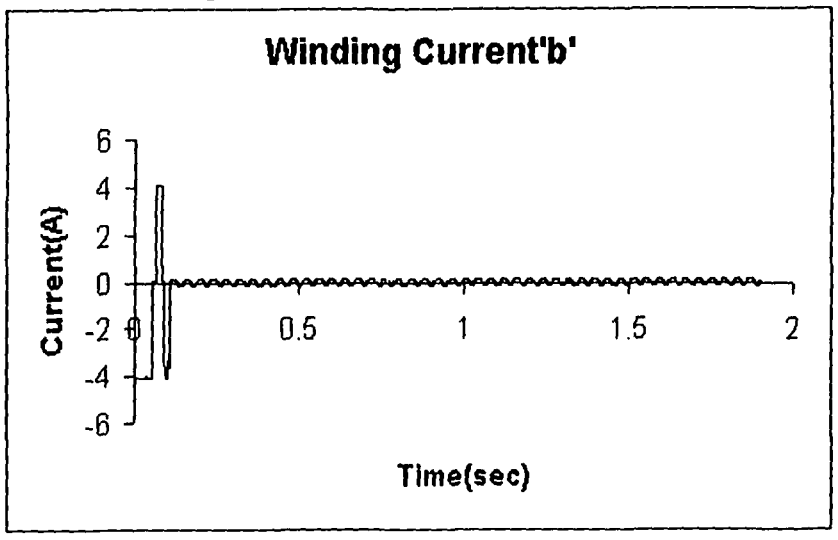

Figure 5.146: Motor Current 'i_b'

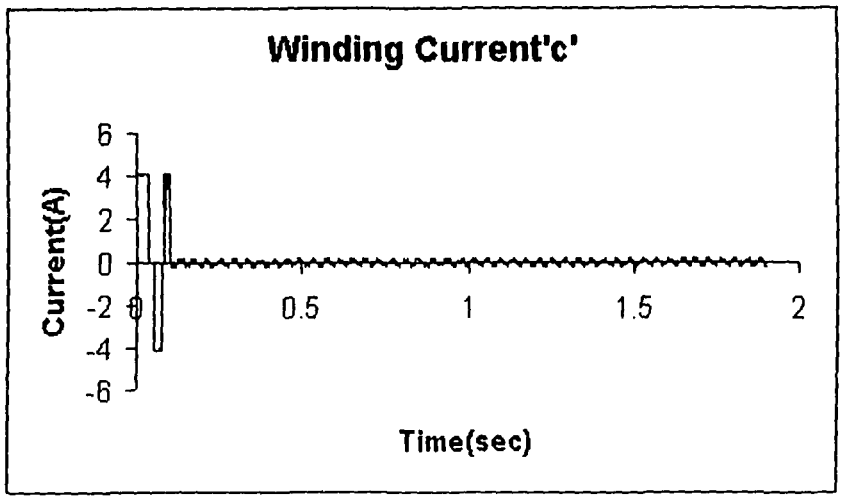

Figure 5.147: Motor Current 'i_c'

5.10.1.1 Response of PMBLDC Motor Speed with hybrid FP+ID Controller During Starting

The starting response of the PMBLDC drive system using hybrid fuzzy FP+ID controller is shown in Figure 5.148 with the motor at rest, the reference speed is set at 157rad/s (1500rpm). Within 140 msec the motor speed reaches the reference speed without any overshoot and zero-steady-state error in speed. The facts point to the existence of faster response of speed controllers. The starting response of the PMBLDC drive with conventional PID controller is slower than that of hybrid FP+ID speed controller. The former controller shows an overshoot in speed, which is undesirable. The drive takes maximum permissible current to start the motor from standstill. The results prove that the response of the drive is faster than the conventional PID controller. Improved of hybrid FP+ID controller is of immense help to industrial applications.

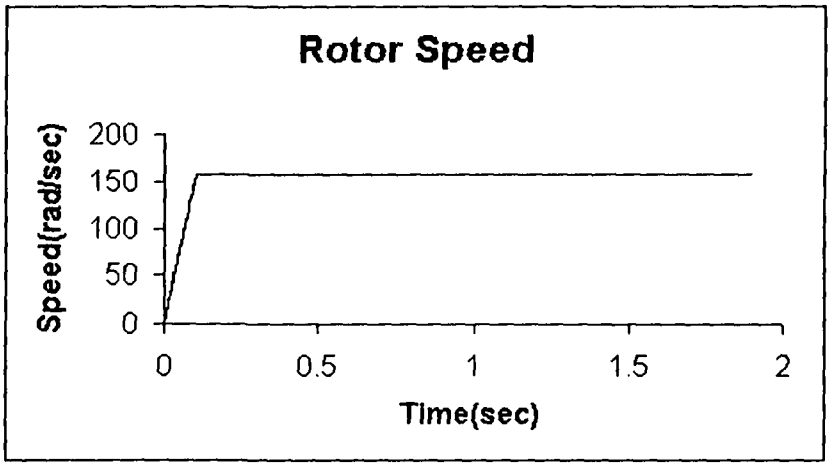

Figure 5.148: Rotor speed Vs time plot during Starting

5.10.1.2 Response of PMBLDC Motor Torque with hybrid FP+ID Controller During Starting

Figure 5.149 shows the motor electromagnetic torque which rises to 10 Nm (maximum permissible value) during the starting of the motor from standstill. The rise in torque is almost instantaneous to start the motor from the standstill condition. By the time the motor reaches the steady-state condition, the torque also undergoes a fast transient decrease and settles down to the steady-state level of 0.35 Nm and maintains the same level over the remaining period of time. The level of electromagnetic torque under steady- state is decided by the extent of the load torque on the motor shaft.

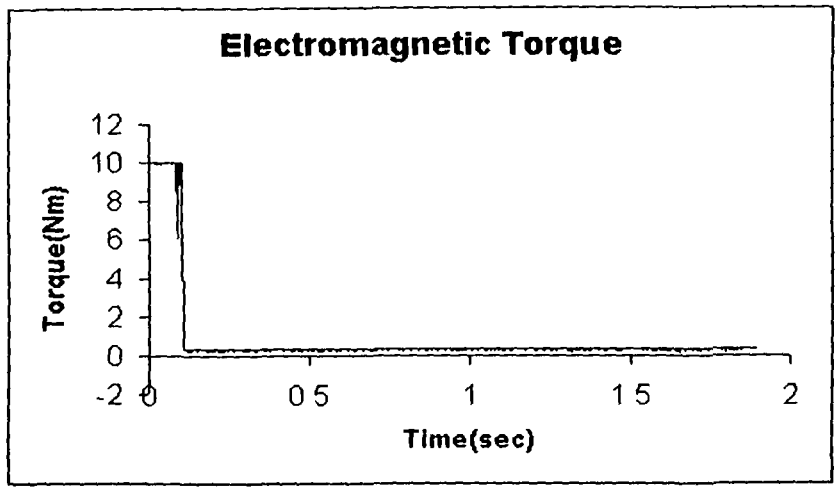

Fig. 5.149: Electromagnetic Torque Vs time plot during Starting

5.10.1.3 Response of PMBLDC Motor Voltage with hybrid FP+ID Controller During Starting

Figure 5.150 shows the motor voltage response of one of the phases. Winding voltage is increases up to 300 V /305V (peak) in all the three phases.

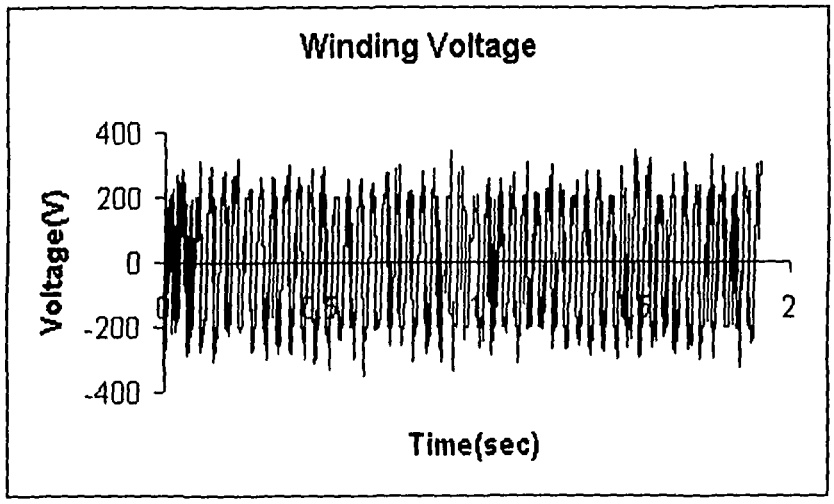

Figure 5.150: Motor winding Voltage Vs time plot during Starting

5.10.2 Responses of PMBLDC Motor Current with hybrid FP+ID Controller During Reversal

Figures 5.151 –5.153 shows the motor currents (i_a, i_b and i_c) which increase up to 4.05 A (peak) at the time of starting without any load and settle down at 0.15 A(peak) during the steady-state condition. At 775 msec currents again rise up to 4.05A (peak) due to the speed reversal. The drive takes 230 msec for a reversal of speed and currents reach the original value of 0.15 A.

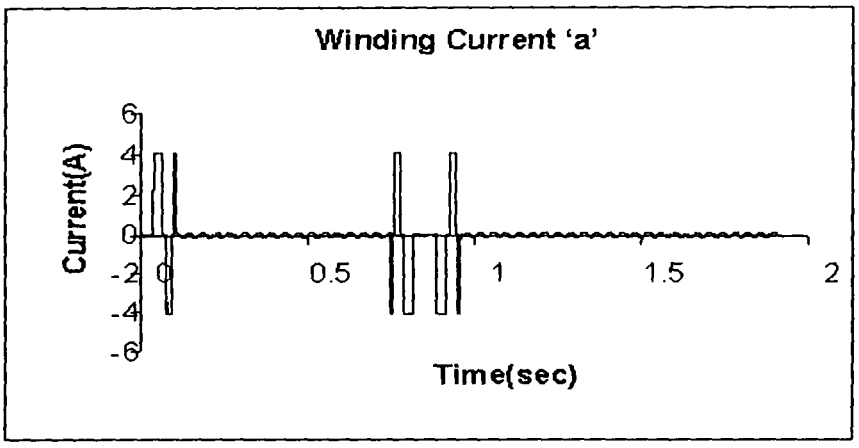

Figure 5.151: Motor Current 'i_a'

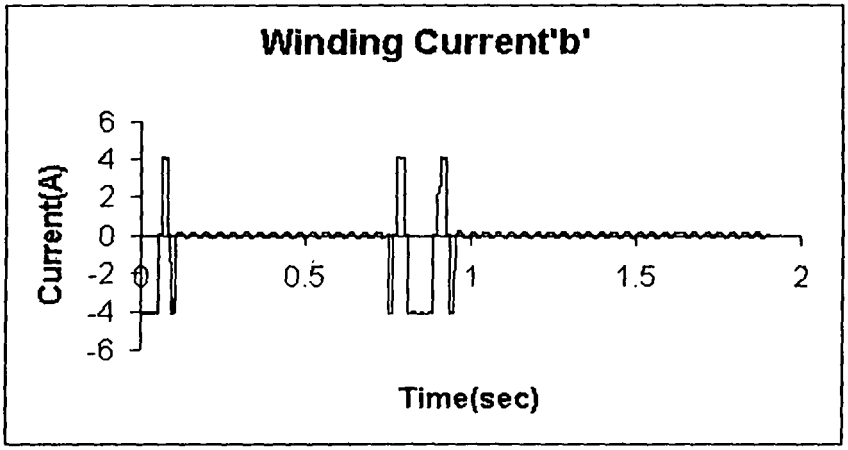

Figure 5.152: Motor Current 'i_b'

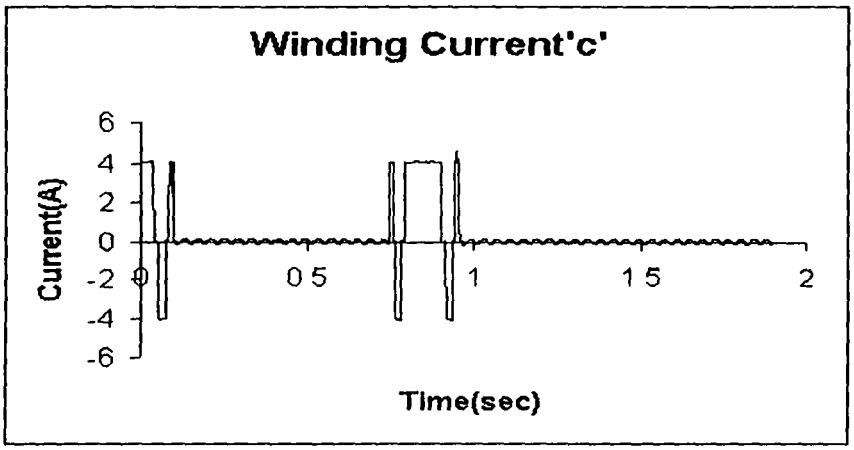

Figure 5.153: Motor Current 'i_c'

5.10.2.1 Response of PMBLDC Motor Speed with hybrid FP+ID Controller During Speed Reversal

Figure 5.154 shows the speed reversal dynamics of the PMBLDC motor with hybrid FP+ID speed controller. When the set speed is changed to −157 rad/sec (speed reversal), hybrid FP+ID Speed Controller becomes active and brings the motor

speed equal to the reference speed. The drive takes 230 msec for the speed reversal. The response is smooth without oscillations. This is due to robust and accurate control structure proposed in the present investigation.

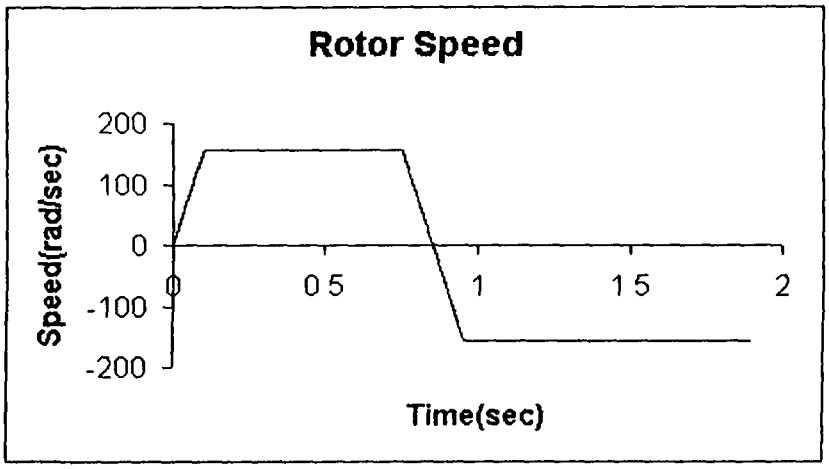

Figure 5.154: Rotor Speed Vs time plot during Reversal

5.10.2.2Response of PMBLDC Motor Torque with hybrid FP+ID Controller During Speed Reversal

Figure 5.155 shows the electromagnetic torque which rise instantaneously to 10.0 Nm (Maximum permissible value) to start the motor from standstill. By the time of the motor reaches the steady-state condition, the torque also undergoes a quick decrease to settle down to the steady-state level of 0.35 Nm and is maintained till the reversal condition. When the speed is changed suddenly the torque becomes maximum with negative value (-10.0 Nm) and the motor speeds up in reverse direction. Once the motor reaches the steady state in (-ve) direction, the torque is maintained at its initial value of 0.35 Nm.

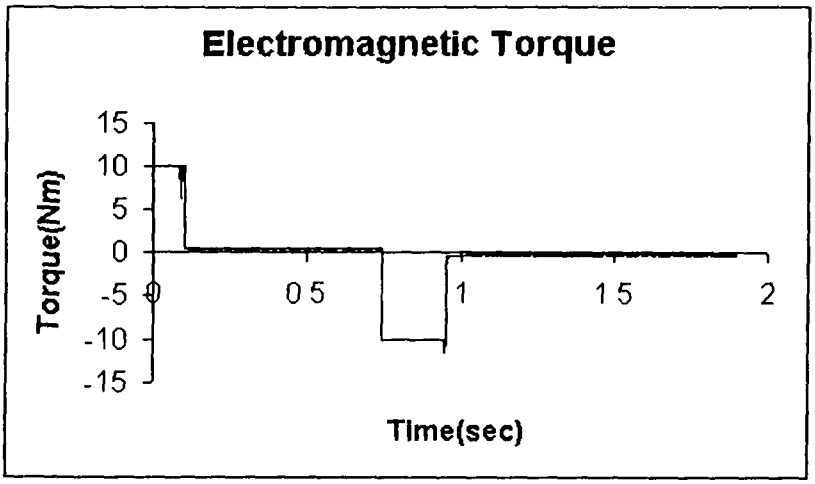

Figure 5.155: Electromagnetic Torque Vs time plot during Reversal

5.10.2.3 Response of PMBLDC Motor Voltage with hybrid FP+ID Controller During Reversal

Figure 5.156 shows the motor voltage response of one of the phases. Winding voltage is increases up to 300 V / 305 V (peak) in all the three phases.

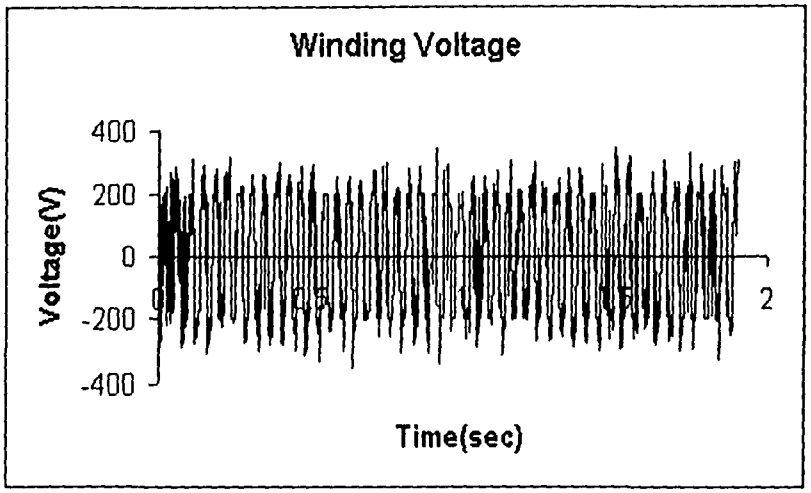

Figure 5.156: Motor winding Voltage Vs time plot during Reversal

5.10.3 Responses of PMBLDC Motor Current with hybrid FP+ID Controller During Load Perturbations

Figures 5.157 – 5.159 show the motor currents (i_a, i_b and i_c) which increase up to 4.05 A (peak) at the time of starting without any load settle down to 0.15 A(peak) during the steady-state condition. During the load perturbation, the current increases to 1.75 A to meet the demand of the load. When the load is removed, the current returns to the original value. The winding currents are found to follow the reference currents even during the conditions of load perturbations.

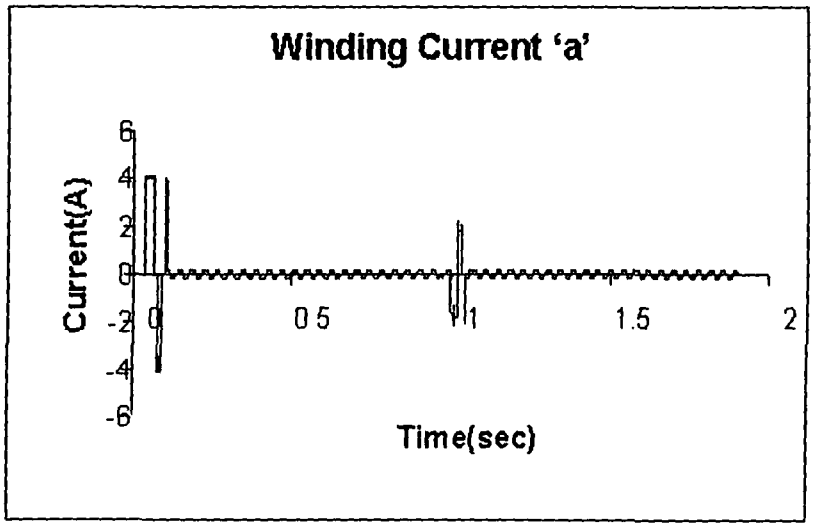

Figure 5.157: Motor Current 'i_a'

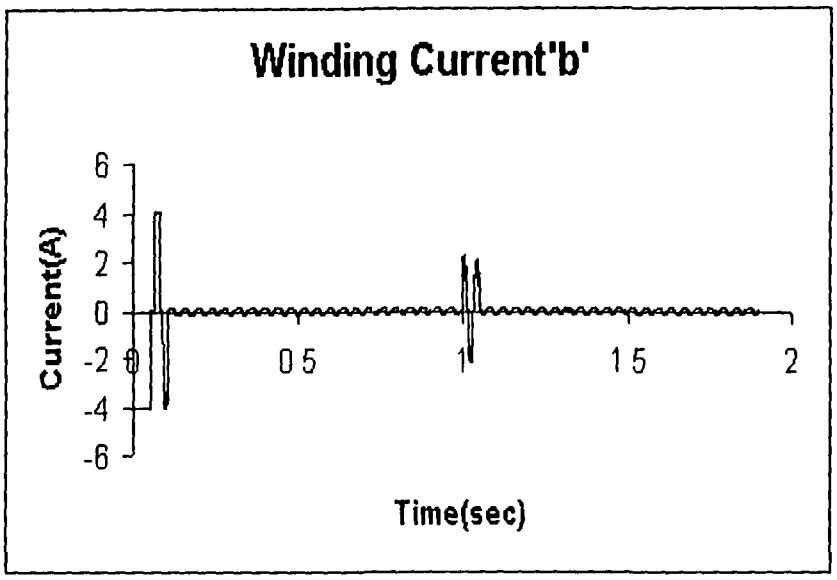

Figure 5.158: Motor Current 'i_b'

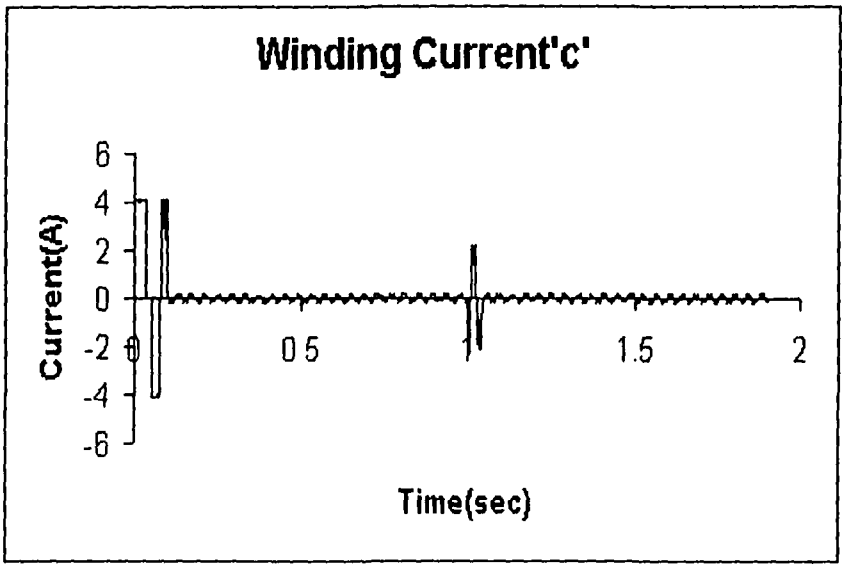

Figure 5.159: Motor Current 'i_c'

5.10.3.1 Responses of PMBLDC Motor Speed with hybrid FP+ID Controller During Load Perturbations

Figure 5.160 shows the response of the hybrid FP+ID speed controller under load perturbations. The sudden application of full-load at t =1.0sec and removal at t =1.05sec on the motor shaft cause a negligible variation in speed. It takes no time to reach the reference speed. The result shows significant improvement in the response of the drive with the hybrid FP+ID speed controller. The hybrid FP+ID controller makes the drive robust under the load perturbations.

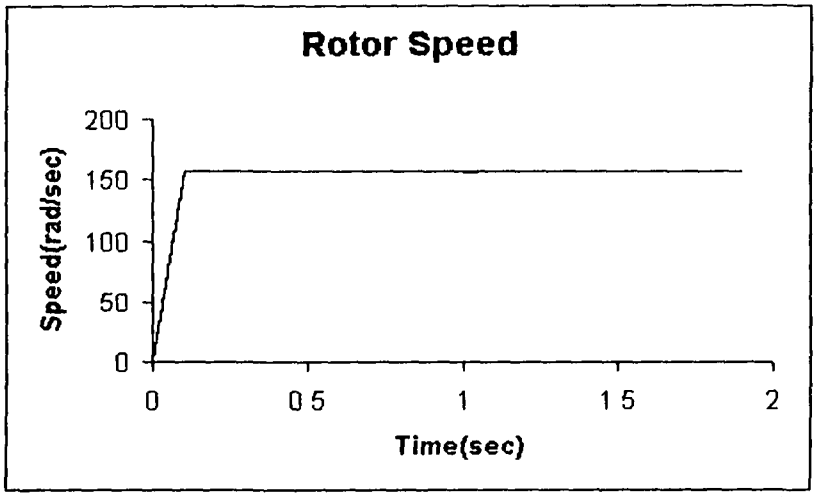

Figure 5.160: Rotor Speed Vs time plot during Load Perturbations

5.10.3.2 Response of PMBLDC Motor Torque with hybrid FP+ID Controller During Load Perturbations

Figure 5.161 shows the electromagnetic torque which increases to 5.15 Nm on application of load and is maintained at that value till the load is removed. It is observed that the hybrid FP+ID controller shows superior response over PID controller in terms of the improved dynamics under load perturbations.

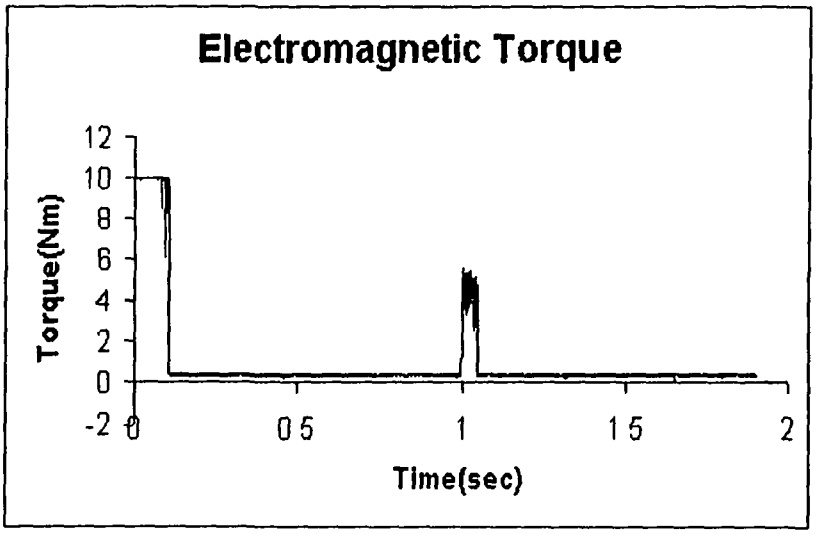

Figure 5.161: Electromagnetic Torque Vs time plot during load Perturbations

5.10.3.3 Responses of PMBLDC Motor Voltage with hybrid FP+ID Controller During Load Perturbations

Figure 5.162 shows the motor voltage response of one of the phases. Winding voltage is increases up to 300 V / 305 V (peak) in all the three phases.

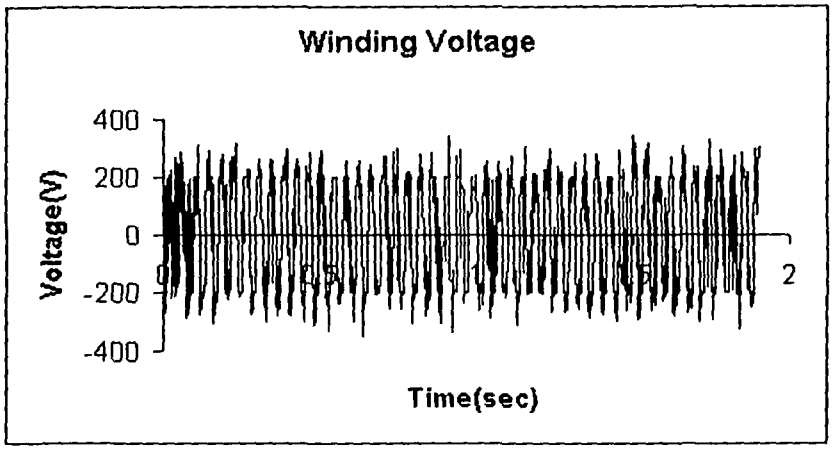

Figure 5.162: Motor winding Voltage Vs time plot during load Perturbations

5.11 Performance Comparison of Controllers

The results of the investigation have confirmed the viability of the simplified models used in the present studies. The different types of control structure proposed in the work are capable of taking care of transients in speed, current and torque variations during starting, speed reversal and load perturbations. Since the transient currents drawn by the motor never exceeded the maximum permissible, it is observed that the motor control structure has an in-built over-current protection. The dynamic responses of the drive are observed to improve with SMC and Fuzzy-based controllers. It is revealed from this investigation that all the speed controllers used have their own advantages and disadvantages, and the choice is to be made depending on the requirements of a particular application. It is also noticed that PI and PID controllers are simple and easy to simulate. But they exhibit poor performance under load disturbances and nonlinearities. SMC is observed to suffer from chattering problems. Fuzzy-PI controller is highly robust to load variations than PI and SMC controllers. Fuzzy-PI controller also shows significant improvement in transient and steady-state responses of the PMBLDC drive. Compared to PI and PID speed controllers, the Gain-Scheduled PI controller, Hybrid FP+ID controller and Self-Organizing controller show better performance in terms of overshoot, rise-time and load disturbances.

Conventional solutions to controller requirements were based on classical control theory or modern control theory. Classical control-theory-based design of PID family of controllers requires precise linear mathematical models. The PID family of controllers failed to perform satisfactorily under parametric variation, non-linearity,

load disturbances, etc. For example DC-DC converters with one power switch have three possible configurations within a single switching cycle. In this case, the most widely used method to obtain mathematical model is state-space-averaging method.

Modern controllers are state-feedback controllers, self-tuning controllers and model-reference-adaptive controllers. These controllers also need mathematical models and are therefore sensitive to parametric variation. To alleviate the need for accurate mathematical models, sliding-mode controllers (SMC) were introduced. The SMC does not need accurate mathematical models but requires the knowledge of the range of parametric variation to ensure stability conditions. The SMC is designed to have first- order response irrespective of the order of the system. In the process of ensuring the first- order response, the control law ensures the optimum dynamic responses.

In the recent times Fuzzy Logic Controllers (FLC) have generated a good deal of interest in certain applications. The advantages of FLC over the conventional controllers are due to the fact that it offers flexibility and lends itself to the mathematical model selected; and it can work with imprecise inputs. It can handle non linearity, and is more robust than conventional non-linear controllers.

The reference speed of the motor is set at 157 rad/sec (1500 rpm). The starting responses of the drives were studied with PI, PID, SMC, FPI, FPID, FSMC, Self-Organizing Fuzzy Logic Controller, Gain Scheduling PI Controller and Hybrid (FP+ID) Controller. From the graphics it is clear that the motor takes nearly (125 – 170) msec, depending upon the type of speed controller used, to reach the set reference speed. For easy comparison, their exact values are given in Table-5.1 from which one can find the difference in starting time between the fastest (FSMC taking 125 msec) and the slowest (PID taking 170 msec) controller. It may also be observed from the figures that in all cases (with different controllers), as soon as the rotor speed reaches the set reference value, the controller becomes effective in maintaining the rotor speed at the set reference value without oscillations in speed. Only during the starting, the speed shows marginal oscillations. These facts point to fast response of the speed controllers.

With PI and PID controllers, more oscillations are observed in speed, current and torque during the settling period. These oscillations get reduced in the case of SMC in which case the change over is relatively smooth from starting to the running condition. The starting performance is further improved with fuzzy-based

controllers (all types) as can be seen from reduction in the torque pulsation. But winding voltage is same in all types of controllers as can be seen in the figures.

In speed reversal the set reference speed is suddenly changed from +157 rad/sec to-157.0 rad/sec. In response to this change, the control structure is activated which implements the regenerative braking at controlled frequencies and this is followed by the reverse motoring up to the set reference speed. It is observed that right at the moment when the reference speed is changed from positive to the negative value, there is an instantaneous change in reference currents. The motor current follows the change in reference currents. This is possible due to the fast and accurate closed-loop control structure used in the present investigation. In the case of reverse-speed operation, spikes are observed in PI and PID controllers during the settling period. Where as this problem is minimized to a great extent in the case of SMC, the results get further improved in FLC, namely FPI, FPID, FSMC, Gain Scheduling PI and hybrid FP+ID etc.

The responses of the above controllers were also studied under load perturbations. From the graphics it is clear that the motor takes time to recover from load perturbations (nearly 5–100 msec) depending upon the type of speed controller used in order to reach the set reference speed (Table-5.1). The sudden application of load on the motor causes a small dip in the motor speed, which recovers very quickly due to the fast controller action. It can be observed from the figures that, almost immediately after the change of load, the speed recovers and comes back to its normal value. In PI and PID controllers, some small oscillations are observed during the load perturbations in speed, torque and current but winding voltage of all phases are same in all the three phases. These oscillations are found to get reduced in the SMC scheme. The performance of the drive system gets improved in the case of FLC in terms of speed, torque and current responses.

The transient and steady-state responses of the drive were studied with Self-Organizing Fuzzy-logic controller. This controller gives fast response similar to fuzzy- logic controller. For reaching the reference speed of 157rad/sec, the drive takes 145msec. The speed reversal dynamics is also shown. For reversal, it takes 240msec. Also sudden application of load causes negligible variation in speed.

The starting response of the PMBLDC drive system using hybrid-fuzzy-logic controller was studied at the reference speed of 157rad/s (1500rpm). Within 140 msec, the motor speed reaches the reference speed without any appreciable overshoot

and zero steady-state-error in speed. The response shows only marginal oscillations. The fact points to the fast response of speed controller. The starting response of the PMBLDC drive with conventional PID controller is slower than that of FP+ID speed controller. The former shows an overshoot in speed, which is undesirable. It also takes maximum permissible current to start the motor from standstill. The results prove that the response of the drive is faster with FP+ID controller than the conventional PID controller. Improved response of FP+ID controller is of immense help to industrial applications. The performances of the PMBLDC Motor under different speed controllers are compared in Tables 5.1 and 5.2.

It has been shown that there is a quick and instantaneous corrective change in the motor current in response to any disturbances in the set operating conditions of the drive system. In all cases, the actual winding currents are found to follow the variations in the reference currents. The oscillations present in the current and torque in the PI and PID speed controllers during changeover from starting to steady-state condition have been found to improve considerably when the SMC and FLC are used in the closed-loop operation of the drive. It has been observed that the PI and PID controllers (in comparison to Fuzzy PI and Fuzzy PID controllers) are easier to implement. But they exhibit a slower response and cause some steady-state errors with a settling period. The SMC on the other hand is found to be robust but slower, and suffers from the problem of chattering. Apart from being relatively difficult to realize FSMC, it is found to be superior to SMC in terms of intelligence and load-bearing capability. FPID and hybrid FP+ID are more intelligent than FSMC and exhibit the fastest response besides having an excellent load-bearing capability. Gain-Scheduled PI controller is also superior to the PI controller.

Table 5.1 Performance comparison of the drive with different speed controllers

Speed controller	Starting time (msec)	Dip in speed under load perturbation (%)	Time for recover from load perturbation(msec)	Speed reversal (msec)
PI	160	0.6	100	280
PID	170	0.6	100	260
SMC	140	0.45	Steady state error	205
FP-PI	130	0.01	5	230
FP-PID	150	0.01	5	230
FP-SMC	125	0.07	10	215
Self-Organizing Fuzzy	145	0.08	10	240
Gain-Scheduled PI	125	0.3	25	240
Hybrid FP+ID	140	0.15	10	230

Table 5.2 Performance summary

Speed controller	Accuracy	Transient Response	Robustness
PI controller	Excellent	Fair	Poor
PID controller	Excellent	Fair	Poor
SMC	Good	Good	Excellent
FP-PI Speed controller	Excellent	Very Good	Excellent
FP-PID Speed controller	Excellent	Very Good	Excellent
FP-SMC Speed controller	Excellent	Very Good	Excellent
Self-Organizing Fuzzy	Good	Very good	Very Good
Gain-Scheduled PI	Excellent	Good	Fair
Hybrid FP+ID	Good	Very Good	Excellent

5.12 RESPONSES OF SENSORLESS CONTROL OF PMBLDC MOTOR DRIVE

5.12.1 Starting Algorithm

To start the motor, the first phase sequence is consequently known. However, the phase back-emf magnitude is still too low to assure a synchronization of the phase switchings on the back-emf position detection. The motor is started differently by applying a specific PWM (Pulse Width Modulation) pattern (say, devices T1 and T2 are turned ON and OFF) to the inverter. This is repeated several times to align the rotor in the direction of a particular phase winding. The regular sensorless control strategy is then followed.

5.12.2 Results and Discussions

The sensorless operation of PMBLDC motor without a shaft position sensor has been simulated. By sensing the motor terminal voltage, it is possible to start the motor with maximum torque and operate properly over entire speed range. In this prototype drive; simulation of this technique requires minimum external components since most of the processing is ensured by a low-cost microcontroller. Electronic commutation is achieved properly without shaft encoder.

The simulated responses of winding currents of three phases, speed, torque and winding voltage of a 3-phase, 4-pole, 2 HP PMBLDC motor with its reference speed set at 1500 rpm (157 rad/sec) were studied for each of these cases results pertaining to three modes of dynamic operations. The simulated responses of the drive, thus obtained are shown in Figures 5.163 to 5.165. These Figures 5.163 to 5.165 show the starting responses of the drive with each of the speed controllers considered in this investigation.

5.12.3 Responses of Sensorless Control of PMBLDC Motor Current During Starting

Figures 5.163 – 5.165 show the motor currents (i_a, i_b and i_c). The transient current increases to 3.25A (peak) and drops to 250 mA (peak) at steady-state at the time of starting without any load. The starting procedure is based on applying a specific PWM pattern to the inverter. The motor current is limited to a desired level and the line current is regulated within a hystresis band.

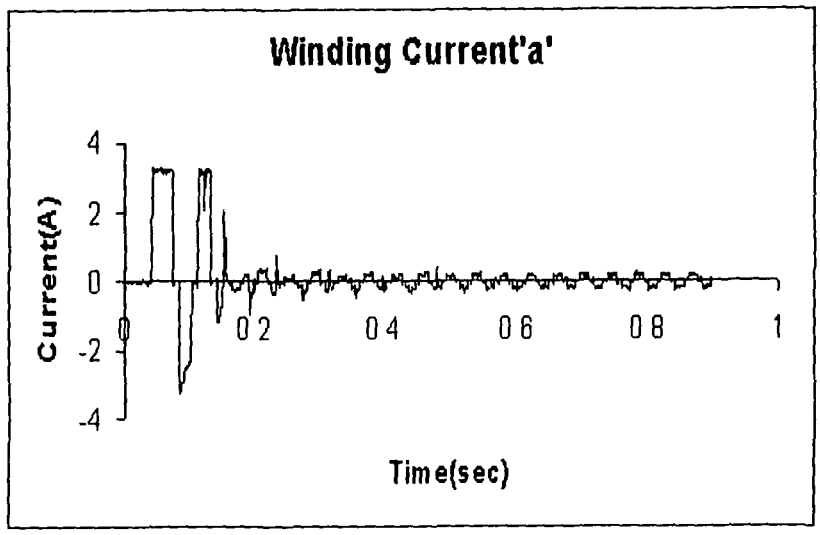

Figure 5.163: Motor Current 'i_a'

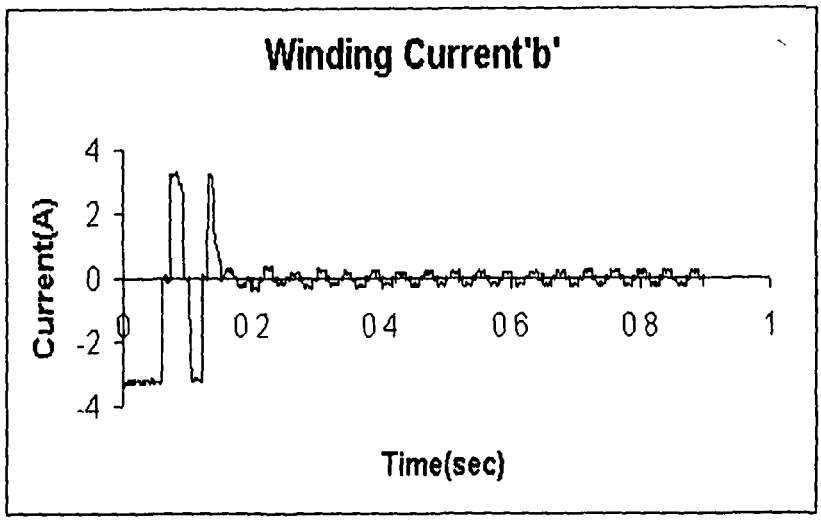

Figure 5.164: Motor Current 'i_b'

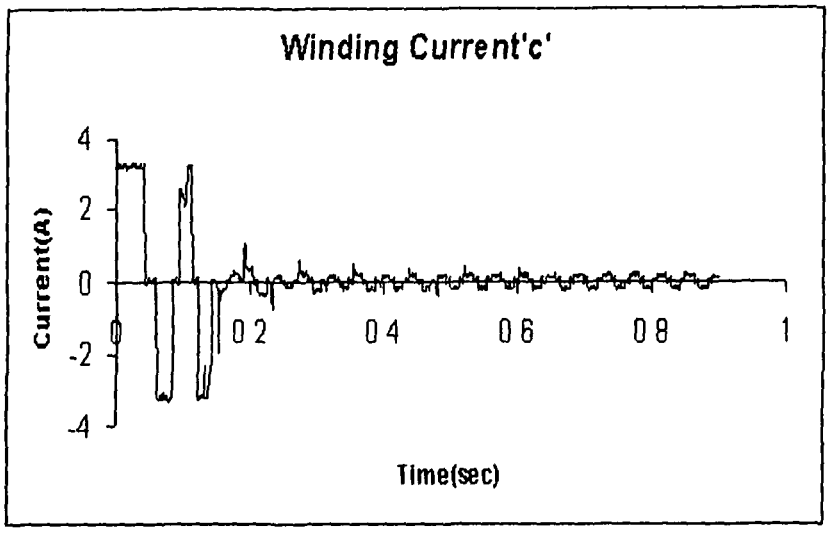

Figure 5.165: Motor Current 'i_c'

5.12.4 Response of Sensorless Control of PMBLDC Motor Speed During Starting

Figure 5.166 shows the rotor speed which is set at 1500 rpm (157 rad/sec). The drive takes the 170 msec to reach the reference speed. The developed torque rises to maximum permissible value to start the motor from standstill.

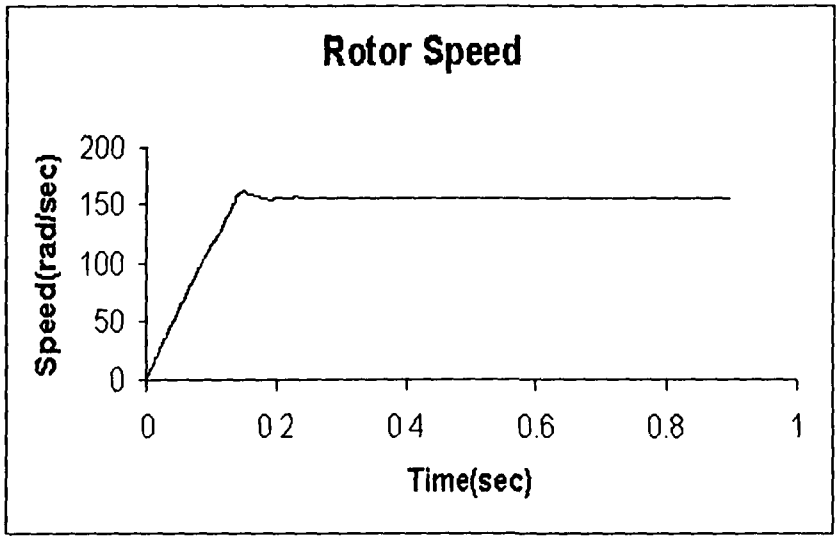

Figure 5.166: Rotor Speed Vs time plot during Starting

5.12.5 Response of Sensorless Control of PMBLDC Motor Torque During Starting

The torque response is shown in Figure 5.167. The motor torque which rises to 8 Nm at starting settles to 0.55 Nm after reaching the set speed.

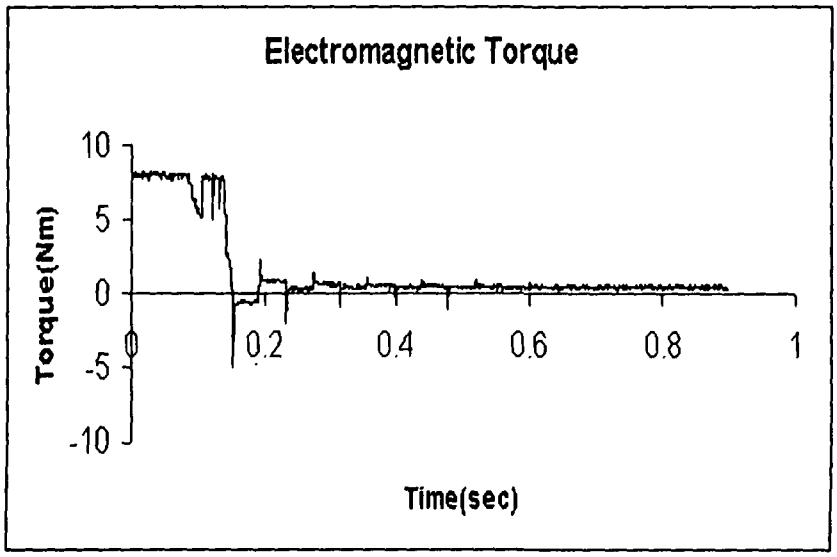

Figure 5.167: Electromagnetic Torque Vs time plot during Starting

5.12.6 Response of Back EMF and Its Corresponding Position Signal

Figure 5.168 shows the back emf and its corresponding position signal obtained from the zero crossings.

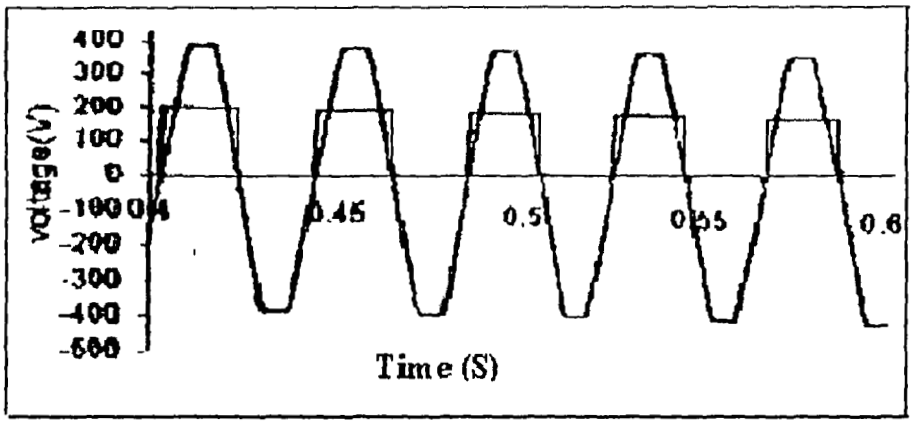

Figure 5.168: Motor back emf and its corresponding position signal

5.12.7 Response of Back EMF and Its Corresponding Three Position Signal

Figure 5.169 shows the three-phase back emf's from which the three-position signals are deducted. The three-position signals are 180° pulses displaced by 120°. Initially the drive is started by applying a specific PWM pattern (say, devices T1 and T2 are turned ON and OFF) to the inverter. This is repeated several times to align the rotor in the direction of a particular phase winding. The regular sensorless control strategy is then followed. The PMBLDC motor used for this work is of rating 2.0 H.P and 1500 rpm. The speed of the motor is set at 1500 rpm (157rad/sec). The transient current rises to 4.05A and in steady-state the drive takes 405 mA.

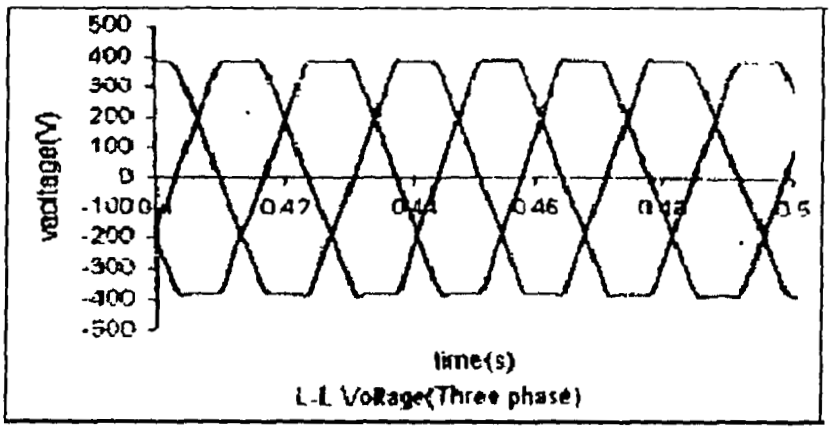

Figure 5.169: Motor back emf and its corresponding three position signal

5.13 Conclusion

The results of the investigation have confirmed the viability of the simplified model currently used. The different types of control structures proposed in the work are capable of taking care of speed transients, current and torque variations during starting, reversal and load perturbations. Since the transient currents drawn by the motor never exceeded the maximum permissible value, it is observed that the motor control structure takes care of the over-current protection. The dynamic responses of the drive are observed to be improved with SMC and Fuzzy based controllers. It is revealed from this investigation that all the speed controllers used have their own advantages and disadvantages, and the choice is made depending on the requirement of a particular application. It is also noticed that PI and PID controllers are simple and easy to implement. But they exhibit poor performance under load disturbances and nonlinearities. SMC is observed to suffer from chattering problems. Fuzzy PI controller is highly robust to load variations than PI and SMC controllers. Fuzzy PI controller also shows significant improvement in transient and steady state responses of the PMBLDC drive. Compared to PI and PID speed controllers, the Gain-Scheduled PI controller, hybrid FP+ID controller and Self Organizing controller show better performance in terms of overshoot, rise time and load disturbances.

CHAPTER 6

SIMULATION RESULTS OF PMSM DRIVE

6.1 General

The performance of a closed-loop speed-controlled drive system depends on the choice of controllers. The equations governing the model of a drive system are presented in the chapter 4. As the model of the PMSM drive is nonlinear, a numerical technique namely Runge-Kutta method is used to get the solution of these equations for the variables such as i_a, i_b, i_c, ω_r and θ_r. The motor torque, winding currents, reference speed, reference currents and rotor speed were simulated for studying the dynamic responses of the drive. The performance of the PMSM drive is influenced by parameter variations and external load disturbances. This has resulted in a continuous thrust on exploring the use of modern control schemes such as adaptive control and sliding-mode control. Controllers based on fuzzy logic are being increasingly applied to systems with non-linearity and uncertainty. With this scenario, a range of speed controllers starting from conventional to modern ones has been tried for the simulation of the PMSM drive. In this investigation, the transient and steady-state response of the drive is examined with different speed controllers like PI, PID, SMC and Fuzzy-Logic controllers. Among different current controllers the PWM current controller has been of immense help in this investigation. An algorithm is also developed for the simulation in real-time operating conditions. The PMSM drive used for this simulation is a prototype motor of 0.5 H.P, 6 pole, 3-phase, 1000 rpm (100 rad/sec), and star-connected one. The specification of the motor is given in Table-B.1 and the gain parameters of different speed controllers are given in Table-C.10 to Table-C.11.

The results of several simulation runs have been compiled for the comprehensive study of the performance behavior of the PMSM drive under of a wide range of controllers. Figures 6.1 to 6.42 illustrate the simulation results and are presented in this chapter in the following sections.

6.2 Simulation Results of PMSM drive with PI Controller

The simulated responses of a 0.5 HP, 3-phase, 6 pole PMSM with its reference speed set at 100 rad/sec are shown in Figure 6.1 to 6.21. To examine the effectiveness of PI controller with improved source of excitation applied to PMSM drive, the various simulation results were critically studied.

6.2.1 Response of PMSM Motor Current with PI Controller during Starting

Figures 6.1 – 6.4 show the motor currents (i_a, i_b and i_c) which increase to 5.0A (peak) at the time of starting without any load and reduce to a 75 mA (peak) at the steady-state condition. The control structure maintains the motor winding currents within the hystresis band around the reference currents. The winding currents always follow their reference counterparts due to the effectiveness of the current controller.

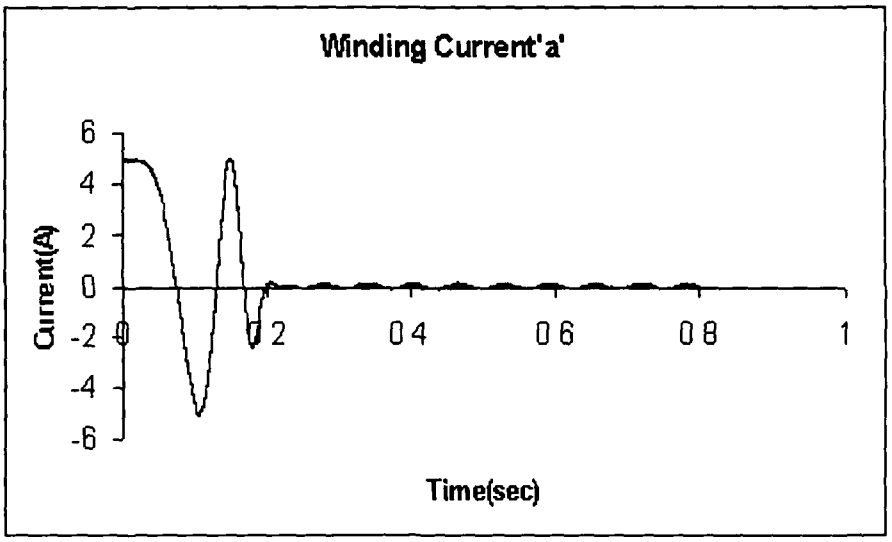

Figure 6.1: Response of Motor Current ('i_a') with PI Controller

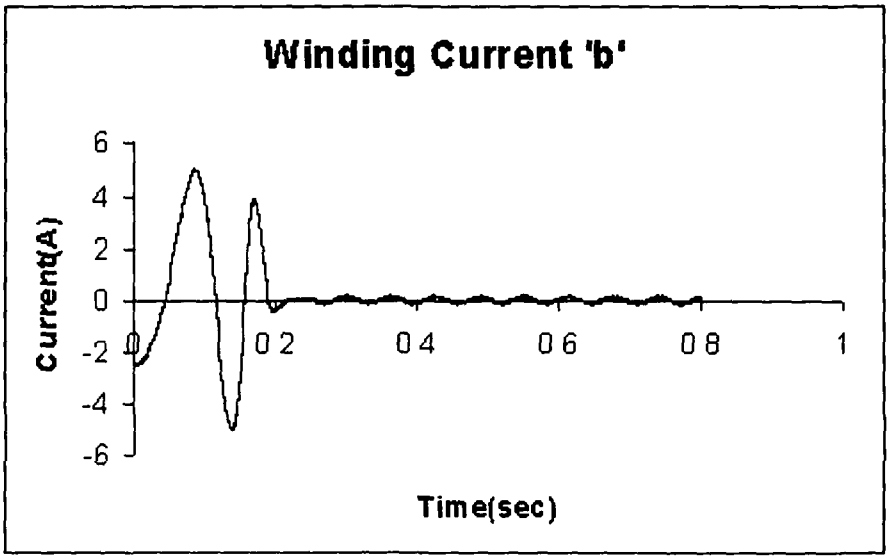

Figure 6.2: Response of Motor Current ('i_b') with PI Controller

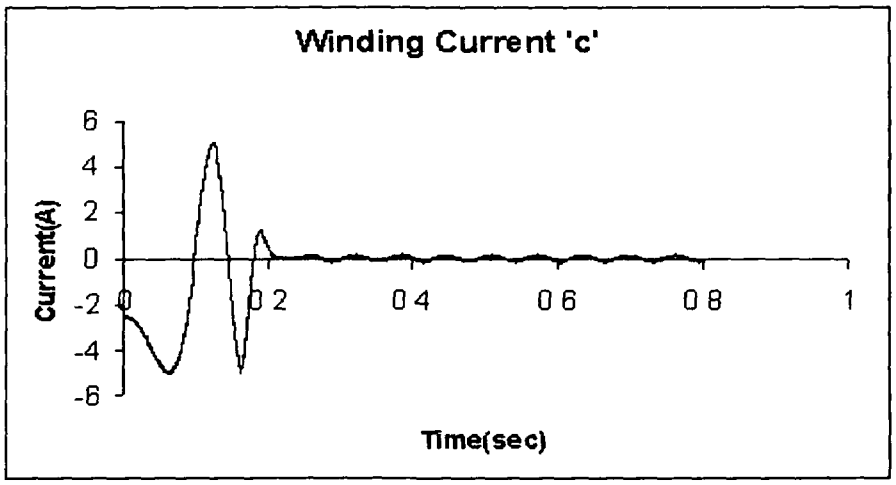

Figure 6.3: Response of Motor Current ('i_c') with PI Controller

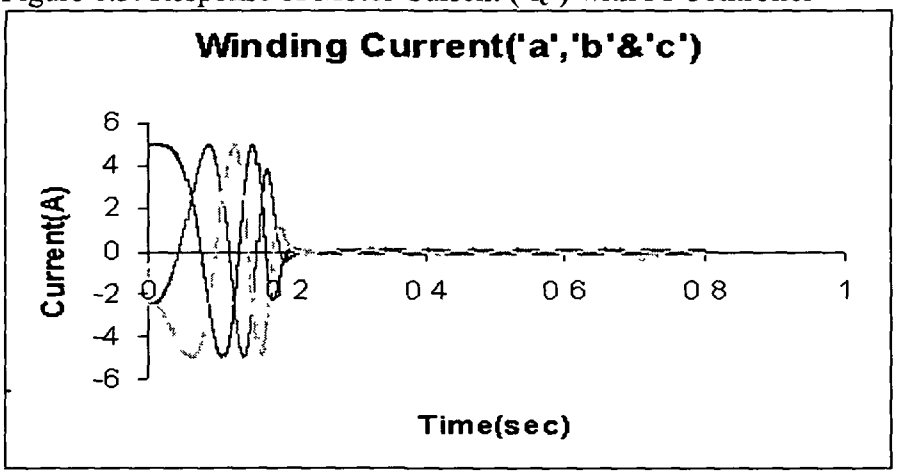

Figure 6.4: Response of Motor Currents (i_a, i_b and i_c) with PI Controller

6.2.2 Response of PMSM Speed with PI Controller during Starting

. Figure 6.5 shows the starting response of the drive in which it takes around 240 msec to reach the reference speed. As soon as the rotor reaches the reference speed, the PI speed controller becomes active, and maintains the rotor speed at the reference speed.

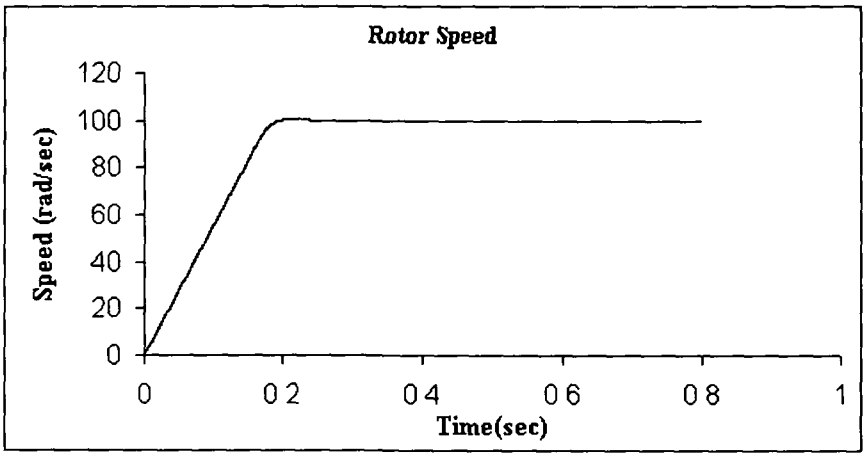

Figure 6.5: Rotor speed Vs time plot during starting

6.2.3 Response of PMSM Torque with PI Controller during Starting

Figure 6.6 shows the motor electromagnetic torque which rises instantaneously to 15 Nm (maximum permissible value) during the starting of the motor from standstill condition. After the motor reaches the steady-state speed, the developed torque decreases to 0.35 Nm and is maintained at that level over the remaining period of time.

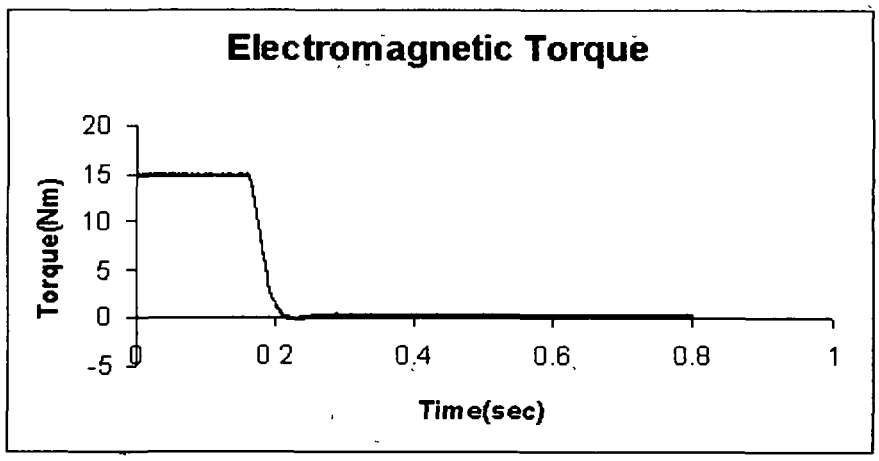

Figure 6.6: Electromagnetic Torque Vs time plot during starting

6.2.4 Response of PMSM Voltage with PI Controller during Starting

Figure 6.7 shows the motor voltage. The winding voltage increases up to 109V (peak). The winding voltages are the same in all the three phases.

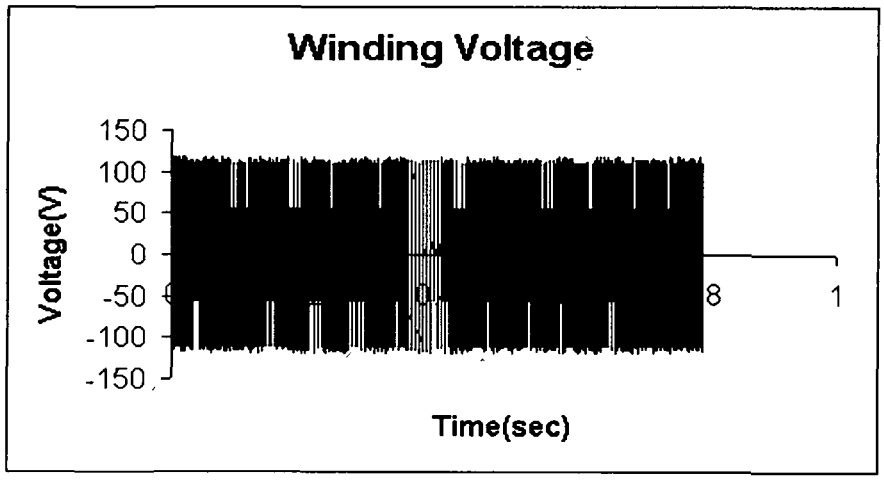

Figure 6.7: Motor winding Voltage Vs time plot during starting

6.3 Response of PMSM Current with PI Controller During Speed Reversal

Figures 6.8– 6.11 show the motor currents (i_a, i_b and i_c) which increase up to 5.0 A (peak) at the time of starting without any load and reduce to a 0.195A (peak) during the steady-state condition and it takes time 195 msec to settle down and then

after 105 msec currents again rise up to 5.0 A due to the speed reversal. The drive takes 350 msec for a reversal of speed and currents come to the original value having mean equal to 0.195 A (peak).

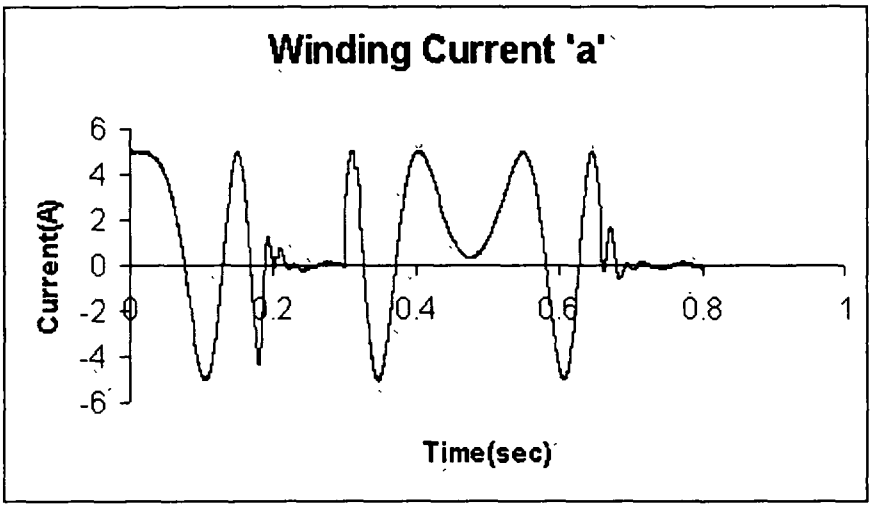

Figure 6.8: Response of Motor Current ('i_a') during Reversal

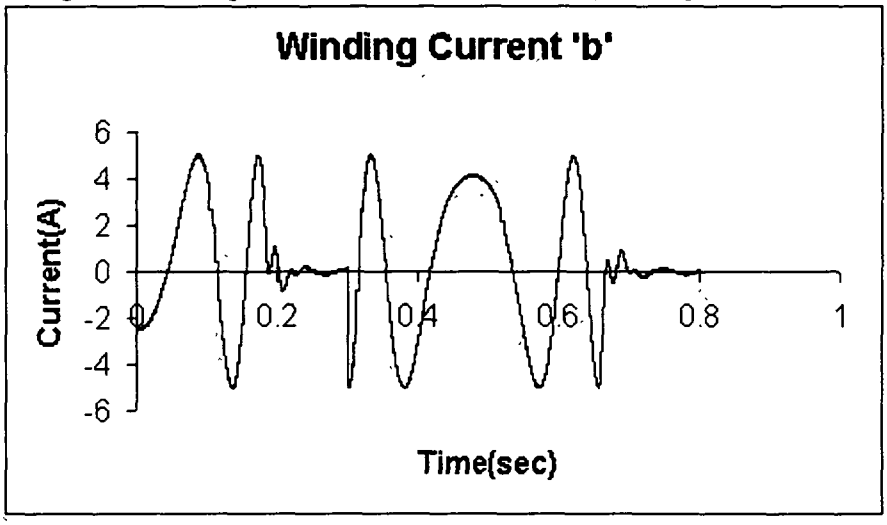

Figure 6.9: Response of Motor Current ('i_b') during Reversal

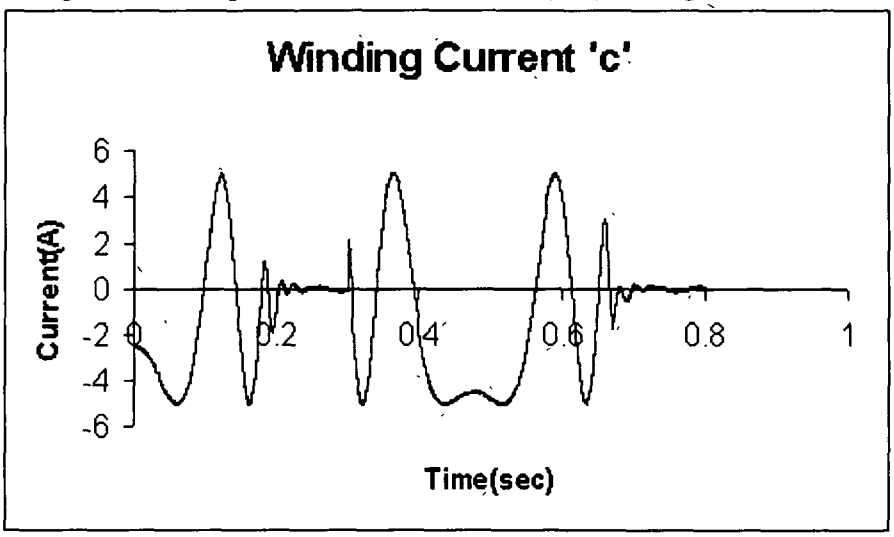

Figure 6.10: Response Motor Current ('i_c') during Reversal

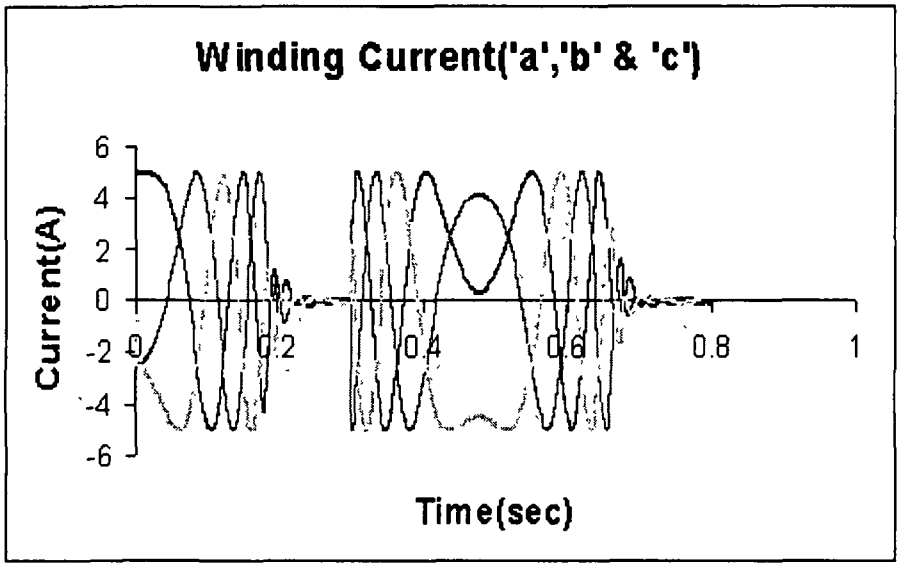

Figure 6.11: Response of Motor Currents (i_a, i_b and i_c) during speed Reversal

6.3.1 Response of PMSM Speed with PI Controller During Speed Reversal

Figure 6.12 shows the speed reversal dynamics of the PMSM motor with PI speed controller. The motor runs stable as the positive set reference speed is changed to –100 rad/sec (speed reversal). In response to this sudden change, the PI controller is actuated and control structure of the drive system becomes active and makes the motor speed equal to the reference speed. The drive takes 350 msec for the speed reversal.

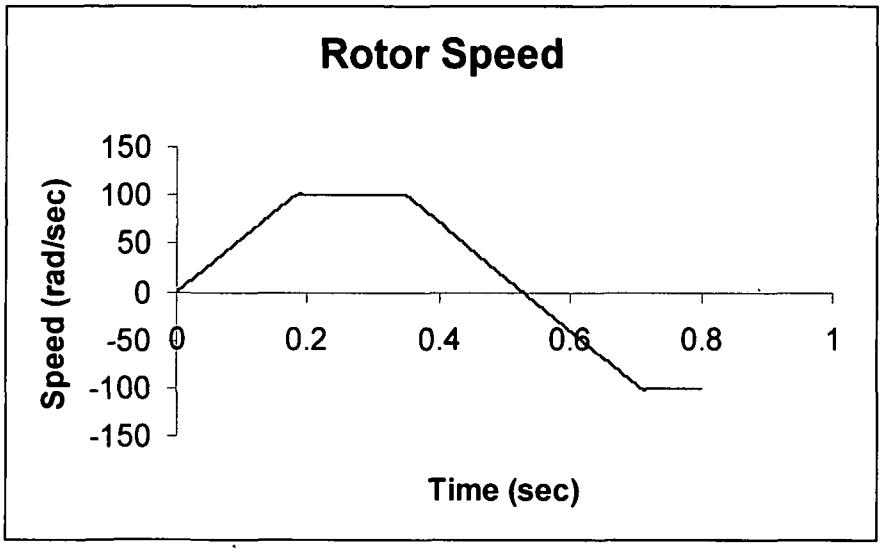

Figure 6.12: Rotor speed Vs time plot during Reversal

6.3.2 Response of PMSM Torque with PI Controller During Speed Reversal

Figure 6.13 shows the electromagnetic torque which rises instantaneously to 15 Nm (Maximum permissible value) to start the motor from the standstill condition.

By the time the motor reaches the steady-state speed, the torque undergoes a quick transient settlement to the steady-state level of 1.5 Nm till the application of reversal condition. When the speed is changed suddenly the torque becomes maximum with negative value (-15 Nm) and the motor speeds up in the reverse direction. Once the motor reaches the steady-state in negative direction, the torque is maintained at its initial value (1.5 Nm).

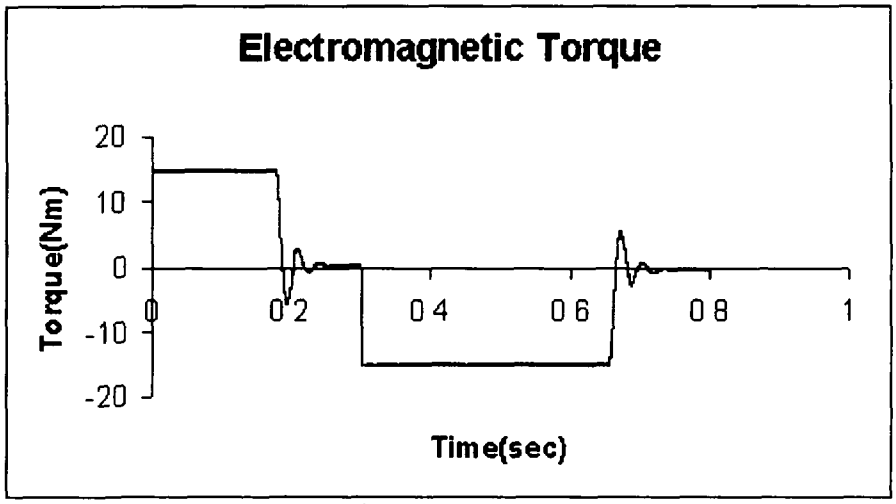

Figure6.13: Electromagnetic Torque Vs time plot during speed Reversal

6.3.3 Response of PMSM Voltage with PI Controller During Speed Reversal

Figure 6.14 shows the motor voltage. The winding voltage increases up to 109V (peak). The winding voltages are the same in all the three phases.

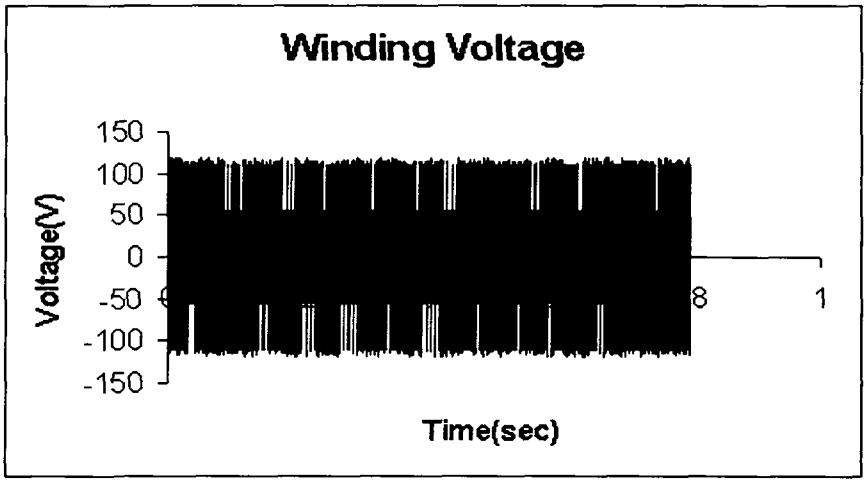

Figure 6.14: Motor winding Voltage Vs time plot during speed Reversal

6.4 Response of PMSM Current with PI Controller During Load Perturbations

Figures 6.15 – 7.18 show the motors currents (i_a, i_b and i_c) which increases to 5.0 A (peak) at the time of starting without any load and reduce to 0.15 A (peak)

during the steady-state condition. During the load perturbation, the current increases to 2.25 A to meet the demand of the load. When the load is withdrawn, the current reduces to a value decided by the small load that remains effective due to friction and windage etc. The winding currents are found to follow the reference currents even during the condition of load perturbation.

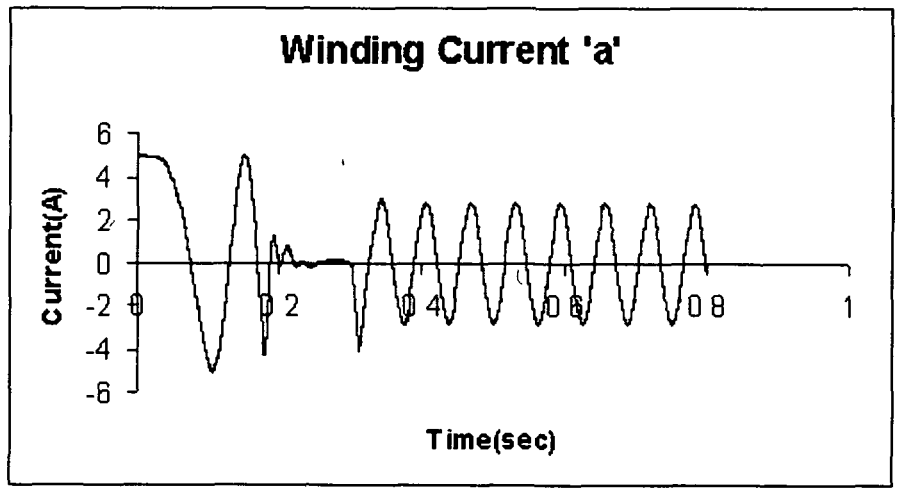

Figure 6.15: Response of Motor Current ('i_a') during load Perturbations

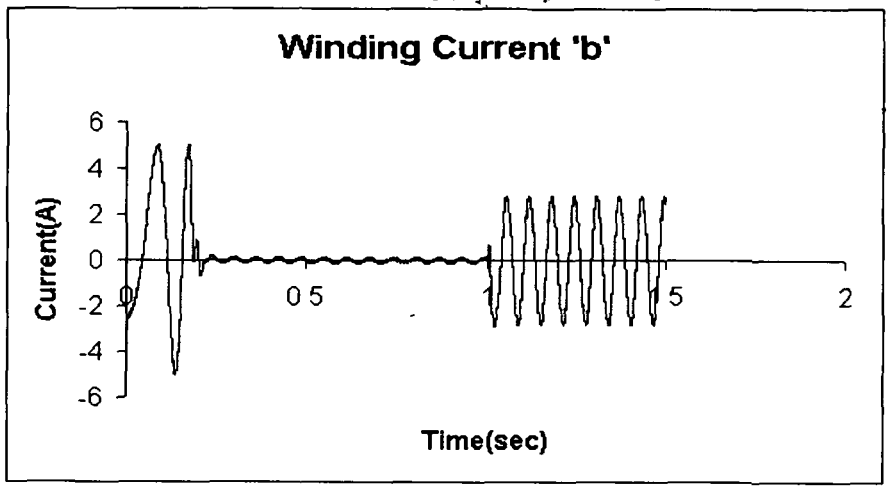

Figure 6.16: Response of Motor Current ('i_b') during load Perturbations

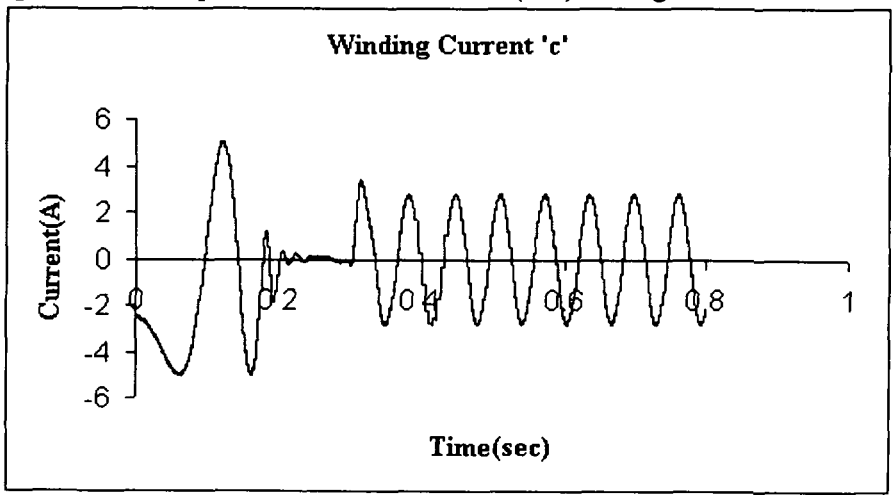

Figure 6.17: Response of Motor Current ('i_c') during load Perturbations

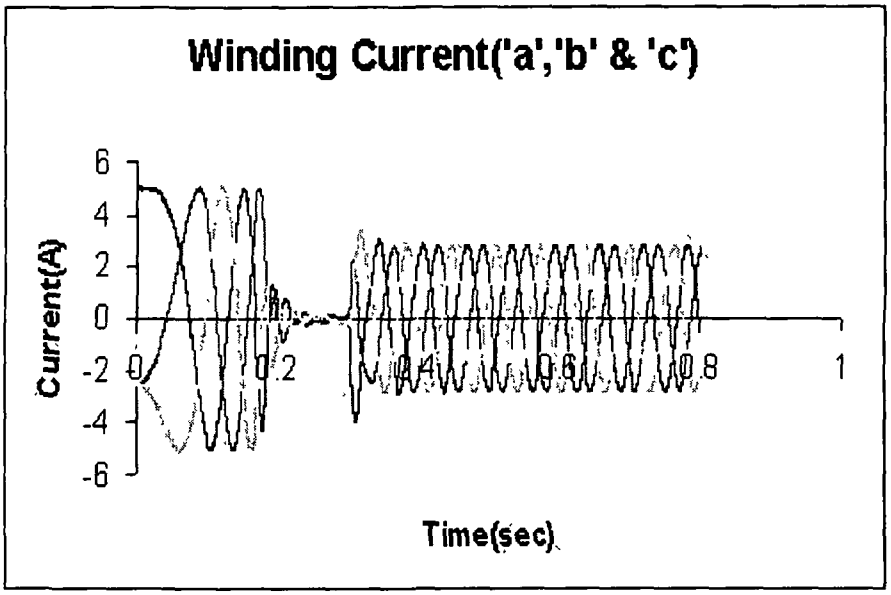

Figure 6.18: Response of Motor Currents (i_a, i_b and i_c) during load Perturbations

6.4.1 Response of PMSM Speed with PI Controller During Load Perturbations

Figure 6.19 shows the performance of the drive with the PI speed controller under load perturbation. The sudden application of load on the motor causes a small dip in the motor speed which is clearly visible in the Figure. However, the speed returns quickly to its normal value.

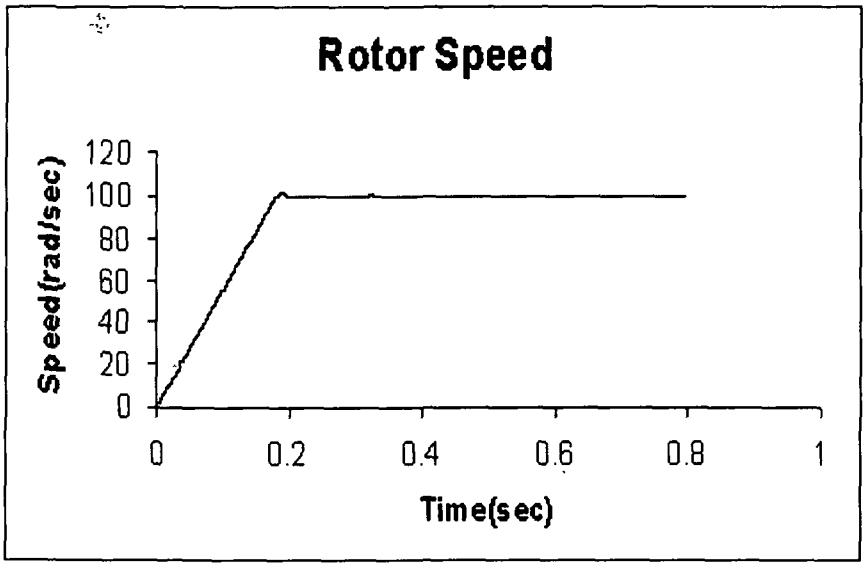

Figure 6.19: Rotor speed Vs time plot during load Perturbations

6.4.2 Response of PMSM Torque with PI Controller During Load Perturbations

Figure 6.20 shows the electromagnetic torque which increase to 8.5 Nm and is maintained at the higher value till the load is removed.

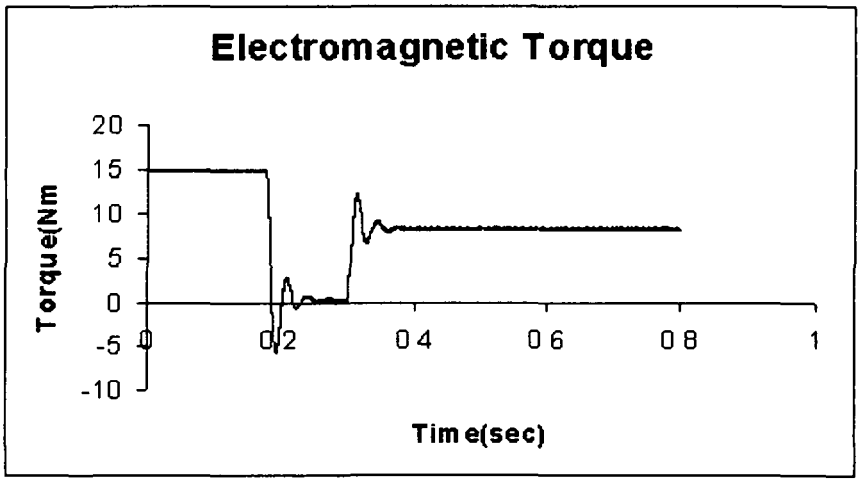

Fig. 6.20: Electromagnetic Torque Vs time plot during load Perturbations

6.4.3 Response of PMSM Voltage with PI Controller During Load Perturbations

Figure 6.21 shows the motor voltage. The winding voltage increases up to 109V (peak). The winding voltages are same in all the three phases.

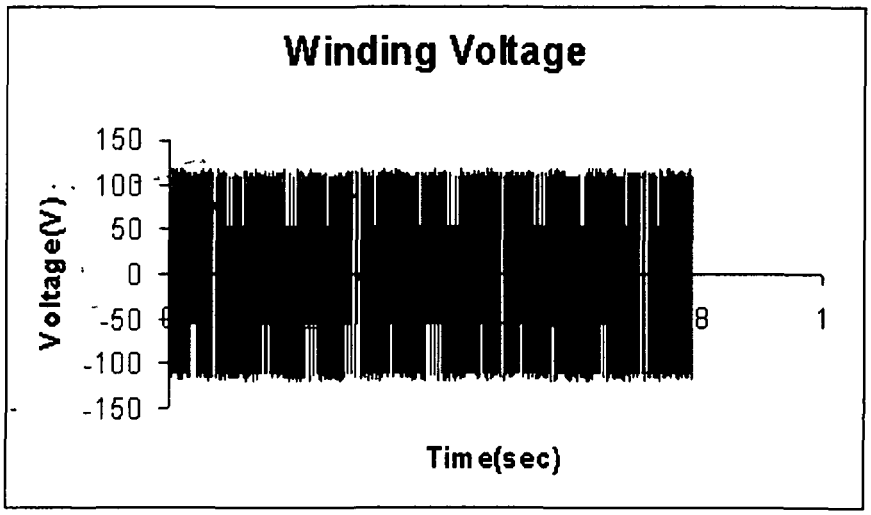

Figure 6.21: Motor winding Voltage Vs time plot during load Perturbations

6.5 Response of PMSM with PID Controller

The simulated responses of a 3-phase, 6-pole and 0.5 HP PMSM motor with its reference speed set at 100 rad/sec are shown in Figures 6.22 to 6.42. To examine the effectiveness of PID speed controller with the improved excitation applied to PMSM drive, the various simulation results were critically studied.

6.5.1 Response of PMSM Motor Current with PID Controller during Starting

Figures 6.22–8.25 shows the motor currents (i_a, i_b and i_c) which increase up to 5.0 A (peak) at the time of starting without any load and reduce to a 35 mA during the

steady-state condition. The control structure maintains the motor winding currents within the hystresis band around the reference currents. The winding currents always follow their reference counterparts due to the effectiveness of the current controller.

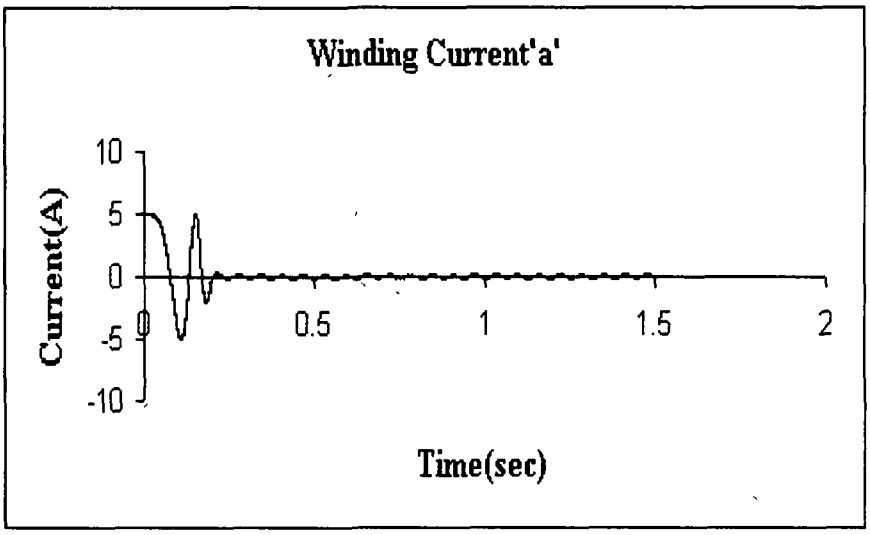

Figure 6.22: Response of Motor Current ('i_a') during Starting

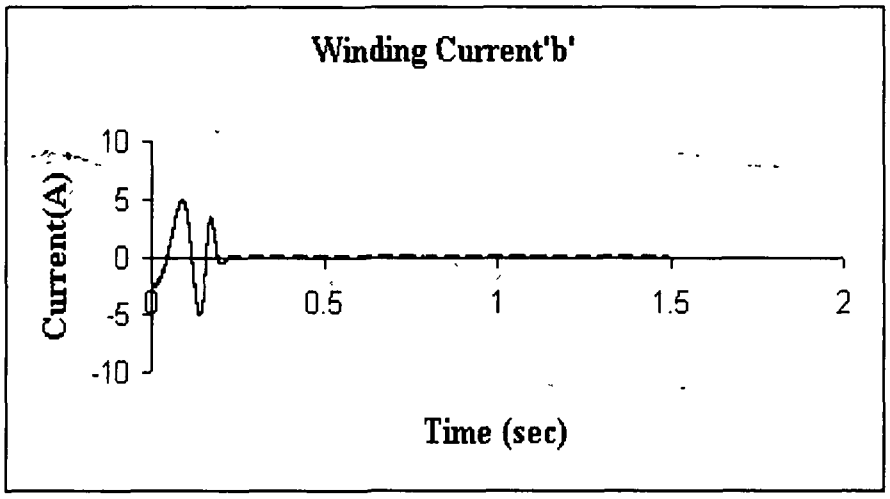

Figure 6.23: Response of Motor Current ('i_b') during Starting

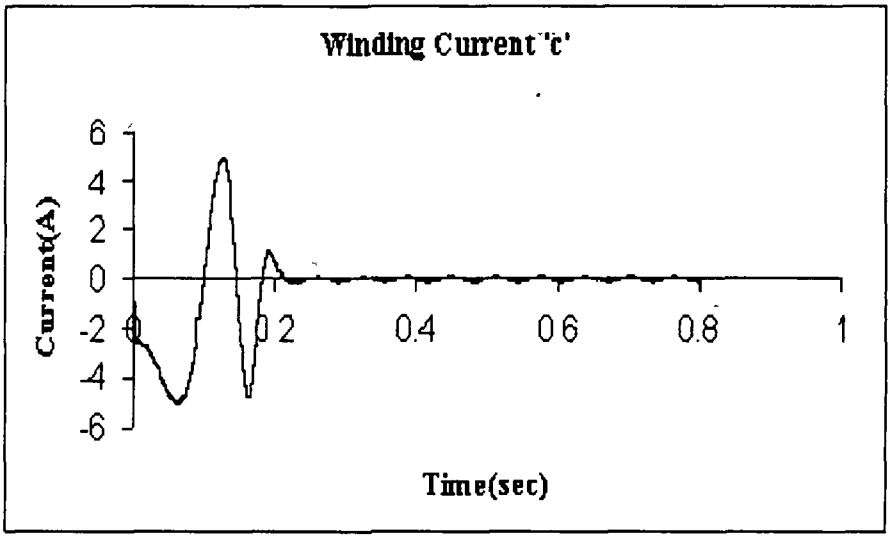

Figure 6.24: Response of Motor Current ('i_c') during Starting

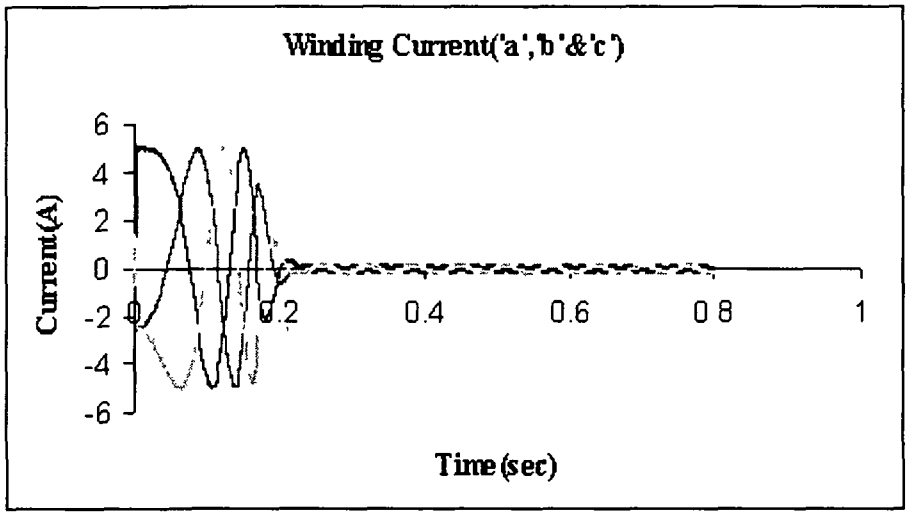

Figure 6.25: Response of Motor Currents (i_a, i_b and i_c) during Starting

6.5.2 Response of PMSM Speed with PID Controller During Starting

Figure 6.26 shows the starting response of the drive in which it takes around 225msec to reach the reference speed. As soon as the rotor reaches the reference speed, PID speed controller becomes active, and maintains the rotor speed at the reference speed.

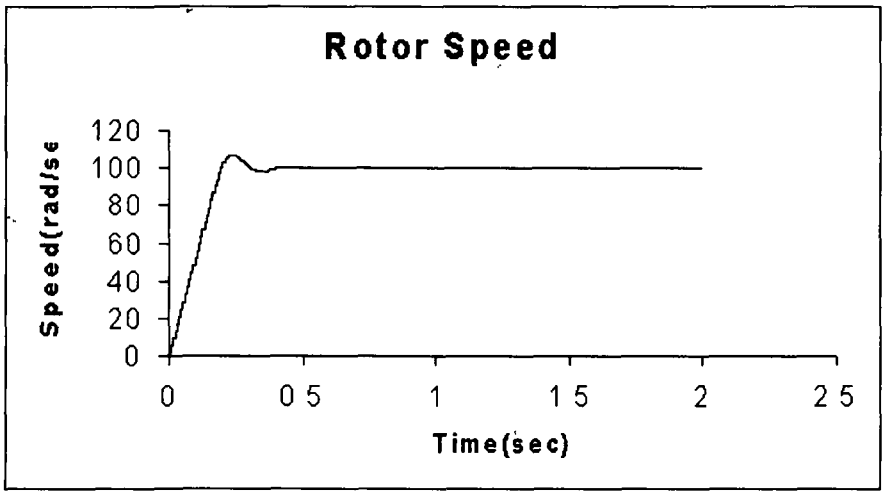

Figure 6.26: Rotor speed Vs time plot during Starting

6.5.3 Response of PMSM Torque with PID Controller during Starting

Figure 6.27 shows the motor electromagnetic torque which rises to 15 Nm (maximum permissible value) during starting from standstill. The rise in torque is almost instantaneous. After the motor reaches the steady-state condition, the developed torque decreases to 0.30 Nm and is maintained at the level over the remaining period of time.

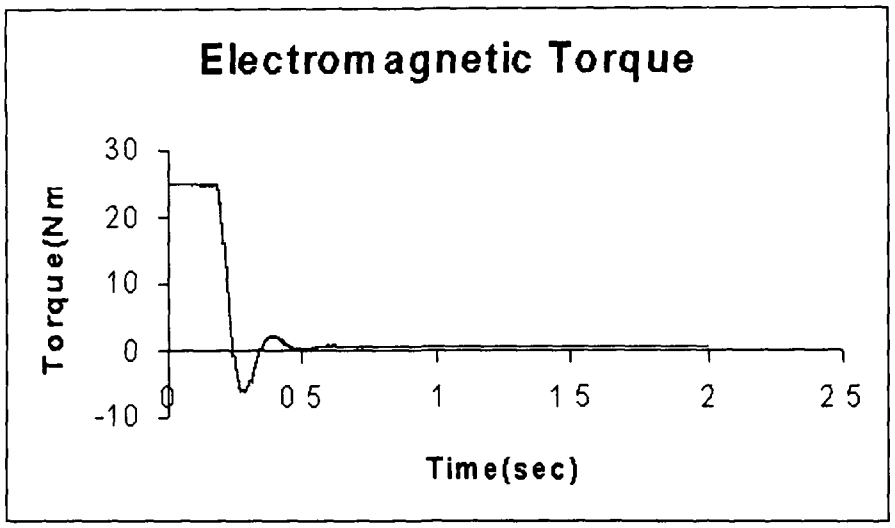

Figure 6.27: Electromagnetic Torque Vs time plot during Starting

6.5.4 Response of PMSM winding Voltage with PID Controller during Starting

Figure 6.28 shows the motor voltage. The winding voltage increase up to 109V (peak). The winding voltages are constant in all the three phases.

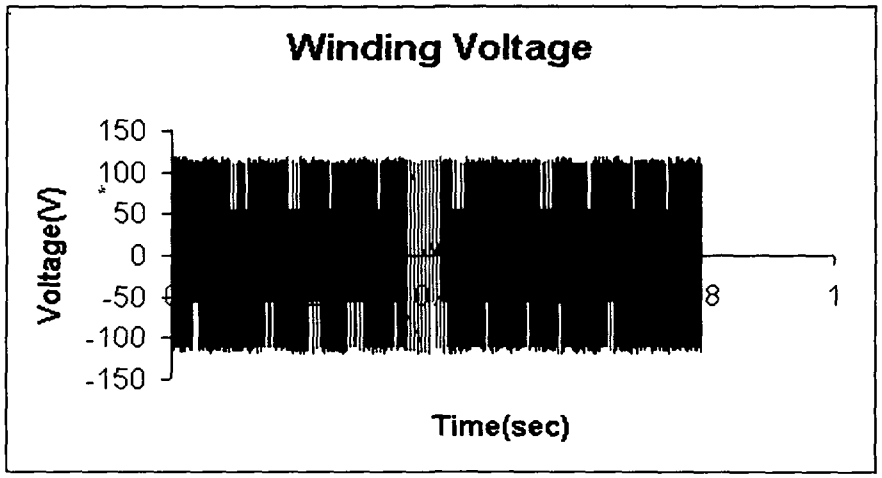

Figure 6.28: Motor winding Voltage Vs time plot during Starting

6.6 Response of PMSM Current with PID Controller During Speed Reversal

Figures 6.29 –6.32 show the motor currents (i_a, i_b and i_c) which increase up to 5.0 A (peak) at the time of starting without any load and reduce to 0.08 A during the steady-state condition. It takes 210 msec to settle down and then after 400 msec currents again rise up to 5.0 A due to the speed reversal. The drive takes 405 msec for a reversal of speed and currents come to the original value having mean equal to 0.08 A.

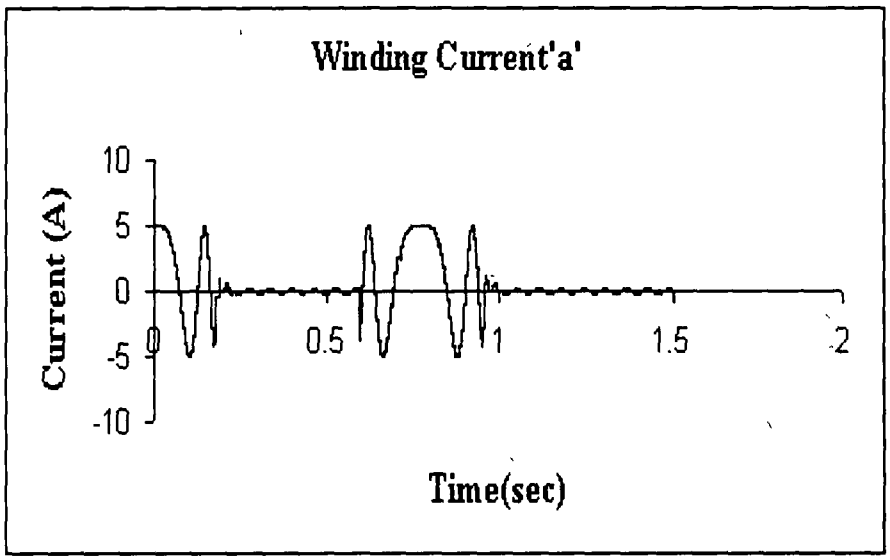

Figure 6.29: Response of Motor Current ('i_a') during speed Reversal

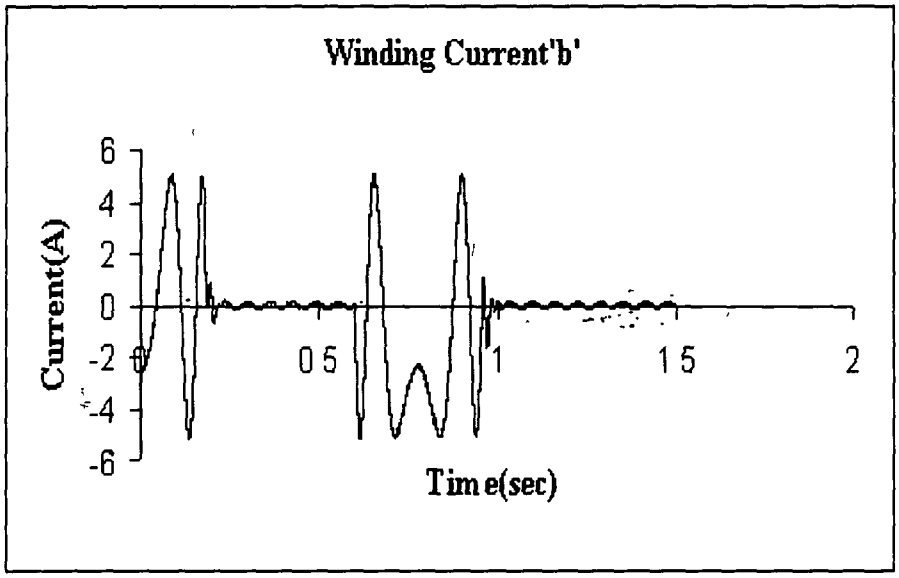

Figure 6.30: Response of Motor Current ('i_b') during speed Reversal

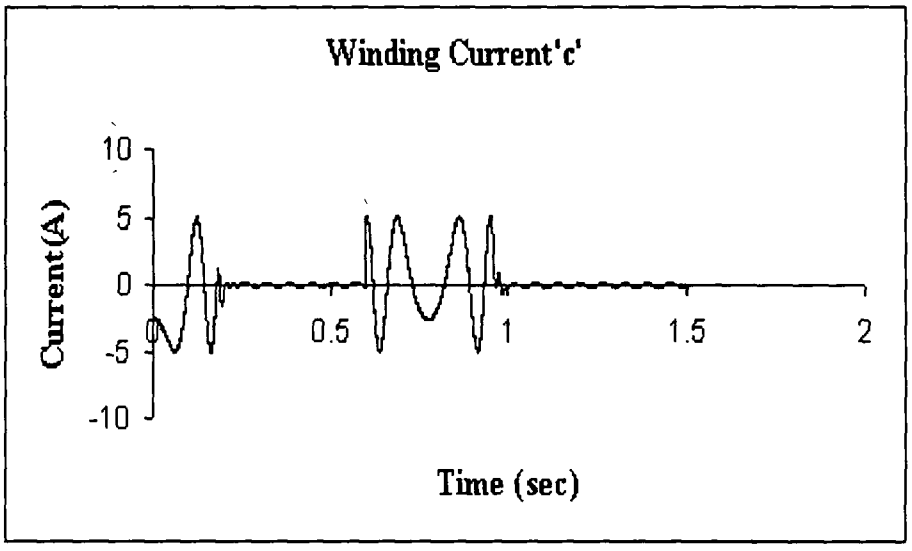

Figure 6.31: Response of Motor Current ('i_c') during speed Reversal

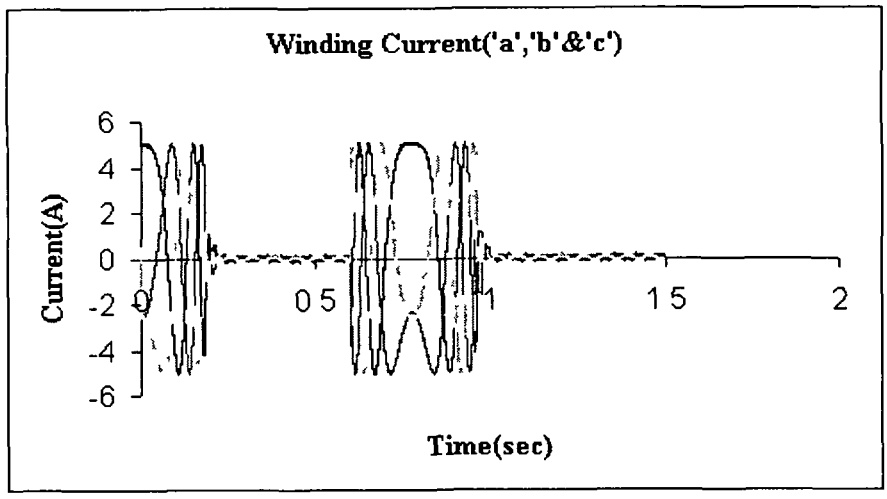

Figure 6.32: Response of Motor Currents (i_a, i_b and i_c) during speed Reversal

6.6.1 Response of PMSM Speed with PID Controller During Speed Reversal

Figure 6.33 shows the speed reversal dynamics of the PMSM motor with PID speed controller. The motor runs stable as the positive set reference speed is changed to –100 rad/sec (speed reversal). In response to this sudden change, the PID controller becomes active and makes the motor speed equal to the reference speed. The drive takes 405 msec for the speed reversal.

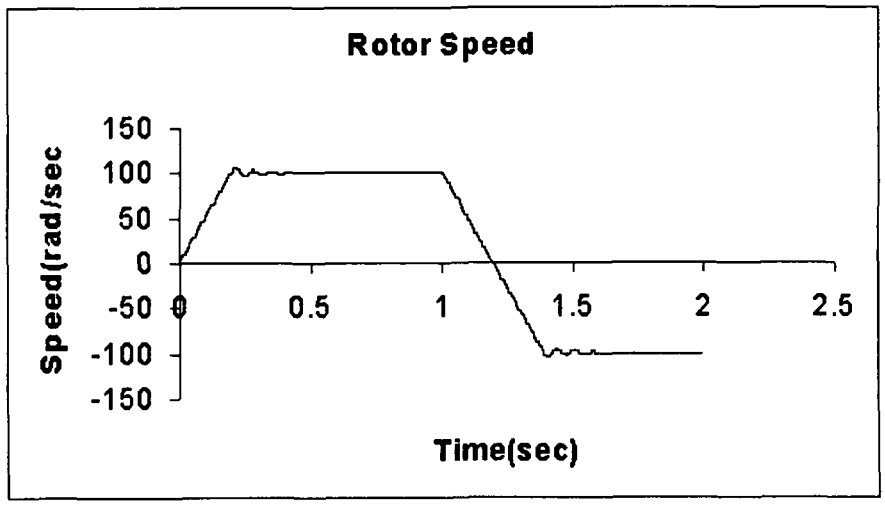

Figure 6.33: Rotor speed Vs time plot during speed Reversal

6.6.2 Response of PMSM Torque with PID Controller During Speed Reversal

Figure 6.34 shows the electromagnetic torque which rises instantaneously to 15 Nm (Maximum permissible value) to start the motor from the standstill. By the time the motor reaches the steady-state condition, the torque also undergoes a quick transient settlement to the steady-state level of 0.35 Nm until the application of speed reversal condition. When the speed is changed suddenly the torque becomes

maximum with negative value (-15 Nm) and the motor speeds up in the reverse direction. Once the motor reaches the steady state in negative direction, the torque is maintained at its initial value (0.35 Nm).

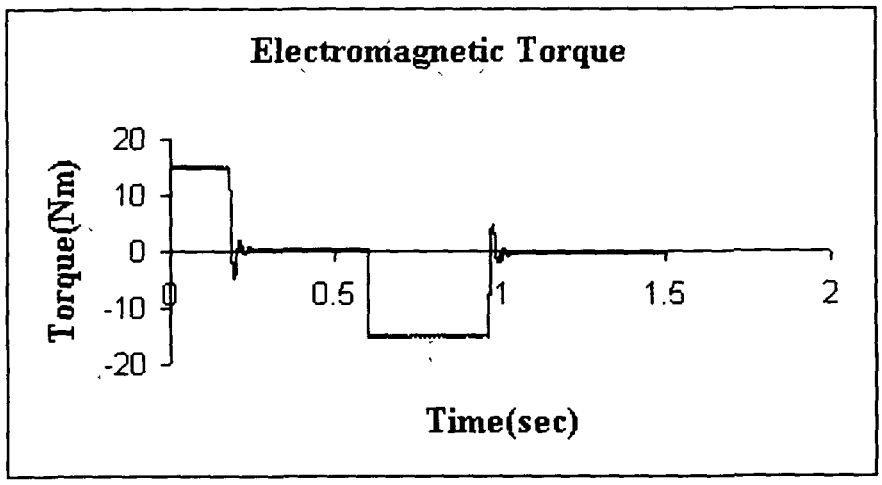

Figure 6.34: Electromagnetic Torque Vs time plot during speed Reversal

6.6.3 Response of PMSM winding Voltage with PID Controller During Speed Reversal

Figure 6.35 shows the motor voltage. The winding voltage increases up to 109V (peak0. The winding voltages are the same in all the three phases.

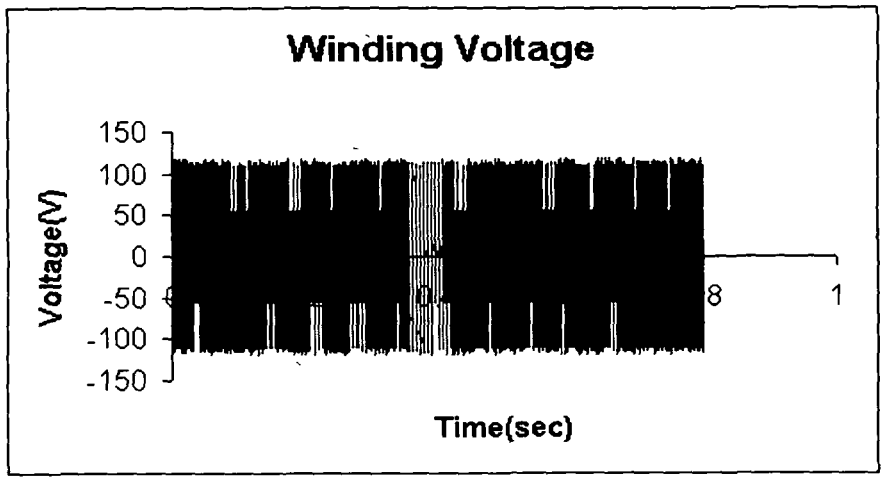

Figure 6.35: Motor winding Voltage Vs time plot during speed Reversal

6.7 Response of PMSM Motor Current with PID Controller During Load Perturbations

Figures 6.36–6.39 show the motor currents (i_a, i_b and i_c) which increase up to 5.0 A (peak) at the time of starting without any load and reduces to a 0.35 A during the steady-state condition. During the load perturbation, the current increases to 2.55A (peak) to meet the demand of load. When the load is withdrawn, the current reduces to a value decided by the small load that remains effective due to friction and windage

etc. The winding currents are found to follow the reference currents even during the condition of load perturbation. Assymetry is noted in all the 3-phase currents indicating the presence of a decaying dc component. This may be the result of non-zero switching of the controller.

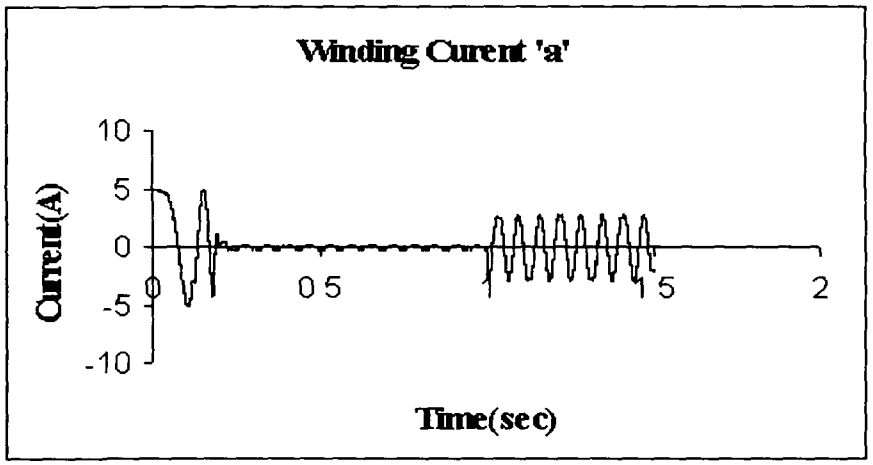

Figure 6.36: Response of Motor Current ('i_a') during load Perturbations

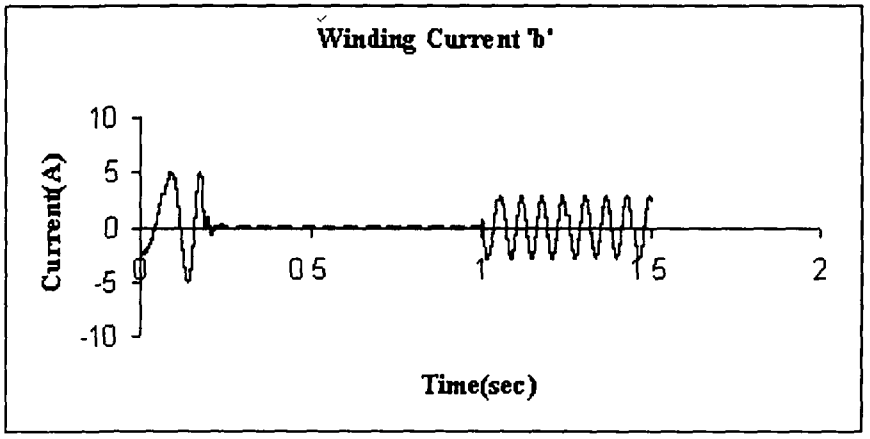

Figure 6.37: Response of Motor Current ('i_b') during load Perturbations

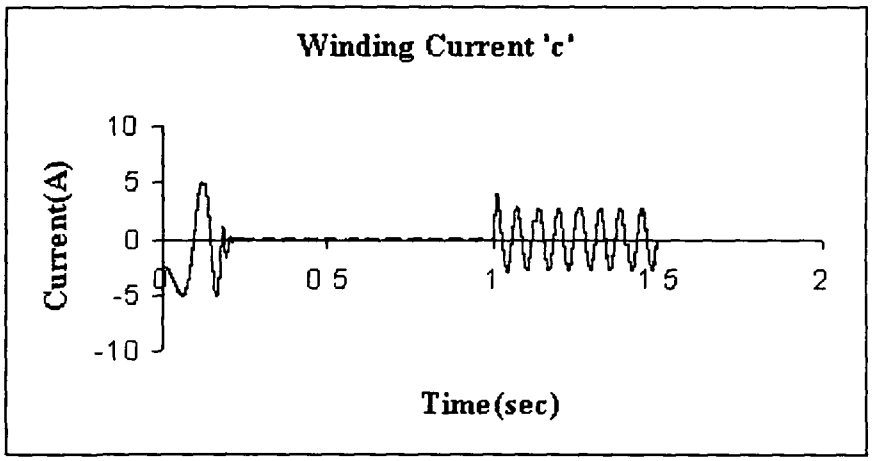

Figure 6.38: Response of Motor Current ('i_c') during load Perturbations

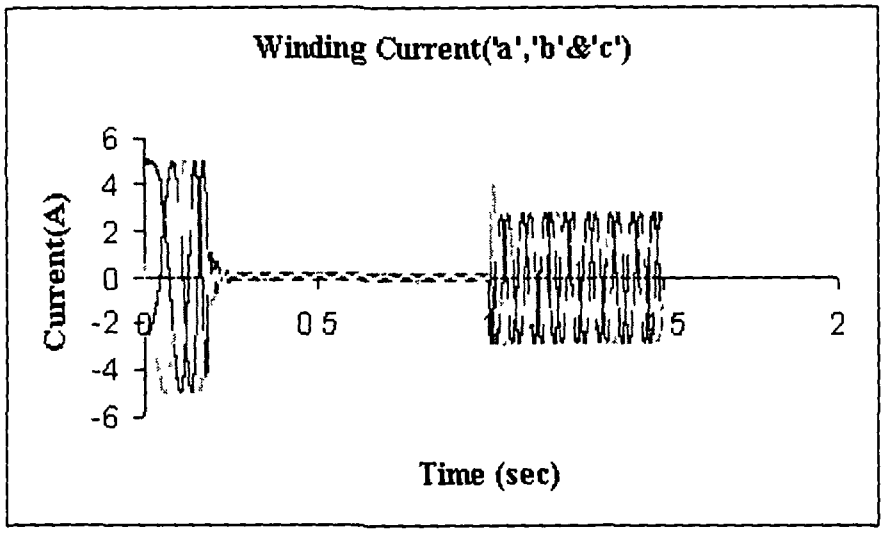

Figure 6.39: Response of Motor Currents (i_a, i_b and i_c) during load Perturbations

6.7.1 Response of PMSM Speed with PID Controller During Load Perturbations

Figure 6.40 shows the performance of the drive with the PID speed controller under load perturbations. The sudden application of the load on the motor causes a small dip and oscillation in the motor speed which is clearly visible in the Figure. However, speed returns quickly to its normal value.

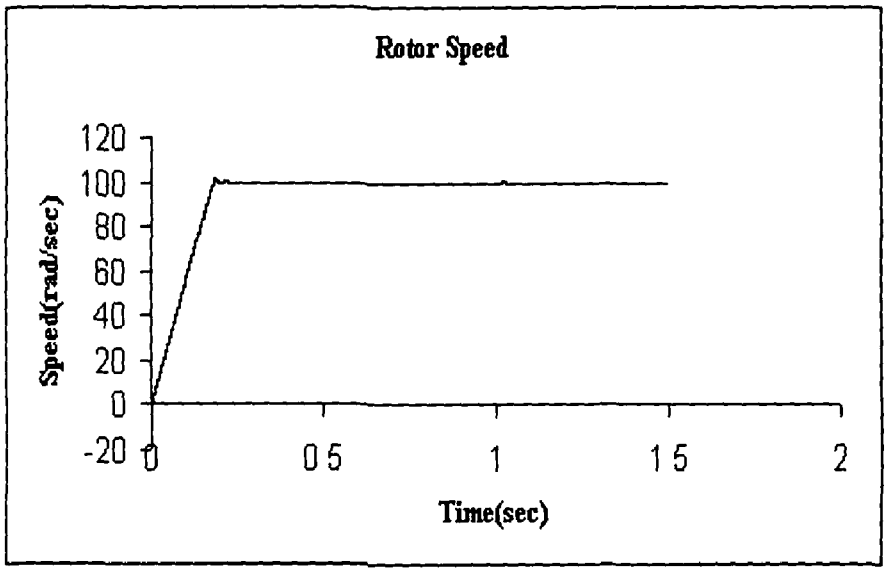

Figure 6.40: Rotor speed Vs time plot during load Perturbations

6.7.2 Response of PMSM Torque with PID Controller During Load Perturbations

Figure 6.41 shows the electromagnetic torque which increases up to 15 Nm and is maintained at the higher value till the load is removed.

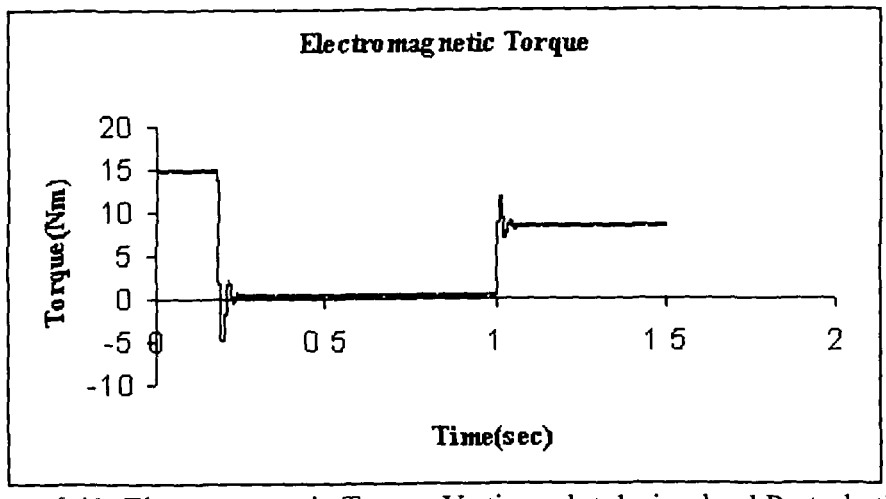

Figure 6.41: Electromagnetic Torque Vs time plot during load Perturbations

6.7.3 Response of PMSM Motor winding Voltage with PID Controller During Load Perturbations

Figure 6.42 shows the motor voltage. The winding voltage increases up to 109V (peak). The winding voltages are the same in all the three phases and seem to be unaffected by the load perturbations.

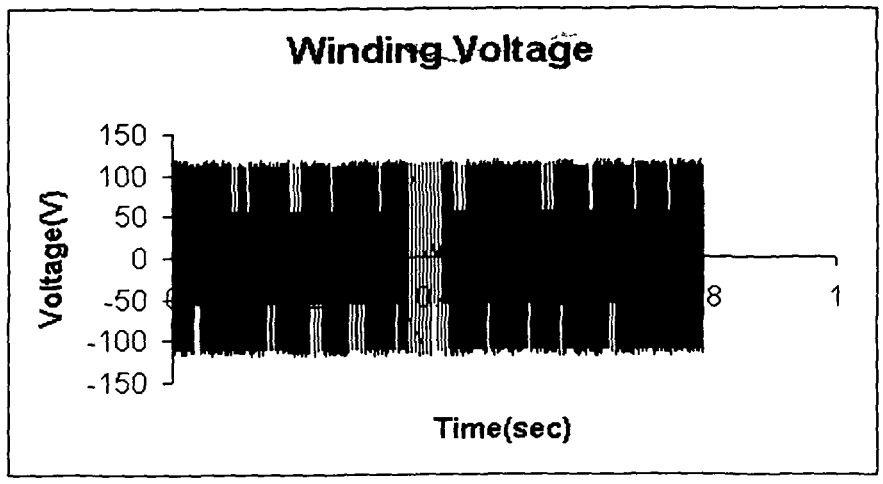

Figure 6.42: Motor winding Voltage Vs time plot during load Perturbations

6.8 Comparison of PMSM with PMBLDC Motor Drive System

The permanent magnet synchronous motor (PMSM) is a brushless PM motor, in which, the windings of the motor are sinusoidally distributed and generate sinusoidal induced emfs. The salient features of PMSM are higher power density, improved efficiency, high torque to inertia ratio and faster dynamic response etc.

Brushless dc motor, is actually not a DC motor, but is a Permanent Magnet Motor with electronic commutation, whose operating characteristics can be made to

resemble those of a DC shunt motor with constant field current. The similarity is achieved by supplying the permanent magnet synchronous machine from a source the frequency of which always corresponds to the speed of the rotor. These motors basically fall into two main categories of sinusoidally excited and square-wave excited (trapezoidal) motors. The former is known as Permanent Magnet synchronous Motor (PMSM) and operates on the principle of rotating magnetic field while the latter is termed as the Permanent Magnet Brushless DC (PMBLDC) motor and uses the method of electronic commutation

For a motor of PMBLDC type the phase model is usually preferred as the transformation of trapezoidal wave shape of induced emf into d-q axis is more complicated. For PMSM motor, on the other hand, the model is based on the frequently used d-q axis as the sinusoidal wave-shape of induced emf can be easily handled.

PMSM motor also offers many advantages similar to those of PMBLDC motor. The analysis of PMSM motor is carried out in this investigation to study its dynamic behavior under different operating conditions.

A model of the PMSM drive system is developed by including all the accessories used in the closed-loop operation of the system. The PI and PID speed controllers are used in the closed loop operation of speed control owing to its wide application in industry and ease of implementation. A computer algorithm has been developed to simulate the model of PMSM drive system to obtain its dynamic performance for starting, speed reversal and load perturbations.

The connection of a PMDC commutator motor is similar to a DC motor with the electromagnetic excitation system replaced by permanent magnets. PMBLDC motor and AC synchronous motor designs are practically the same with a polyphase stator and PMs located on the rotor. The only difference is in the control and shape of the excitation voltage. An AC synchronous motor is fed with more or less sinusoidal waveforms which in turn produce a rotating magnetic field. In PM brushless DC motors, the armature current has a shape of square (trapezoidal) waveform, only two phase-windings (for Y connection) conduct the current at the same time and switching pattern is synchronized with the rotor angular position (electronic communication).

The armature current of synchronous and brushless DC motor is not transmitted through brushes, which are subject to wear and require maintenance. Another advantage of the brushless motor is the fact that the power losses occur in the

stator, whereas the heat-transfer conditions are good. Consequently the power-density can be increased in comparison to a DC Commutator motor. In addition, considerable improvements in dynamics can be achieved because the air-gap flux-density is high, the rotor has a lower inertia and there are no speed dependent current limitations. Thus, the volume of a brushless PM motor can be reduced by more than 40% for still keeping the same rating as that of a PM commutator motor.

The results of the investigation have confirmed the viability of the simplified model used in the investigation. The different types of control structures proposed in the work are capable of taking care of transients in speed, current and torque variations during starting, reversal and load perturbations. Since the transient currents drawn by the motor never exceeded the maximum permissible, it is observed that the motor control structure takes care of the over current protection. The dynamic responses of the PMSM Motor drive are observed to be improved with PI and PID based controllers. It is revealed from this investigation that the speed controllers used have their own advantages and disadvantages, and the choice is made depending on the requirement of a particular application. It is also noticed that PI and PID controllers are simple and easy to implement.

The dynamic responses of the PMBLDC Motor drive are observed to be improved with SMC and Fuzzy PI based controllers. It is also noticed that PI and PID controllers are simple and easy to implement. But they exhibit poor performance under load disturbances and nonlinearities. SMC is observed to suffer from chattering problems. Fuzzy-PI controller is highly robust to load variations than PI and SMC controllers. Fuzzy-PI controller also shows significant improvement in transient and steady-state responses of the PMBLDC drive. Compared to PI and PID speed controllers, the Gain-Scheduled PI controller, hybrid FP+ID controller and Self-Organizing controller show better performance in terms of overshoot, rise time and load disturbances.

It has been shown in this study that there is a quick and instantaneous corrective change in the motor current in response to any disturbances in the set operating conditions of the drive system. In all cases, the actual winding currents are found to follow the variations in the reference currents. The oscillations present in the current and torque in the PI and PID speed controllers during changeover from starting to steady-state have been found to improve considerably when the SMC and FLC are used in the closed-loop operation of the drive. It has been observed that the

PI and PID controllers in comparison to Fuzzy PI and Fuzzy PID speed controllers are simpler and easier to implement. But they exhibit a slower response and cause some steady state errors with a settling period. The SMC on the other hand is found to be robust but slower, and suffers from the problem of chattering. Apart from being relatively difficult to realize FSMC, the latter is found to be superior to SMC in terms of intelligence robustness and load bearing capability. FPID is more intelligent than PID and exhibits the fastest response besides having an excellent load bearing capability.

6.9 Conclusion

The mathematical model developed has been found to be very useful in analyzing the dynamic performance of the PMSM drive. The PI and PID speed controlles used in a closed-loop control of PMSM has been found to be capable of maintaining the accurate control of speed in either direction of rotation of the drive. It has been confirmed that the control structure of the drive takes care of the transients. It has been observed that the transient currents drawn by the motor never exceed the permissible values. The instant variation of the motor currents and developed torque provide fast response of the drive system making it suitable for a number of applications such as machine tools, robotics and servo drives.

CHAPTER 7

SUMMARY AND CONCLUSIONS

7.1 General

The main objective of the research is to develop modelling and simulation techniques for selecting a digital speed controller for Permanent Magnet Brushless DC Motor drive. A model of the drive system is developed and pertinent parameters identified to examine the dynamic performances of the drive system under different operating conditions. The drive is simulated with different speed controllers to study the effectiveness of different speed controllers in improving the drive performance. The hardware complexity of the system is reduced to minimum possible extent. The cost of the drive system is reduced by eliminating position sensors. The results highlighted in the preceding chapters fulfilled these objectives. A brief summary of the main conclusions drawn is presented in the thesis in section 7.2.

7.2 Major Contributions and Summary of the Main Conclusions Drawn

The major contributions that have been carried out during the research reported in the thesis are summarized as follows:

1. The main effort of the research is centered around dynamic performance evaluation of PMBLDC motor. The investigation seeks to develop a suitable model for the PMBLDC motor with the help of which the dynamic performances of the drive system can be studied and analyzed.
2. The model has flexibility to use the various controllers and/or excitation schemes apart from improving upon the motor's overall performance.
3. A simulation model for prediction of both the dynamic and the steady state performances of the Permanent Magnet Brushless motor has been developed.
4. Motor performances with different types of speed controllers for the PMBLDC motor have been considered, namely, PI (Proportional plus Integral), PID (Proportional plus Integral plus Derivative), SMC (Sliding Mode Controller), FP-PI (Fuzzy Precompensated Proportional plus Integral), FPID (Fuzzy Proportional plus Integral plus Derivative) and FSMC (Fuzzy

Sliding Mode Controller), Gain-scheduling PI, Self-Organizing Fuzzy-Logic and Hybrid (FP+ID) controllers; and the dynamic performances of the motor under starting, speed reversal and load perturbation are studied in detail.

5. Effort is directed to develop the mathematical model of the PMBLDC motor drive system using its fundamental volt-ampere equations. This has led to the development of the model equations in abc reference frame for PMBLDC motor and d-q axis model for PMSM. A simulation model for prediction of both the dynamic and the steady state performances of PM brushless motors is presented.

6. The abc modelling approach has been used to simulate the drive, and five differential equations (three electrical, two mechanical) of the system have been solved simultaneously using the Runge-Kutta numerical integration method. In the closed loop control, the performance indices of the drive system are defined in terms of its dynamic responses during transient conditions such as starting, speed reversal and load perturbation.

7. The model allows direct examination of the motor's speed, current, position and torque. The overall performances of the PMBLDC and PMSM motors have been found satisfactory in both the steady-state and the transient state. The simulation results presented in the thesis have been specifically chosen to study the effectiveness of different speed controllers in improving the performance of the PMBLDC drive.

8. The study has also revealed that each controller has its own advantages and disadvantages and, therefore, the choice of a particular controller is specific application.

9. Gain-Scheduling PI speed controller is simulated for improving the performance of the PMBLDC drive. The PI gains are allowed to vary as a function of speed in Gain-Scheduled PI controller. This controller shows better performance than conventional PI controllers.

10. The Sliding Mode Controller suffers from the problem of chattering. The fuzzy based controllers like FP-PI, FPID, FSMC, Self-Organizing and Hybrid (FP+ID) controllers have superior performance compared to conventional controllers (PI, PID and SMC) in terms of robustness and sudden load disturbances.

11. Fuzzy-based controllers are also observed to be highly robust against load disturbances. Considering all these aspects, and by striking a balance between advantages and disadvantages of different controllers, the Gain-Scheduled PI controller is considered to be a better choice and is easier to simulate as well as to implement, besides giving comparable performance.

12. It can be concluded that the motor control structure takes care of the over-current protection requirement of devices used in the inverter circuit. It has also been shown from this study that there is a quick corrective change in the motor current in response to any disturbances in the set operating conditions of the drive system. The oscillations present in the current and torque characteristics of the PI and PID speed controllers during changeover from starting to steady-state condition have been found to be curbed considerably when the sliding-mode and Fuzzy-logic controllers are used in the closed-loop operation of the drive.

13. It has been observed that the PI and PID controllers are simpler and easier to implement in comparison to Fuzzy PI and Fuzzy PID speed controllers. But they exhibit a slower response and cause some steady-state errors with a longer settling period.

14. The Sliding Mode Controller (SMC), on the other hand, is found to be robust but slower. Apart from being relatively difficult to realize, Fuzzy Sliding Mode Controller (FSMC), is found to be superior to SMC in terms of intelligence. FPID and hybrid (FP+ID) controllers are more intelligent than FSMC and exhibit the fastest responses. Gain-Scheduling PI controller is also superior to the PI controller.

15. Elimination of the mechanical sensor from the rotor basically moves the sensor to the electrical side, which is accessible through the motor's terminals. Sensorless operation not only eliminates the number of connections between the motor and the controller, it also increases the noise immunity of position sensing. Position is sensed from the zero crossings of the back-emf signals. This has worked satisfactorily for higher speeds. It is difficult to detect position at standstill. To overcome this problem a separate starting procedure is employed by applying a specific PWM pattern. To validate the simulation, a low-cost sensorless scheme is simulated and the simulation results are shown

in Section 5.12. The sensorless scheme based on back-emf sensing is simple and cost effective for steady-state operation.

16. The digital speed controllers developed for PMBLDC motor have operated satisfactorily. All the control functions were incorporated in software for implementation. This in turn increases the accuracy in speed control of the drive system. Sensorless scheme based on motor terminal voltage sensing has been employed and found to be working effectively.

7.3 Limitations

Following are the main limitations identified for the controllers:

1. The conventional controllers have failed to show good transient and steady state performances under sudden load disturbances. So, the problem of developing a simple tuning procedure working in wide range of operating conditions is still open.
2. The gain parameters (like K_p, K_I and K_D) for each controller are selected on the basis of 'trial and error' method. If original values based on the experimental results are used instead, it will be more effective for each of the controllers.
3. The analysis carried out in the present investigation is limited to some known controllers like PI, PID, SMC, FP-PI, FPID and FSMC, Gain scheduling PI, Self organizing Fuzzy Logic and Hybrid (FP+ID) controllers.
4. The Sensorless operation has limitations because of it is difficult to detect position at zero speed. Overall the sensorless scheme based on back-emf sensing method is very simple and can be practically implemented easily.
5. The induced back-emf is decreased by imposing a demagnetizing current component in the stator windings. For a PMSM model expressed in the dq-frame, the demagnetizing current component is in the negative d-axis direction. Consequently, when a part of the current rating is used for flux weakening, there is less current left to be used for torque productions.

7.4 Scope for Future Work

Although the objectives set for this work have been completed successfully, certain problems are observed during the course of the present investigation. For further extension of the present work, some of these problems are listed as follows:

1. The conventional controllers have failed to show good transient and steady state performances under sudden load disturbances. So, there is scope for simplification of the tuning procedure covering a wide range of operating conditions.
2. The analysis carried out in this investigation is limited to some selected controllers. However, this can be further extended by using the modern control techniques of ANN (Artificial Neural Network), neuro-fuzzy, genetic algorithms and anti-windup controllers.
3. The concept of application specific integrated circuits (ASICs) into the drive system needs further work.
4. Sensorless operation of the motor needs further investigations.
5. Simulated results may be authenticated with the help of prototype; there are a number of areas where there is ample scope for further extension of this work.

REFERENCES

Bernal - Fernandez, F., A. Garcia-Cerrada, and R. Faure, "Determination of Parameters in interior permanent magnet synchronous motors with iron losses without torque measurement," IEEE Trans. Ind. Applicat., vol. 37, pp. 1265-1272, Sept. /Oct. 2001.

Betz, R.E. and M. G. Jovanovic, "The brushless doubly-fed reluctance machine and The synchronous reluctance machine - a comparison," IEEE Trans. Ind. Applicat., vol. 36, pp. 1103-1110, Jul./Aug. 2000.

Barakat, G., T. El-meslouhi and B. Dakyo, "Analysis of the cogging torque Behavior of a two-phase axial flux permanent magnet synchronous machine," IEEE Trans. Magn., vol. 37, pp. 2803-2805, Jul. 2001.

Butt, C. B., Hoque, M. A. and Rahman, M.A., "Simplified fuzzy-logic-based MTPA Speed control of IPMSM drive", IEEE Transactions Industry Applications, pp.1529- 1535, vol. 40, Nov./Dec. 2004

Bhowmik, S., A. Renespee and Enslin, "Sensorless current control for active rectifiers", IEEE Transactions on Industry Applications, vol.33, no.3, May/Jun. 1997.

Chern, T.L. and L.Chang, "DSP Based Integral Variable Structure Model following control for Brushless DC motor drives", IEEE Transactions on Power Electronics, vol.12, no.1, pp.53-63, Jan.1991.

Cerrupto,E., A. Consoli and A. Raciti, "Fuzzy Adaptive vector control of Induction motor drives", IEEE Transactions of Power Electronics, vol.12, no.6, pp.1028-1040, Nov. 1997.

Carvajal, J., G. Chen and H. Ogmen, "Fuzzy PID control: Design, performance evaluation, and stability analysis," Inform. Sci., vol. 123, pp. 249-270, 2000.

Consoli, A. and A. Testa, "Experimental low chattering sliding mode control of a PM motor drives", EPE, FIRENZE, 1991, pp. 13-18.

Cerrupto, E. A.Consoli, A. Raciti and A.Testa, "A robust adaptive controller for PM Motor drives in robotic applications", IEEE Transactions on Power Electronics, , vol. 10, no.1, pp.62-71, Jan.1995.

Chung, M.J. and D.G. Gweon, "Modelling of the armature slotting effect in the Magnetic field distribution of a linear permanent magnet motor," Arch. Elektrotech., 2002, vol. 84, pp. 101-108.

Chaaban, F.B., P. H. Mellor and K J Binns, "Practical Modelling of Permanent Magnet Synchronous Machines with Rare Earth Magnets" IEEE annul Meeting, 1990, pp.140-145.

Carrara, G. D., A. Landi Casini and L. Taponecco, "Sliding Mode Speed Controller for Trapezoidal Brushless Motors", Electric Machines & Power Systems, vol.19, pp. 157-169, 1991.

Consoli, Alfo, Salvatore Musumeci, Angelo Raciti and Antonio Tesla, "Sensorless Vector & Speed Control of Brushless DC Motor Drives", IEEE Transactions on Industrial Electronics,vol.41, no. 1, pp 91-96, Feb. 1994.

Chaaban, F.B., "Determination of the Optimum Rotor/Stator Diameter Ratio of Permanent Magnet Machines", Electric Machines and Power Systems, vol.22, pp. 521-531, 1994.

Dote, Y. and K. Kano, "DSP based Neuro fuzzy position controller for servo motor", IEEE International conference on industrial Electronics (IECON) 1992, pp. 986-989.

Dhaoudi, R. and N.Mohan, "Design and Implementation of an Extended Kalman Filter for the state Estimation of a Permanent Magnet Synchronous Motor", IEEE Transactions on Power Electronics, vol.6, no.3, 1991.

Dote, Y., and S. Kinoshita, "Brushless Servomotors fundamentals and applicat.," Clarenton press, 1990.

Demerdash, N.A., "T.W. Hijari and A.A. Arkadan, "Computation of Winding Inductances of Permanent Magnet Brushless DC Motors with Damper Windings by Energy Perturbation", IEEE Transactions on Energy Conversion,Vol. 3. No.3. Sept. 1988, pp. 705-713.

Erdman, D.M., H.B.Harms, J.J.Olderkamp, "Electronically commutated DC motors for the appliance industry," IEEE IAS Conference Records, 1984, pp. 1339-1345.

Ehasani, M. and K. M. Rahman, "Application of a clustering adaptive fuzzy logic controller in a brushless motor", Proceedings of the International Conference on Industrial Electronics (IECON), 1997, pp. 1001-1005.

Ertugrul, N. and P. Acarnley, "A new algorithm for sensorless operation of Permanent magnet motors", IEEE Transactions on Industry Applications, vol.30,no.1, Jan/Feb. 1994, pp. 126-133.

Erdman, D.M. and H. B. Harms, "Estimating Speed-Torque Profiles of the Brushless DC motor", Proceedings of MOTORCON, pp.1-7, Oct.1985.

Ertugal, N., "Position Estimation and performance prediction for permanent magnet motor drives" A Ph.D Thesis, The University of Newcastle upon Tyne, 1992.

Friedrich, G. and M. Kant, "Choice of drives for electric vehicles: A comparison between two Permanent Magnet AC Machines," IEE Proceedings on Electric Power Applications, vol.45, no.3, pp. 247-252, May 1998.

Gieras, J.F. and M.Wing, "Permanent magnet motors drives", IEEE Tutorial, PEDES, IIT Delhi, 1996.

Gieras, J. F. and M. Wing, Permanent Magnet Motors Technology: Design and Applications, 2nd ed. New York: Marcel Dekker, 2002.

Gieras, J. F. and M. E. Marler, "Analytical prediction of torque ripple in permanent magnet brushless motors," in Proc. Int. Conf. Electric Machines (ICEM'02) Brugge, Belgium, pp. 33-34, 2002.

Galvan, E., A. Torralba and L.G. Franquelo, "ASIC Implementation of a Digital Tachometer with High Precision in a Wide Speed Range", IEEE Transactions on Industrial Electronics, vol. 43, no. 6, pp. 655- 661, Dec. 1996.

Howlett, J.F., "Brushless DC motors", Proceedings on MOTORCON, pp.1- 41, Mar. 1982.

Honsinger, V.B., "Performance of Polyphase Permanent Magnet Machines", IEEE Transactions on Power Apparatus and Systems, vol. PAS-99, no.4, pp.1510-1518, July/Aug. 1980.

Hwang, G. C. and S. C. Lin, "A Stability Approach to Fuzzy Control Design for Non-linear Systems", Fuzzy Sets & systems, vol. 48, pp. 279-286, 1992.

Hu, J., D.M. Dawson and K. Anderson, " Position Control of a Brushless DC Motor without Velocity Measurements", IEE Proceedings of Electrical Power Application, vol.142, no.2, pp. 113-122, Mar. 1995.

Hanselman, Duene C.,"Brushless Permanent Magnet Motor Design" (Book) McGraw - Hill, Inc.1994.

Hzuka, K., H. Uzuhashi, Rano, Endo and K. Mohri, "Micro computer control for Sensorless brushless motor", IEEE Transactions on Industry Applications, vol.1A-21, no. 4, pp. 595-601, May/Jun.1985.

H. Han, C. Y. Su, and S. Murakami, "Adaptive fuzzy control for a class of discrete - time nonlinear systems," in Proc. 10th IEEE Int. Conf. Fuzzy Systems, vol. 2, pp. 892-895, 2002.

Irdand, J.K., "Ceramic Permanent Magnet Motors," Mc.Graw Hill Book Company, 1968.

Jack, A.G. and P.P. Acarnley, "The design of small high speed DC drives with precise speed stability," IEEE IAS meeting, pp.501-506, 1988.

Jespersen, T., "Self organizing fuzzy logic control of a PH neutralization process", Rapport No.8102, Technical University of Denmark, Lyngby, Mar. 1981.

Jahns, T.M., G.R. Kliman and T.W. Neuman, "Interior Permanent Magnet Synchronous Motors for adjustable speed drives", IEEE Transactions on Industry Applications, vol. IA -22, no.4, pp. 738 – 747, Jul./Aug. 1980.

Jahns, M. Thomas, "Flux Weakening Regime Operation of an Interior Permanent-Magnet Synchronous Motor Drive", IEEE Transactions on Industry Applications, vol. IA-23, no.4, pp 681-689, Jul./Aug. 1987.

Johns, TM, "Motion control with permanent magnet a.c. machines", Proc IEEE 82(8): 1241-1252, 1994.

Krishnanan, R. and S. Lee, "PM Brushless DC motor drive with a new power converter Topology", IEEE Transactions on Industry Applications, vol. 33, no. 4, pp. 973-982, Jul./Aug. 1997.

Krishnanan, R., "PM Brushless DC motor drive with a new power converter Topology", IEEE Transactions on Industry Applications, vol. 33, no. 4, pp.983-992, Jul./Aug. 1997.

Kovacic, Z. and S. Bogdan, "Sensitivity based self learning Fuzzy logic control for a Servo System", IEEE Transactions on Control Systems, pp 41– 51, Jun. 1998.

Kenjo, T. and S. Nagamori, "Permanent Magnet Brushless DC Motors," Clarendon press, Oxford, U.K, 1985.

Karunadasa, J.P. and A.C. Renfrew, "Analysis of Torque Production in Brushless DC and AC Motor Drives", IEE. CD No.324, Fourth International Conference on Power Electronics and Variable Speed Drives, pp.451–456, July 1993.

Kung, Y. S. and C. M. Liaw, "A Fuzzy Controller Improving a Linear Model Following Controller for Motor Drives", IEEE Transactions on Fuzzy Systems, vol. 2, no.3, pp.194, Aug. 1994.

Krishnan R. and Geu Hie Rim, "Modelling, Simulation & Analysis of Variable-Speed Constant Frequency Power Conversion Scheme with a Permanent Magnet Brushless DC Generator", IEEE Transactions on Industrial Electronics, vol. 37. no. 4 pp. 291-296, Aug. 1990.

Kim, Kyeong Hua, Cheng S.K., Moon G.W., "Parameter Estimation and Control for Permanent Magnet Synchronous Motor Drive Using Model Reference Adaptive Technique", IECON 95, pp. 387-392.

Kim, E. and D. Kim, "Stability analysis and synthesis for an affine fuzzy system Via LMI and ILMI: Discrete case," IEEE Trans. Syst., Man, Cybern. B, Cybern. vol. 31, no. 1, pp. 132-140, Feb. 2001.

Kim, K. H. and M. J. Yoon, "A nonlinear speed control for a PM synchronous Motor using simple disturbance estimation technique," IEEE Trans. Ind. Electron., vol. 49, no. 3, pp. 524-535, Jun. 2002.

Kim, Y.H., B.G. Cho and Yoko, "Generalized Techniques of Reducing Torque Ripples", IEEE International Conference on Industrial Electronics, pp.514-519, 1994.

Kenjo, T. and S. Nagamori, "Permanent Magnet Brushless DC Motors," Clarendon press, Oxford, U.K, 1985.

Kumar, K.,"Choice of Electric Drives for Mine Equipment", Minetech, vol. 14, no. 1, pp.29-31, Jan./Feb.1993.

Kumar, K., A. K. Singh, and P. K. Bordoloi, "Improved PID Controller Using Fuzzy Precompensated Algorithm for PMBLDC Motor Drive", Accepted in AMSE Journal (France).

Kumar, K., A. K. Singh and P. K. Bordoloi, "Optimum PI Controller for Permanent Magnet Brushless DC motor", Electrical Review Journal (India), vol.1, pp.16-23, Jun. 2005.

Kumar, K. and A. K. Singh, "Sensorless Control of Permanent Magnet Brushless Motor"– The present Trends in Development on 15th Sept. 2002 and published by Arunachal Pradesh Engineering Service Association Constiuted by INDEF, Itanagar.

Kumar K., O.P. Roy, A.K. Singh, " Dry type Distribution transformers and their applications", National Seminar on Application of Dry Transformer in Electrical Distribution System, Apr. 7, IE(I), Assam State Center, Guwahati, 2002.

Ko, J.S., "Robust position control of BLDC motors using Integral-Proportional-Plus Fuzzy logic controller", IEEE Trans. On IE, vol, pp.308-315, Jun. 1994.

Kim, J.H. and Chong, "Fuzzy pre-compensated PID controllers", IEEE Transactions on Control Systems Technology, vol.2, no.4, pp. 406-410, Dec. 1994.

Kappas, E., D. J. Kinniment, P. P. Acarhley, "Design of an Integrated Circuit Controller for Brushless DC drives," IEE 4th International Conference on Power Electronics and Variable Speed drives, 1990, pp. 336-341.

Lee, V.N. and T.W. Kim, "Design of self organizing plus PID controller using the lookup tables", Proceedings of the 1992 IEEE International Conference on Intelligent robots and systems, Raleigh, NC, 1992, pp. 775 - 781.

Low,Teck-Seng, M.A.Jabbar, and M.A.Rahman, "Permanent Magnet Motors for Brushless Operation", IEEE Transactions on Industry Applications, vol.26, no.1, pp 124 – 129, Jan./Feb. 1980.

Low, T. S and Binns, K. J, "Multistacked imbricated rotors with Permanent Magnet Excitation: Design for new magnetic materials" Proc. IEE, 1986, vol. 133, no.4, pp. 205-211.

Lu, Yu-Sheng and Jain-Shiang Chen, "A Self Organizing Fuzzy Sliding-Mode Controller Design for a Class of Nonlinear Servo Systems", IEEE Transactions on Industrial Electronics, vol. 41, no. 5, oct. 1994.

Le-Huy, H, P. Viarouge and I. Kamwa, "Model reference Adaptive Fuzzy Control of a Permanent Magnet Synchronous Motors", IECON-95, pp 1440-1445.

Le-huy, Houng, Rober Perret and Rene Feuillet, "Minimization of Torque Ripples in Brushless DC Motor Drives", IEEE Transactions on Industry Applications, vol. 1A-22, no.4, pp 748-755, Jul./Aug.1986.

Lee, C. C., "Fuzzy logic in control systems: Fuzzy logic control- part1 & part 2", IEEE Trans. Syst., Man, Cybern, vol.20, no.2, pp. 404-435, Mar./Apr. 1990.

Luk, P. C. K. and C.K. Lee,"Efficient Modelling for a Brushless Motor drive", IEEE International Conference on Industrial Electronics (IECON), 1994, pp.188-191.

Luneau, J.R., "New Developments in Feedback Devices for Brushless DC Servo Systems", EMCA, Regional Meeting King of Prussia, PA, Sept 11, 1984, pp.86-95.

Lo, J.C. and Y. H. Kuo, "De - coupled fuzzy sliding mode control", IEEE Trans. on Fuzzy Systems, vol.6, no.3, pp. 426-435, Aug. 1998.

Li, N., "Design of a Hybrid Fuzzy logic Proportional plus conventional Integral Derivative Controller", IEEE Transactions on Industry Applications, vol. 27, no.4, pp. 449-463, Nov. 1998.

Lee, B. K and M. Ehsani "Advanced Simulation Model for Brushless DC Motor Drives" Electrical Power Components and Systems, vol.31, pp. 841-868, Jul. 2003.

Matavelli, P. and G. Spiazzi, "General Purpose Fuzzy controller for DC-DC converters", IEEE Transactions on Power Electronics vol. 12, No.1, Jan 1997, pp. 77 – 86.

Matsui, Nobuyuki and Masakane Shigyo, "Brushless DC Motor Control Without Position and Speed Sensors", IEEE Transactions on Industry Applications, vol. 20, no.l, pp. 339-346, Jan./Feb. 1992.

Mayer J., "Design News 3rd (March 27): 182, 1995.

Morimoto, Shigeo, Masayuki Sanada and Yoji Takeda, "Wide-Speed Operation of Interior Permanent Magnet Synchronous Motors with High-Performance Current Regulator", IEEE Transactions on Industry Applications, vol. 30, no.4, pp. 920-926, Jul./Aug. 1994.

Miraoui, A, L.D. Fang and J. M. Kauffman, "Performance Analysis of Permanent Magnet Brushless DC motor", CD No. 376, Sixth International Conference on Electric Machines and Drives, 8-10th Sept. 1993, Oxford, UK,

Mecrow, B.C., A.G. Jack and T.M. Masterman, "Determination of Rotor Eddy Current Losses in Permanent Magnet Machines", CP. No. 376, Sixth International Conference on Electrical Machines and Drives, 9-10th Sept. 1993, Oxford, UK. pp. 1120-1126.

Miller, T.J.E., "Brushless Permanent Magnet and Reluctance Motor Drive," Clarendon Press, Oxford, U.K, 1989.

Matsunga, N. and S. Kawaji, "Fuzzy hybrid control of dc servo motor," Elec. Engr. Japan, vol.11, no.6, pp.105-111, 1991.

Matsui, N. "Sensorless PM Brushless DC motor drive", IEEE Transactions on Industrial Electronics, vol. 43. no. 2, pp. 300 – 308, Apr. 1996.

Matsui, N. and H. Ohashi, "DSP based adaptive control of a brushless Motor", IEEE Transactions on Industry applications, vol.28, no.2, pp. 442-454, Mar./Apr.1992.

Moreia, J.C., "Indirect sensing for rotor flux position of permanent magnet AC motor operating in a wide range", Conference Proceedings of IEEE IAS Annual Meeting, 1994, pp. 401-407.

Mellor, P.H., F.B. Chaaban and K.J.Binns, "Estimation of parameters and Performance of Rare-Earth Permanent Magnet Motors Avoiding Measurement of Load Angle", IEE Proceedings-B, vol.138, no.6, pp.371-375, 1991

Miller, T. J. E. M., Popescu, C. Cossar, M. McGilp and J. A. Walker, "Calculating The interior permanent-magnet motor," in Proc. IEEE IEMDC, 2003, pp. 1181-1187.

Osheiba, A.M. and M.A. Rahman, "Effect of Parameter Variations on the Stability Limits of Permanent Magnet Synchronous Machines", Electric Machines and Power Systems, vol.18, pp. 519-534, 1990.

Ostovic, Vlado, "Computation of Saturated Permanent Magnet AC Motor Performance By Means of Magnetic Circuits", IEEE Transactions on Industry Applications, vol. IA-23, no.5, pp 836-841, Sep./Oct. 1987.

Ogasawara, S. and H.Akagi, "An approach to position sensorless drive for brushless DC motors", IEEE Transactions on Industry Applications, vol.27, pp. 928-933, Sept./Oct 1991.

Procyk, T. and E.H. Mamdani, "On the performance of rule based self organizing controller", IEEE conference on Applications of Adaptive and Multivariable control, Hull, U.K., 1982, pp. 50-55.

Pillay, P. and R. Krishnan, "Application Characteristics of Permanent Magnet Synchronous Motor and Brushless DC Motors for Servo Drives", IEEE IAS Annual Meeting, 1987, pp. 380-390.

Patterson, E.B. and D. Morley, "Total ASIC control for an Induction Motor drive", IEE Colloquium on ASIC Technology for Power Electronics Equipment, 1992, pp. 211-214.

Panda, S. K., J. M. S. Lim and P.K.Dash, "Gain Scheduled PI speed controller for PMSM Drive", IEEE International Conference on Industrial Electronics (IECON) 1997, pp. 925-929.

Puttaswamy, C.L., "Fuzzy based sliding mode control of permanent magnet Brushless DC motor", Journal of IETE, India 1995, pp. 245-252.

Pillay, P. and R. Krishnan, "Modelling, Simulation and Analysis of a Permanent Magnet Brushless DC motor drive part II: The brushless DC motor drive", IEEE Transactions on Industry Applications, Vol.25, May/Apr. 1989, pp.274-279.

PuttaSwamy, C.L., B. Singh and B.P. Singh, "Investigations on Dynamic behavior of Permanent Magnet Brushless DC motor drive," Journal of Electrical Machines and Power Systems", vol.23, no.6, pp. 689-701, Nov./Dec. 1995.

Popescu, M., T. J. E. Miller, M. I. Mc Gilp, G. Strappazzon, N. Trivillin, and R. Santarossa, "Line start permanent magnet motor: single-phase starting performance analysis," in Conf. Rec. IEEE-IAS Annu. Meeting, 2002, pp. 2499-2506.

Parviainen, A. J., Pyrhönen, and M. Niemelä, "Axial flux interior permanent Magnet synchronous motor with sinusoidally shaped magnets," in Proc. X Int. Symp. Electromagnetic Fields in Electrical Engineering Krakow, Poland, Sept. 2001, pp. 507-512.

Quian Jainhua and M.A. Rahman, "Analysis of Field Oriented Control of Permanent Magnet Hysteresis Synchronous Motors", IEEE Transactions on Industrial Applications, vol. 29., no. 6, pp1156-1163, Nov./Dec.1993

Qu R. and T. A. Lipo, "Dual-rotor, radial-flux, toroidally-wound, permanent-Magnet machines," in Conf. Rec. IEEE-IAS Annu. Meeting Pittsburgh, PA, vol. 2, pp. 1281-1288, Oct. 2002.

Rajasekhara, K., A. Kawamura and K. Matsuse, "Sensorless control of AC motor drives," Editorial, IEEE press, New York, 1996, pp.259-425.

Ramsden, V.S. and H.T. Nguyen, "Brushless DC Motors Using Neodymium Iron Bron Permanent Magnets", Electric Energy Conference, pp 22-27, 6-9 Oct. 1987.

Ritchter, Eike, T.J.E. Miller and T.W.Neumann and T.L.Hudson, "The Ferrite Permanent Magnet AC Motors-A Technical and Economical Assessment", IEEE Transactions on Industry Applications, vol. IA-21, no.4, pp. 644-650, May/Jun. 1985.

Rahman, M.A. and G.R.Slemon, "Promising Applications of Neodymium, Boron and Iron magnets in Electrical Machines", IEEE Transactions on Magnetic, vol. Mag.-21, no.5, pp 1712-1716, Sept.1985.

Rahman, M. A., M. Vilathgamuwa, M. N. Uddin and K. J. Tseng, "Non-linear control of interior permanent magnet synchronous motor drive," IEEE Trans. Ind. Applicat., vol. 39, pp. 408-416, Mar./Apr. 2003.

Rubaai, A., Rubaai, R. Kotaru, and M. D. Kankam, "A continually online-trained Neural network controller for brushless dc motor drives," IEEE Trans. Ind. Applicat., vol. 36, pp. 475-483, Mar. /Apr. 2000.

Rubaai, A., D. Ricketts and D. Kankam, "Experimental verification of a hybrid Fuzzy control strategy for a high performance brushless DC drive," IEEE Trans. Ind. Applicat., vol. 37, no. 32, pp. 503-512, Mar./Apr. 2001.

Sebastian, T. and V. Gangla, "Analysis of Induced EMF waveforms and Torque ripple in a Brushless Permanent Magnet Machine", IEEE Transactions on Industry Applications, vol. 32, no.1, pp. 195-200, Jan/Feb. 1996.

Slemon, G.R. and A.V. Gumaste, "Steady State Analysis of Permanent Magnet Synchronous Motor Drive with Current Source Inverter", IEEE Transactions on Industry Applications, vol. IA-19, no.2, pp. 190 – 197, Mar.-Apr. 1983.

Sebastian, T. and G.R.Slemon , "Transient Modeling and Performance of Variable Speed Permanent Magnet Motors", IEEE Transactions on Industry Applications, vol. 25, no.1, pp. 101-106, Jan./Feb. 1989.

Sebastian, T., G. R., Slemon and M. A. Rahman, "Modelling of Permanent Magnet Synchronous Motors", IEEE Transactions on Magnetic, vol. MAG-22, no.5, pp. 1069-1071, Sept.1986.

Soulard, J. and H. P. Nee, "Study of the synchronization of line-start permanent Magnet synchronous motors," in Conf. Rec. IEEE-IAS Annu. Meeting, Rome, Italy, vol. 1, pp. 424-431, Oct. 2000.

Singh, B., B. P. Singh and C. L. PuttaSwamy, "Modelling of Variable structure Controlled Permanent Magnet Brushless DC Motor", Journal of Institution of Engineers (INDIA), vol. 75, pp 183-189, Feb. 1995.

Slemon, Gordon R. and Xian Liu, "Modelling and Design Optimization of Permanent Magnet Motors", Electric Machines and Power Systems, vol. 20, pp. 71-92, 1992.

Say, M.G., "The Performance and Design of Alternating Current Machines - (book), Pitman, 1948.

Singh, A. K. and K .Kumar, "Modelling and Simulation of PID Controller Type PMBLDC Motor", Proceedings of National Seminar on Infrastructure

Development: Retrospect and prospects, vol.1, pp.137-146, Institution of Engineers (I), Patna (India), 2002.

Singh, A.K., K. Kumar and P.K. Bordoloi, "Energy Conservation Study of PMBLDC Motor" Proceedings of the All India Seminar on Energy & Environment: Issue & challenges, vol. 1, pp. 239-245, Institution of Engineers (I), Dehradun (India), 2004.

Singh A.K and. K. Kumar, "Energy Efficiency and Torque Analysis of PMSM Motor", - Proceedings of the 1st National Conference on Emerging Technologies in Electrical Systems (ETES-2005), March, 10-11, 2005 organized by Noorul Islam College of Engineering Kumaracoil, Thuckalay-629180 (India).

Singh, A.K. and K. Kumar, "Hybrid Fuzzy Controller for Permanent Magnet Brushless DC Motor", Accepted in Electrical Review Journal (India).

Singh, B, S. S Murthy, B. P. Singh, A. H. N. Reddy and A. K. Singh, "Fuzzy precompensated PID Controller for permanent Magnet Brushless DC Motor Drive" Proceedings of 23rd national Conference (NSC-99) on Systems Approach to Social Engineering,vol.1, pp 290-296, Institute of Technology, B.H.U, Varansi (India).

Singh, A.K. and K. Kumar, "Hybrid Fuzzy Versus Conventional PID Controller For PMBLDC Motor" Communicated in AMSE Journal (France).

Souza, C.D. and B.K.Bose, "A Fuzzy Set Theory based control of a Phase-Controlled Converter DC Machine Drive", IEEE Transactions on Industry Applications, vol.30, no.1, pp.34-44, Jan. /Feb. 1994.

Silva, J.E. Neto and H.L.Huy, "A Fuzzy Controller with a Fuzzy Adaptive mechanism for the speed control of a PMSM", IEEE Conference on Industrial Electronics pp. 995-1000, 1997.

Song, T., M.F. Rahman and K.W. Lim, "Digital realization of sensor drive: Some practical considerations", Conference records of IEEE IECON 1997, pp. 983-98.

Sawyer, B. and J.T. Edge, "Design of a samarium cobalt brushless DC motor for Electromechanical actuator applications", IEEE Proceedings on National Aerospace Electronics Conference (NAECON 77), Dayton, Ohio, pp.1108-1112, May 17-19, 1977.

Slemon, Gordon R., and Xian Liu, "Modelling and Design Optimization of Permanent Magnet Motors", Electric Machines and Power Systems, vol.20, pp.71-92, 1992.

Tripathi, A. and Sen P. C., "Comparative analysis of fixed and sinusoidal band Hysteresis current controllers for voltage source inverters", IEEE Transactions on Industrial Electronics, vol.30, no.l, pp 63- 73, Jan. /Feb. 1992.

Tzou, Y. and T.S. Kuo, "Design and Implementation of an FPGA Based Motor Control IC for Permanent Magnet AC servomotors", IEEE Conference on Industrial Electronics (IECON) 1997, pp. 943-947.

Thakur, T. and Singh A. K.; Electronic Supervision of Agricultural Sector, National Level Seminar on Agricultural Infrastructures on Economics, 20-21 October 2001. N.E.R.I.S.T., Nirjuli, Arunachal Pradesh-791 109.

Uddin, M. N., T. S. Radwan and M. A. Rahman, "Performances of fuzzy logic Based indirect vector control for induction motor drive," IEEE Trans. Ind. Applicat., vol. 38, pp. 1219-1225, Sept. /Oct. 2002.

Uddin M. N. and M. A. Rahman, "Fuzzy logic based speed control of an IPM synchronous motor drive," J. Adv. Comput. Intell., vol. 4, no.3, pp.212-219, 2000.

Uddin, M. N., T. S Radwan and M. A. Rahman, "Performance of interior Permanent magnet motor drive over wide speed range," IEEE Trans. Energy Conversion, vol. 17, pp. 79-84, Mar. 2002.

Uddin, M.N., Abido, M.A. and Rahman, M. A., "Development and implementation of a hybrid intelligent controller for interior permanent-magnet synchronous motor drives", IEEE Trans. Ind. Applicat., vol. 40 pp. 68- 76, Jan./Feb. 2004.

Uddin, M. N., Abido, M. A. and Rahman, M.A., "Real-time performance evaluation of a genetic-algorithm-based fuzzy logic controller for IPM motor drives", IEEE Transactions Industry Applications, vol. 41, pp. 246 252, Jan./Feb. 2005.

Verster, J.P. and J.H.R. Enslin, "Practical Design Approach for PWM Technique Controllers in the Applications of Permanent Magnet Synchronous Machine (PMSM) Drives", CD-324, Fourth International Conference on Power Electronics and Variable Speed Drives", Jul.17-19, 1990, London, UK. pp. 40-45.

Yoshitsugu, J. and K.Inove, "DC Brushless servo motor drive systems using Automatic Learning Control Based Auto gain parameter Tuning scheme", IEEE International Conference on Industrial Electronics (IECON) 1997, pp.1006-1011.

Yamamoto, H. and T. Furuhashi, "A new sufficient condition for stable fuzzy control system and its design method," IEEE Trans. Fuzzy Syst., vol. 9, no. 4, pp. 554-569, Apr. 2001.

Y. Yang, Artificial neural networks based vector control of interior permanent Magnet synchronous motor, Masters Thesis, Singapore: School Elect. Electron. Eng., Nanyang Technological Univ., 2001.

Zhang, B. S. and J. M .Edmunds, "Self-Organizing fuzzy logic controller", IEEE Proceedings, vol.139, no.5, Sept.1992, pp. 460-464.

Zhuang, M. and D. P. Atherton, "Automatic Tuning of PID Controllers" IEE Proceedings-D, vol.140, no.3, pp. 215-224, May 1993.

Zhou, P., M.A. Rahman and M. A. Jabbar, "Field Circuit Analysis of Permanent Magnet Synchronous Motors", IEEE Transactions on Magnetics, vol. 30, no.4, pp.1350-1359, Jul.1994.

Ziyad M. Salameh and William A. Lynch, "Polarized Film Resolver for the Control of Permanent Magnet Synchronous Machines", IEEE Transactions on Energy Conversion, vol.6,no.3, pp. 560-563, Sept. 1991.

Zhu, Z. Q. and D. Howe, "Influence of design parameters on cogging torque in permanent magnet machines," IEEE Trans. Energy Conversion, vol. 15, pp. 407-412, Dec. 2000.

Zhu, Z. Q., Zhu, J. D. Ede and D. Howe, "Design criteria for brushless DC motors for high-speed sensorless operation," Int. J. Appl. Electromagn. Mech., vol. 15, pp. 79-87, 2001/2002.

Zhang, B., Y. Li, and Y. Zuo, "A DSP-based fully digital PMSM servo drive using on-line self-tuning PI controller," in Proc. PIEMC 2000, vol. 2, 2000, pp. 1012-1018.

APPENDIX - A

PARAMETERS OF PMBLDC MOTORS

Table A.1: PMBLDC motor (1) Specifications

HP	2
No. of Poles	4
No. of Phases	3
Type of connection	Star
Rated Speed	1500 rpm
Rated current	4A
Rated Voltage	400 V
Resistance/Ph	2.8Ω
Back EMF Constant	1.23V-Sec/rad
Self & Mutual Inductance	0.00521 H/phase
Moment of Inertia	0.013 N/m^2

Table A.2: PMBLDC Motor (2) Specifications

HP	0.5
No. of Poles	4
No. of Phases	3
Type of connection	Star
Rated Speed	1500 rpm
Rated current	1A
Rated Voltage	400 V
Resistance/Ph	2.8Ω
Back EMF Constant	0.017 Volt -sec/rad
Self & Mutual Inductance	0.006 H/phase
Moment of Inertia	0.013 N/m^2

APPENDIX - B

PARAMETERS OF PMSM MOTOR

Table B.1: PMSM Motor Specifications

HP	2
No. of Poles	6
No. of Phases	3
Type of connection	Star
Rated Speed	1000 rpm
Rated current	4.0A
Rated Voltage	400 V
Resistance/Ph	0.8 Ω
Back EMF Constant	0.0143 Volt-sec/rad
Self & Mutual Inductance	0.00945 H/phase
Moment of Inertia	0.080 kg/m^2

APPENDIX – C

CONTROLLER PARAMETERS FOR PMBLDC MOTOR

Table C.1: Controller gains for PI Speed Controller

$K_P = 0.3$

$K_I = 0.0005$

Table C.2: Controller gains for PID Speed Controller

$K_P = 0.3$

$K_I = 0.0005$

$K_D = 0.12$

Table C.3: Controller gains for SMC Speed Controller

$K_P = 2.0$

$K_1 = 10.0$

$K_2 = 0.12$

Table C.4: Controller gains for FP-PI Speed Controller

Scaling Parameter of Speed error	$K_e = 0.0064$
Scaling Parameter of change in Speed error	$K_{ce} = 0.0064$
Scaling Parameter of Output	$K_{du} = 0.5$

Table C.5: Controller gains for Fuzzy PID Speed Controller

Scaling Parameter of Speed error	$K_e = 50.0$
Scaling Parameter of change in Speed error	$K_{ce} = 100.0$
Scaling Parameter of Output	$K_{du} = 15.0$

Table C.6: Controller gains for Fuzzy SMC Speed Controller Simulation

Scaling Parameter of Speed error	$K_e = 50.0$
Scaling Parameter of change in Speed error	$K_{ce} = 100.0$
Scaling Parameter of Output	$K_{du} = 10.0$

Table C.7: Controller gains for Self-Organizing Fuzzy Speed Controller Simulation

Scaling Parameter of Speed error	K_e= 10.0
Scaling Parameter of change in Speed error	K_{ce} = 15.0
Scaling Parameter of Output	K_{du} = 200.0

Table C.8: Controller gains for Gain-scheduling PI Speed Controller Simulation

$K_P(max) = 2.0$

$K_P(min) = 0.5$

$K_I(max) = 0.0008$

Table C.9: Controller gains for Hybrid (FP+ID) Speed Controller Simulation

$K_P = 023$

$K_I = 0.0005$

$K_D = 0.0012$

Scaling Parameter of Speed error	K_e= 50.0
Scaling Parameter of change in Speed error	K_{ce} = 100.0
Scaling Parameter of Output	K_{du} = 30.0

CONTROLLER PARAMETERS FOR PMSM MOTOR DRIVE

Table C.10: Controller gains for PI Speed Controller

$K_P = 1.05$

$K_I = 0.004$

Table C.11: Controller gains for PID Speed Controller

$K_P = 1.2$

$K_I = 0.004$

$K_D = 0.1$

APPENDIX - D

Table D.1: ELECTRICAL AND ELECTRONIC CIRCUIT PARAMETERS

Details of the MOSFETs: *IRF840, 8A, 600V*

DC Link Parameters: $C_d = 0.22\ \mu F$, $R_s = 10$ ohms, $L_d = 3.0$ mH

Table D.2: POWER SUPPLY

Two Transformers: 220V/20V

Capacitors: (i) 50 V, 1000 μF

(ii) 25 V, 4700 μF

Diode: 8A, 600V

Voltage Regulation: IC's, (i) 7818

(ii) 7812

(iii) 7912

Fuse: Six Semi Conductor Fuse: 450 V/ 10A

CORRIGANDUM

Page No. xxxi,

B = Frictional coefficient

Is Changed to

B = Damping coefficient

Page No. 1 & 11

PMBLDC Motor
Is Changed to

PMBLDC Motor Drive **at both the above mentioned pages.**

akaing
24/7/06

Page No. 18

Figure 2.1: Armature waveforms: for sinusoidally excited and square wave

is changed by the following figure

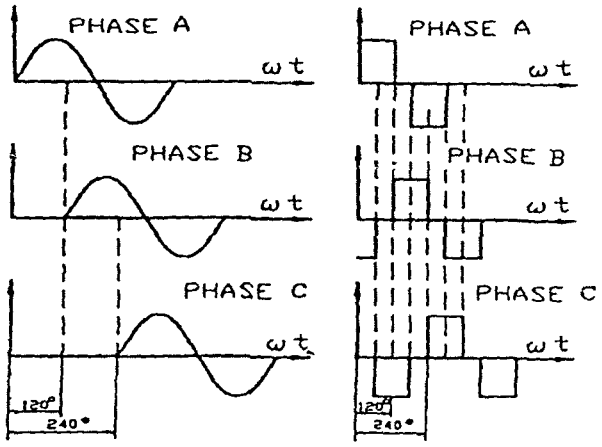

Figure 2.1: Armature waveforms: for sinusoidally excited and square wave

Page No. 75 Para 4.2 (first line)

Is changed by

The electromagnet field poles of a synchronous motor are replaced by permanent magnet in PMSM Motor Drive as shown in Figure 4.1

Page No. 84

P is changed by p

Page No. 194 (First Line)

Whereas
Is changed by
where

aksingh
24/7/06

Page No. 213 & 214 (Table A.1, Table A.2 and Table B.1)

Unit of moment of inertia kg/m^2
Is changed by
$Kg\text{-}m^2$

Volt-sec/rad
Is changed by
V-s/rad

Volt
Is changed by
V or volt

Rated current
Is changed by
Rated Current

Page No. 215 & 216
No requirement of units.

24/7/06

(A. K. SINGH)
& Ph.D. Scholar,
Regn. No. 011/2003
Deptt. of Energy,
Tezpur University, Assam

Recommended by:

24/07/06

(Prof. K. Kumar)
Director, NERIST
& Ph.D. Supervisor

DIRECTOR
North Eastern Regional Institute of
Science and Technology, ITANAGAR
NIRJULI-791109,
ARUNACHAL PRADESH